

LEVEL III

AD E 500 391
Copy of 205 copies

AD A104993

2

IDA PAPER P-1604

A STUDY OF TWENTY-FOUR NATIONWIDE FALLOUT PATTERNS FROM TWELVE WINDS

Leo A. Schmidt

September 1981

Prepared for
Federal Emergency Management Agency

This report has been reviewed in the Federal Emergency Management Agency and approved for publication. Approval does not signify that the contents necessarily reflect the views and policies of the Federal Emergency Management Agency.

DISTRIBUTION STATEMENT A

Approved for public release;
Distribution Unlimited

DTIC
ELECTE
OCT 6 1981

S

D



INSTITUTE FOR DEFENSE ANALYSES
PROGRAM ANALYSIS DIVISION

DTIC FILE COPY

81 9

29 022

IDA Log No. HQ 81-23813

Approved for public release; distribution unlimited.

REPORT DOCUMENTATION PAGE		READ INSTRUCTIONS BEFORE COMPLETING FORM
1. REPORT NUMBER	2. GOVT ACCESSION NO. AD-A104993	3. RECIPIENT'S CATALOG NUMBER
4. TITLE (and Subtitle) A Study of Twenty-Four Nationwide Fallout Patterns from Twelve Winds	5. TYPE OF REPORT & PERIOD COVERED Final	
	6. PERFORMING ORG. REPORT NUMBER IDA Paper P-1604	
7. AUTHOR(s) Leo A. Schmidt	8. CONTRACT OR GRANT NUMBER(s) FEMA EMW-C-0377	
9. PERFORMING ORGANIZATION NAME AND ADDRESS Institute for Defense Analyses Program Analysis Division 400 Army-Navy Drive Arlington, VA 22202	10. PROGRAM ELEMENT, PROJECT, TASK AREA & WORK UNIT NUMBERS Work Unit 4112C	
11. CONTROLLING OFFICE NAME AND ADDRESS Federal Emergency Mangement Agency Washington, DC 20472	12. REPORT DATE September 1981	
	13. NUMBER OF PAGES 344	
14. MONITORING AGENCY NAME & ADDRESS (if different from Controlling Office)	15. SECURITY CLASS. (of this report) UNCLASSIFIED	
	15a. DECLASSIFICATION/DOWNGRADING SCHEDULE N/A	
16. DISTRIBUTION STATEMENT (of this Report) APPROVED FOR PUBLIC RELEASE: DISTRIBUTION UNLIMITED		
17. DISTRIBUTION STATEMENT (of the abstract entered in Block 20, if different from Report)		
18. SUPPLEMENTARY NOTES		
19. KEY WORDS (Continue on reverse side if necessary and identify by block number) Fallout Deposition, Model, Winds, Attack, Effective Fallout Winds, Counterforce, Counterforce plus Countervalue		
20. ABSTRACT (Continue on reverse side if necessary and identify by block number) The research conducted under this contract deals with an assessment of fallout deposition resulting from two different types of attacks on the conti- nental United States (counterforce-only and counterforce plus countervalue) given twelve typical wind patterns--one for each month of the year. Representa- tions of fallout deposition are given in two categories--one accenting higher dose ranges to indicate shelter requirements and the other accenting lower dose ranges to present the complete spectrum of the fallout threat. (continued)		

Item 20 (continued)

The research is reported in descriptive presentation of the model, the winds, the attack, and the results. Appendices present the fallout deposition maps.

IDA PAPER P-1604

A STUDY OF TWENTY-FOUR NATIONWIDE FALLOUT PATTERNS FROM TWELVE WINDS

Leo A. Schmidt

September 1981



INSTITUTE FOR DEFENSE ANALYSES
PROGRAM ANALYSIS DIVISION

400 Army-Navy Drive, Arlington, Virginia 22202

Contract FEMA (EMW-C-0377)
Work Unit 4112C

S DTIC
ELECTE
OCT 6 1981
D

Accession For		
NTIS GRA&I	<input checked="" type="checkbox"/>	
DTIC TAB	<input type="checkbox"/>	
Unannounced	<input type="checkbox"/>	
Justification		
By _____		
Distribution/		
Availability Codes		
Dist	Avail and/or	
	Special	
A		

DISTRIBUTION STATEMENT A
Approved for public release;
Distribution Unlimited

PREFACE

This paper was prepared by the Institute for Defense Analyses for the Federal Emergency Management Agency under Contract EMW-C-0377 (Work Unit 4112C) issued August 1980.

The research conducted under this contract deals with an assessment of fallout deposition resulting from two different types of attacks on the continental United States (counterforce-only and counterforce plus countervalue) given twelve typical wind patterns--one for each month of the year. Representations of fallout deposition are given in two categories--one accenting higher dose ranges to indicate shelter requirements and the other accenting lower dose ranges to present the complete spectrum of the fallout threat.

The research is reported in descriptive presentation of the model, the winds; the attack, and the results. Appendices present the fallout deposition maps.

The research was scheduled for completion and publication as the contract deliverable on 15 September 1981. This paper is issued in fulfillment of the contract.

FOREWORD

This paper was prepared by the Institute for Defense Analyses under Contract EMW-C-0377 (Work Unit 4112C) for the Federal Emergency Management Agency. The author wishes to express his appreciation to Mr. James Jacobs, Project Officer for this Contract, for his assistance and suggestions.

TABLE OF CONTENTS

PREFACE.	111
FOREWORD	v
SUMMARY.	S-1
A. THE BASIC FALLOUT CALCULATIONS.	S-1
B. THE MODEL	S-2
C. THE WINDS	S-3
D. THE ATTACK.	S-3
E. RESULTS	S-4
F. RECOMMENDATIONS	S-5
1. Planning.	S-5
2. Operations.	S-6
CHAPTER I: INTRODUCTION.	1
CHAPTER II: THE MODEL.	3
A. GENERAL DESCRIPTION	3
B. AREA COVERED AT VARIOUS DOSE LEVELS	6
C. FALLOUT PATTERN SHAPES.	53
CHAPTER III: THE WINDS	85
A. GENERAL DESCRIPTION	85
E. OVERALL WIND SPEED AND WIND SHEAR	99
C. MONTHLY AND REGIONAL WIND SPEED AND WIND SHEAR STATISTICS.	107
D. OVERALL WIND DIRECTION STATISTICS	116
E. MONTHLY AND REGIONAL WIND DIRECTION STATISTICS.	135

CHAPTER IV: THE ATTACK. 151
A. GENERAL DESCRIPTION. 151
B. DEPICTION. 161
CHAPTER V: THE RESULTS. 195
A. PRESENTATION OF FALLOUT MAPS 195
B. COMBINED STATISTICS. 203
REFERENCES 223

APPENDICES

- A. FULL ATTACK, HIGH DOSE RANGE
- B. FULL ATTACK, LOW DOSE RANGE
- C. COUNTERFORCE ATTACK, HIGH DOSE RANGE
- D. COUNTERFORCE ATTACK, LOW DOSE RANGE

SUMMARY

A. THE BASIC FALLOUT CALCULATIONS

This report presents a set of maps drawn from results of calculations of fallout deposition as a result of two attacks on the continental United States--a counterforce-only attack and a counterforce plus countervalue attack. These maps are drawn for twelve typical wind patterns--one representing each month of the year. Two types of representations of the fallout deposition are presented, one accenting higher dose ranges to indicate shelter requirements and the other accenting lower dose ranges to present the complete spectrum of the fallout threat. The principal outputs of the study are these fallout deposition maps (in Appendices A through D); their persual is recommended to see how the fallout threat varies with the type of attack and the winds.

The fallout model used in the predictions is the WSEG-10 fallout model. This model has remained in its present form for about two decades and is used extensively for fallout predictions. A computer program called GUISTO, developed for FEMA, drives the WSEG-10 model under appropriate attack and wind conditions to produce the data files from which the fallout maps are generated. The winds are twelve historical winds, one selected from each month to give patterns typical of those particular months. The counterforce attack is 2,570 megatons and is directed principally against missile silos. The full attack consists of 6,541 megatons--the counterforce attack plus additional weapons directed primarily against urban-industrial targets. It was developed by FEMA to assist in their crisis relocation planning.

B. THE MODEL

The WSEG-10 model computes a radiation dose as a function of yield, fission fraction, height of burst (always taken as zero in this study), effective fallout wind speed, effective fallout wind shear, downwind distance, and crosswind distance. The model predicts either an H+1 hour dose rate or an "effective maximum biological dose." It is the latter quantity which is used exclusively in this study.

The area covered from a single weapon at various dose levels was determined for a variety of wind conditions. The area varies drastically as a function of dose level. The area coverage does not vary in any simple way with dose level; however, the area times dose level as a function of dose level approximates a log normal distribution.

To study the variation of area coverage with the wind, a set of contours of constant area coverage at a particular dose level as a function of wind speed and wind shear was developed. At low dose levels, increasing either wind speed or wind shear (i.e., moving outward from the origin) increases area coverage, whereas at high dose levels, just the opposite effect occurs. At intermediate dose levels, ridges of higher area coverage are seen at intermediate wind values, sloping to lower levels at more extreme values.

If coverage is presented as a function of dose divided by total fission yield, only a relatively small sensitivity to yield is observed with the coverage decreasing with yield especially at high dose levels.

Pattern shapes are presented for a variety of conditions which appear as ellipses (somewhat flattened downwind) with the bomb location near the upwind edge of the ellipse. The shape does not vary strongly with dose level over an appreciable range of levels. As a rough approximation the ratio may be taken to vary directly with wind speed and inversely with wind shear.

Finally, pattern shapes for a cluster of nearby weapons, such as would be obtained from an attack on a missile field, show a widening from an ellipse near the upwind section but a much smaller dependence on wind shear.

The fallout maps in the Appendices present examples of all of these effects.

C. THE WINDS

The winds used in this study for the fallout maps are "effective fallout winds;" these are real winds averaged over several altitudes through which a "typical" fallout particle falls. Such winds may show somewhat different properties than actual winds.

The mean wind speed averaged over all parts of the country and over all 12 monthly winds was 40 mph, and the mean wind shear was 0.126 mph/kilofoot. There was only a small correlation (0.12) between wind speed and wind shear. The wind speed distribution was close to a normal distribution over its mid range. The wind shear distribution was close to half of a normal distribution, where the mean value of the distribution was zero.

Wind speeds and angles can be approximately represented as the sum of a mean wind vector which points Eastward and a random wind vector which has a circular normal distribution.

Considerable variation in wind statistics is found for different seasons of the year and different sections of the country. In particular, mean wind speeds for winter months are a factor of two larger than for summer months. This would imply that the ratio of pattern length to width is twice as great in summer as in winter.

D. THE ATTACK

The counterforce attack consists primarily of an attack on nine missile fields in the Western and West Central part of the

United States. The full attack adds clusters of weapons in major urban areas plus an appreciable number of weapons scattered throughout the country. For assessing risk for blast damage where effects are relatively localized, the precise weapon locations are needed, whereas for estimating the fallout risk, a means of defocusing the weapon locations is desired. A "weapon density" was defined for a monitor point as the sum of yields of weapons about a monitor point times a distance weighting factor which decreased with distance from the monitor point. When contours of constant weapon density are drawn for the counterforce-only attack (see Figure IV-8), a peak in weapon density is seen covering the Colorado to North Dakota missile fields which slopes downwind to low values in each direction. For the full attack (see Figure IV-7), to this peak is added another peak centered in the Washington-New York corridor with a ridge extending Westward.

Since the prevailing winds are West to East, a modification of the weapon density calculation emphasizing upwind weapons should better indicate fallout risk. A weapon density was computed which has the distance weighting factor constant on an ellipse which has its downwind focus at a monitor point. With an ellipse with semi major axis 200 miles and semi minor axis 100 miles (see Figure IV-9), weapon density contours were obtained which had marked similarity to the observed mean fallout dose, i.e., those averaged over all twelve months. Decreasing the semi minor axis to 40 miles (see Figures IV-13 and IV-14) gave results which are similar in appearance to fallout deposition contours from a single wind.

E. RESULTS

The fallout deposition maps in the Appendices present directly the results of the calculations. The mean doses averaged for all attacks (see Figures V-3 and V-4) show rather smooth general contours. A number of hot spots, of dimension of one to several

hundred miles across, are seen in areas where a large number of weapons are concentrated.

The doses in a particular locality can vary over wide ranges for different winds. Histograms for the counterforce-only attack (see Figure V-4) show only a small chance of significant doses for most of the country. However, in some locations there is only a low chance of an insignificant dose, with the chances of being in low, medium or high ranges are rather uniformly spread. For the full attack (Figure V-5), the histograms show much smaller sections of the country with low chance of significant fallout, while much of the country shows the rather uniformly spread chances of low, medium or high doses.

F. RECOMMENDATIONS

This report has concentrated exclusively on describing the fallout threat. It is appropriate at this point to hypothesize implications for countermeasures to this threat. These recommendations should be placed in context by recalling first that the relation between blast-devastated areas and fallout-infected areas is not explicitly considered, and second that procedural or cost limitations may impede following up some of these recommendations.

1. Planning

For counterforce attacks, the primary threats are the downwind tails of attacks on missile fields which usually extend over an angle within 45 degrees from the East. The high intensity region of the tails are about 40 to 80 miles wide and extend downwind for close to 1,000 miles. A number of missile fields are located significantly close together so that for many attacks the tails merge in the crosswind direction. In those areas behind several adjacent missile fields,

a high level of fallout protection (a protection factor of 40 or greater) is required to achieve a moderate chance of surviving an attack. Further downwind the chances of any significant dose are less and the doses received are of less intensity. If high quality shelter is to be installed, it should be nearer the missile site where the chance of need is greater. If lower quality shelter is installed, it should be done further away where it is more likely to be adequate.

The Eastern section of the country generally has only a low chance of insignificant risk for a full attack and often high quality shelter is required. Especially along and east of the Washington-Boston corridor a very high quality shelter is required.

Most sections of the country and usually all of the East is covered with at least some levels of fallout (see Appendix B). Even if the levels are not high enough for immediate sickness or lethal effects, they are almost always high enough to give an appreciable radiation burden which could have significant long term effects.

2. Operations

A great amount of detail is not seen in the fallout patterns; effects occur over tens of miles rather than a few miles. (The patterns shown are averages over ten miles square, but only in the near vicinity of explosion would a higher resolution be appropriate.) Thus the general level of radiation observed at a local observation post should apply over an appreciable area. For many areas, detailed monitoring of individual weapon fallout patterns will not appreciably help in overall fallout prediction.

The above comments ignore the problem of hot spots, which might arise from individual weapon explosion,¹ details of surface wind patterns, terrain and cultural features. After assessing

¹ The WSEG-10 model does not attempt to predict hot spots.

the general background levels, the prime question in local radiation level determination should be the location of hot spots. These may range in size from a few feet to tens of miles, and these locations are often determined by random factors.

The fallout maps seem sensitive only to very gross scale features, extending over most of the continent. This gives rise to the hope that such gross features may tend to be reasonably enduring so that pre-attack predictions of such fallout patterns may be held reasonably accurate.

Chapter I

INTRODUCTION

This study deals with the problem of providing protection against radioactive fallout resulting from nuclear weapon detonations--a major element of Civil Defense programs. Planning such programs is made more difficult because of the uncertainty associated with nuclear attack as well as the daily variability in the winds which transport the radioactive material. The purpose of this study is to illustrate the range of variability from these uncertainties by presenting nationwide maps of fallout deposition from two different attacks and a set of twelve different winds. These maps are presented in four appendices as the principal output of this study.

The basic attack used is the current "Crisis Relocation Planning Attack" developed by FEMA; it uses a SALT II compatible Soviet Union inventory of weapons. For Attack A, all weapons are surface burst to produce a representation of the maximum fallout threat which might be expected. For Attack B, only those weapons against time-urgent strategic targets are used. This produces a threat representative of a counter-force-only attack, or an attack where most weapons are air burst.

A set of 12 historical winds are used, one for each month of the year. These winds might be considered typical of the type and range of winds to be expected during each month and throughout the year.

Chapters II through V are descriptive presentations of the model, the winds, the attack, and the results, respectively. Appendices A and B present Attack A with a dose intensity scale which emphasizes the higher intensities (A) and the lower intensities (B); Appendices C and D present Attack B with high intensity dosage (C) and low intensity dosage (D). Each of the 48 plots covers the entire continental United States; the plastic overlay may be used to identify specific locations. We believe these fallout maps will enhance the readers' judgment by their visual presentation of representative fallout threats. We recommend that a reader study the results presented in the appendices first, and then proceed to the more detailed chapters as interest directs.

Chapter II

THE MODEL

A. GENERAL DESCRIPTION

In this report all fallout deposition is estimated using the WSEG-10 fallout model which was originally defined in 1959 [Ref. 1]. Reference 2 documents the final version of the model after modifications were made to better represent fallout deposition near ground zero. The model has the advantage of being able to produce a prediction of dose from a nuclear weapon for given values of downwind distance and crosswind distance in a relatively short time; this characteristic makes it well suited for use in damage assessment models. It has been the standard model used in a large percentage of nationwide damage assessment calculations, including those at FEMA.

The WSEG-10 model predicts directly the H+1 dose rate as a function of position, that is, the radiation rate one hour after the detonation of all fallout which will eventually be deposited at a location. A biological dose is defined as a peak total dose received, modified by biological repair rates. A formula in the WSEG-10 model enables converting from H+1 dose rate to biological dose.

Beside the downwind distance, x (miles), and crosswind distance, y (miles), to the weapon, the inputs to the model are: the weapon yield, Y (MT), the weapon fission fraction, F , the height of burst, HOB (feet), an effective fallout wind speed, W (miles/hour), and a crosswind shear, S (miles/hr/kilo-foot). For a surface burst, the total amount of fission

deposited is proportional to the product of the weapon yield and the fission fraction. For an air burst this total deposition is reduced by some fraction of the burst height. The shape of this deposition pattern is determined by the weapon yield, wind speed and wind shear. The effective fallout wind speed is obtained by averaging winds from the top of the cloud to the ground. The wind for each layer is weighted by the time an "average" fallout particle stays in that layer. The crosswind shear is the rate of change in wind speed with height at the "cloud stabilization" altitude in a direction perpendicular to the wind. If V is the wind speed at an altitude h , and α is wind direction at altitude h , and α' is the wind direction at altitude $h+\Delta h$, the wind shear is defined as $(V|\sin(\alpha-\alpha')|)/\Delta h$.

The complete formulation of the model is too complex to present in this report; it is given in [Refs. 2 and 3].

At distances reasonably far from ground zero several simplifications can be made to the basic model without introducing significant error. With these simplifications, Reference 3 gives the following equation for biological dose, D_B (roentgens):

$$D_B = K\bar{F} \frac{2.71}{\sqrt{2\pi}BT} \frac{W^{0.382}}{S} \frac{\exp(-x/WT)}{x^{1.382}} \exp\left(-\frac{1}{2}\left(\frac{y}{xBS}\right)^2\right),$$

where \bar{F} = fission yield = YF ,

K = normalization factor = $2 \times 10^6 \cdot \text{Roentgens/hr/MT/}$
 $\text{mile}^2, ^1$

¹The WSEG-10 model is designed so that the H+1 dose rate can be written as

$$D_{H+1} = K\bar{F} f(x) g(y)$$

$f(x)$ and $g(y)$ are chosen so $\int_{-\infty}^{\infty} f(x) dx = 1$ (almost) and $\int_{-\infty}^{\infty} g(y) dy = 1$.

Thus K represents the area integral of the total radioactivity deposited, normalized to radiation rates at one hour, which is independent of wind speed and wind shear, and any explicit dependence on yield. Since the ratio of biological dose to H+1 dose rate depends on deposition time, this normalization does not apply to biological dose.

$$B = 7.5 + 1.5 \log_{10} Y,$$

$$T = \text{characteristic time} = 7.5 + 1.66 \log_{10} Y.$$

The last exponent represents the decay crosswind. The coefficient could be written y/σ_c with $\sigma_c = \frac{xBS}{W}$. The crosswind spread is proportional to downwind distance and shear and is inversely proportional to wind.

If it is desired to compute the maximum dose at some distance, i.e., the hotline dose, the last exponential term is equal to one since $y=0$. To determine the distance at which a particular hotline dose is obtained one would have to solve for x in

$$\frac{\exp\left(-\frac{x}{WT}\right)}{x^{1.382}} = \frac{\sqrt{2\pi}BT}{2.71 K\bar{F}} \frac{S \cdot D_B}{W^{.382}}.$$

Unfortunately this equation must be solved numerically since no explicit representation in terms of elementary functions is possible. We can see, that if for example, the shear is doubled and dose halved, the hotline distance is not changed.

The 1.382 power enters from the conversion from H+1 dose rate to biological dose. The simplified formula for H+1 dose rate is

$$D_{H+1} = \frac{K\bar{F}}{\sqrt{2\pi}TBS} \frac{\exp(-x/WT)}{x} \exp\left(-\frac{1}{2}\left(\frac{y}{xBS}\right)^2\right).$$

Although the expression for x is now somewhat simpler, still no solution in terms of elementary functions is possible.

In many cases in the attacks used (e.g. over missile fields or cities), a number of weapons are so close together that their patterns effectively merge into a single pattern. Although in the actual assessment the weapons were treated separately, it is possible to estimate the effect of such a cluster by approximate methods. As discussed in Reference 3,

this is done by using a pseudo standard deviation for the crosswind dose distribution obtained from

$$\sigma_{cu}^2 = \sigma_c^2 + \sigma_w^2 .$$

There, σ_{cu} is the standard deviation used to estimate cluster effects, σ_c is the usual standard deviation calculated in the WSEG-10 model, and σ_w is the standard deviation in the crosswind direction of the fission yield from the weapons in the cluster.

Since it is necessary to resort to using numerical methods to obtain values of distance to a certain hotline dose level from the simplified model, it is almost as simple, numerically; to exercise the complete model to obtain descriptions of dosage patterns. A simple computer program was written to numerically compute certain values of interest resulting from the detonation of a single weapon. The calculations were restricted to the yield ranges in this attack, i.e. 1 megaton to 20 megatons. The results are described below.

B. AREA COVERED AT VARIOUS DOSE LEVELS

The fraction of the country subjected to radioactive fallout will depend upon the area covered with fallout from individual weapons. This section will present the results of area coverage calculations for different values of the input parameters influencing the model, weapon yield, wind speed and wind shear.

The results will be presented per megaton of fission yield. Thus the area covered in the figures to be presented at a nominal dose of 10 Roentgens for a one megaton weapon with a fission fraction of 1 represents an actual dose of 10 Roentgens; however, for a 1 megaton weapon with a fission fraction of 0.5, this represents an actual dose level of 5 Roentgens, and for a 20 megaton weapon with a fission fraction

of one, this represents an actual dose level of 200 Roentgens. This method of presentation is used for two reasons: first, the area as a function of dose per megaton of fission yield is not very dependent upon weapon yield; second, this method of presentation assists in directly estimating the variations due to different amounts of weapon yield delivered to a target area.

Figure II-1 presents the area covered by at least a particular dose as a function of that dose. This figure is for a nominal wind of 20 mph and wind shear of 0.2 mph/kilo-foot. This graph is presented on linear paper, and as can be seen, three scales are needed to adequately represent the areas covered.¹

In Figure II-2a the area covered is presented as a function of dose on logarithmic paper. These areas are presented for a 20 mph wind and a variety of wind shears. As will be seen in Chapter III, values of wind shear from about 0.0 to 0.4 are typical. At a little over 100 Roentgens dose, the curves all cross. At low dose levels, high values of wind shear spread the patterns and give larger area coverage. This is compensated for at high dose levels where the reverse pattern is evident. Here less area is covered at high shear values. This occurs because at high shear value the dose is spread crosswind more at low dose levels, and since the total amount of radioactivity to spread is almost constant, there isn't as much left at high dose levels.

A 20 mph wind is at the low end of typical wind levels. In Figure II-2b, areas are plotted for a wind speed of 40 mph which is about the mean wind speed; in Figure II-3 the same

¹As a comparison, the area of the Continental United States is about 3,100,000 square miles, Texas is 262,000 square miles, Illinois is 55,000 square miles, Maryland is 9,900 square miles, Rhode Island is 1,000 square miles, and a typical county is 100 square miles.

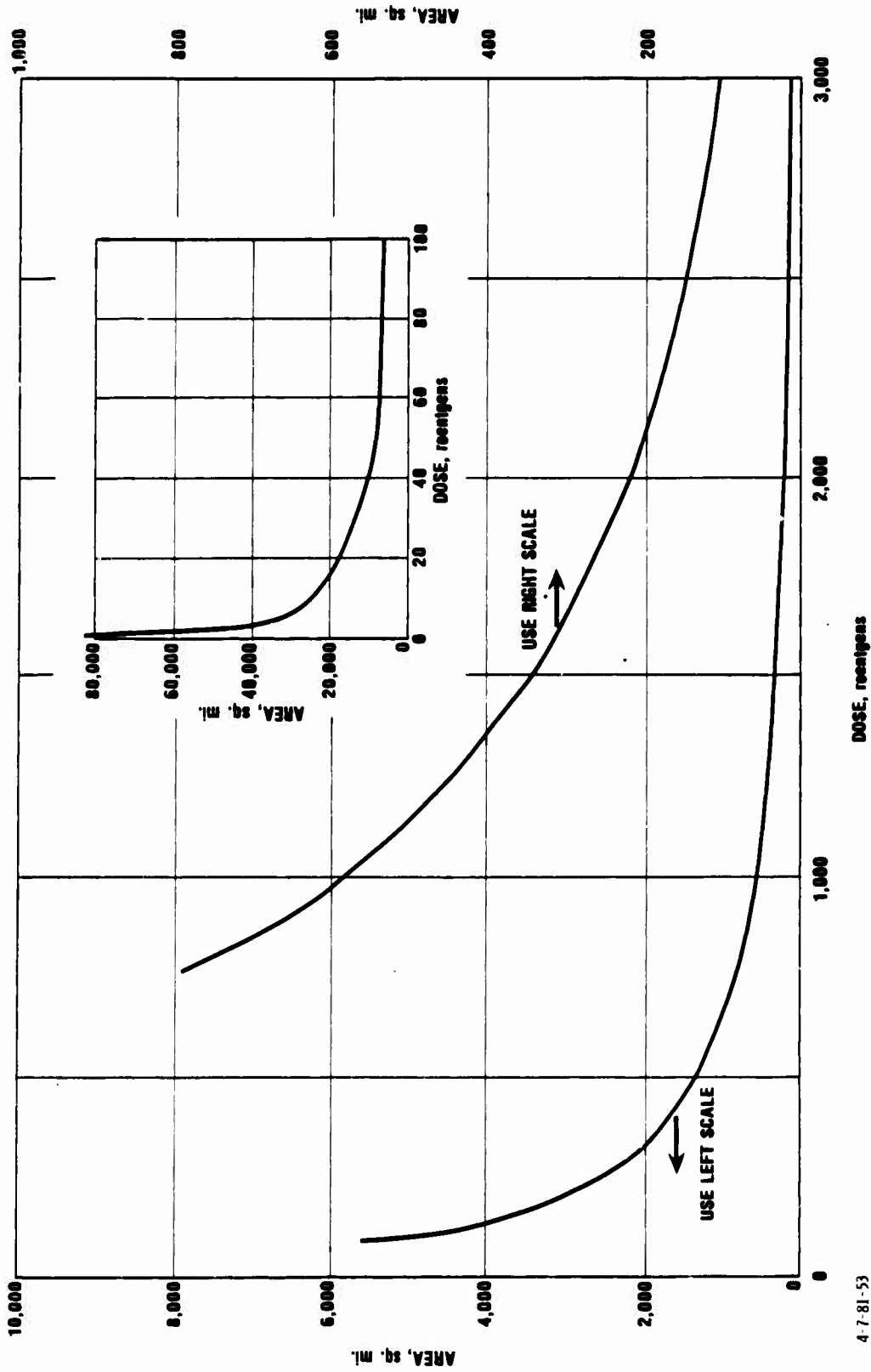
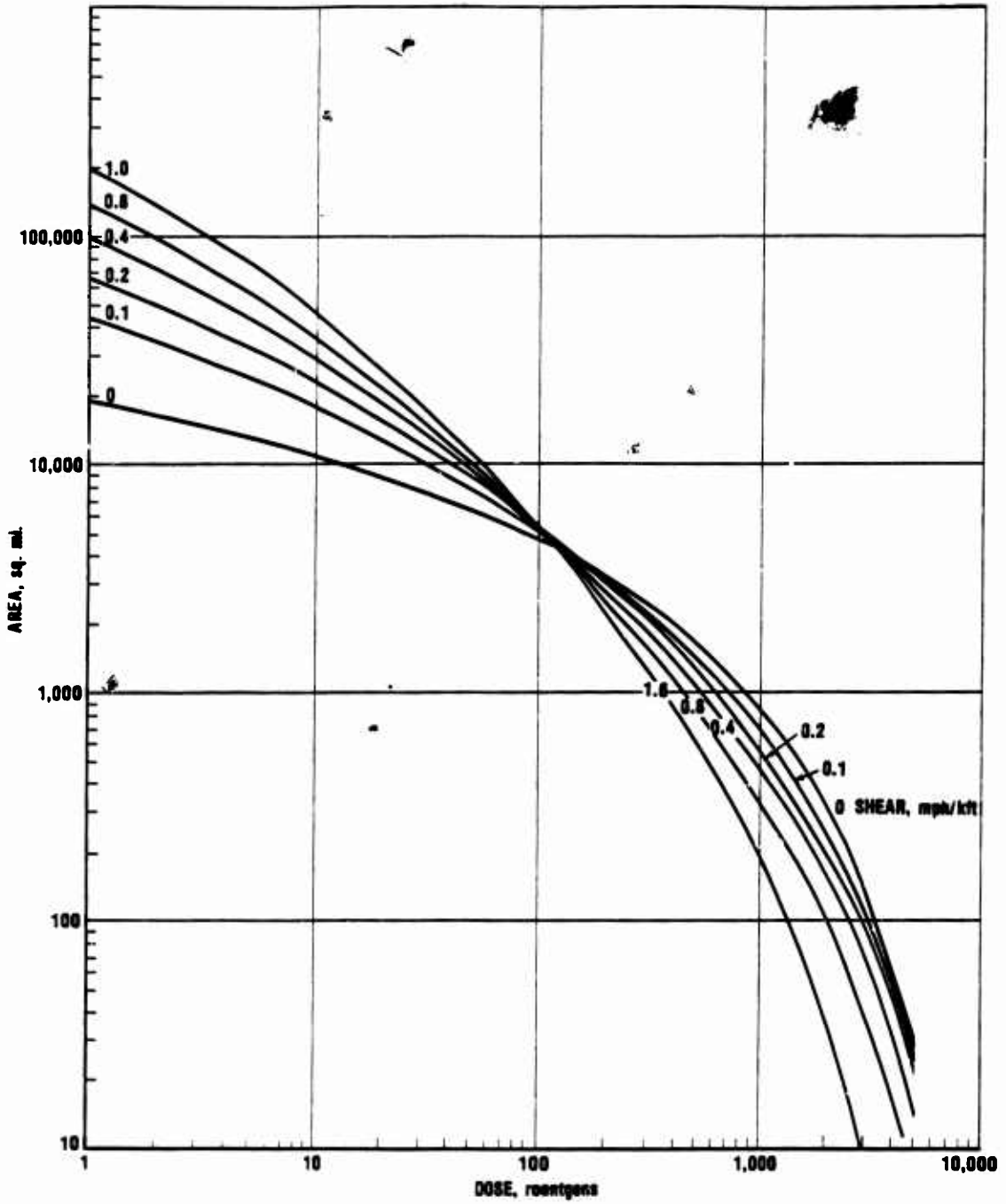


Figure II-1. AREA COVERED AS A FUNCTION OF DOSE FOR A 1 MT YIELD WITH A 20 MPH WIND AND 0.2 MPH/KILOFOOT SHEAR.

4-7-81-53



4-7-61-64

Figure II-2a. AREA COVERED AS A FUNCTION OF DOSE FOR A 1 MT YIELD WITH A 20 MPH WIND AND VARIOUS SHEARS.

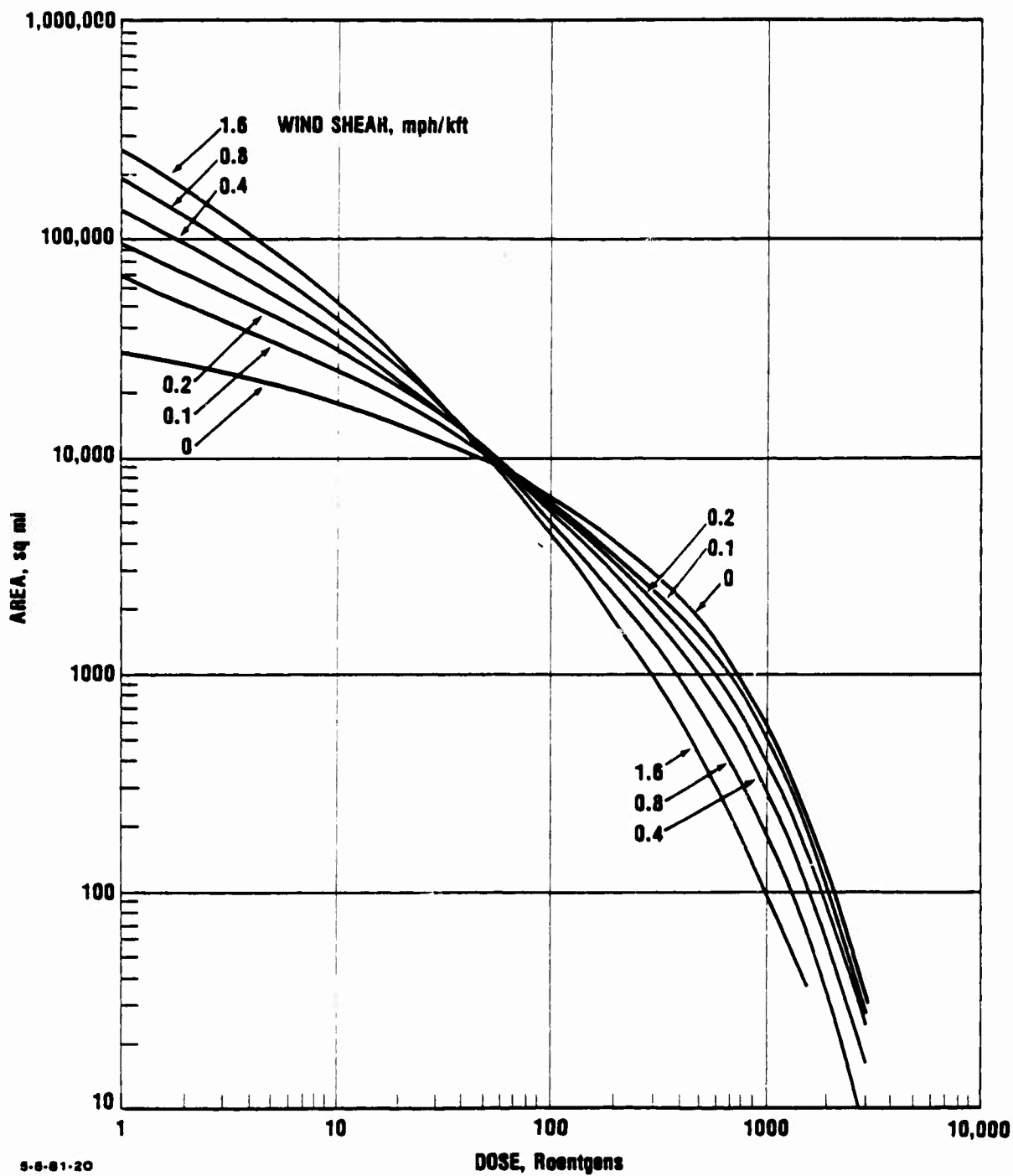
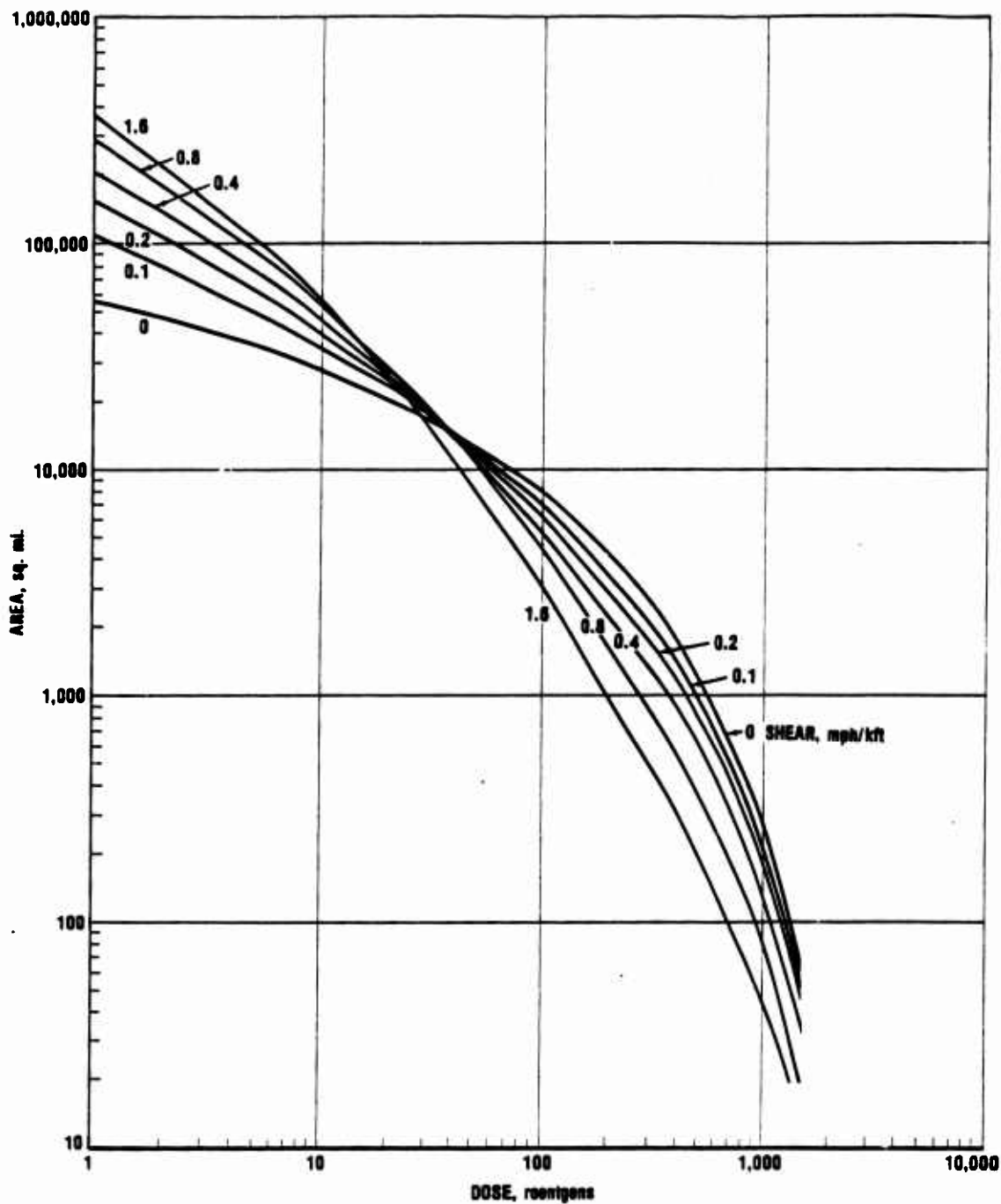


Figure II-2b. AREA COVERED AS A FUNCTION OF DOSE FOR A 1 MT YIELD WITH A 40 MPH WIND AND VARIOUS SHEARS.



4-7-61-00

Figure II-3. AREA COVERED AS A FUNCTION OF DOSE FOR A 1 MT YIELD WITH A 80 MPH WIND AND VARIOUS SHEARS.

values are plotted but for an 80 mph wind, which is near the high end of typical values. The same general patterns are seen, with the high wind speeds giving larger coverage at the lower dose levels.

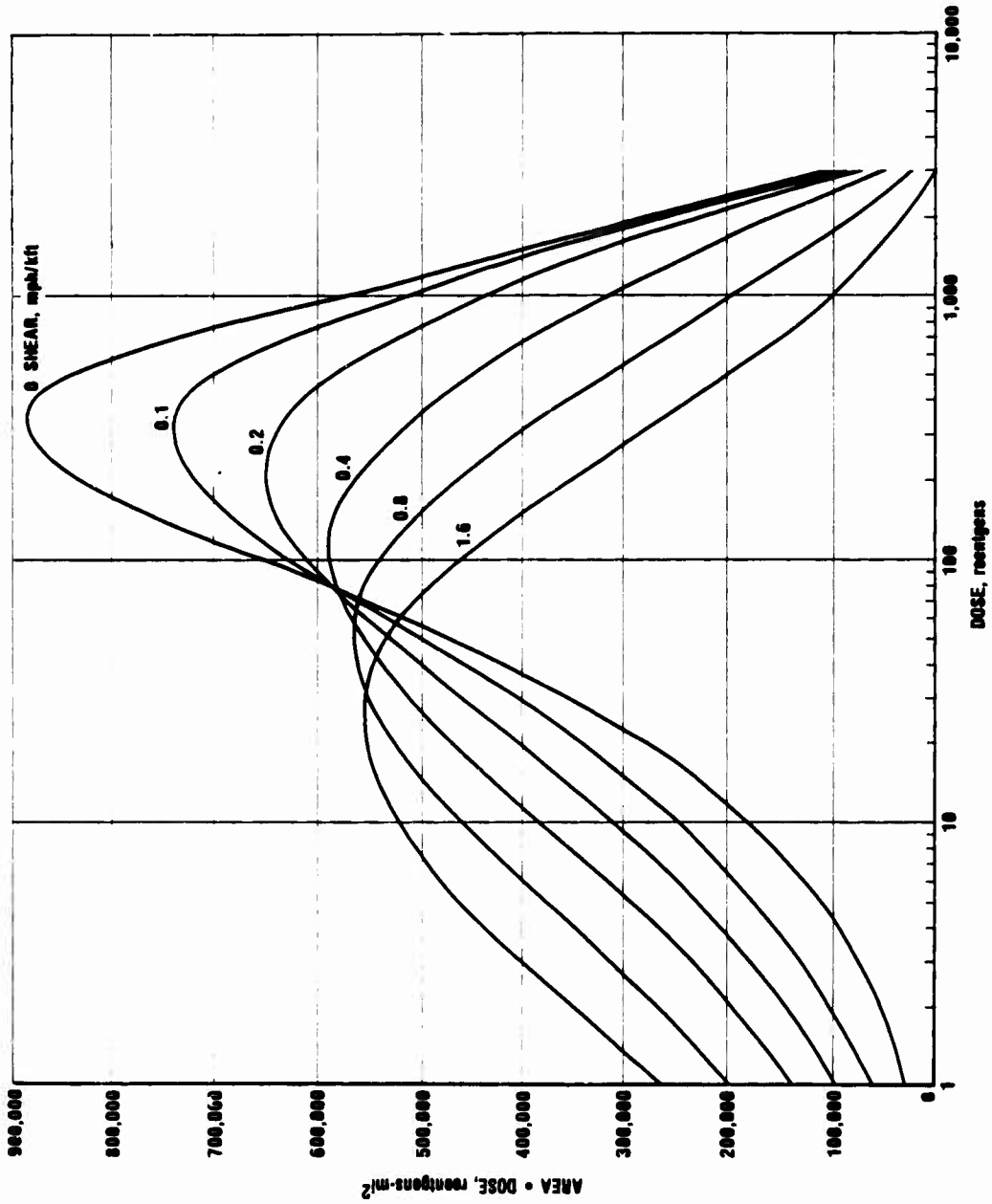
As is seen in Figures II-2 and II-3, the area covered decreases drastically as the dose is increased. The product of area covered times dose should be a slower varying function of the dose. This product is illustrated in Figure II-4 where, in fact, a much slower variation with dose is seen; in fact, the curves appear somewhat like a normal distribution probability density curve. If this is taken to be the case, then an approximate expression for area covered as a function of dose, D, would be

$$A = \frac{K}{D} \exp\left(-\frac{1}{2} \frac{\ln^2(D/D_m)}{\sigma^2}\right),$$

where K, D_m and σ would depend on yield, wind speed and wind shear.

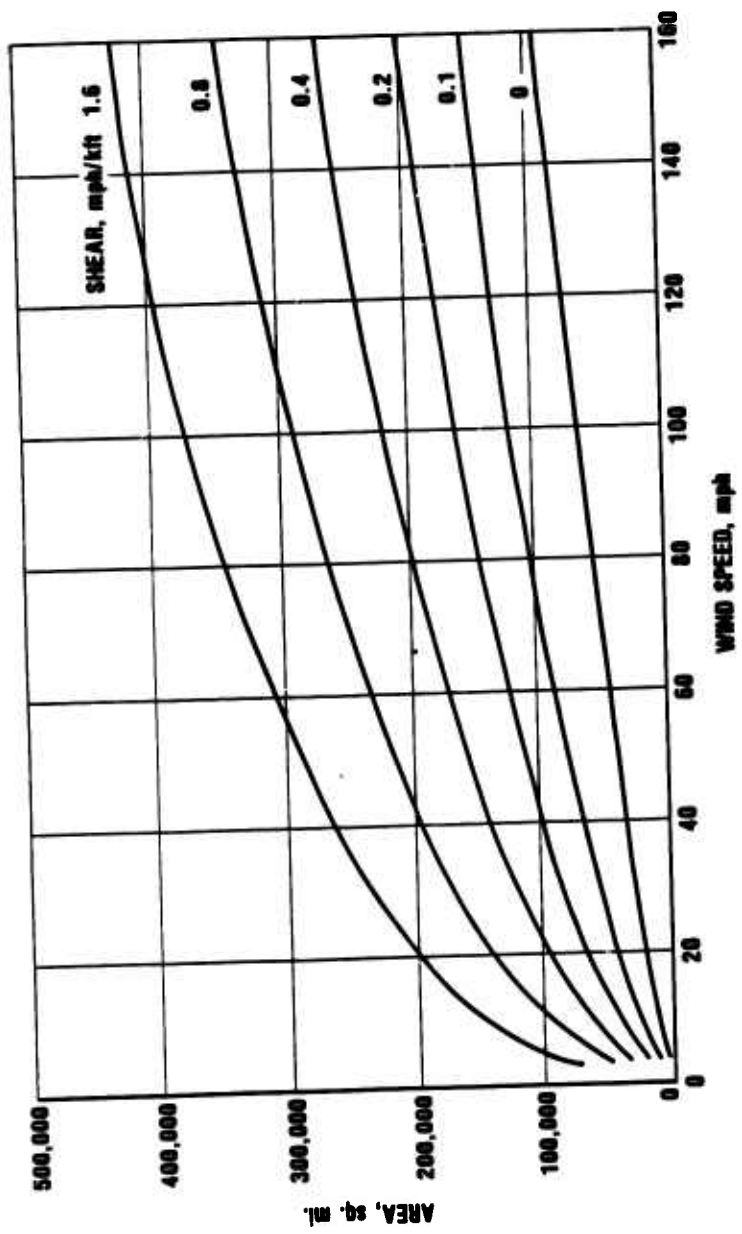
In order to illustrate the variations of area with wind speed and shear, a set of figures are presented giving area covered as a function of wind speed for different shears, all at constant dose levels. The dose levels are 1, 3, 10, 30, 100, 300, 1000 and 3000 Roentgens. In Figures II-5a to II-5h these areas are presented for a 1 megaton weapon with a fission fraction of one. As will be seen later in the report, the maximum value of wind speed and shear for the 12 winds considered are 118 mph and 0.67 mph/kilofoot. For purposes of illustration of the trends, values in these figures are carried beyond the extreme values.

As is evident in the figures, at low dose levels the area covered increases with both increasing wind and increasing shear. This is to be expected since higher winds will blow particles farther downwind during their settling time, and



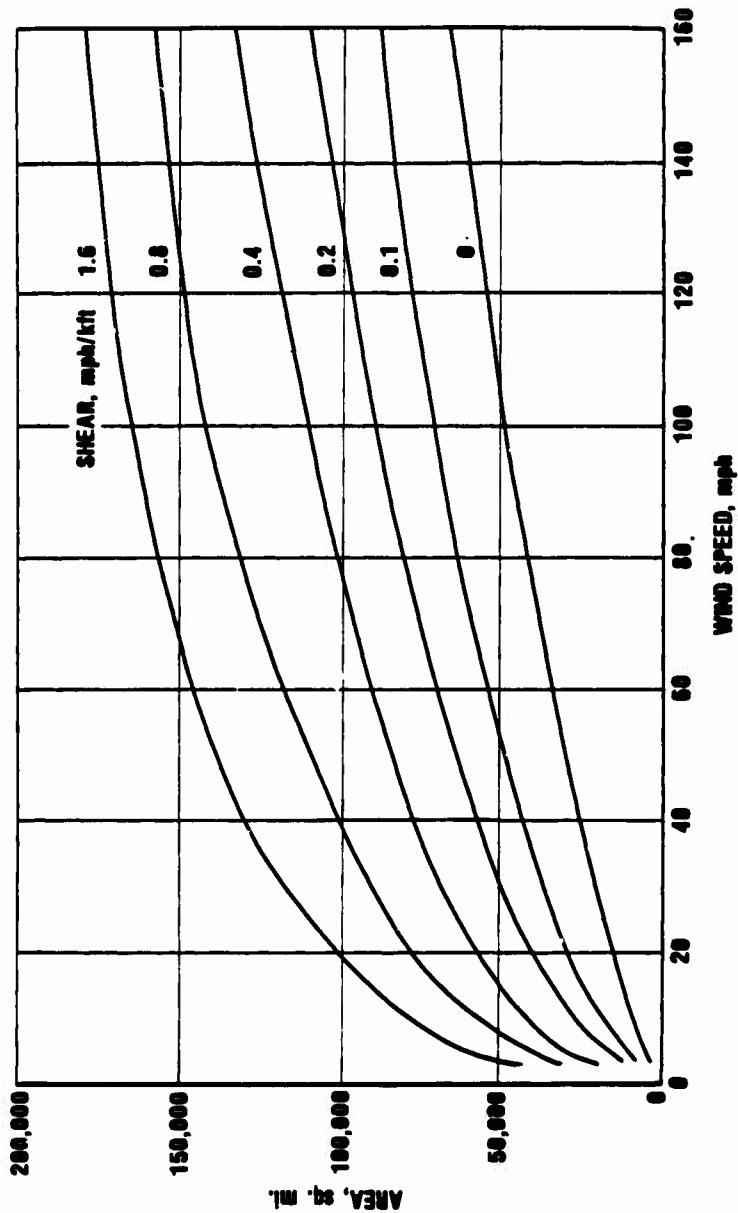
4-7-81-50

Figure II-4. AREA COVERED TIMES DOSE AS A FUNCTION OF DOSE FOR A 1 MT YIELD WITH A 40 MPH WIND AND VARIOUS SHEARS.



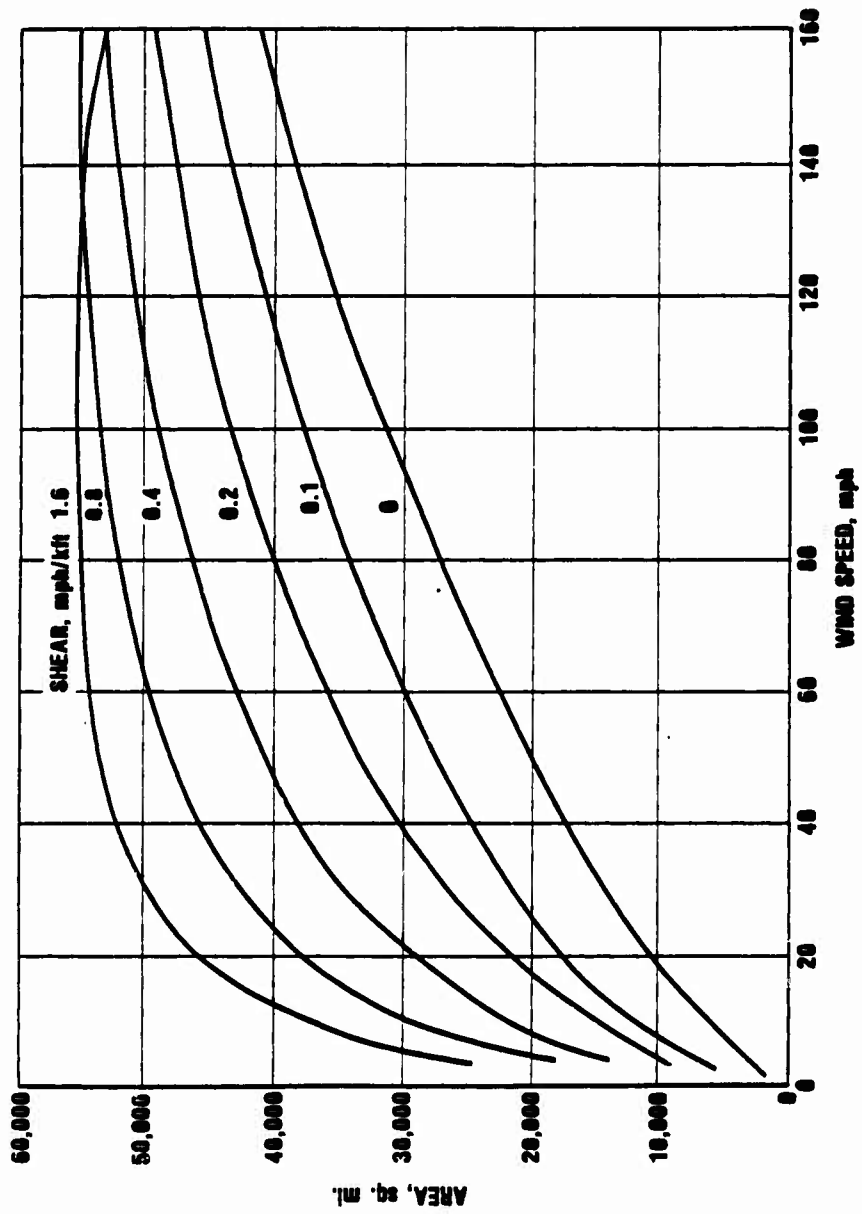
4-7-61-87

Figure II-5a. AREA COVERED AS A FUNCTION OF WIND SPEED AT A DOSE OF 1 ROENTGEN FOR A 1 MT YIELD AND VARIOUS SHEARS.



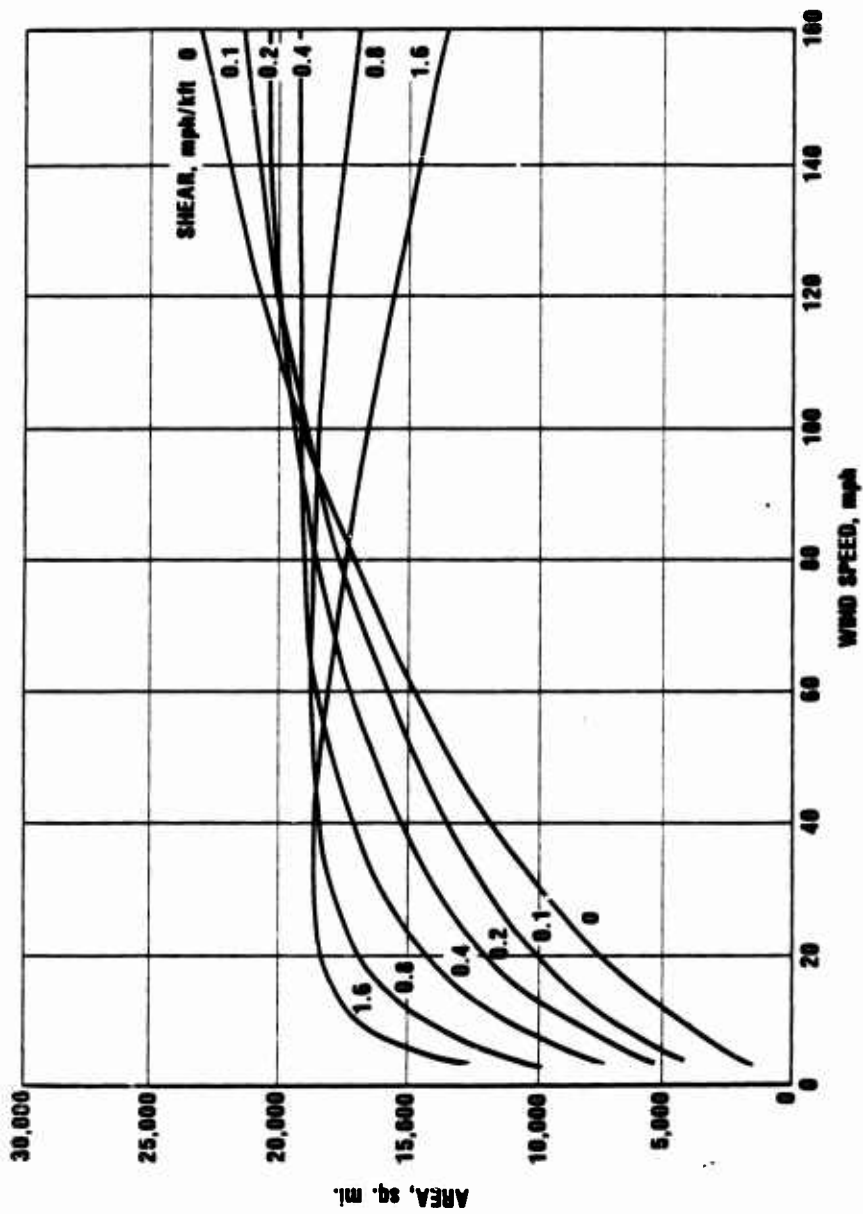
4-7-51-52

Figure II-5b. AREA COVERED AS A FUNCTION OF WIND SPEED AT A DOSE OF 3 ROENTGENS FOR A 1 MT YIELD AND VARIOUS SHEARS.



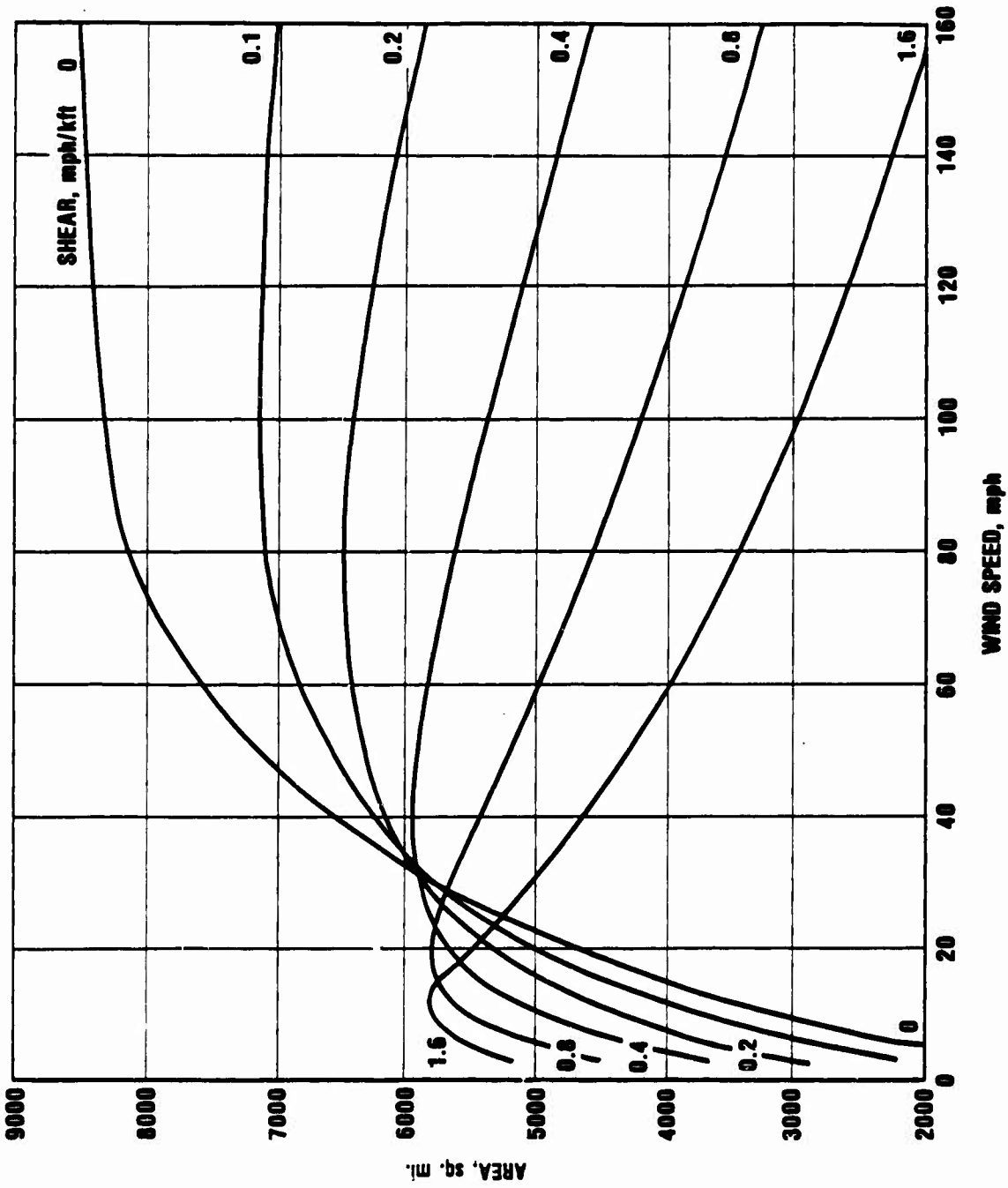
4-7-81-80

Figure II-5c. AREA COVERED AS A FUNCTION OF WIND SPEED AT A DOSE OF 10 ROENTGENS FOR A 1 MT YIELD AND VARIOUS SHEARS.



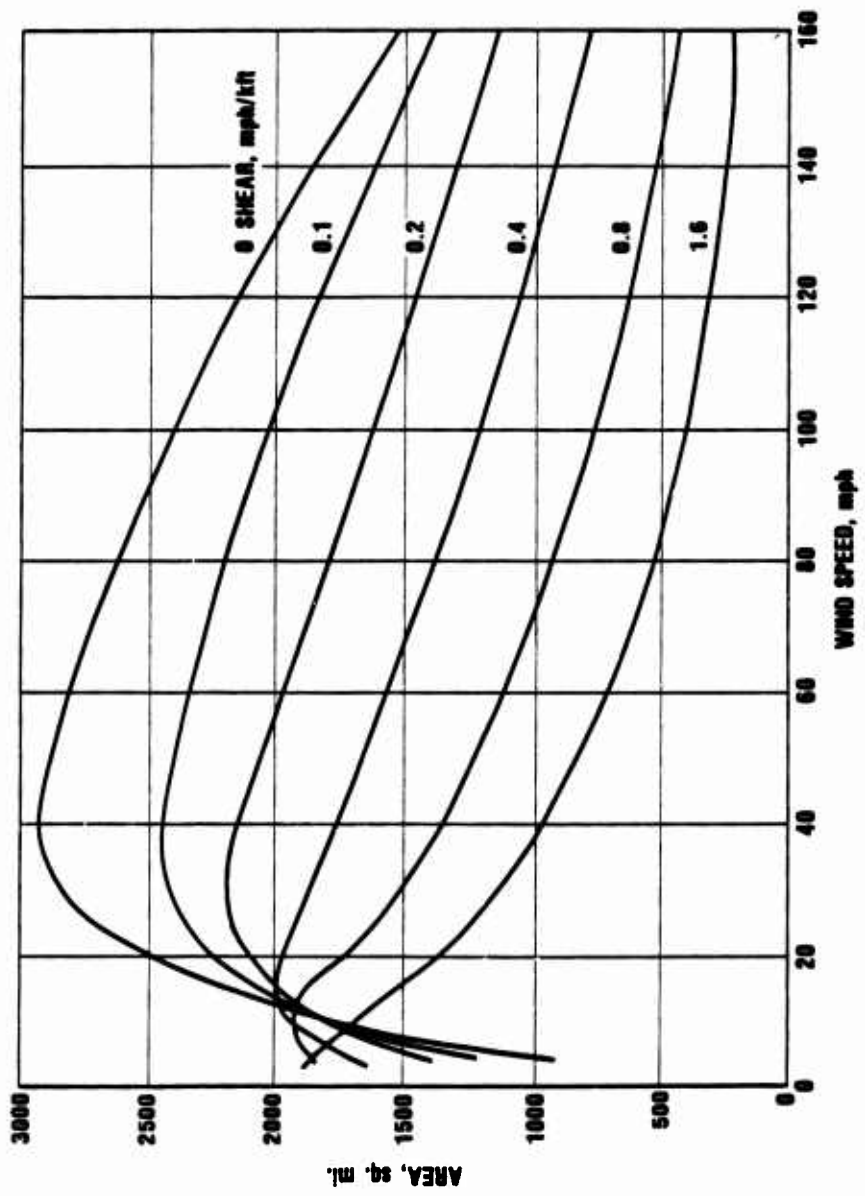
4-7-61-90

Figure II-5d. AREA COVERED AS A FUNCTION OF WIND SPEED AT A DOSE OF 30 ROENTGENS FOR A 1 MT YIELD AND VARIOUS SHEARS.



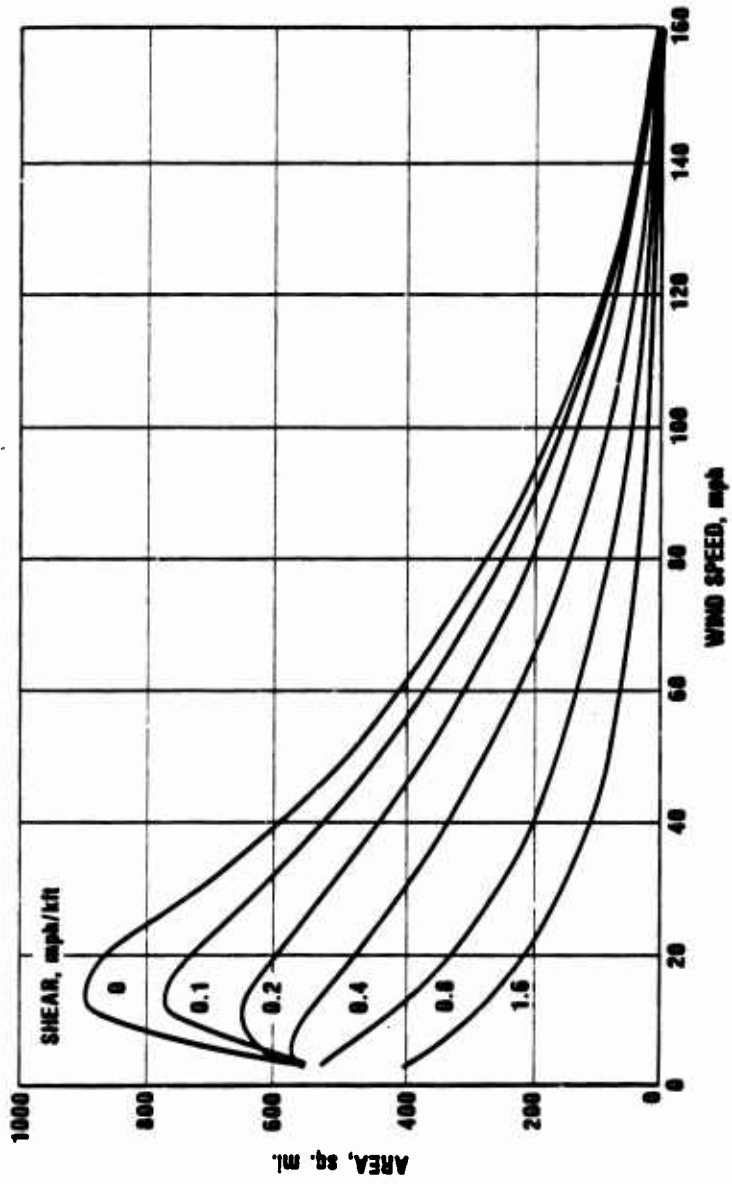
4-7-51-01

Figure II-5e. AREA COVERED AS A FUNCTION OF WIND SPEED AT A DOSE OF 100 ROENTGENS FOR A 1 MT YIELD AND VARIOUS SHEARS.



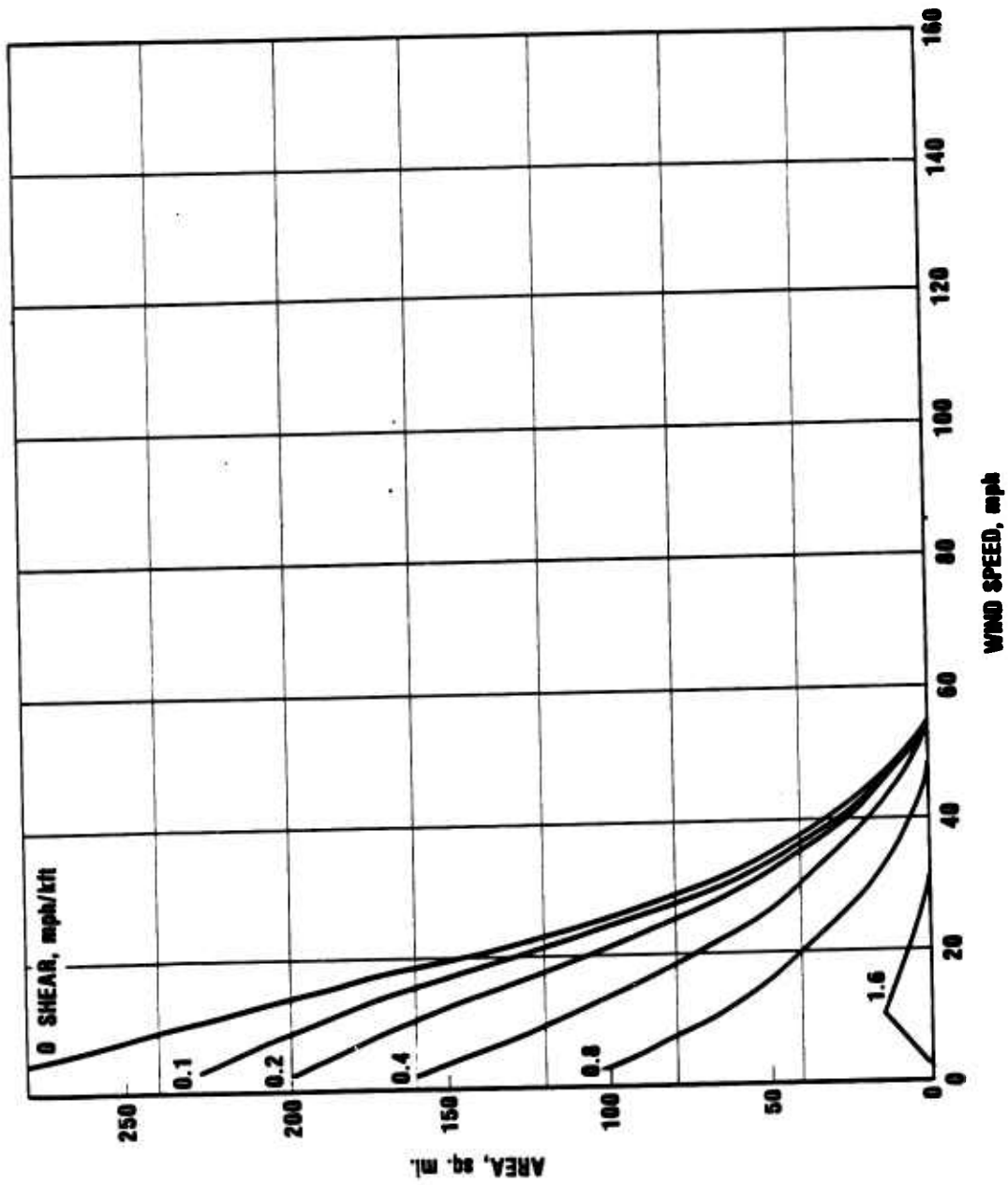
4-7-61-02

Figure II-5f. AREA COVERED AS A FUNCTION OF WIND SPEED AT A DOSE LEVEL OF 300 ROENTGENS FOR A .1 MT YIELD AND VARIOUS SHEARS.



4-7-61-63

Figure II-5g. AREA COVERED AS A FUNCTION OF WIND SPEED AT A DOSE OF 1000 ROENTGENS FOR A 1 MT YIELD AND VARIOUS SHEARS.



4-7-51-54

Figure II-5h. AREA COVERED AS A FUNCTION OF WIND SPEED AT A DOSE OF 3000 ROENTGENS FOR A 1 MT YIELD AND VARIOUS SHEARS.

higher shear will spread the pattern further crosswind. Since the total amount of radioactivity is constant, it is to be expected that this spreading at low dose levels will be achieved at the expense of the area covered at higher dose levels. Again, an inspection of the figures (e.g. Figure III-5g) shows this to be the case (except at very low wind speeds) where either increasing wind speed or shear decreases the area covered. At very low wind speeds, an increasing wind speed will transport the entire pattern further downwind and overcome the loss to lower dose levels.

At intermediate dose levels, a transition occurs between the characteristic patterns seen at low and at high dose levels. Here the curves increase, decrease the cross each other in a rather complicated fashion. As was seen on Figure II-3 for an 80 mph wind, the curves for all different shear values cross near a dose of about 37 Roentgens. This is reflected in Figure II-5d for 30 Roentgens where at 80 mph the areas for a variety of different shear levels are all nearly the same. In fact, in Figure II-5d it can be seen that for a considerable range in wind speeds, the areas are rather close in value for all shears.

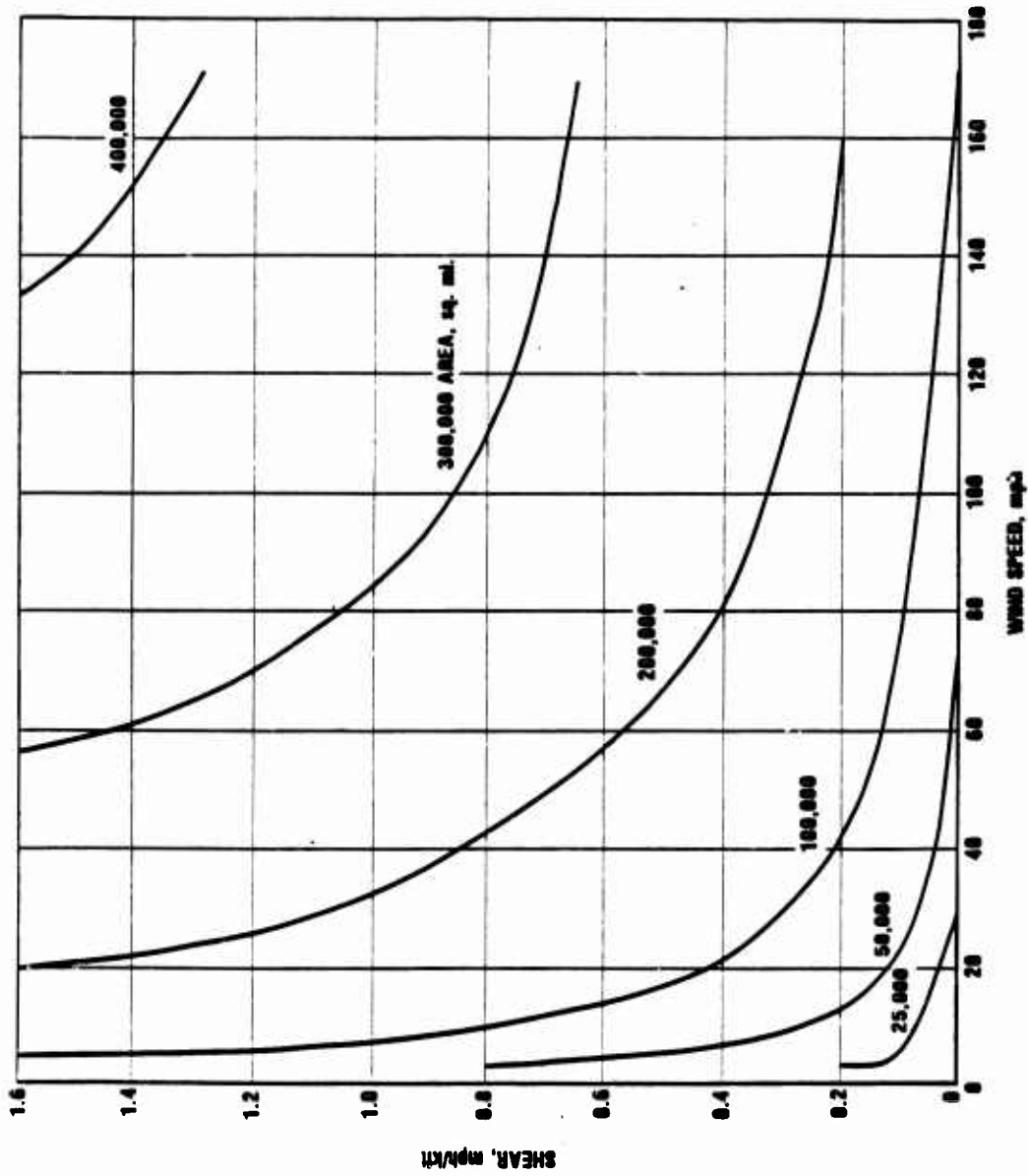
Another way to exhibit the variation of area covered is to plot contours of constant area as functions of wind speed and wind shear. This is done in Figures II-6a through II-6h for dose levels of 1, 3, 10, 30, 100, 300, 1000 and 3000 Roentgens. The tendency shown in the previous figures for area covered at low dose levels to increase with both increasing wind speed and shear is reflected in Figure 6a where, for example, the contours of constant area have their lowest values near the origin, and increase as the distance from the origin is increased. In fact the curves are approximately hyperbolic which indicates that, for a constant product of wind speed times shear, the area is constant. At high dose

levels (see for example Figure II-5h) the tendency is reversed, which is reflected in Figure II-6h by the higher value contours to be near the origin.

At intermediate dose levels both tendencies are reflected. For example, in Figure II-6e for a dose of 100 Roentgens, a ridge of high area in the center of the figure slopes down to lower areas in two directions, both toward the origin and in the opposite direction. As can be seen from inspection of the figures, as the dose increases, the high area ridge moves closer and closer to the origin. Thus, where for typical shear values the ridge is at very high wind speeds at 100 Roentgens, at 300 Roentgens the ridge is located at typical wind speeds.

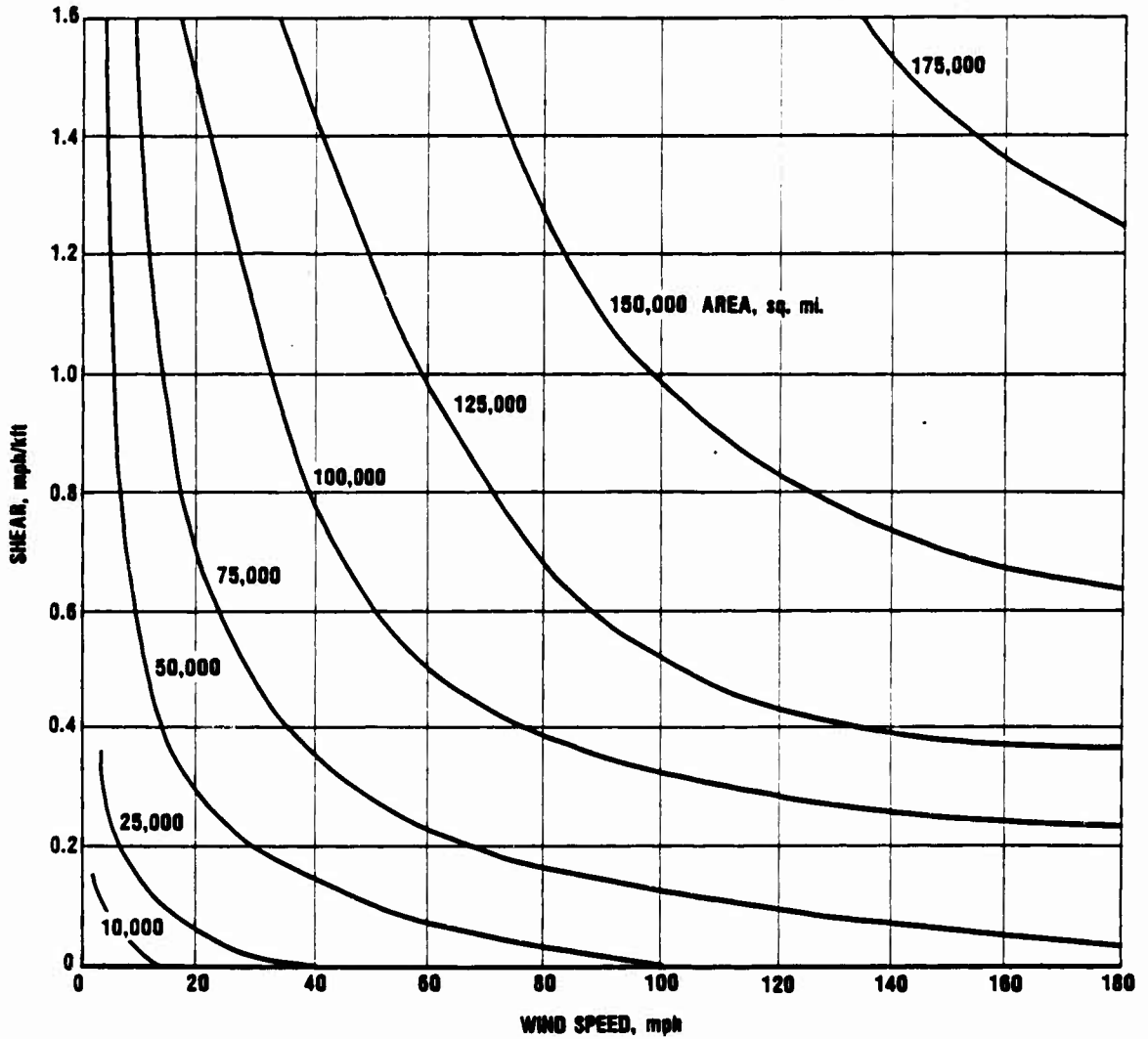
At higher weapon yields larger areas are covered. However, as mentioned before, if the dose level is divided by the yield, comparable area coverages might be expected, at least in the restricted range of yields covered from 1 to 20 MT. Thus a 20 Roentgen contour for a 20 megaton weapon should compare with a 1 Roentgen contour for a 1 megaton weapon with a fission fraction of one. An alternative way of achieving the same effect is to lower the weapon fission fraction. If the fission fraction is divided by the weapon yield, then the total amount of fission materials produced is the same as for a standard 1 megaton weapon and comparable area coverage might be expected. Thus, a 1 Roentgen contour for a 20 megaton weapon with a fission fraction of 0.05 should compare with a 1 Roentgen contour for a 1 megaton weapon with a fission fraction of one.

The following series of figures are for a 20 megaton weapon with a fission fraction of 0.05. Figures II-7 and II-8 show the area covered for a 20 mph wind and a 80 mph wind for a 20 megaton weapon with a fission fraction of 0.05. They are comparable to Figures II-2 and II-3 for a 1 megaton weapon. As can be seen, with a 20 megaton weapon the areas



4-7-61-66

Figure II-6a. CONTOURS OF CONSTANT AREA COVERED AT A DOSE OF 1 ROENTGENS AS A FUNCTION OF WIND SPEED AND SHEAR FOR A 1 MT YIELD.



4-7-81-00

Figure II-6b. CONTOURS OF CONSTANT AREA COVERED AT A DOSE OF 3 ROENTGENS AS A FUNCTION OF WIND SPEED AND SHEAR FOR A 1 MT YIELD.

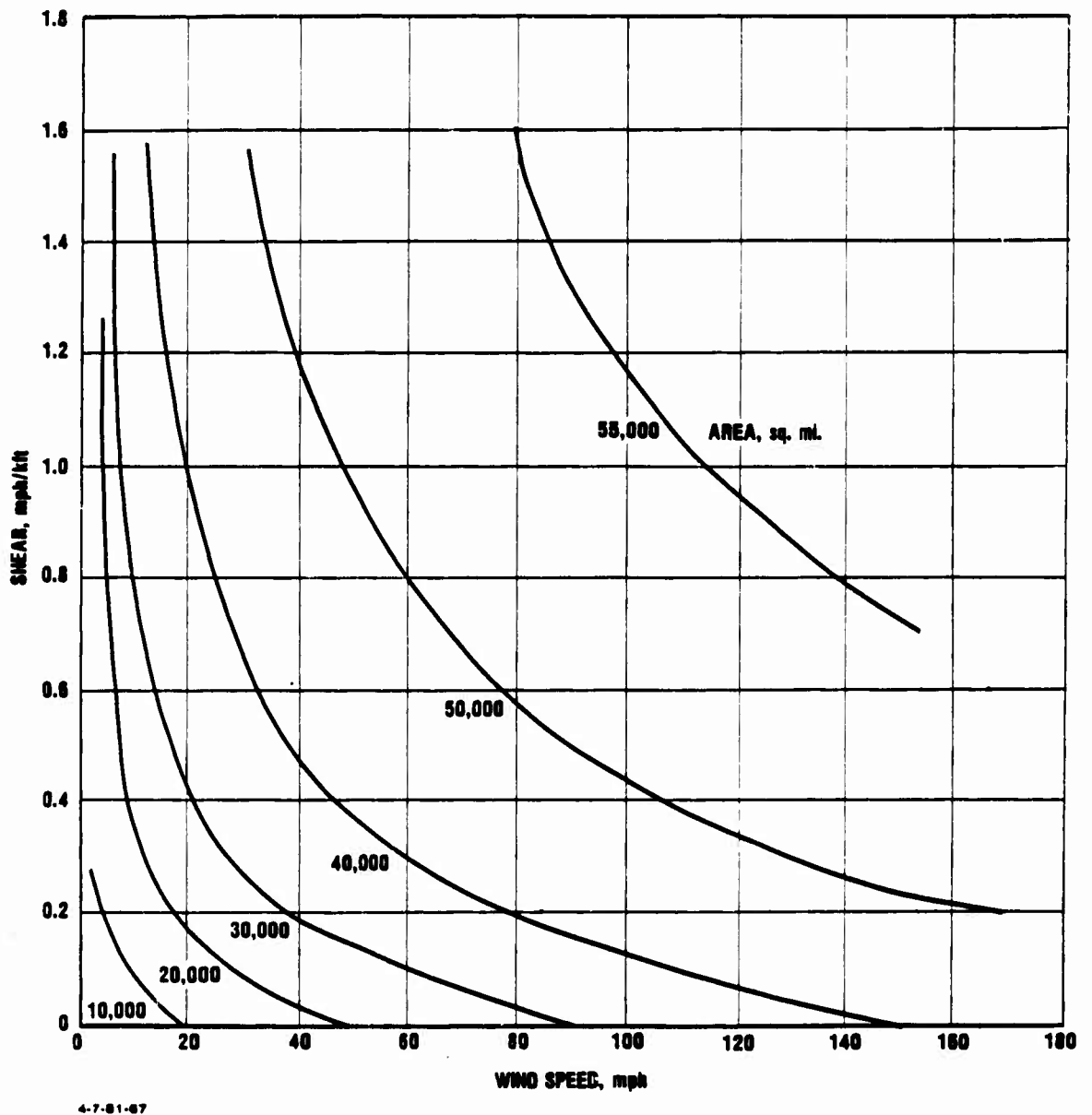
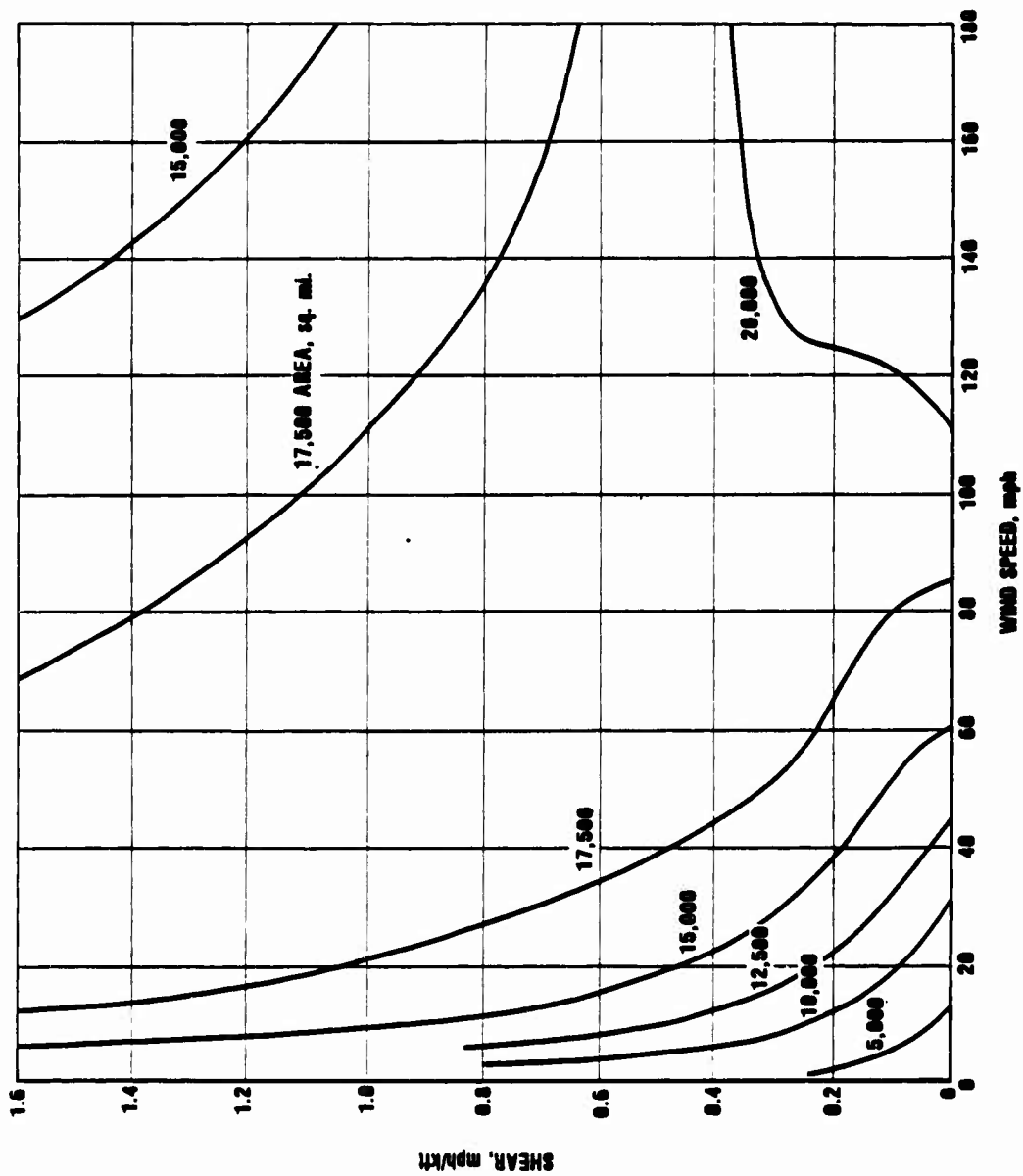


Figure II-6c. CONTOURS OF CONSTANT AREA COVERED AT A DOSE OF 10 ROENTGENS AS A FUNCTION OF WIND SPEED AND SHEAR FOR A 1 MT YIELD.



4-7-61-66

Figure II-6d. CONTOURS OF CONSTANT AREA COVERED AT A DOSE OF 30 ROENTGENS AS A FUNCTION OF WIND SPEED AND SHEAR FOR A 1 MT YIELD.

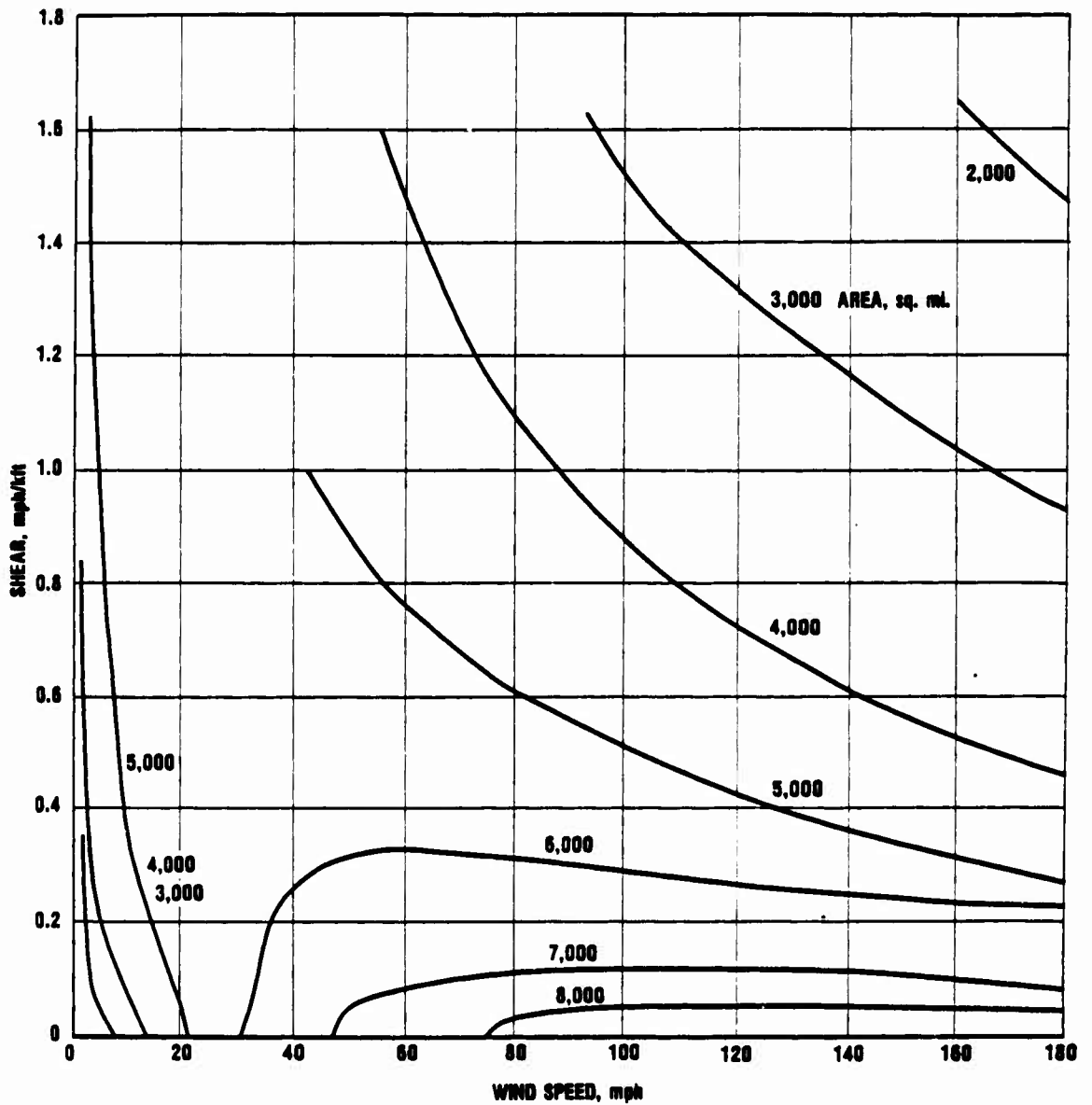
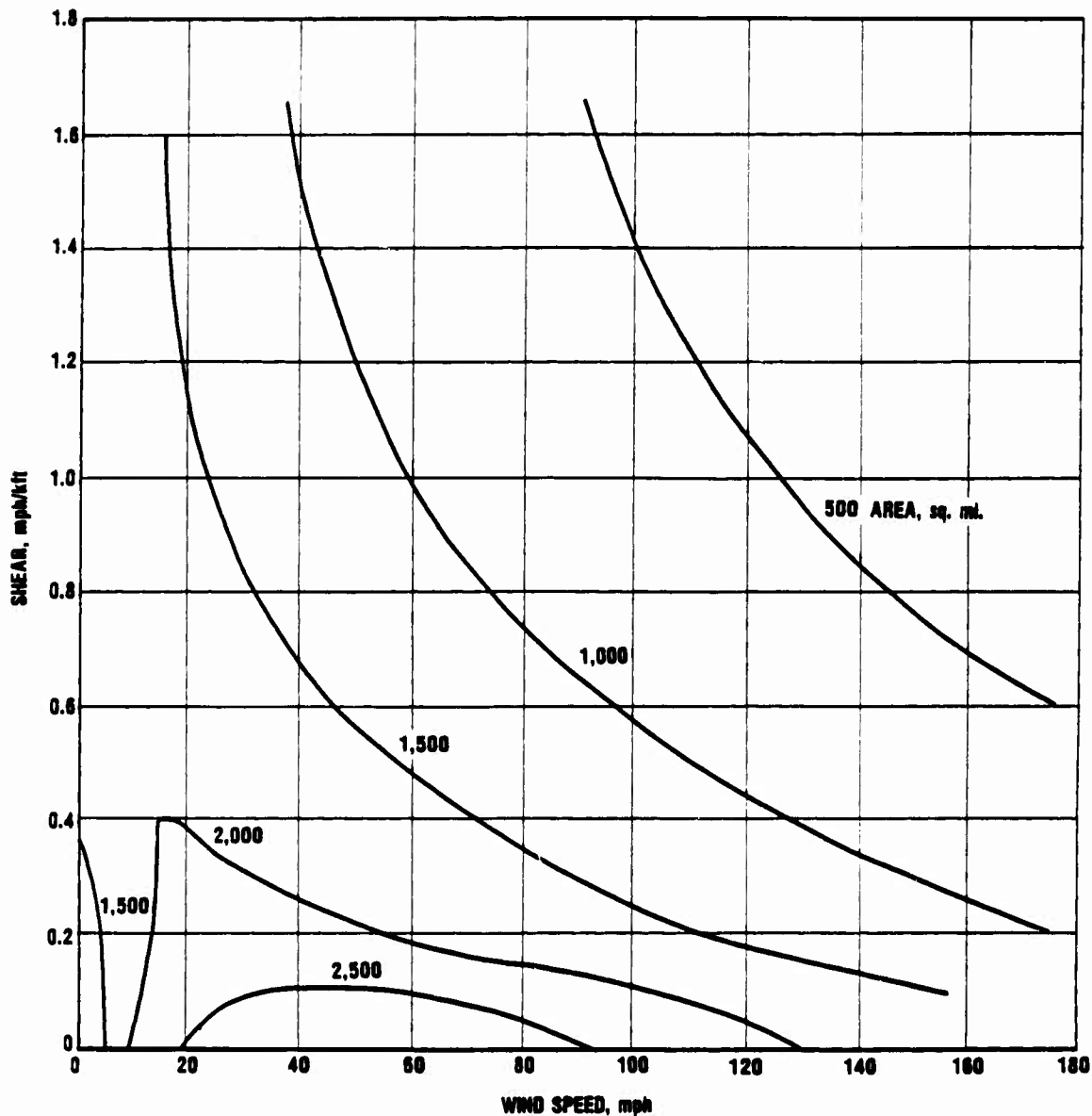
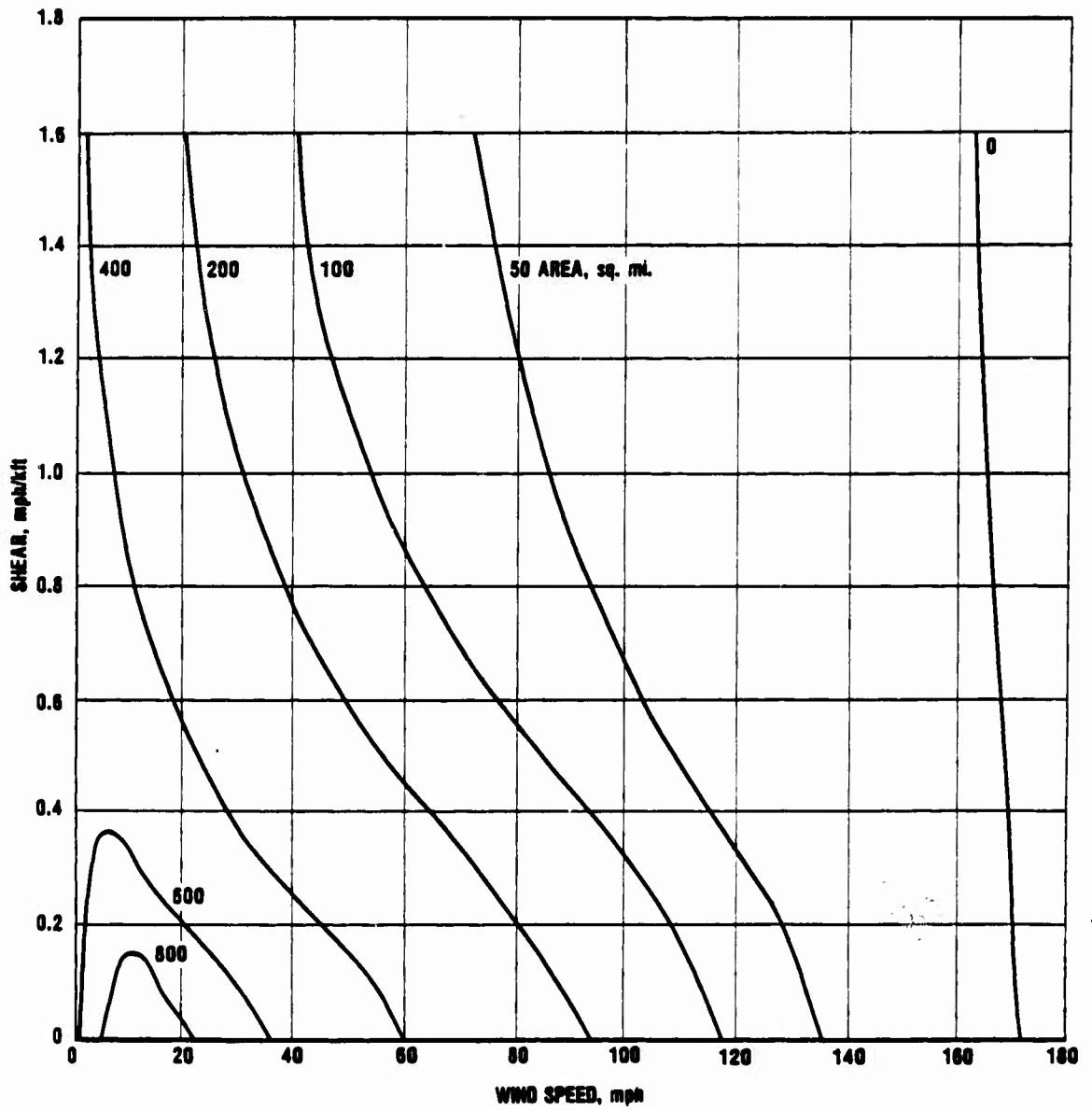


Figure II-6e. CONTOURS OF CONSTANT AREA COVERED AT A DOSE OF 100 ROENTGENS AS A FUNCTION OF WIND SPEED AND SHEAR FOR A 1 MT YIELD.



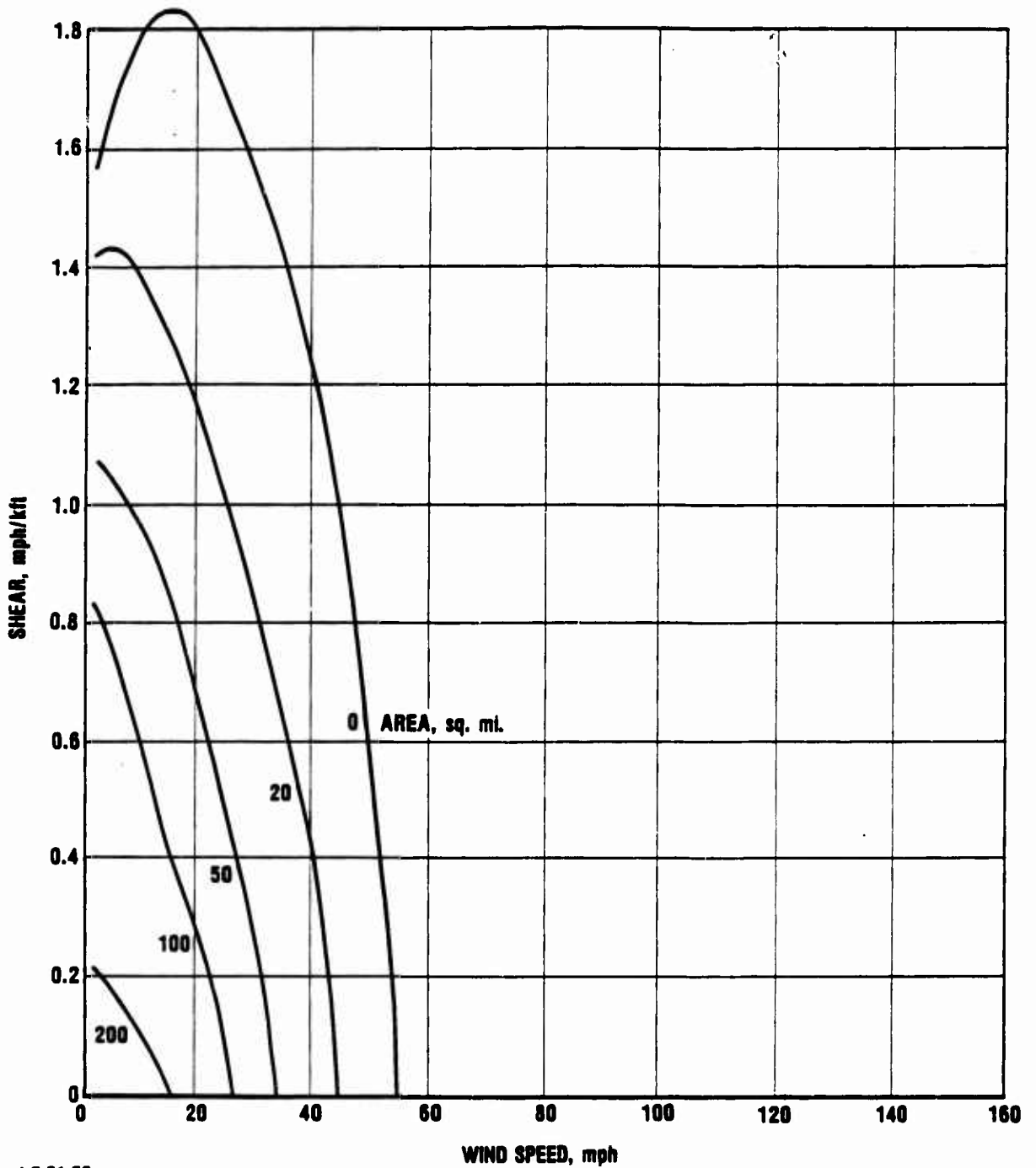
4-7-81-70

Figure II-6f. CONTOURS OF CONSTANT AREA COVERED AT A DOSE OF 300 ROENTGENS AS A FUNCTION OF WIND SPEED AND SHEAR FOR A 1 MT YIELD.



4-7-61-71

Figure II-6g. CONTOURS OF CONSTANT AREA COVERED AT A DOSE OF 1000 ROENTGENS AS A FUNCTION OF WIND SPEED AND SHEAR FOR A 1 MT YIELD.



4-7-81-72

Figure II-6h. CONTOURS OF CONSTANT AREA COVERED AT A DOSE OF 3000 ROENTGENS AS A FUNCTION OF WIND SPEED AND SHEAR FOR A 1 MT YIELD.

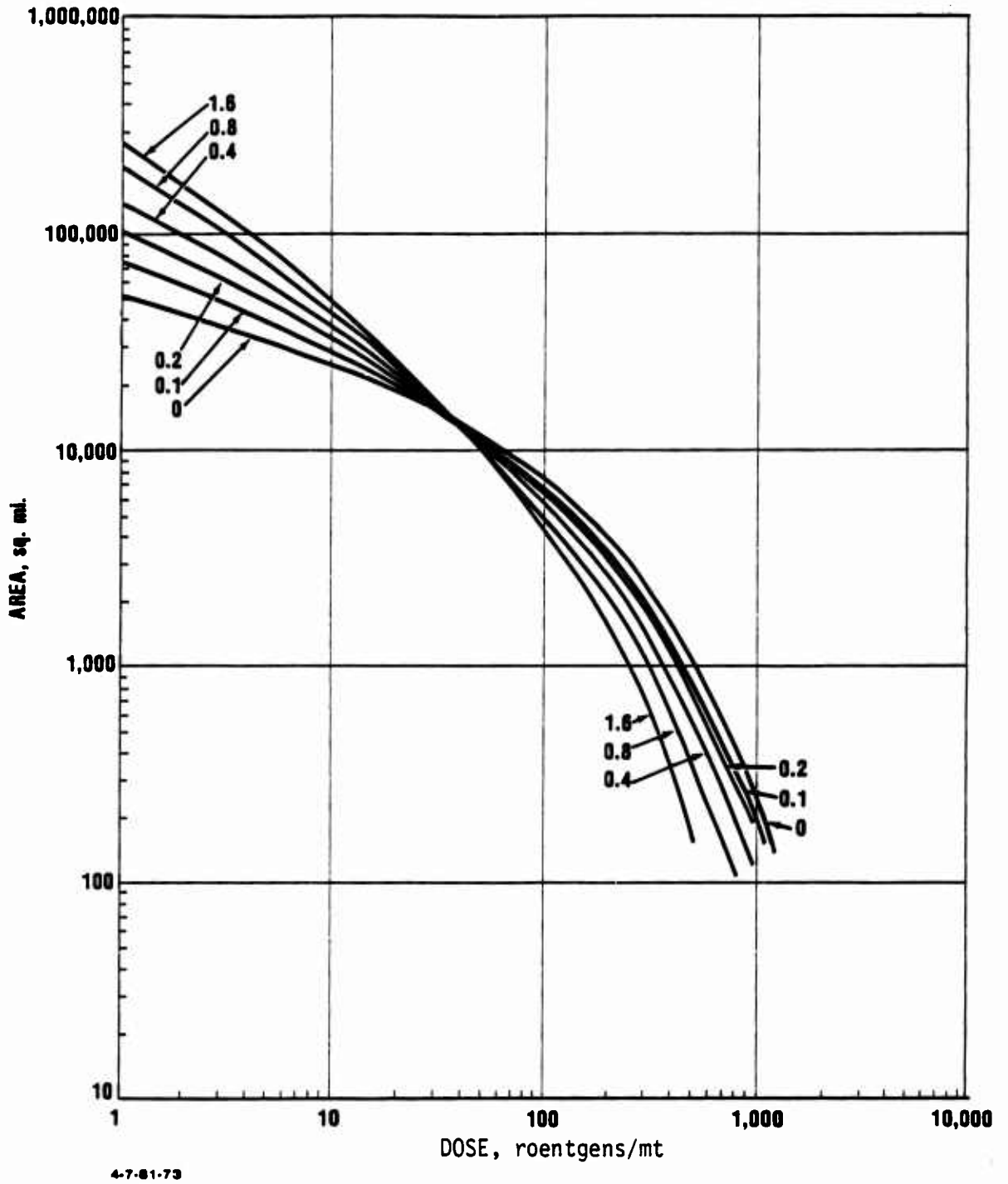


Figure II-7. AREA COVERED AS A FUNCTION OF DOSE/MT FOR A 20 MT YIELD WITH A 20 MPH WIND FOR VARIOUS SHEARS.

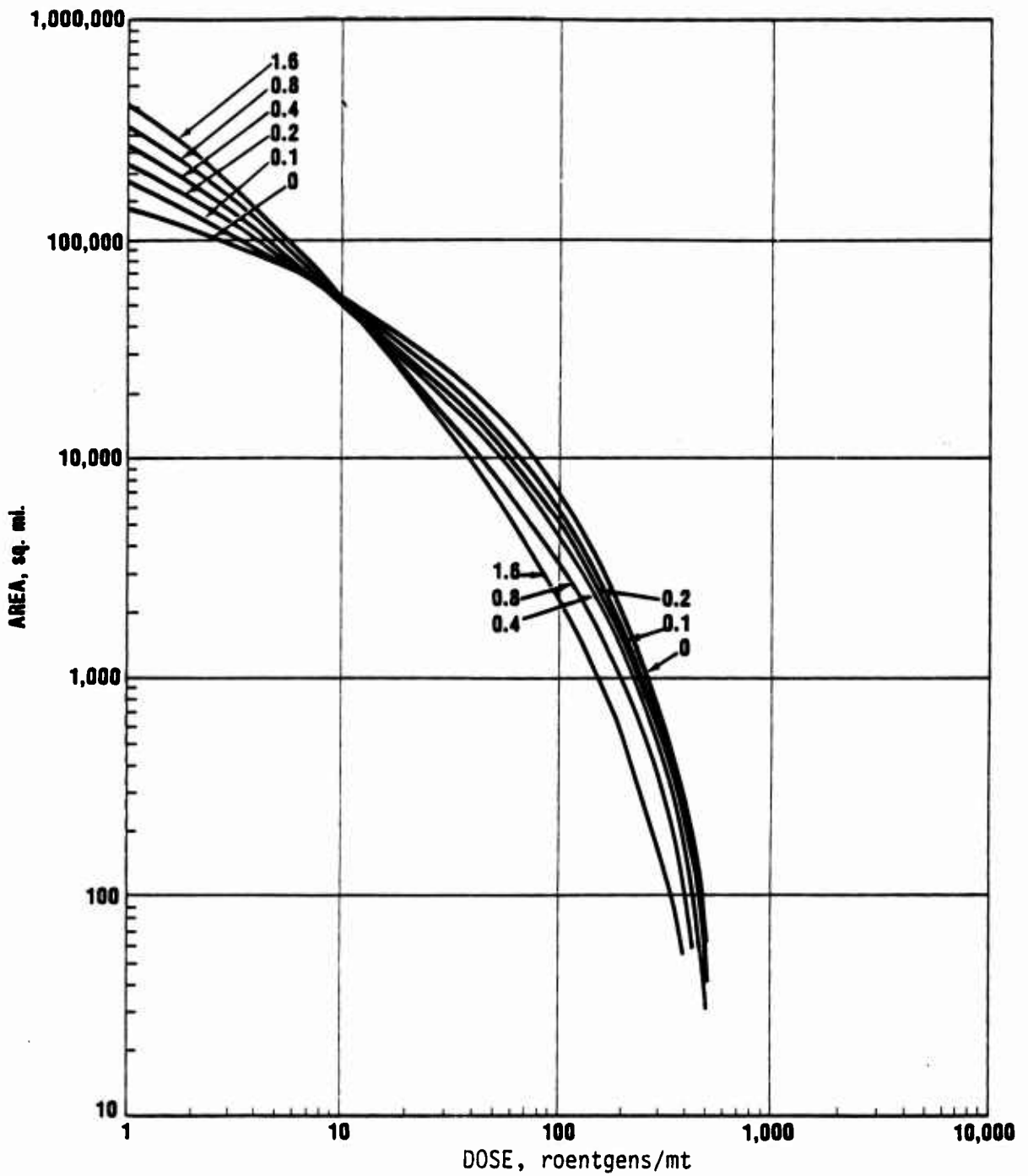


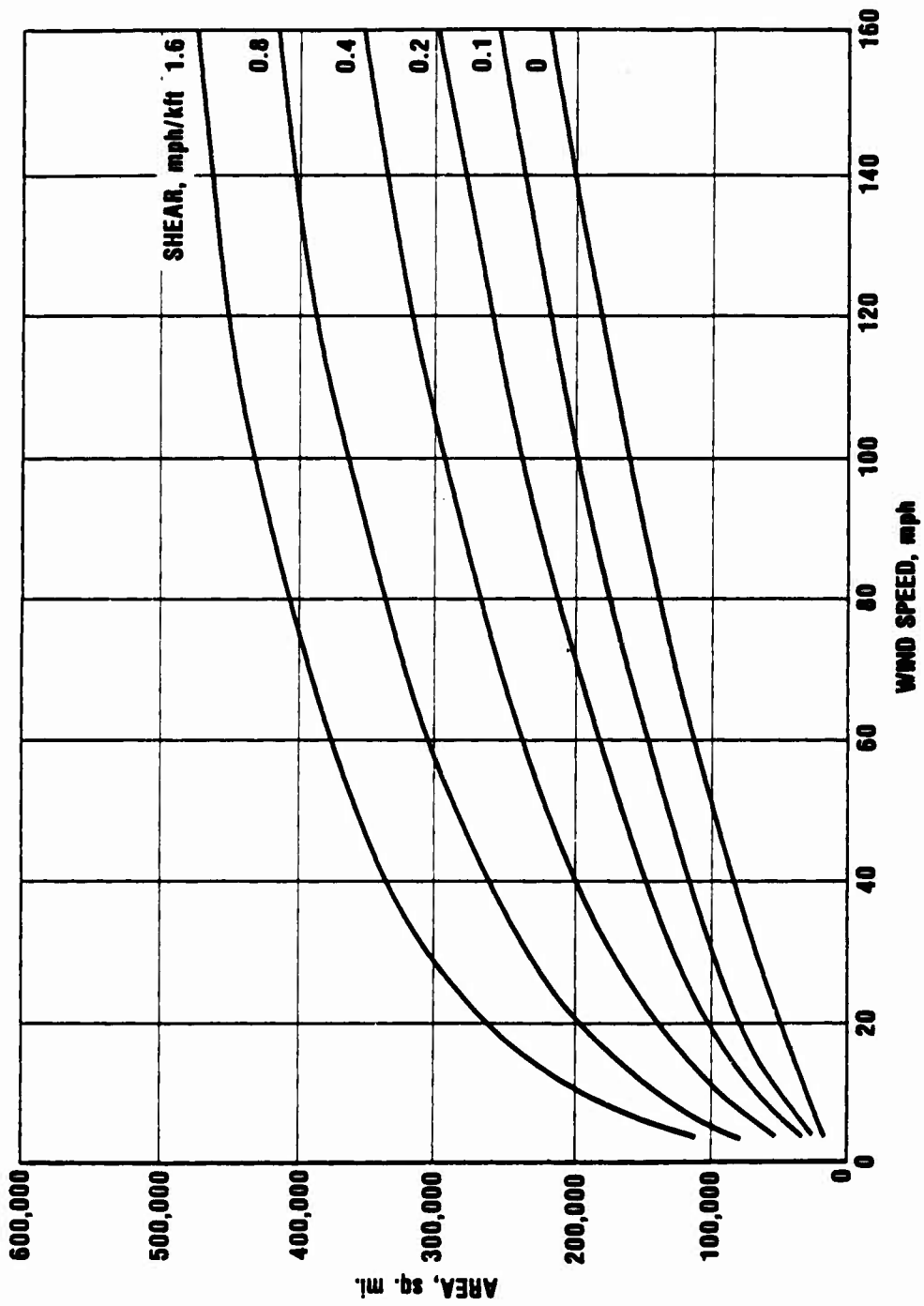
Figure II-8. AREA COVERED AS A FUNCTION OF DOSE/MT FOR A 20 MT YIELD WITH A 80 MPH WIND FOR VARIOUS SHEARS.

are comparable, or slightly higher at low dose levels, but somewhat lower at high dose levels.¹ (Recall, however, a 1000 Roentgen dose level on these figures is actually a 20,000 Roentgen level.) Moreover, the point of crossing for curves with various shears is at a lower dose level for 20 megaton weapons. Thus the crossing at 20 mph goes from about 130 Roentgens for 1 megaton to about 30 Roentgens at 20 megaton, at for an 80 mph wind from about 30 Roentgens to 10 Roentgens.

Two primary mechanisms occur to cause a difference in the shape of the 1 megaton and 20 megaton curves. The first is the higher cloud rise for a 20 megaton weapon which will tend to transport radioactive material further downwind, thus enhancing lower dose level contours for higher yields. The second factor is due to the ratio of WSEG biological yield to H+1 hour dose rate which is lower for higher yield weapons due to the longer fall time for radioactive particles. The structure of the model demands that the integrated area covered by H+1 hour dose rate contour is the same for all yields. However, for biological doses, the lower values of the biological dose to H+1 hour dose rate ratio implies the integrated area is lower. Thus, if the 1 megaton and 20 megaton weapons have comparable areas at low dose levels, the 20 megaton weapons must be lower in area at high dose levels.

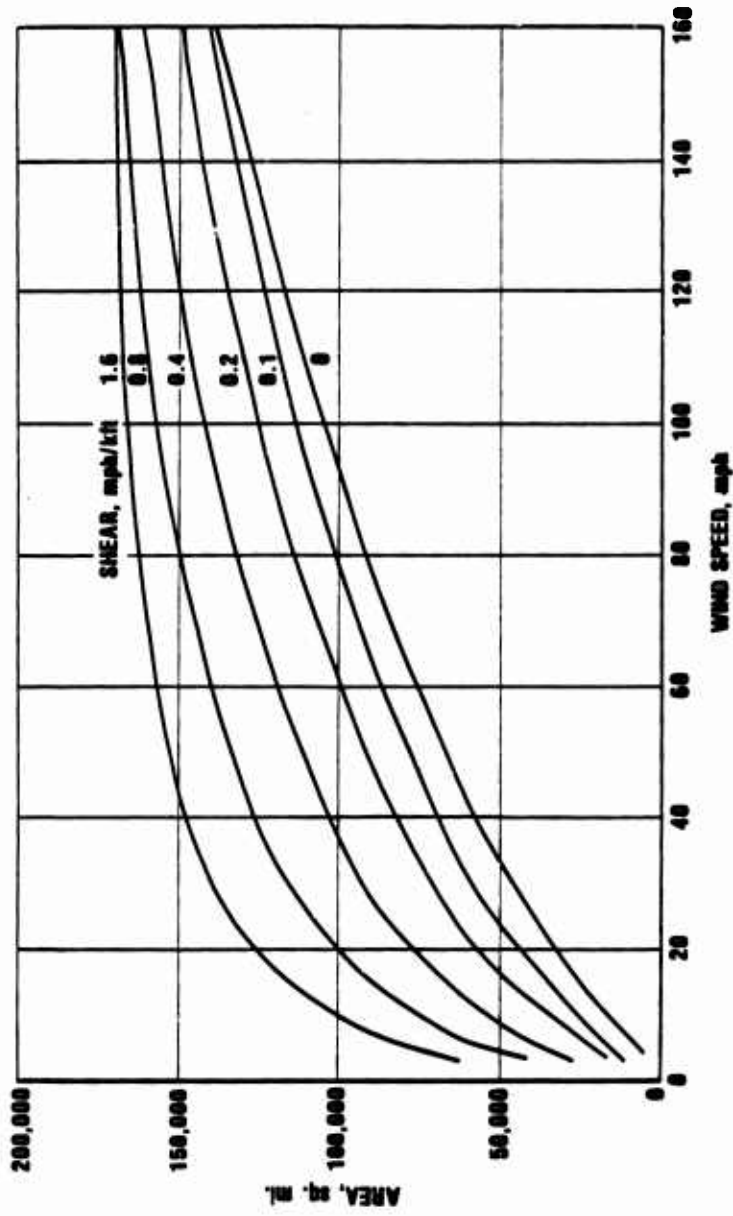
Areas covered as a function of wind speed for various shears are shown in Figures II-9a through g for dose levels of 1, 3, 10, 30, 100, 300 and 1000 Roentgens/MT. The same general behavior is seen as for 1 megaton as presented in Figures II-5. The smaller areas for the 20 megaton weapons at high dose levels are reflected in this set of curves by the transitions from one pattern to another occurring at lower dose levels for the 20 megaton weapons than for the 1 megaton ones.

¹Again the reader is reminded that for weapons appreciably outside the yield range of 1 to 20 MT this approximate correspondence might not hold.



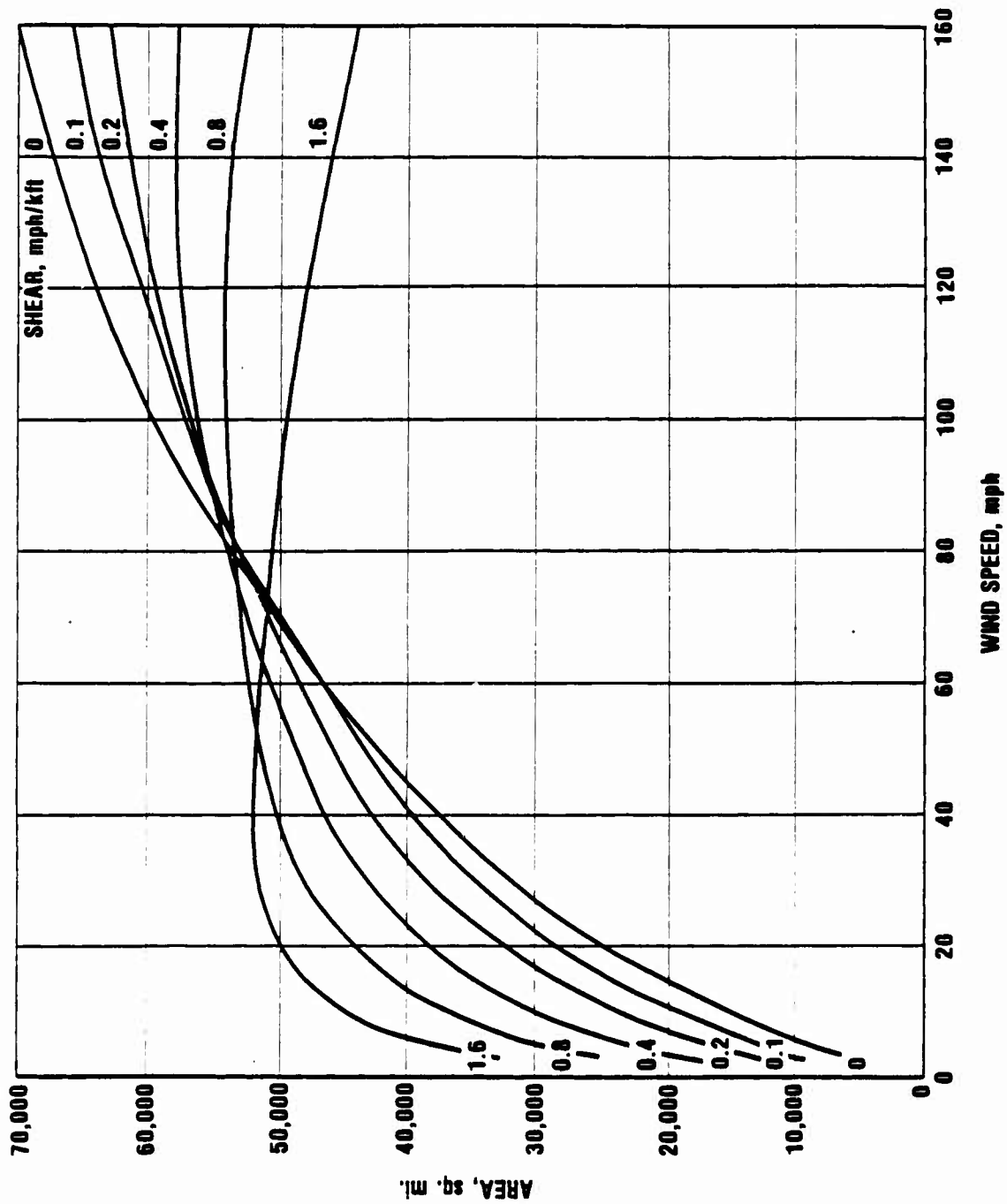
4-7-81. 76

Figure II-9a. AREA COVERED AS A FUNCTION OF WIND SPEED AT A DOSE LEVEL OF 1 ROENTGEN/MT FOR A 20 MT YIELD AND VARIOUS SHEARS.



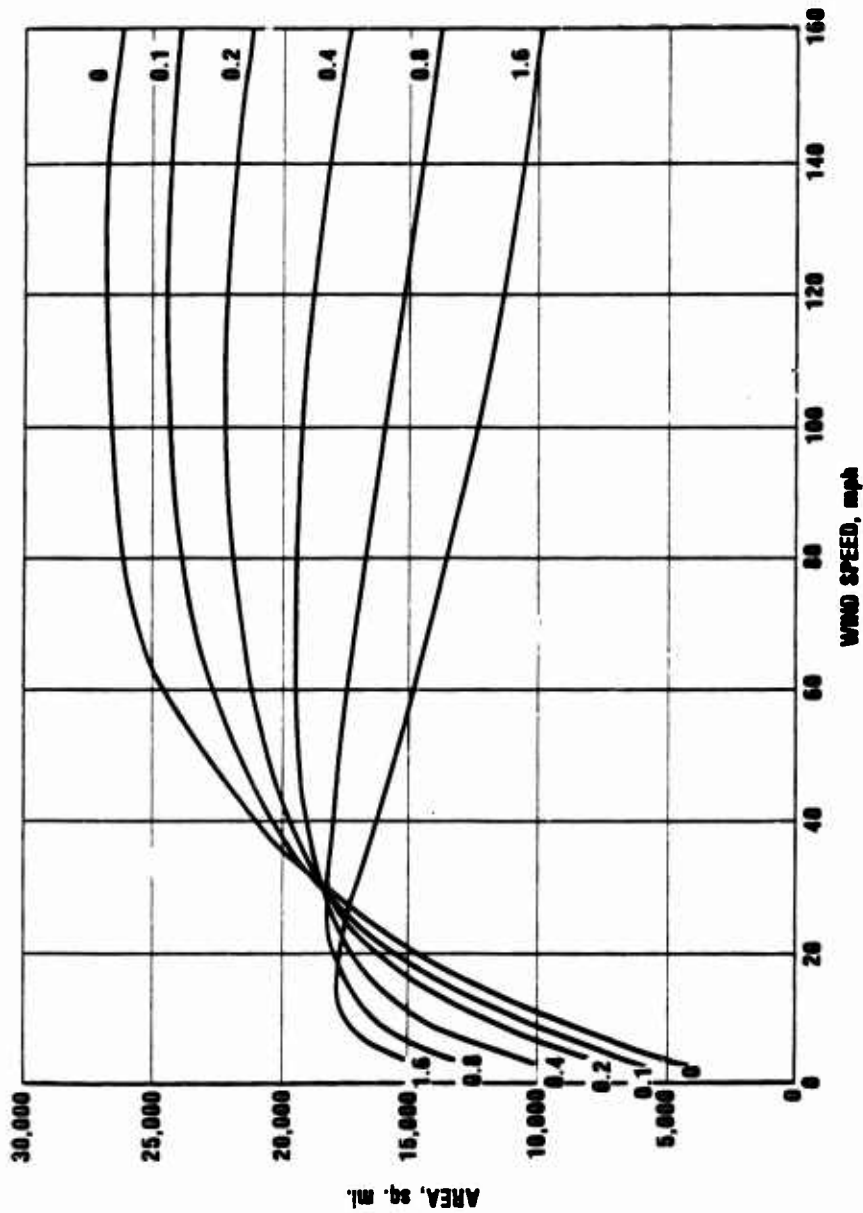
4-7-81-77

Figure II-9b. AREA COVERED AS A FUNCTION OF WIND SPEED AT A DOSE LEVEL OF 3 ROENTGENS/MT FOR A 20 MT YIELD AND VARIOUS SHEARS.



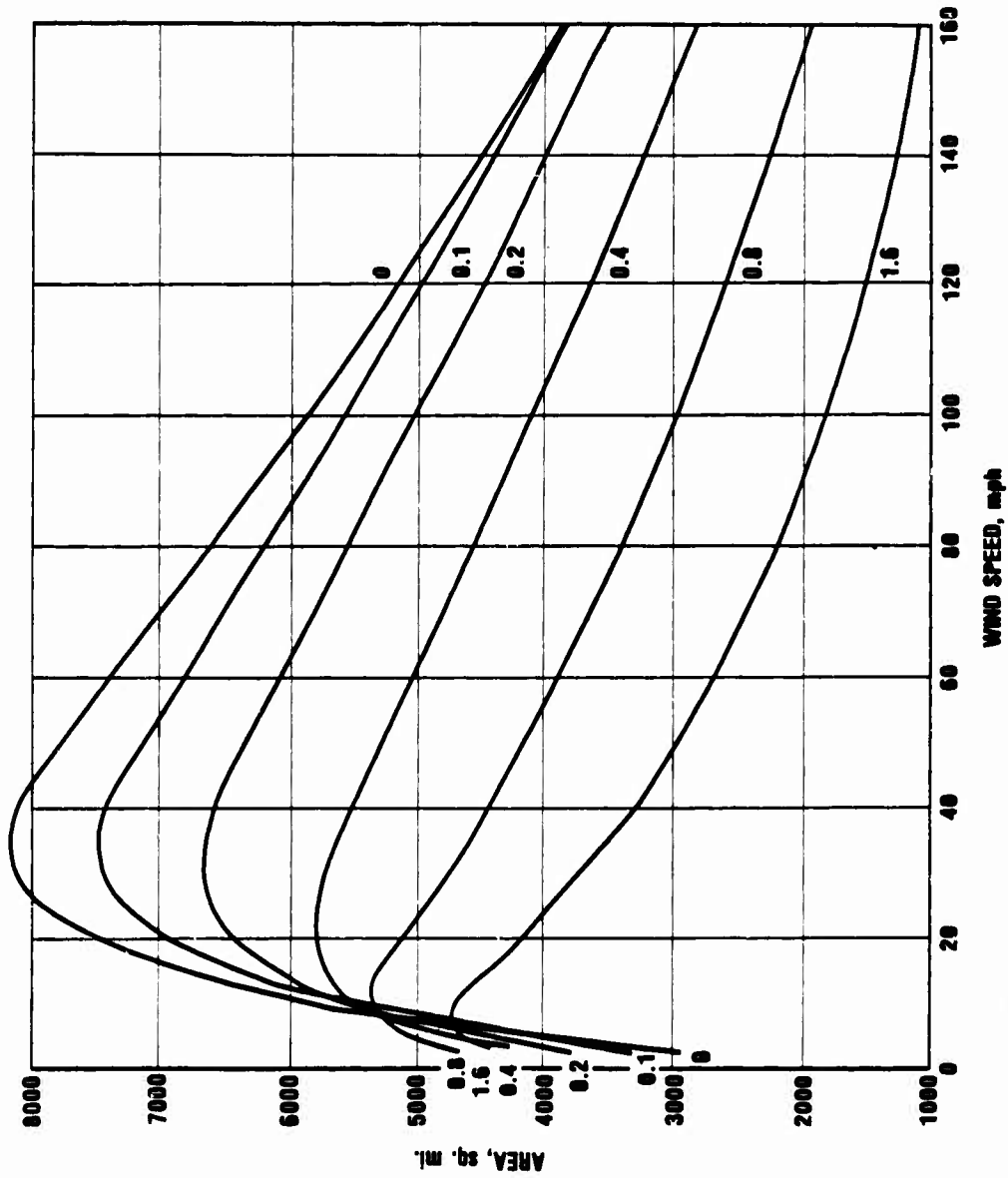
4-7-61-78

Figure 11-9c. AREA COVERED AS A FUNCTION OF WIND SPEED AT A DOSE LEVEL OF 10 ROENTGENS/MT FOR A 20 MT YIELD AND VARIOUS SHEARS.



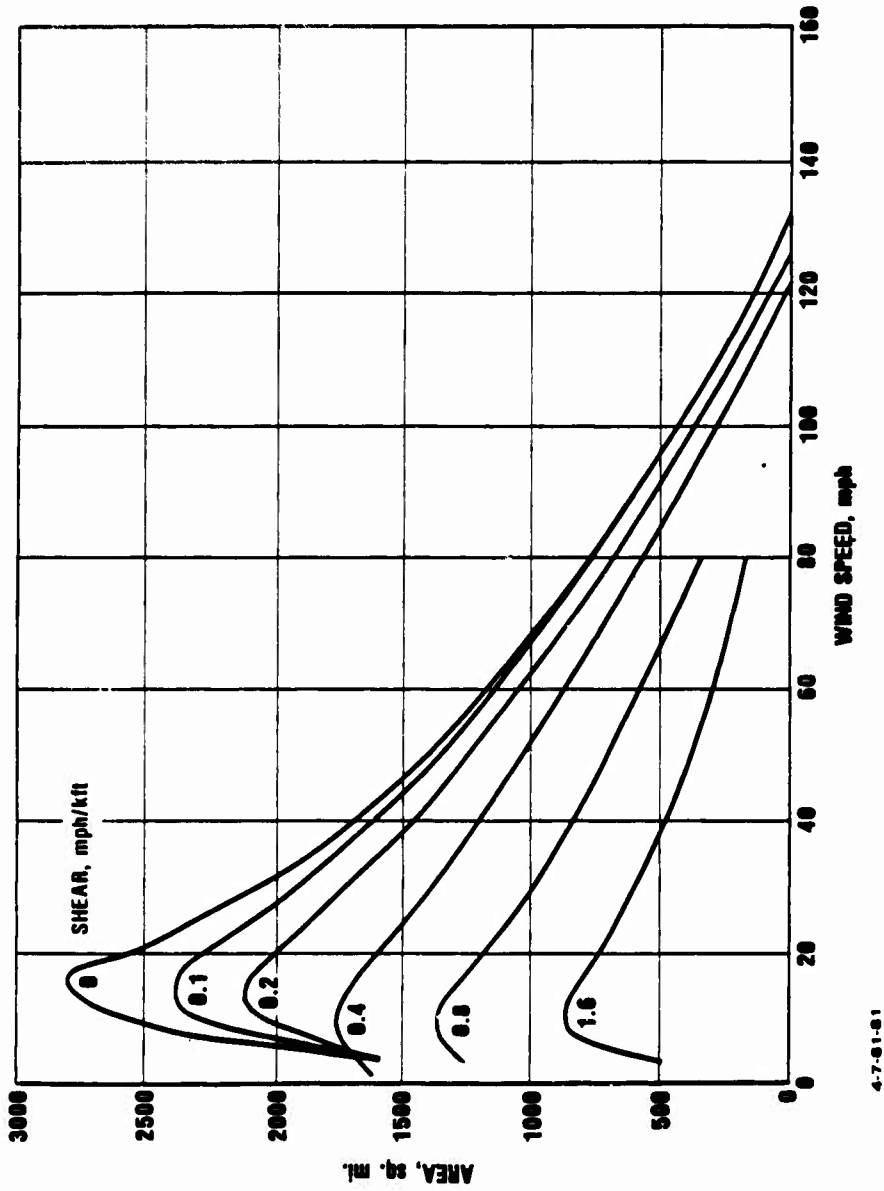
4-7-81-70

Figure II-9d. AREA COVERED AS A FUNCTION OF WIND SPEED AT A DOSE LEVEL OF 30 ROENTGENS/MT FOR A 20 MT YIELD AND VARIOUS SHEARS.



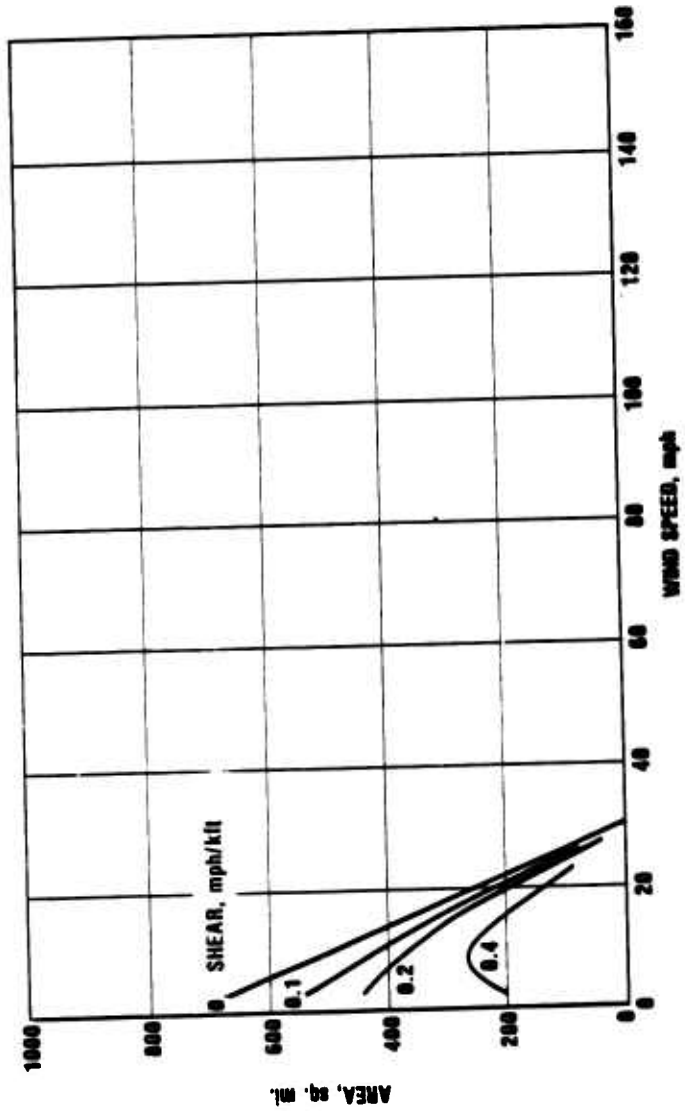
4-7-61-60

Figure II-9e. AREA COVERED AS A FUNCTION OF WIND SPEED AT A DOSE LEVEL OF 100 ROENTGENS/MT FOR A 20 MT YIELD AND VARIOUS SHEARS.



4-7-61-81

Figure II-9f. AREA COVERED AS A FUNCTION OF WIND SPEED AT A DOSE LEVEL OF 300 ROENTGENS/MT FOR A 20 MT YIELD AND VARIOUS SHEARS.



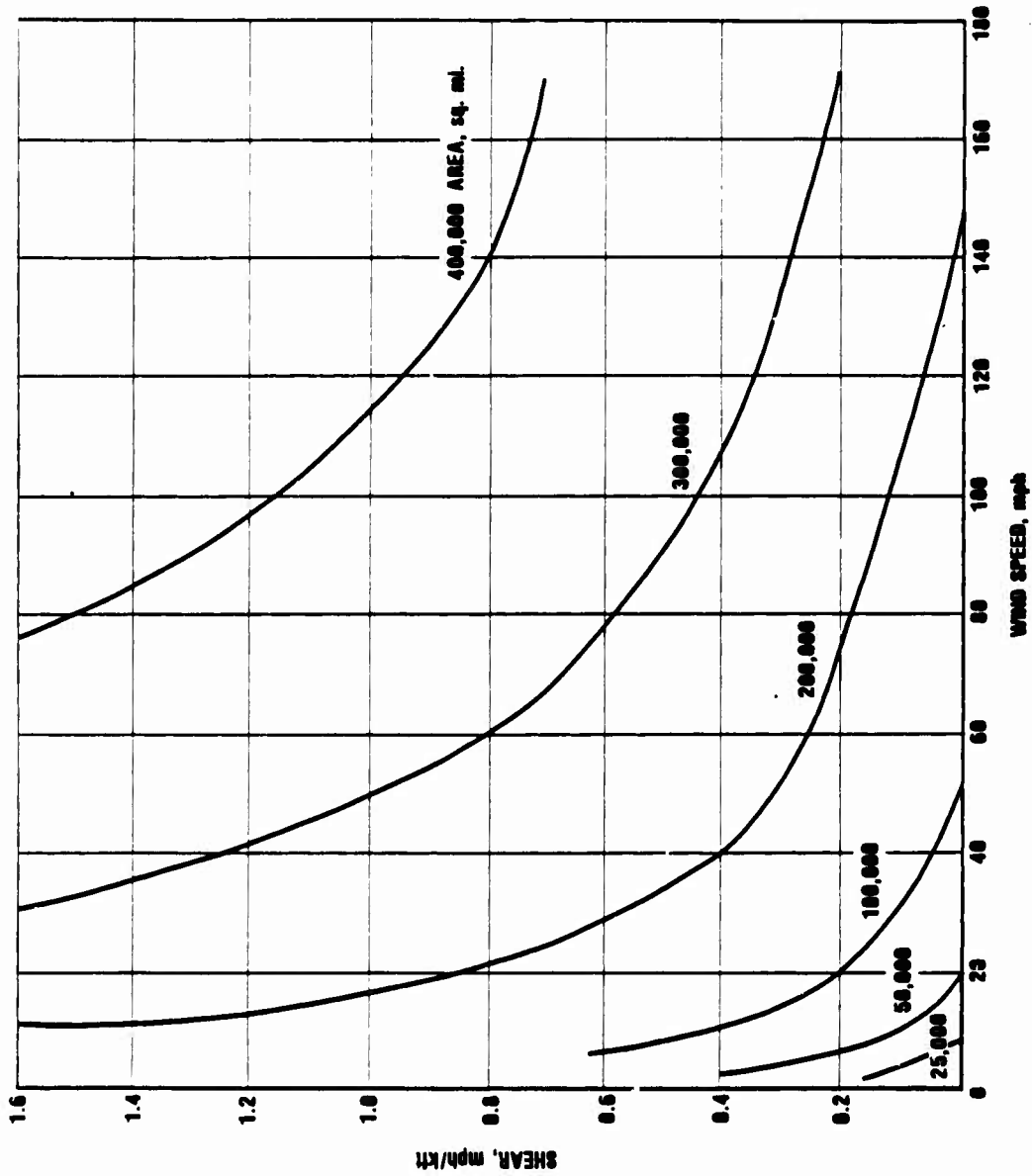
4-7-61-63

Figure II-99. AREA COVERED AS A FUNCTION OF WIND SPEED AT A DOSE LEVEL OF 1000 ROENTGENS/MT FOR A 20 MT YIELD AND VARIOUS SHEARS.

Contours of constant area covered as a function of wind speed and shear are presented in Figures II-10a through f for dose levels of 1, 3, 10, 30, 100, 300 and 1000 Roentgens/MT. Again these figures show the same general features as Figures II-6 except that the transitions occur at somewhat lower dose levels. The main purpose in illustrating the areas covered by 20 megaton weapons is to illustrate the similarities (once the total fission deposition is accounted for) between the different yields. For the purposes of many comparisons for yields in the 1 megaton to 20 megaton range, it is adequate to take the 1 megaton patterns, recalling that at high dose levels the areas covered for larger yield weapons is slightly less.

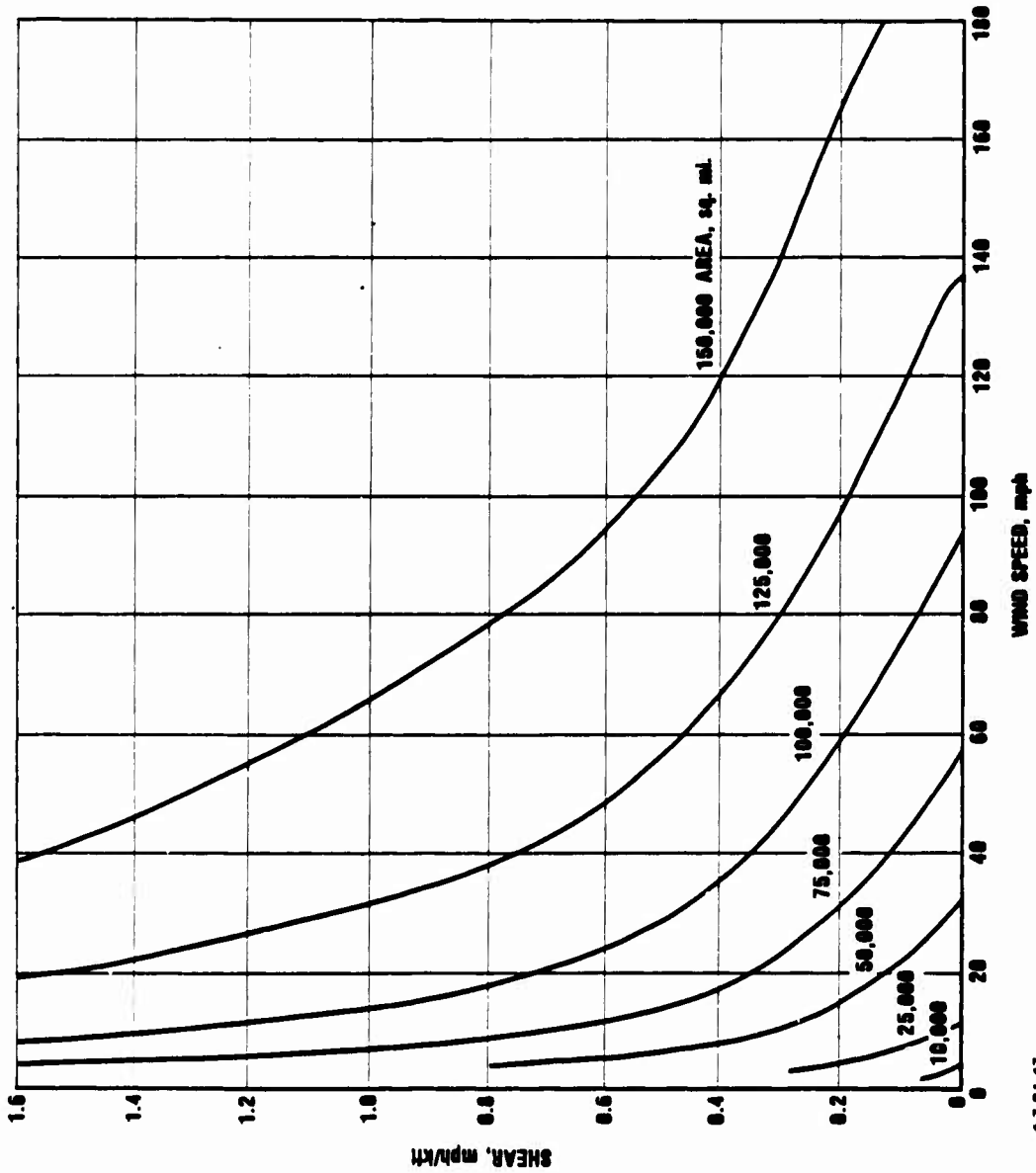
In Figures II-11 to II-13 the areas covered as a function of dose level are presented for weapon clusters of 10, 20 and 40 mile crosswind standard deviations. Each of the figures is for a total of 1 megaton fission yield with a 40 mph wind. This can be compared with Figure II-2b which is for the same conditions but for a single weapon, i.e., with a cluster standard deviation of 0. If, for example, a cluster consisted of 15 one megaton weapons with a total fission yield of 15 megatons, then the dose level for these figures should be multiplied by 15.

As would be expected, a cluster of weapons increases the area covered at low dose levels due to the increased crosswind spread, and decreases coverage at high dose levels due to less concentration of the released fission products. The changes due to different wind shear become less pronounced as the cluster size is increased since the cluster itself contributes an appreciable crosswind spread. (Since the contours are so close in Figures II-12 and II-13, for clarity only three values of shear are plotted.) In Figure II-13, two additional curves are presented for two extremes of high wind speed and low shear, and for low wind speed and high shear. In this



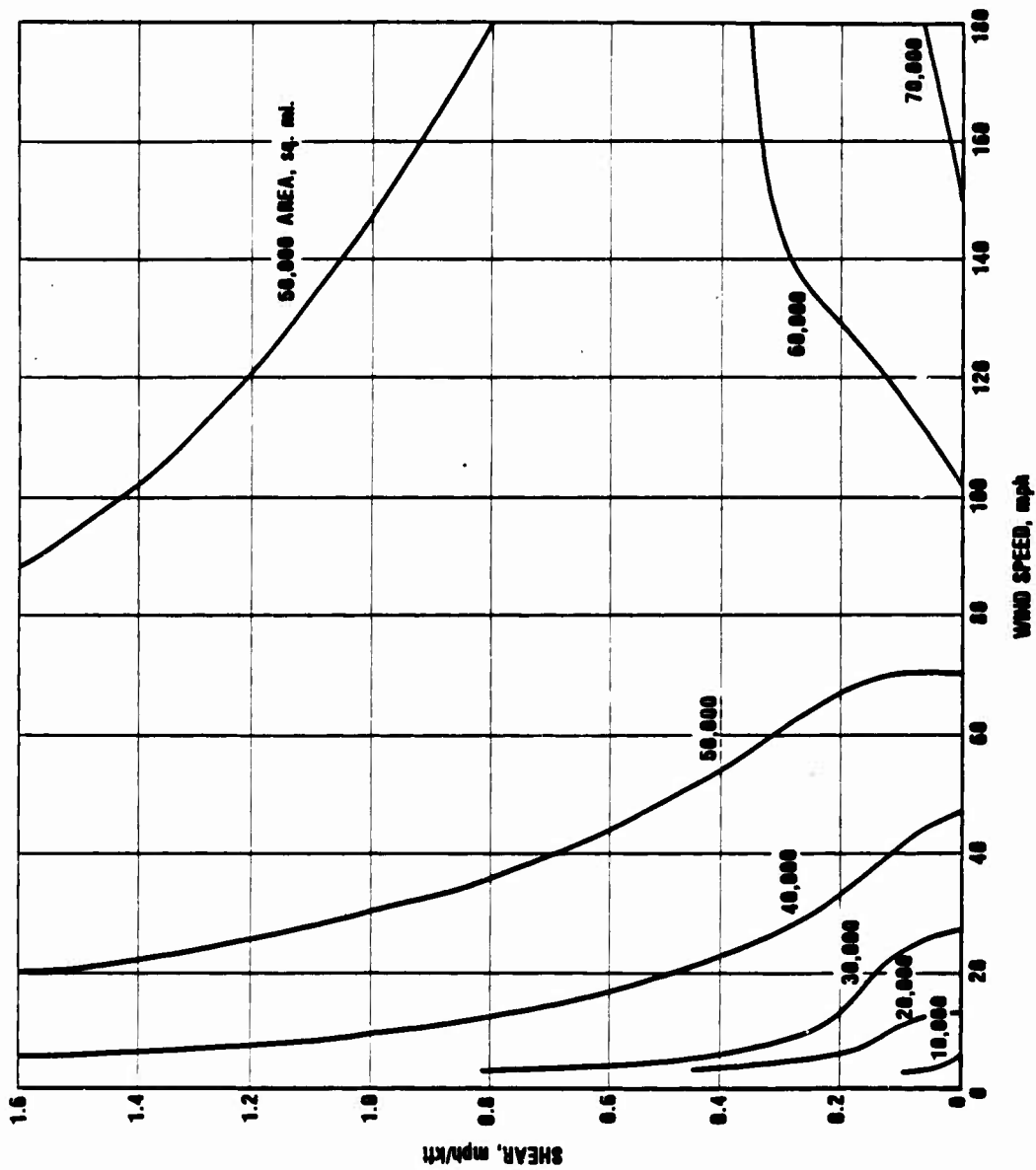
4-7-61-46

Figure II-10a. CONTOURS OF CONSTANT AREA COVERED AT A DOSE OF 1 ROENTGEN/MT AS A FUNCTION OF WIND SPEED AND SHEAR FOR A 20 MT YIELD.



4-7-51-47

Figure II-10b. CONTOURS OF CONSTANT AREA COVERED AT A DOSE OF 3 ROENTGENS/MT AS A FUNCTION OF WIND SPEED AND SHEAR FOR A 20 MT YIELD.



4-7-61-48

Figure II-10c. CONTOURS OF CONSTANT AREA COVERED AT A DOSE OF 10 ROENTGENS/MT AS A FUNCTION OF WIND SPEED AND SHEAR FOR A 20 MT YIELD.

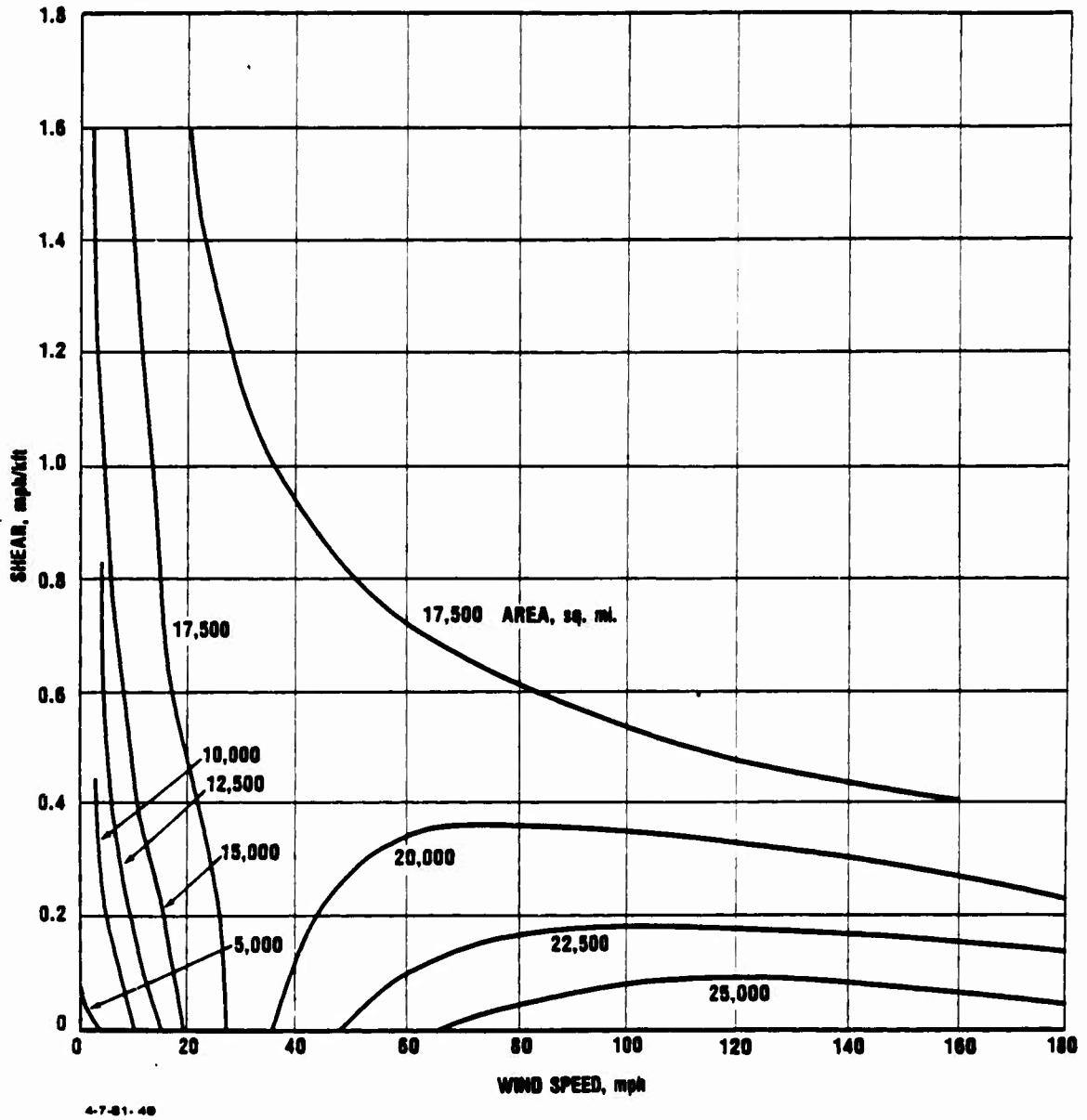
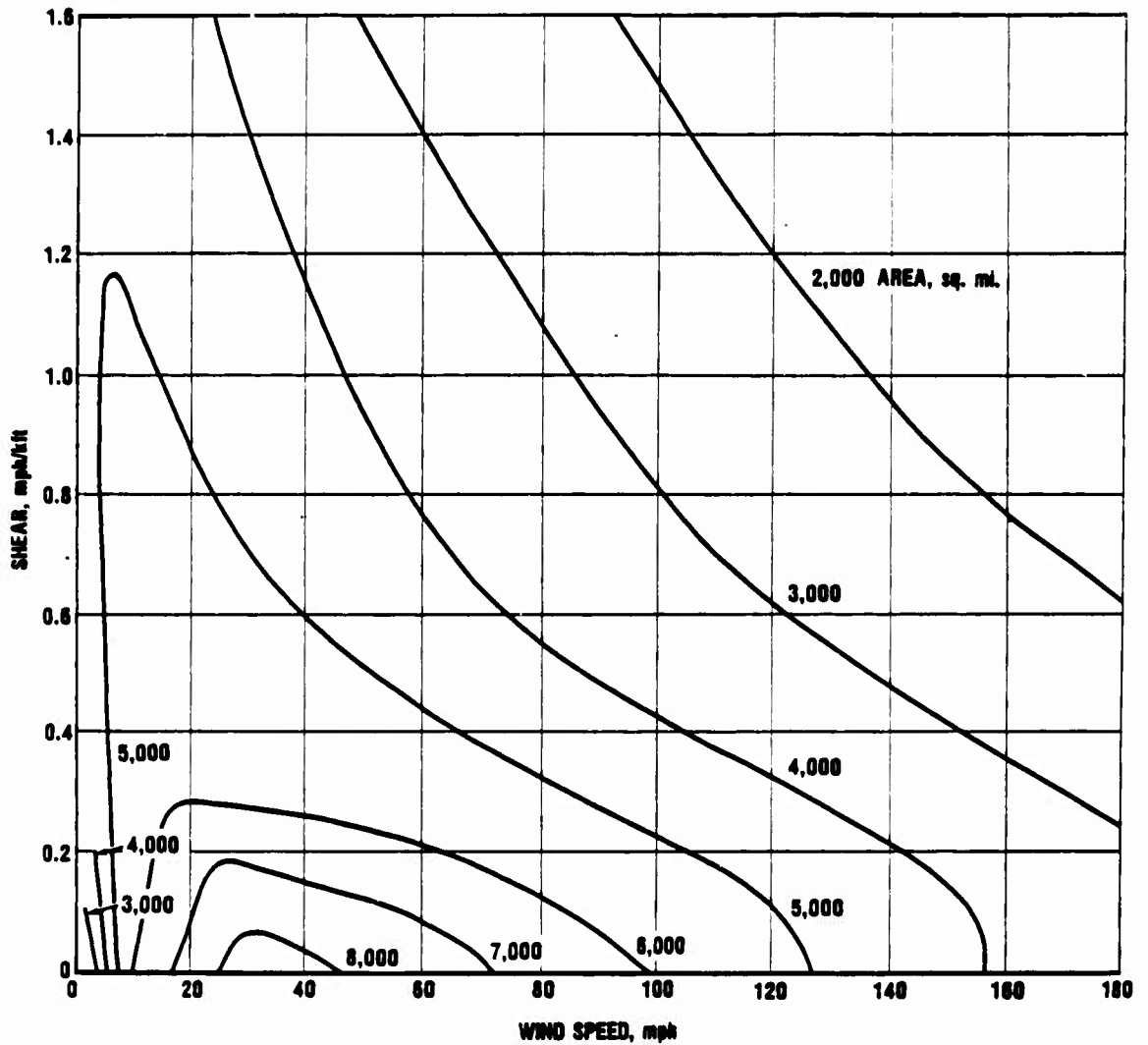
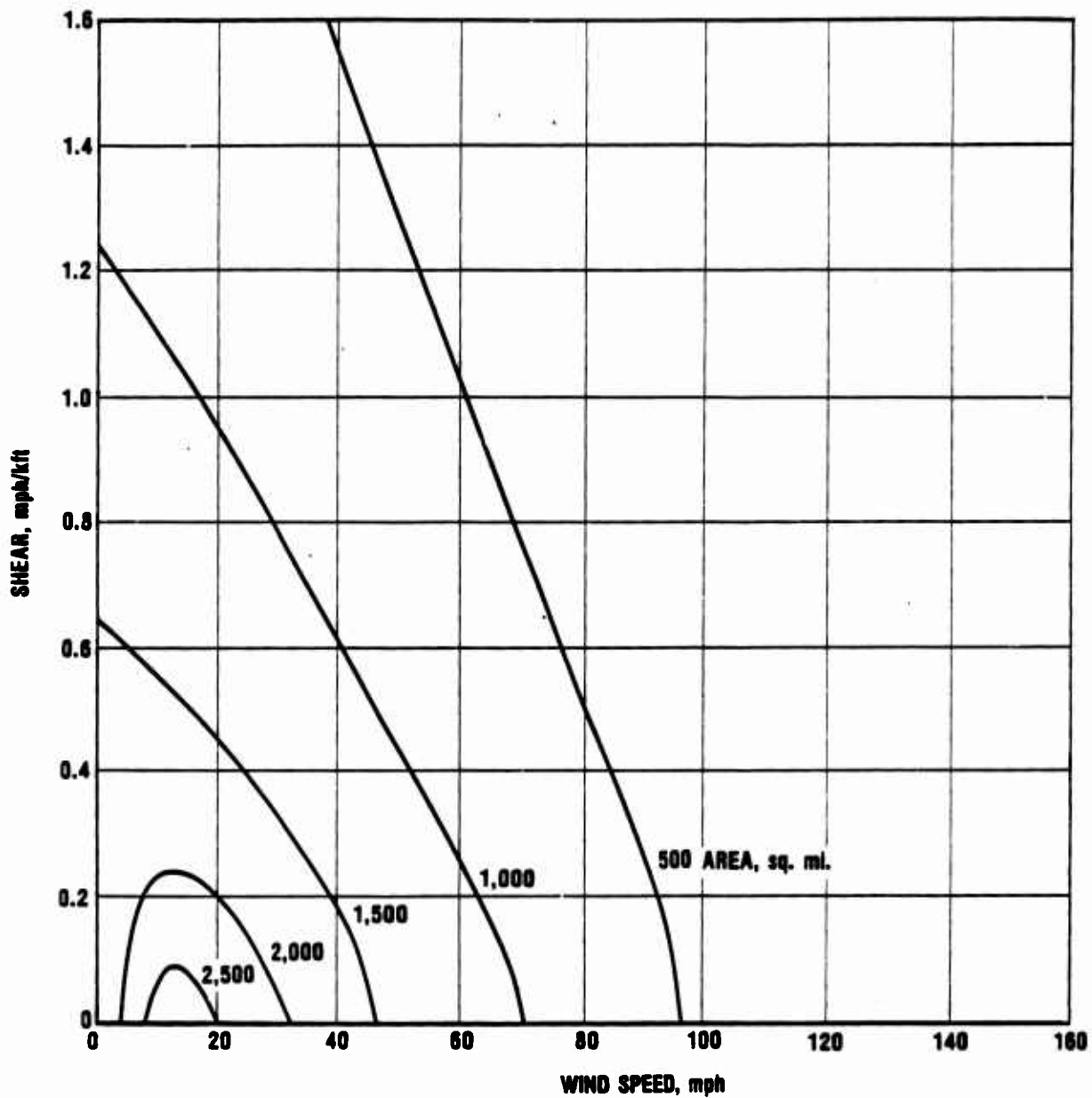


Figure II-10d. CONTOURS OF CONSTANT AREA COVERED AT A DOSE OF 30 ROENTGENS/MT AS A FUNCTION OF WIND SPEED AND SHEAR FOR A 20 MT YIELD.



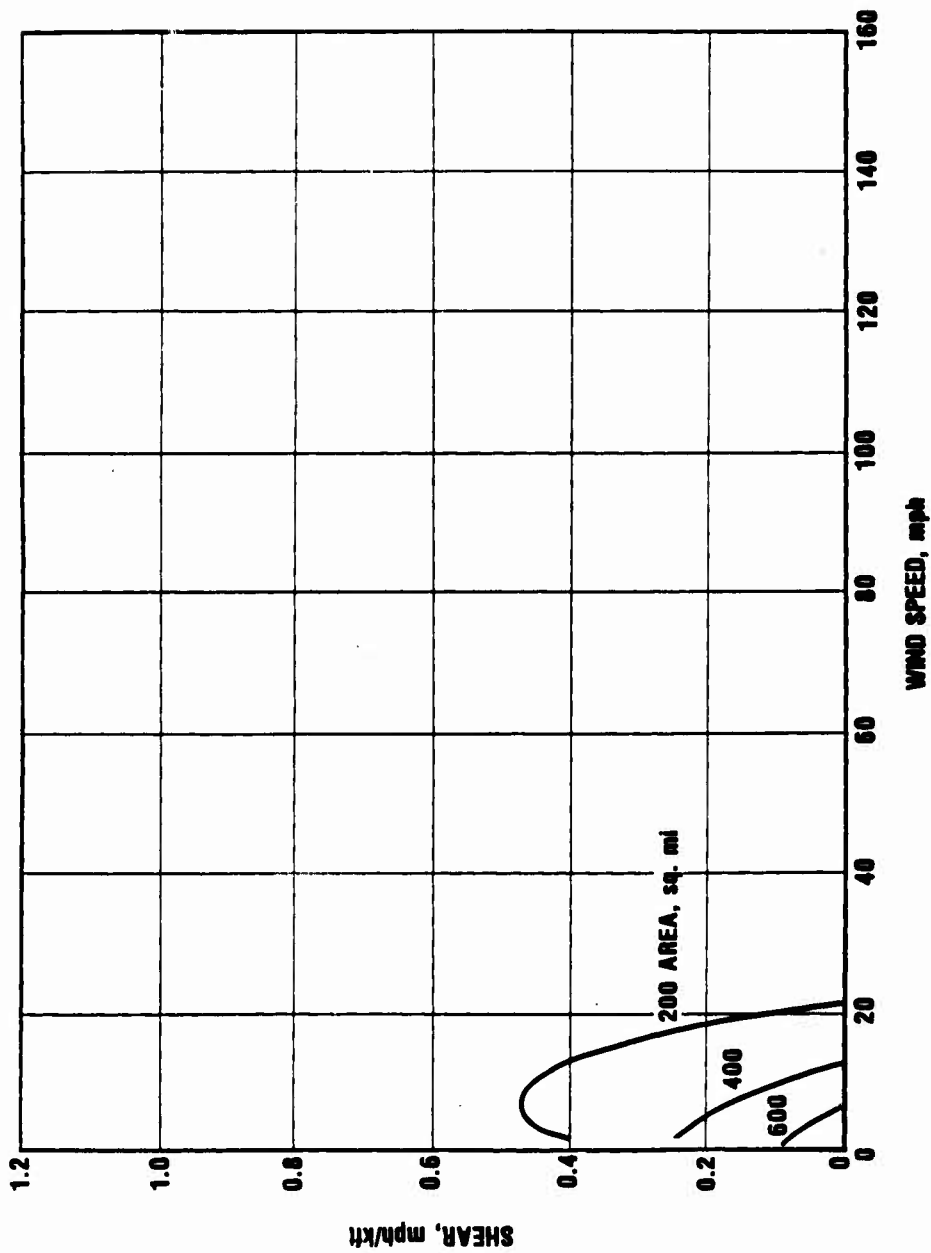
4-7-61-60

Figure II-10e. CONTOURS OF CONSTANT AREA COVERED AT A DOSE OF 100 ROENTGENS/MT AS A FUNCTION OF WIND SPEED AND SHEAR FOR A 20 MT YIELD.



4-7-81-81

Figure II-10f. CONTOURS OF CONSTANT AREA COVERED AT A DOSE OF 300 ROENTGENS/MT AS A FUNCTION OF WIND SPEED AND SHEAR FOR A 20 MT YIELD.



4-7-61-62

Figure II-10g. CONTOURS OF CONSTANT AREA COVERED AT A DOSE OF 1000 ROENTGENS/MT AS A FUNCTION OF WIND SPEED AND SHEAR FOR A 20 MT YIELD.

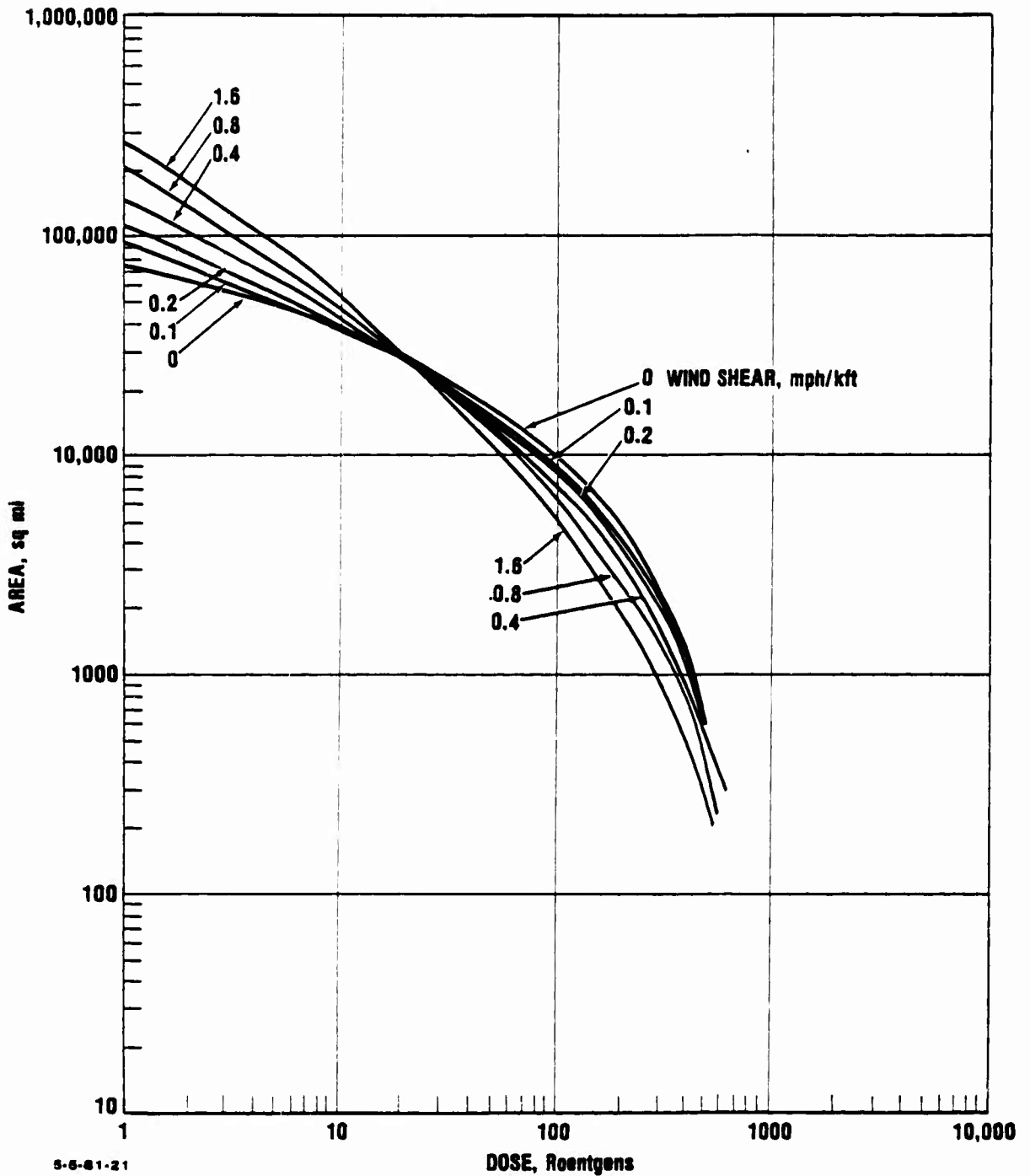


Figure II-11. AREA COVERED AS A FUNCTION OF DOSE FOR A 1 MT YIELD WITH A CLUSTER STANDARD DEVIATION OF 10 MILES WITH A 40 MPH WIND AND VARIOUS SHEARS.

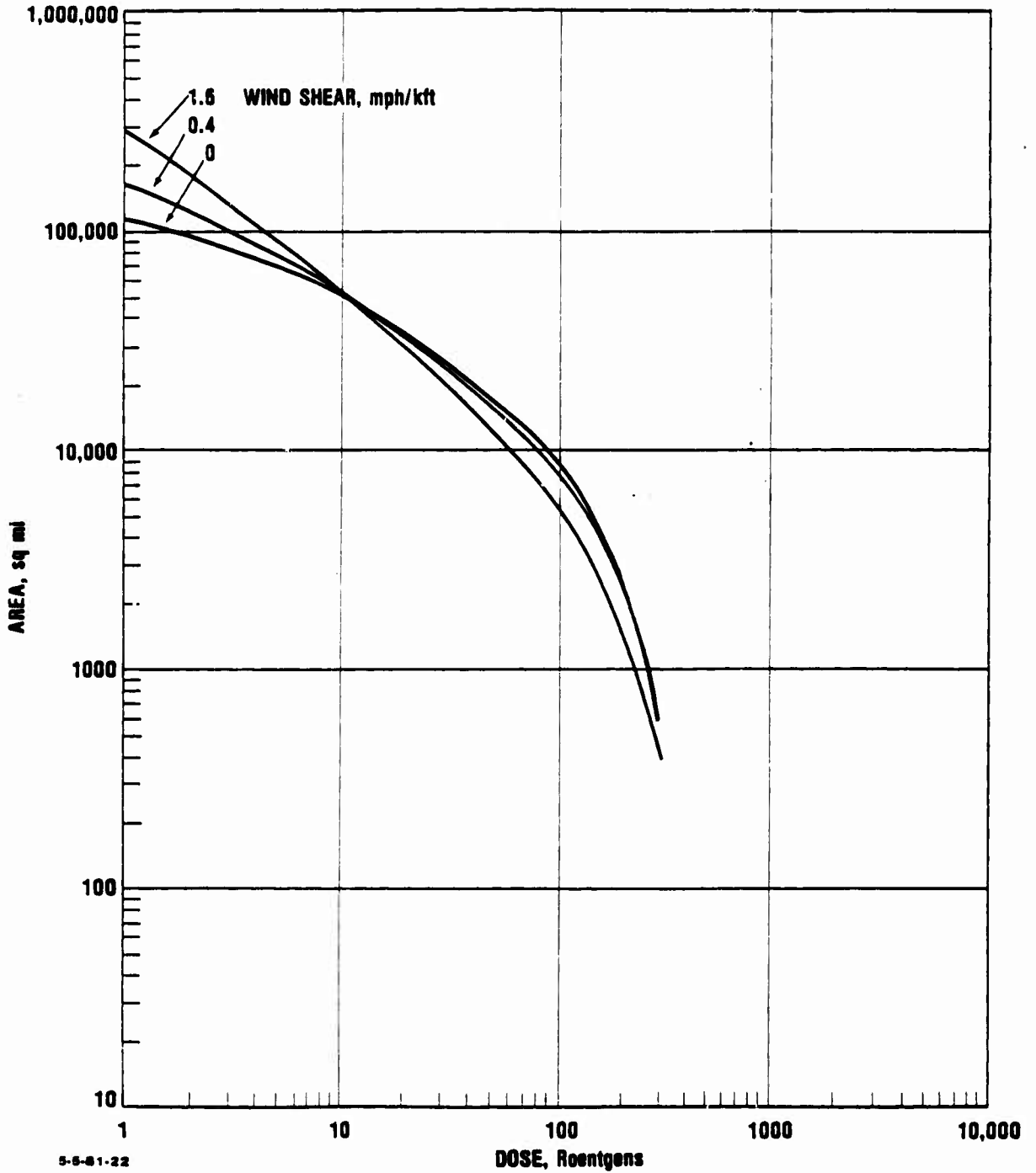


Figure II-12. AREA COVERED AS A FUNCTION OF DOSE FOR A 1 MT YIELD WITH A CLUSTER STANDARD DEVIATION OF 20 MILES WITH A 40 MPH WIND AND VARIOUS SHEARS.

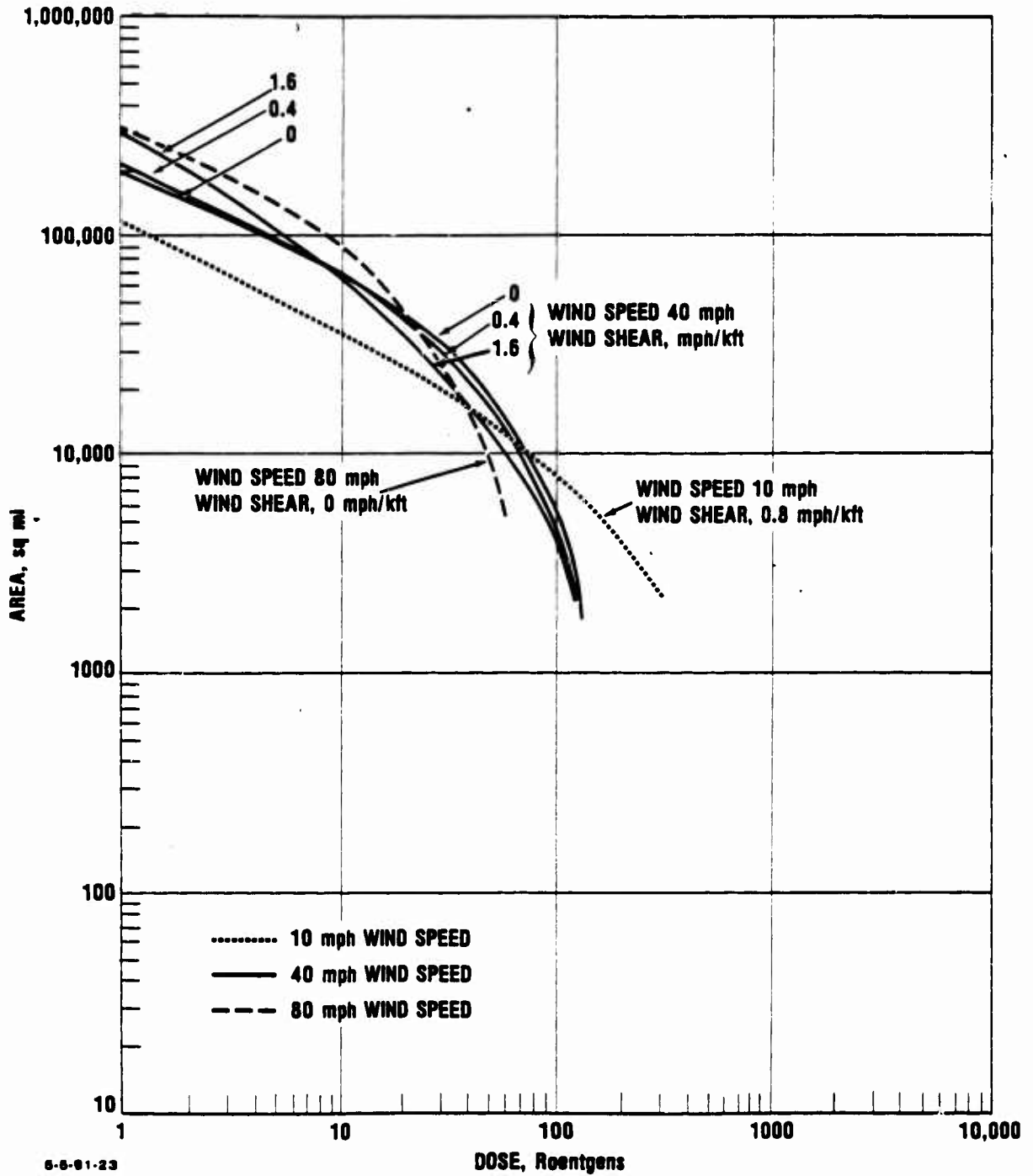


Figure II-13. AREA COVERED AS A FUNCTION OF DOSE FOR A 1 MT YIELD WITH A CLUSTER STANDARD DEVIATION OF 40 MILES WITH VARIOUS WIND SPEEDS AND SHEARS.

case, with a large cluster standard deviation, even these extreme cases do not make too great a difference.

In Figure II-14, areas covered as a function of dose are presented for a range of cluster standard deviations at moderate wind speeds and shears of 40 mph and 0.2 mph/kilofeet. As can be seen, the curves are almost parallel at low dose levels, but turn sharply downward more rapidly as the cluster standard deviation is increased.

C. FALLOUT PATTERN SHAPES

Another output from the WSEG-10 model is ground contours at a number of dose levels. An example of these is presented in Figure II-15 for a 1 megaton weapon with typical wind conditions--a 40 mph wind speed and 0.2 mph/kilofeet wind shear. Each of the contours looks approximately like an ellipse with the downwind end slightly compressed. All the contours appear quite similar in shape, increased in size for the lower dosage levels. A more sensitive test for the similarity in shape is presented in Figure II-16 where contours are presented with the crosswind distance divided by maximum contour width and downwind distance divided by maximum contour distance downwind from ground zero.¹ The difference between the contours represents divergences from perfect similarity. At ground zero a rather appreciable difference is seen, which lessens at further scaled downwind distances. For purposes of comparison, the dashed line in Figure II-16 represents an ellipse, which gives a reasonable approximation. A better match can be obtained by using an "Oval of Cassini." The general form of this equation is

¹In all cases presented here, the upwind distance to a certain contour is small compared to the downwind distance. When a contour length is given, this is defined as the distance from ground zero to the maximum downwind extent of the contour from ground zero.

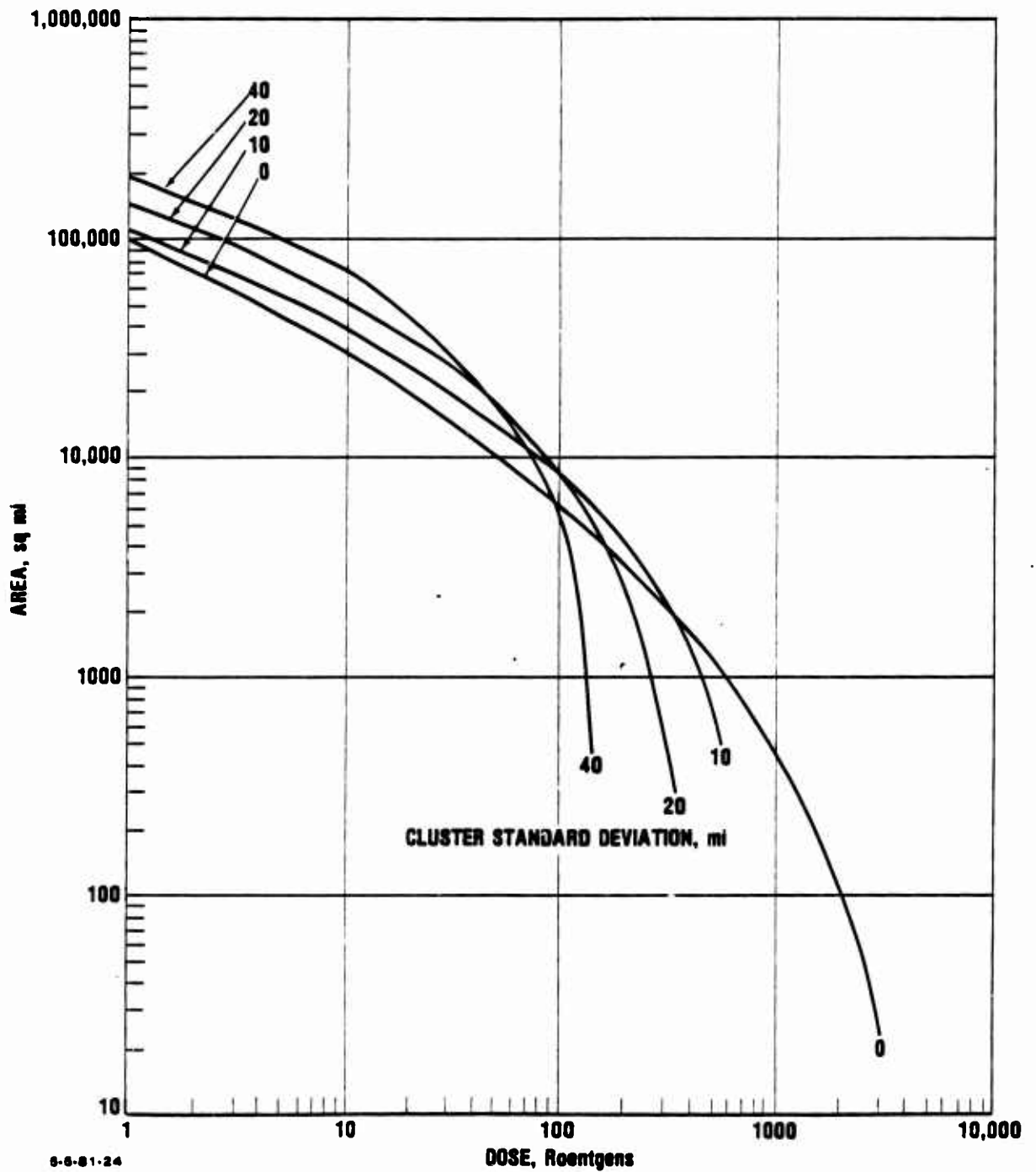


Figure II-14. COMPARISONS OF AREAS COVERED AS A FUNCTION OF DOSE FOR A 1 MT YIELD WITH VARIOUS CLUSTER STANDARD DEVIATIONS WITH A WIND SPEED OF 40 MPH AND WIND SHEAR OF 0.2 MPH/KILOFOOT.

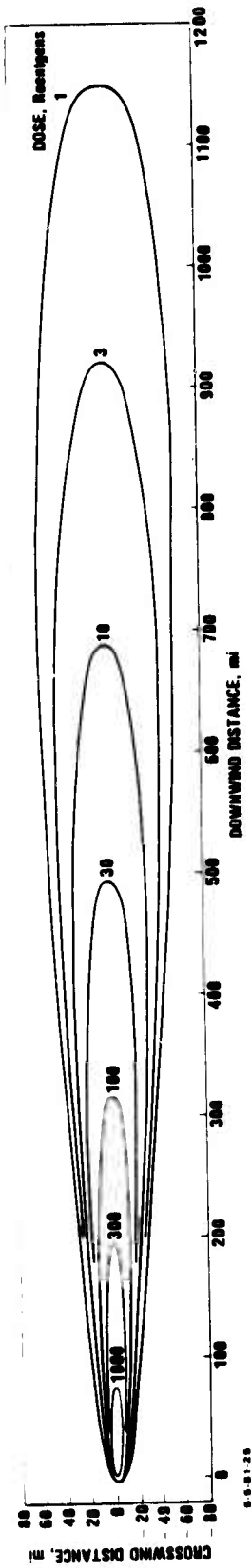


Figure II-15. GROUND CONTOURS FOR VARIOUS DOSES FOR A 1 MT YIELD WITH A 40 MPH WIND SPEED AND 0.2 MPH/KILOFOOT WIND SHEAR.

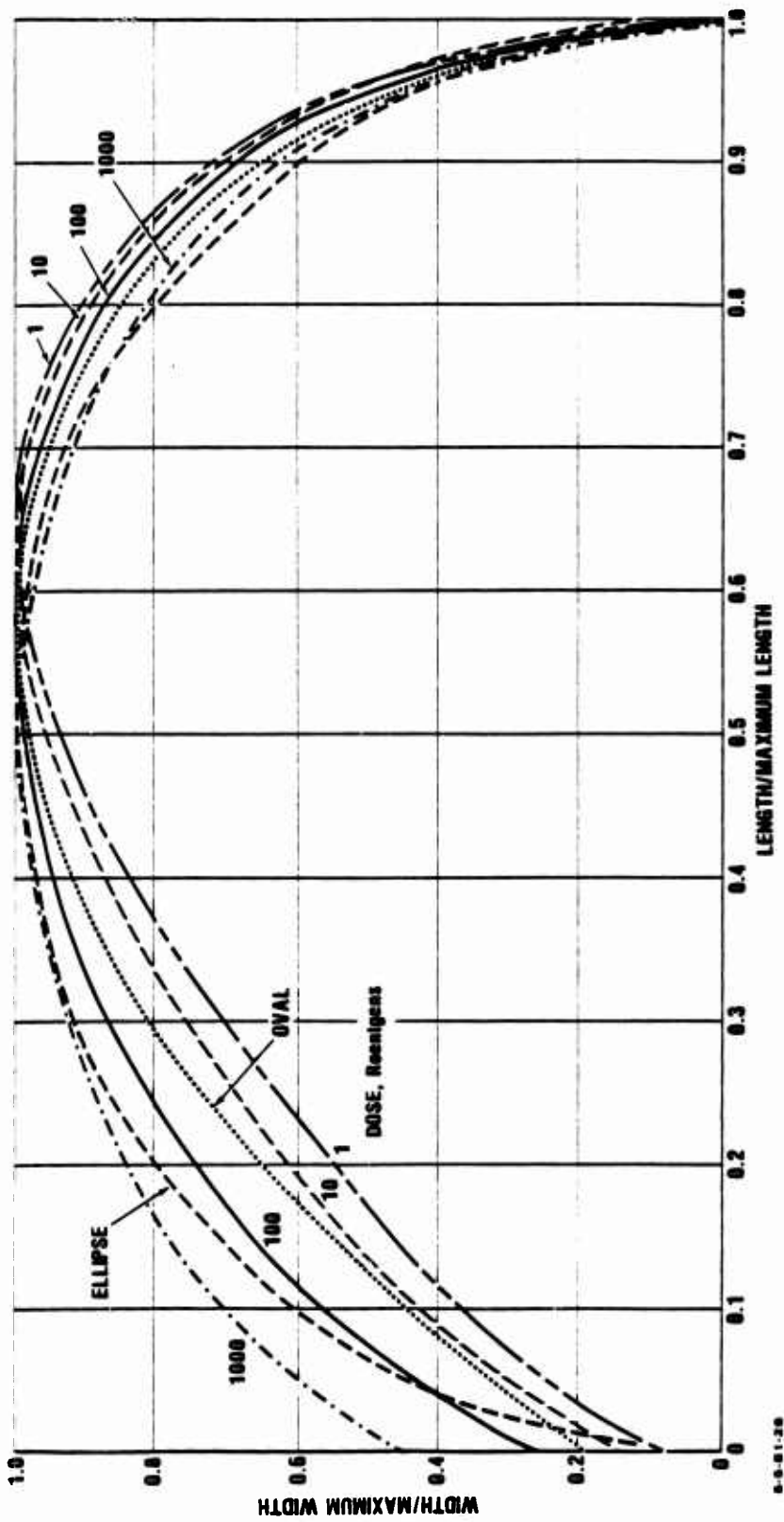


Figure II-16. DIMENSIONLESS CONTOURS FOR VARIOUS DOSES FOR A 1 MT YIELD WITH A 40 MPH WIND SPEED AND A 0.2 MPH/KILOFOOT WIND SHEAR.

$$\left(x^2+y^2+a^2\right)^2 - 4 a^2 x^2 = c^4 .$$

The dotted line in Figure II-16 is a solution of this equation for $a=c=1$. The resulting curve is stretched so that the maximum length is 1, the maximum width is 1, and the value at $x=0$ is .2. The resulting curve differs from the 10R contour by a maximum of 5 percent. This analytical format can be used to give quite close approximations to the shape of the constant dose contours. For simplicity most of the shape comparisons will present contour length and maximum width, assuming the shapes are sufficiently similar.

In Figure II-17, ground contours are given for 100 Roentgen doses for a 0.2 mph/kilofoot wind shear and for a set of wind speeds between 1 and 80 mph. The contours range from short and wide to narrow and thin, but the same general normalized shape is seen.

In Figure II-18 ground contours are given for 100 Roentgen doses for a 80 mph wind and three different shears. The contour for 0 shear is drastically different than the others with the maximum width occurring much closer to ground zero.

One measure of the similarity of the various contours is the distance downwind at which the maximum width occurs, divided by the maximum length. Table II-1 shows the number of occurrences of different values of the ratio for a set of runs with a 1 megaton weapon with wind speeds ranging from 3 mph to 80 mph, and wind shears from 0.1 to 1.6 mph/kilofoot. At low dose levels a high degree of repeatability is seen. As the dose level increases, the position of the maximum width comes closer to ground zero and the spread due to different wind and shear condition increases. However, at doses up to 300 Roentgens, 50 percent of the ratios occur in a spread of 0.03

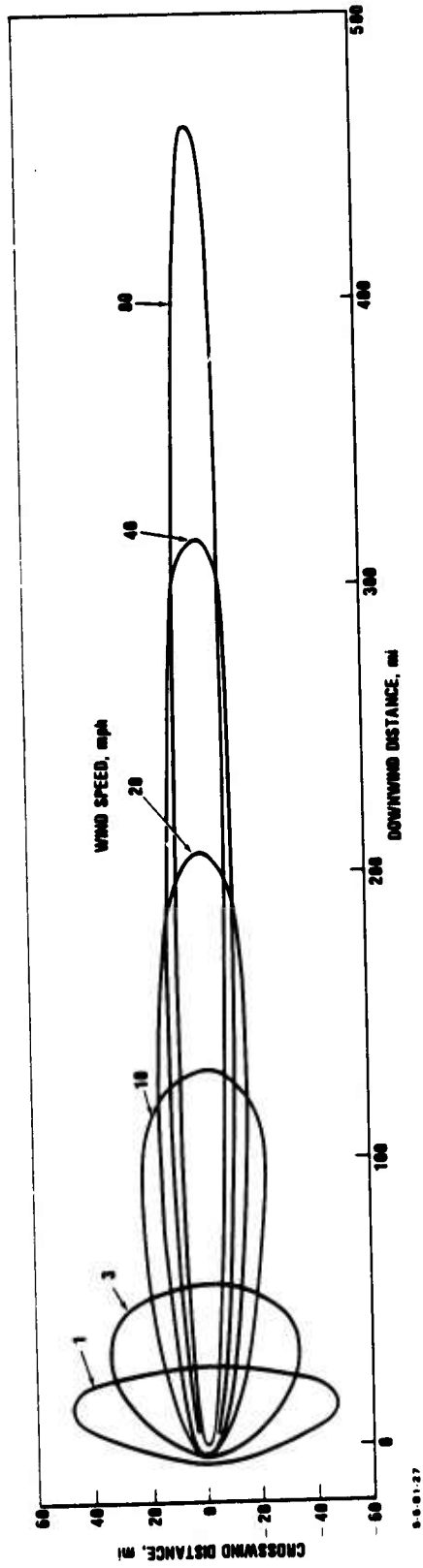


Figure II-17. GROUND CONTOURS FOR 100 ROENTGENS DOSE FOR A 1 MT YIELD WITH A 0.2 MPH/KILOFOOT WIND SHEAR AND VARIOUS WIND SPEEDS.

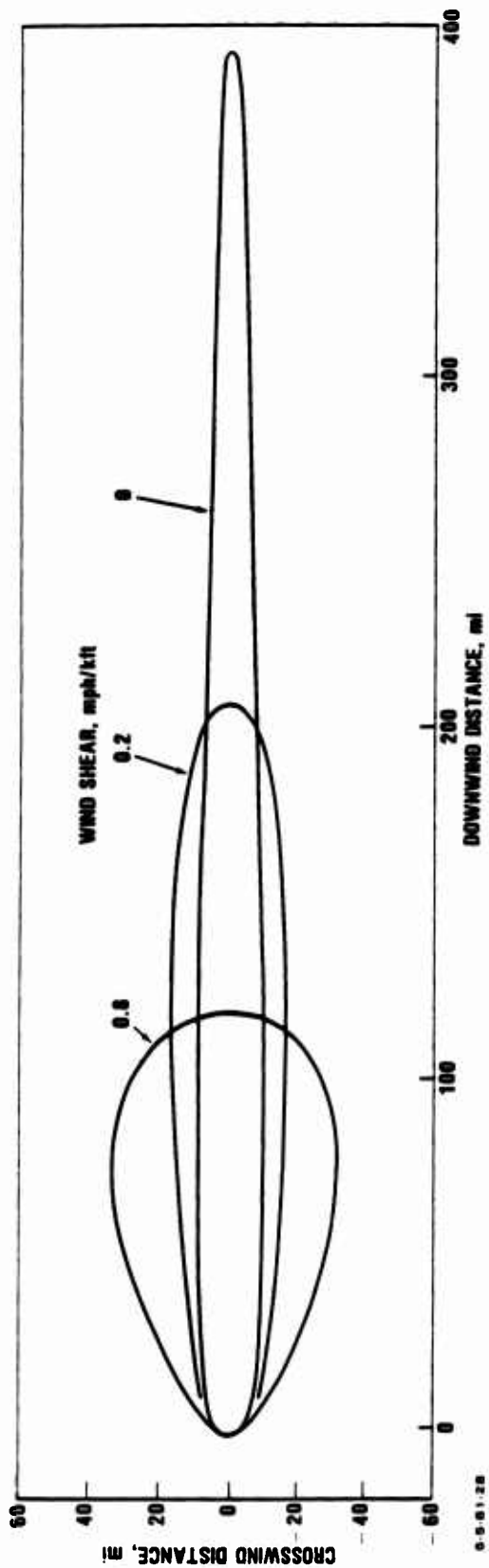


Figure II-18. GROUND CONTOURS FOR 100 ROENTGENS DOSE FOR A 1 MT YIELD WITH A 20 MPH WIND AND VARIOUS SHEARS.

Table II-1. NUMBER OF OCCURRENCES OF RATIO OF DOWNWIND DISTANCE TO MAXIMUM WIDTH TO LENGTH FOR NON-ZERO SHEARS AND VARIOUS WIND SPEEDS.

Downwind Distance at Maximum Width/ Maximum Length	Dose, Roentgens							
	1	3	10	30	100	300	1000	3000
0.0-0.34						1		5
.35								1
.36								
.37					1		2	
.38							1	
.39							1	
.40						1		1
.41							1	2
.42								1
.43						1		
.44								1
.45								3
.46								
.47								1
.48							1	
.49					1	1	2	
.50								
.51								
.52						1	1	
.53					1	1	2	1
.54							3	
.55				1		1	5	
.56					1	1	1	1
.57						1	2	
.58					1	2	2	
.59				1	1	6		1
.60				1	3	4	3	1
.61				1	8	3		
.62			2	9	7			
.63		2	9	13	1	1		
.64	8	20	15		1			
.66	18	4				1		
.67						1		
.68								
.69								
.70								

or less, which can be interpreted to mean that dose level is the prime factor affecting this measure of similarity in this dose range.

Table II-2 gives the rate of downwind distance to maximum width to length for 0 wind shear. Here much lower values of this ratio are seen, reflecting a difference in shapes at 0 wind shear. Increasing values of the ratio are associated with increasing wind speed for all dose levels in this Table except at the 3000 Roentgens.

In Figure II-19 ground contours for a 100 Roentgen dose are shown for different values of weapon cluster standard deviation at a wind speed of 40 mph and a wind shear of 0.2 mph/kilofoot. As the cluster standard deviation is increased, a change in shape is seen bringing the location of maximum width closer and closer to ground zero. For the larger cluster standard deviations patterns similar to those obtained with 0 shear are obtained.

The variations of pattern length and width (here defined as the maximum distance from the center line of the pattern to the crosswind distance where the specified dose occurs) as a function of dose is shown in Figures II-20, II-21 and II-22 for 1 megaton weapons with 20 mph, 40 mph and 80 mph wind speeds and various shears. Similar presentations of length and width as a function of scaled dose for 20 megaton weapons are shown in Figures II-23 and II-24 for the wind speeds of 20 and 80 mph, at the boundaries of the most likely wind speed range.

For a 1 megaton weapon with a 20 mph wind and 0 shear, the maximum length for a 1R dose is 1000 miles, or about 1/3 of the distance across the country. However, for a larger shear of 0.2 mph/kilofoot and larger dose levels of, say 500 Roentgens, distances of only about 100 miles are obtained. At these latter conditions a maximum half-width of a little less

Table II-2. NUMBER OF OCCURRENCES OF RATIO OF DOWNWIND DISTANCE TO MAXIMUM WIDTH TO LENGTH FOR 0 WIND SHEAR AND VARIOUS WIND SPEEDS.

Downwind Distance at Maximum Width/ Maximum Length	Dose, Roentgens								
	1	3	10	30	100	300	1000	3000	10,000
0.01									
0.02									
0.03	1	1							
0.04	1		1						
0.05	1	1		1					
0.06	1	1	1		1				
0.07	1	1				1			
0.08		1	1	1					
0.09			1				1		
0.10				1	1				
0.11									
0.12				1					
0.13					1				
0.14						1			
0.15				1				1	
0.16									
0.17									
0.18					1				
0.19								1	
0.20									
0.21						1			
0.22									
0.23									
0.24								1	1
0.25					1		2		
0.26									
0.27						1			
0.28						1			
0.29									
0.30									
0.30-1.0							2	1	1

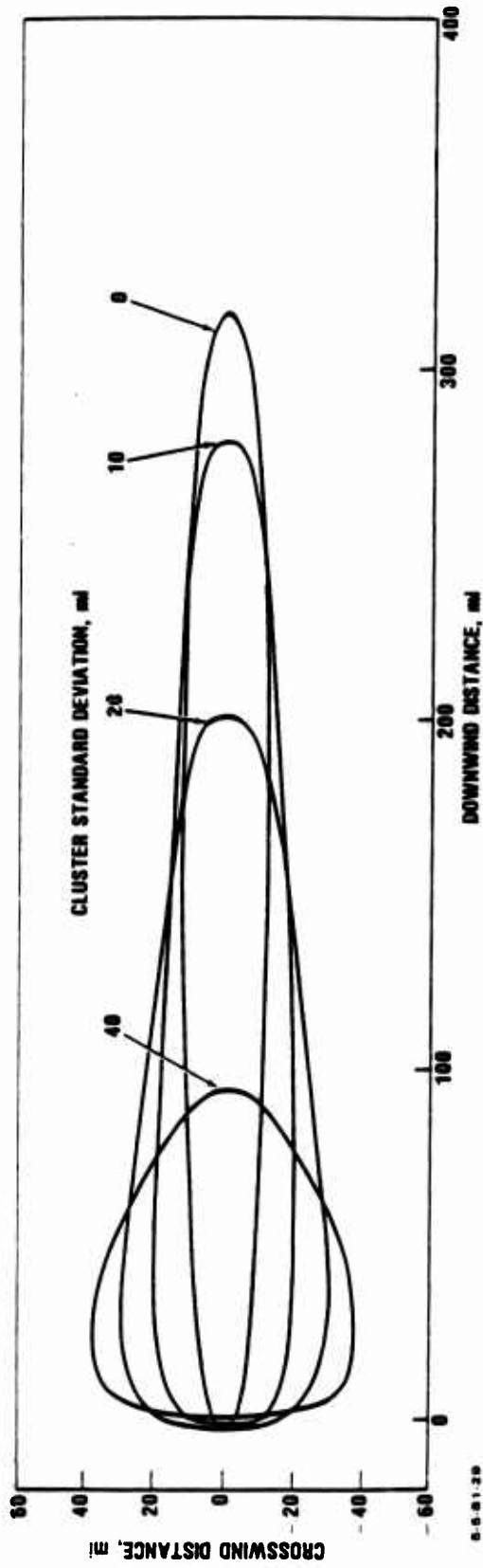


Figure II-19. GROUND CONTOURS FOR 100 ROENTGENS DOSE FOR A 1 MT YIELD WITH VARIOUS WEAPON CLUSTER STANDARD DEVIATIONS WITH A 40 MPH WIND SPEED AND 0.2 MPH/KILOFOOT WIND SHEAR.

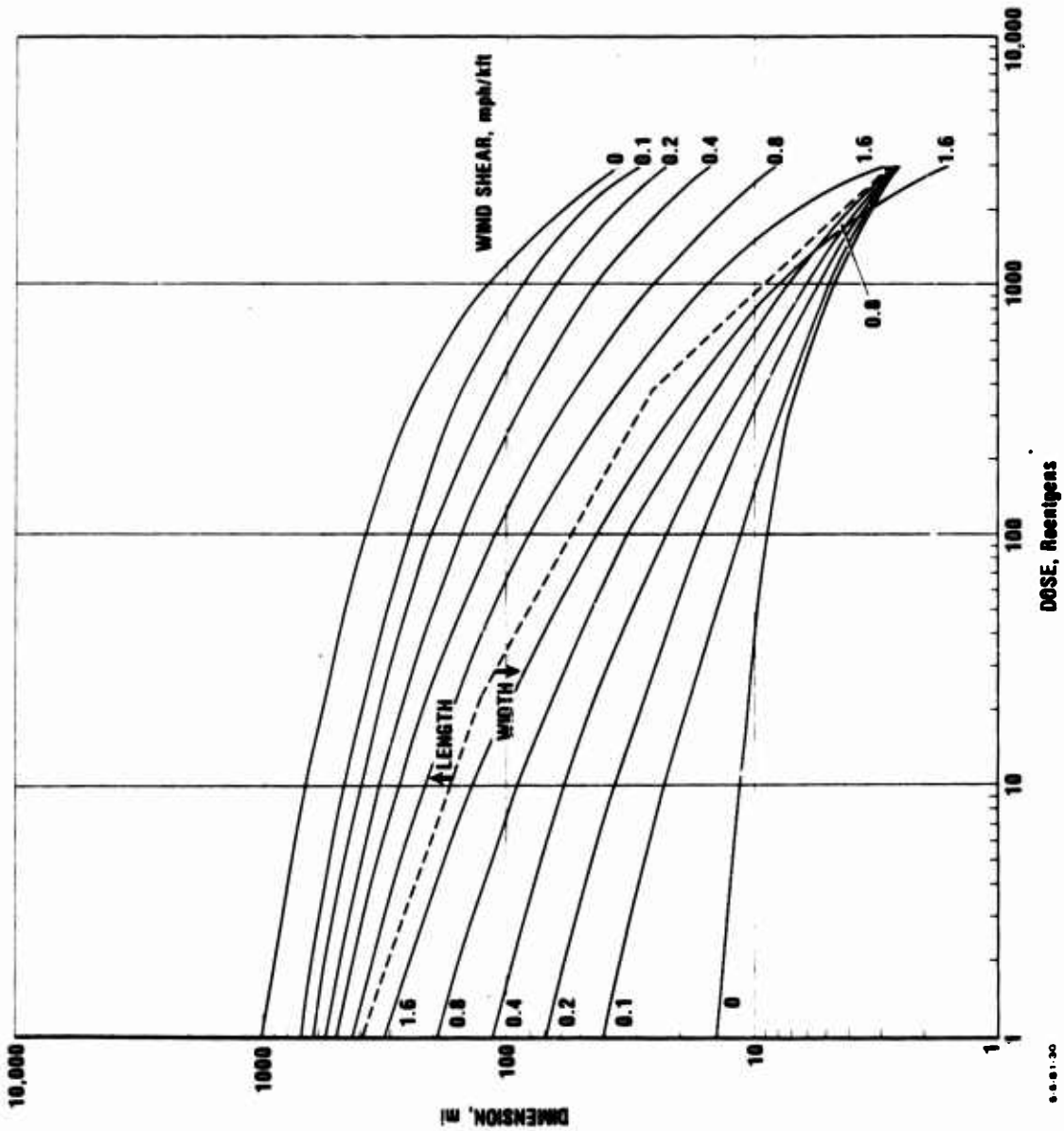


Figure II-20. PATTERN LENGTH AND WIDTH AS A FUNCTION OF DOSE FOR A 1 MT YIELD WITH A 20 MPH WIND SPEED AND VARIOUS WIND SHEAR.

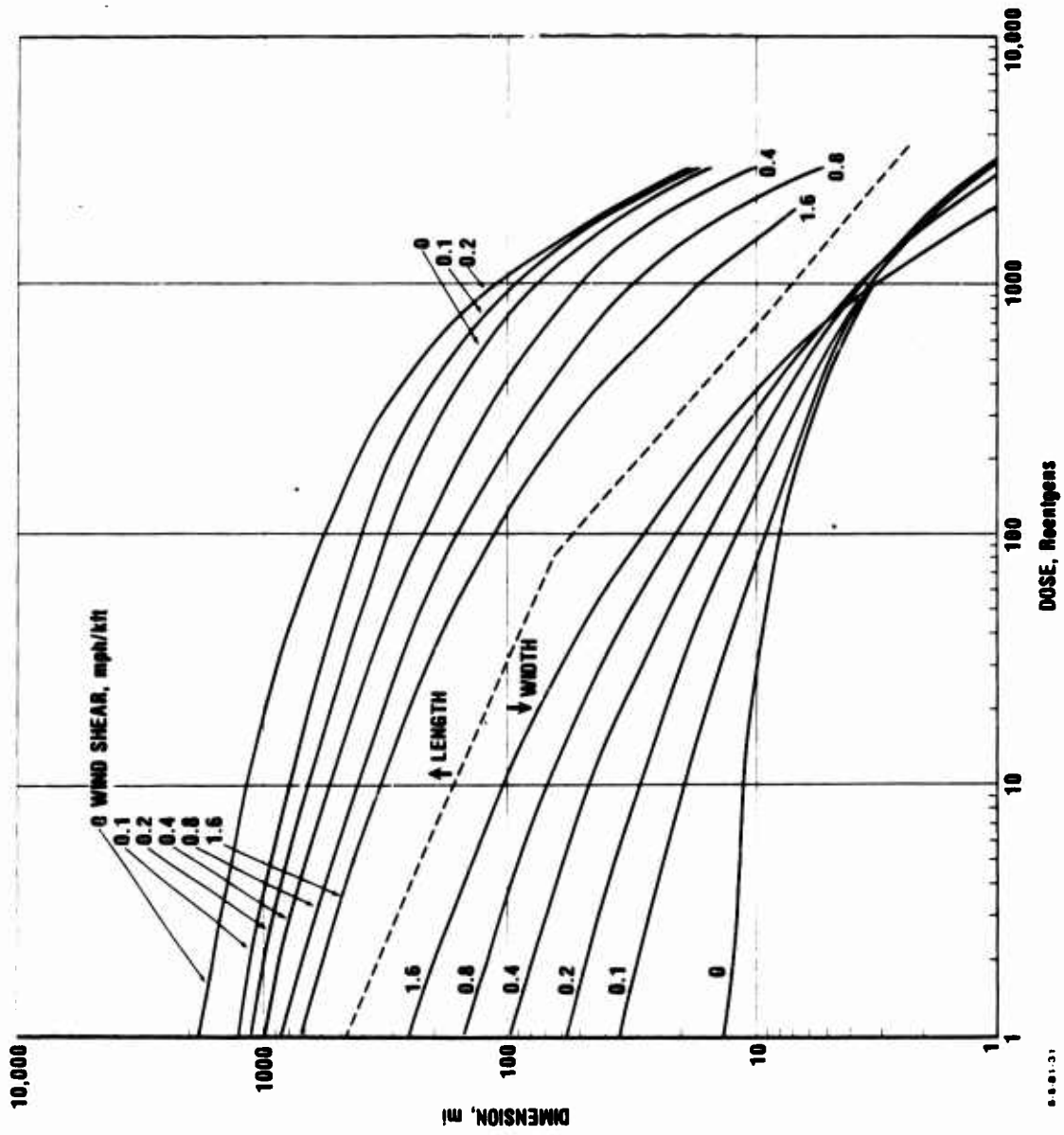
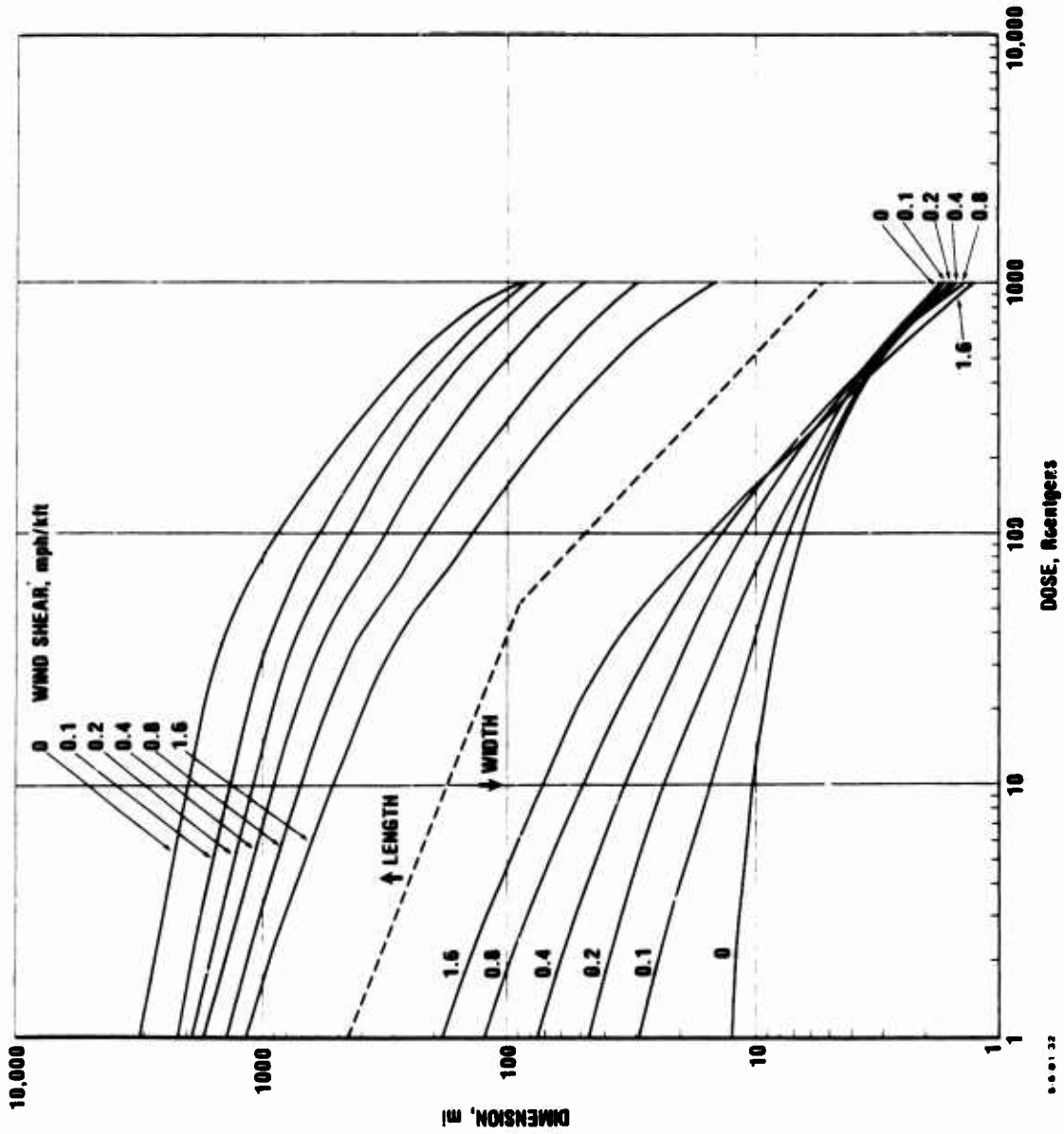


Figure II-21. PATTERN LENGTH AND WIDTH AS A FUNCTION OF DOSE FOR A 1 MT YIELD WITH 40 MPH WIND SPEED AND VARIOUS SHEARS.



9-6-61-22

Figure II-22. PATTERN LENGTH AND WIDTH AS A FUNCTION OF DOSE FOR A 1 MT YIELD WITH A 80 MPH WIND SPEED AND VARIOUS WIND SHEAR.

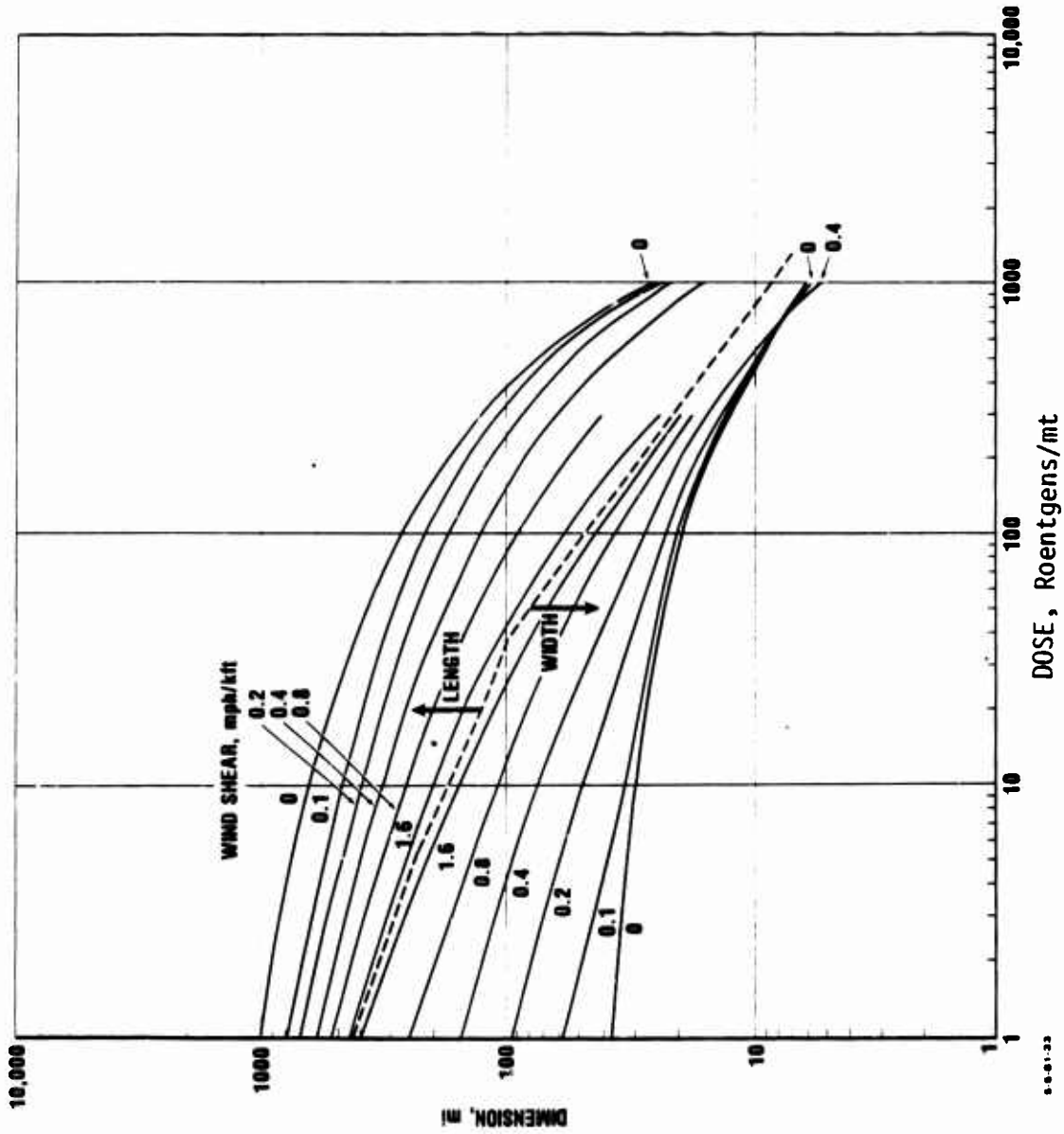


Figure II-23. PATTERN LENGTH AND WIDTH AS A FUNCTION OF DOSE/MT FOR A 20 MT YIELD WITH A 20 MPH WIND SPEED AND VARIOUS WIND SHEARS.

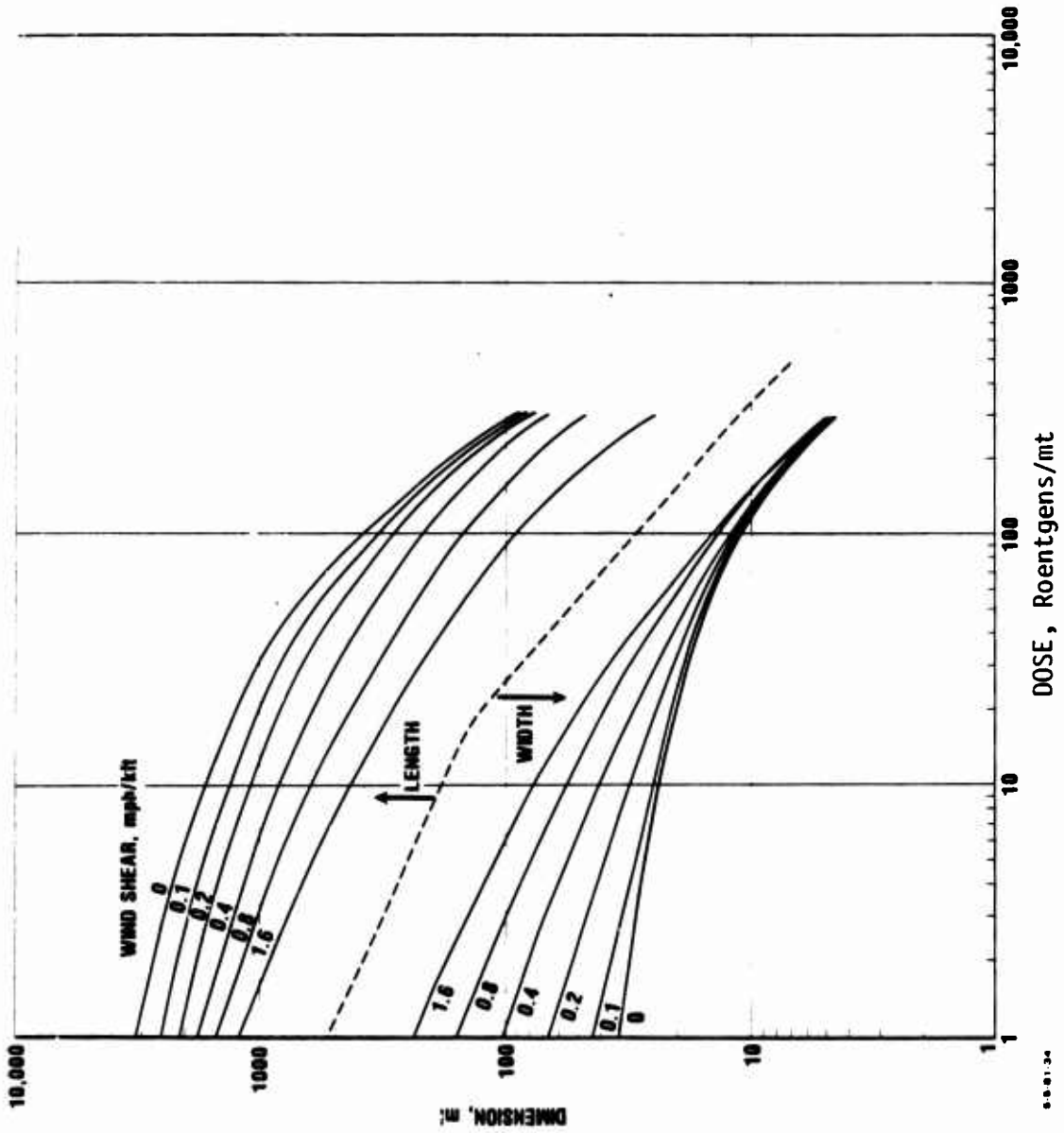


Figure II-24. PATTERN LENGTH AND WIDTH AS A FUNCTION OF DOSE/MT FOR A 20 MT YIELD WITH AN 80 MPH WIND SPEED AND VARIOUS WIND SHEARS.

than 10 miles is obtained, for a total swath width of 20 miles.

With an 80 mph wind at 0 shear condition, a maximum length of 3 times that at 20 mph is obtained. However the decrease of dose with distance is more rapid, so that at a dose of 500 Roentgens with a 0.2 mph/kilofoot shear, a length of only 1.8 times the 20 mph value is obtained. The effect of wind shear on pattern length and width is more pronounced at 80 mph than at 20 mph.

As with pattern areas, increasing the yield to 20 megatons (with 0.05 fission fraction) does not change pattern dimensions much at low dose levels, but the more rapid decrease in pattern size at higher dose levels causes a more rapid decrease in dimensions at high dose levels, as was observed with pattern area.

The ratio of length to pattern half-width (the maximum crosswind distance from the pattern hot line to a particular dose level contour) is a means of describing the relative thickness of a particular pattern. These ratios are presented in Figures II-25 and II-26 for a 1 megaton weapon with 20 mph and 80 mph winds, and in Figures II-27 and II-28 for a 20 megaton weapon with the same 20 mph and 80 mph winds. Only relatively small variations of this ratio are seen as a function of dose level except at the 0 shear value. The ratios for the 80 mph wind in Figure II-26 are about 4 times those for the 20 mph wind shown in Figure II-25. Except at very low shear values, the ratios for the 20 megaton weapon are close to those for a 1 megaton weapon.

Because of the slow variation of pattern shape with dose level, a particular dose level can be chosen to illustrate the variations of length to maximum half-width ratio with wind speed and shear. Figure II-29 shows the variation of length to maximum half-width ratio for a 1 megaton weapon at a

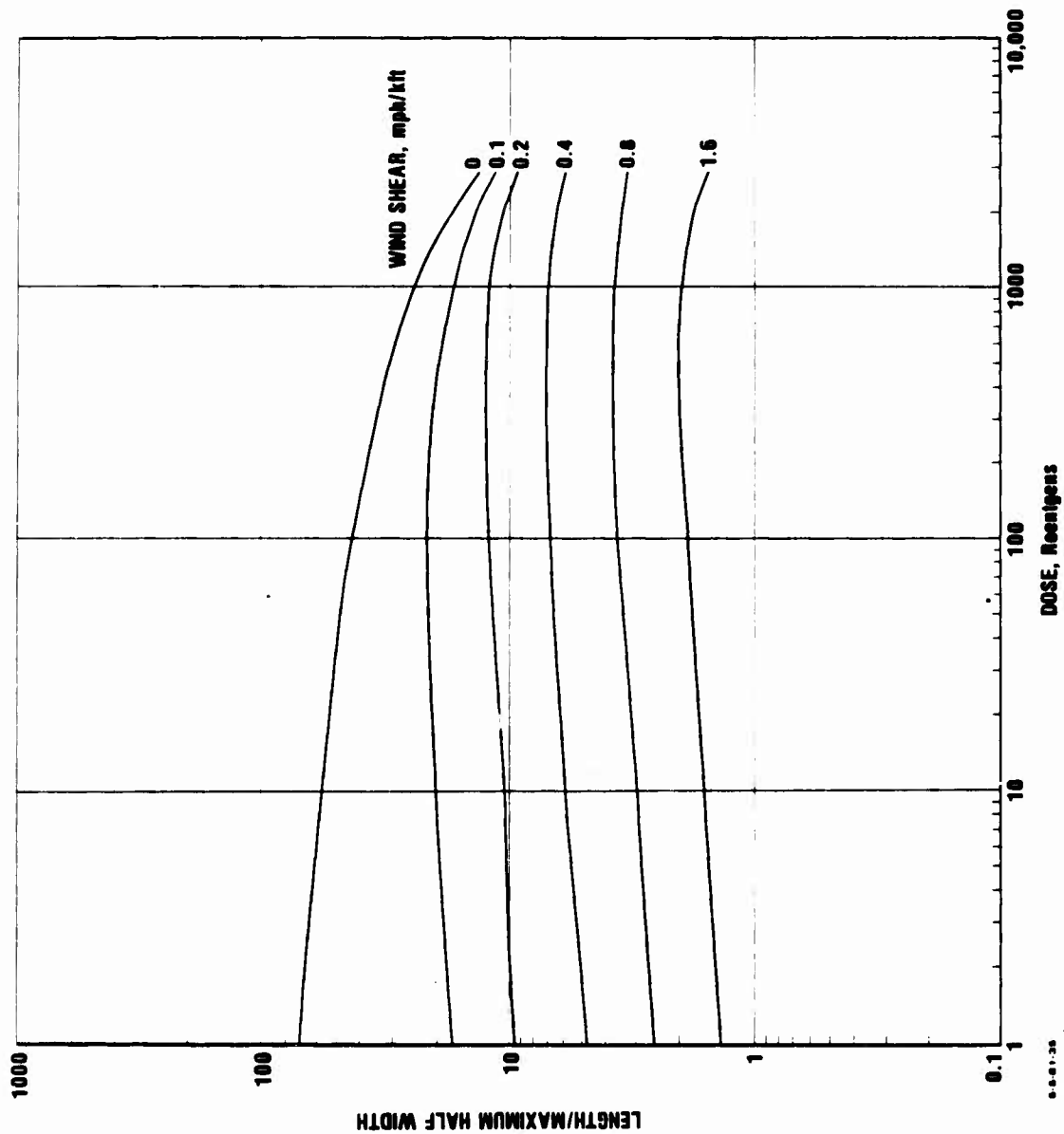


Figure II-25. RATIO OF LENGTH TO MAXIMUM HALF WIDTH AS A FUNCTION OF DOSE FOR A 1 MT YIELD WITH A 20 MPH WIND SPEED AND VARIOUS SHEARS.

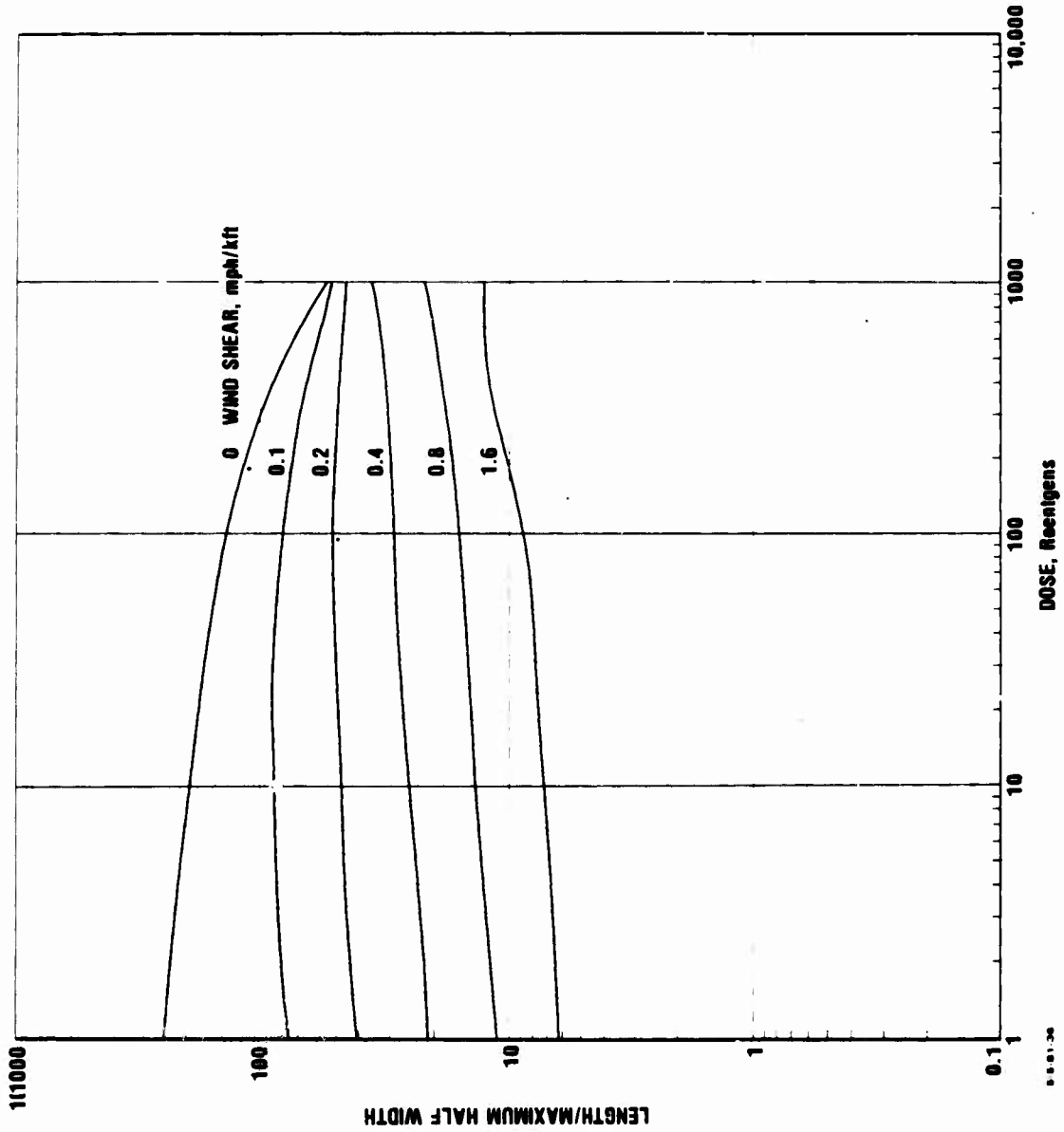


Figure II-26. RATIO OF LENGTH TO MAXIMUM HALF WIDTH AS A FUNCTION OF DOSE FOR A 1 MT YIELD WITH AN 80 MPH WIND SPEED AND VARIOUS SHEARS.

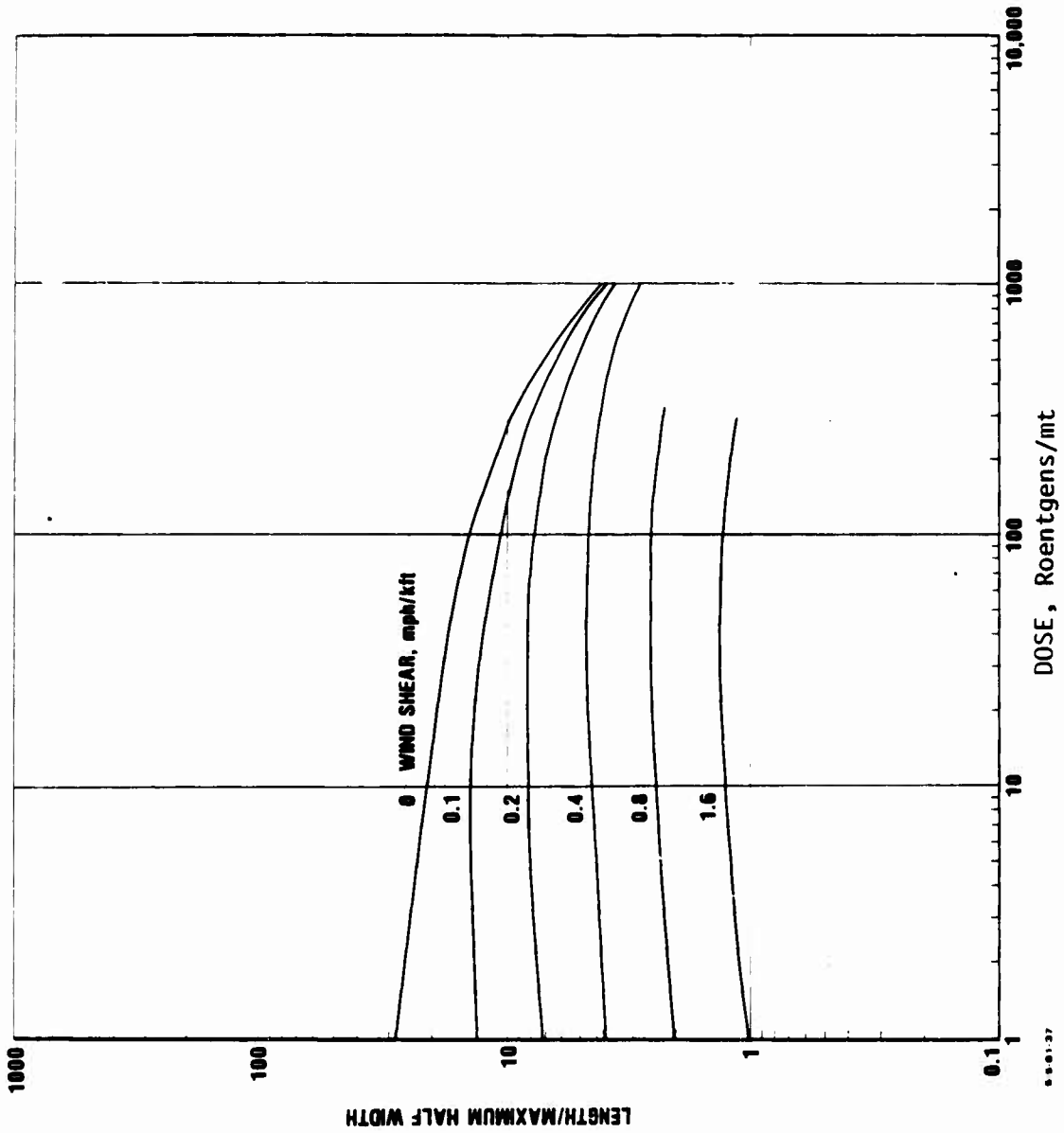


Figure II-27. RATIO OF LENGTH TO MAXIMUM HALF WIDTH AS A FUNCTION OF DOSE/MT FOR A 20 MT YIELD WITH A 20 MPH WIND SPEED AND VARIOUS SHEARS.

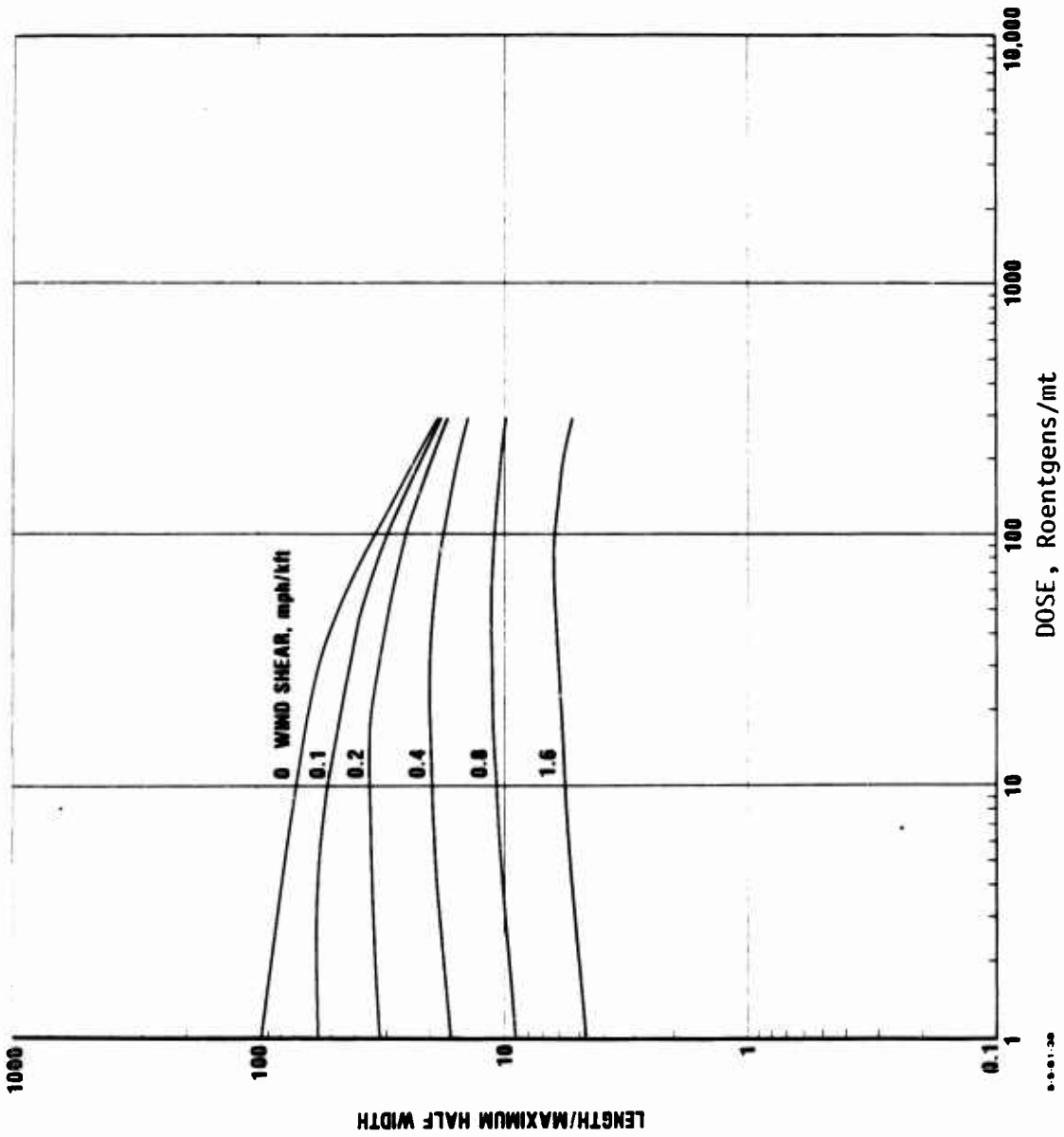


Figure II-28. RATIO OF LENGTH TO MAXIMUM HALF WIDTH AS A FUNCTION OF DOSE/MT FOR A 20 MT YIELD WITH A 80 MPH WIND SPEED AND VARIOUS SHEARS.

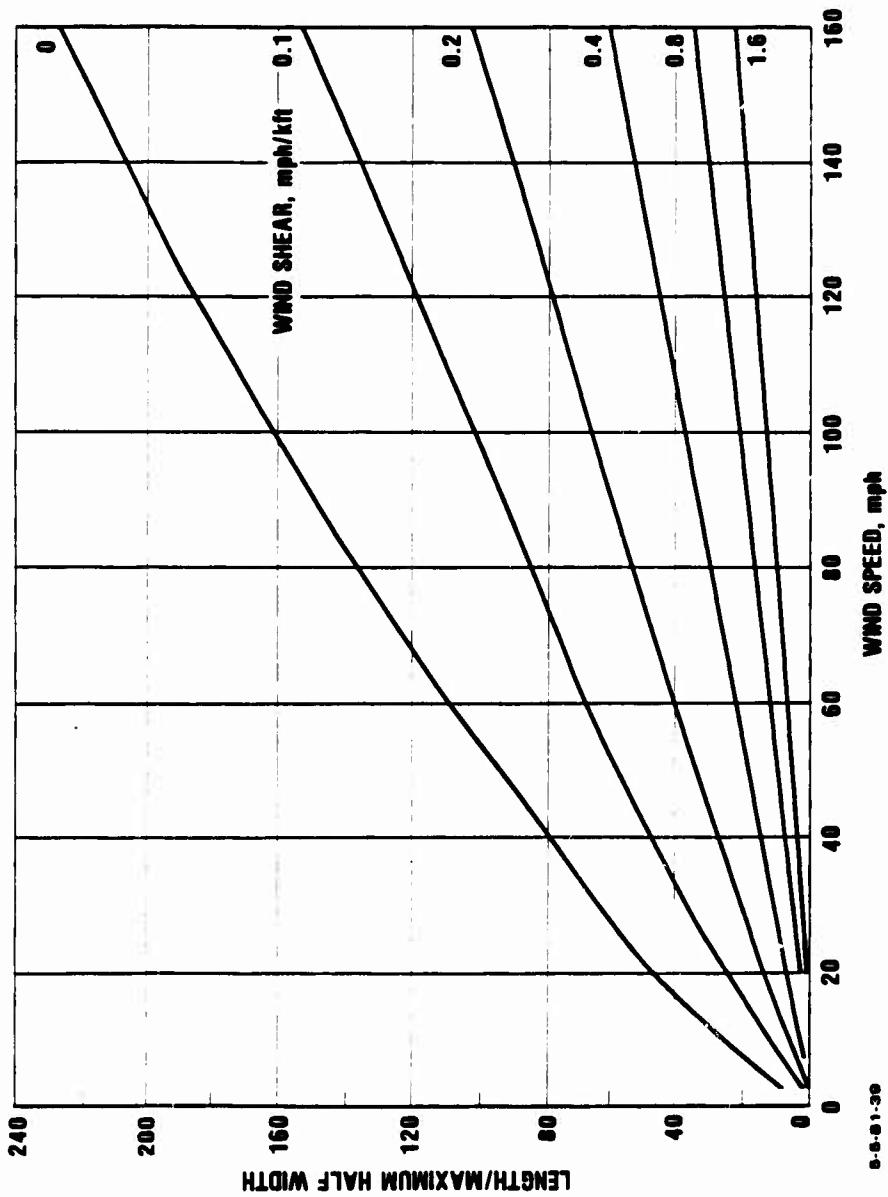


Figure II-29. RATIO OF LENGTH TO MAXIMUM HALF WIDTH AT A DOSE LEVEL OF 100 ROENTGENS AS A FUNCTION OF WIND SPEED FOR VARIOUS WIND SHEARS.

dose level of 100 Roentgens as a function of wind speed for various shears. An almost linear variation of the ratio with wind speed is obtained over the entire range. In Figure II-30 the same plot is presented except that the ordinate is expanded to emphasize the area near the origin. Again an almost linear variation is obtained. In Figure II-31 the same data are presented as contours of constant ratio as a function of wind speed and wind shear. Again nearly straight lines are obtained. From Figures II-29 and II-30 the slope of the ratio, R, as a function of shear can be obtained. This slope is presented in Figure II-32 as a function of wind shear. A linear function on logarithmic paper is obtained. The resulting equation to fit this curve is

$$\frac{dR}{dW} = 0.181 S^{-0.7973}$$

or equivalently

$$R = 0.181 W S^{-0.7973}$$

where W is wind speed in mph and S is wind shear in mph/kilofoot.

The effect of cluster standard deviation is shown in Figures II-33, II-34 and II-35 where pattern length and width are shown as a function of dose for cluster standard deviations of 10, 20 and 40 miles with a 40 mph wind speed and various shears. These figures should be compared with Figure II-21 for zero cluster standard deviation. The effect of a cluster standard deviation is the same as a shear in increasing pattern width. For a cluster standard deviation of 10 miles, pattern widths for shears of 0 to 0.1 mph/kilofoot are the same (within the resolution of the graph), for 20 mile standard deviation, pattern widths for shears of 0, 0.1 and 0.2 mph/kilofoot are the same; and for 40 miles all pattern widths

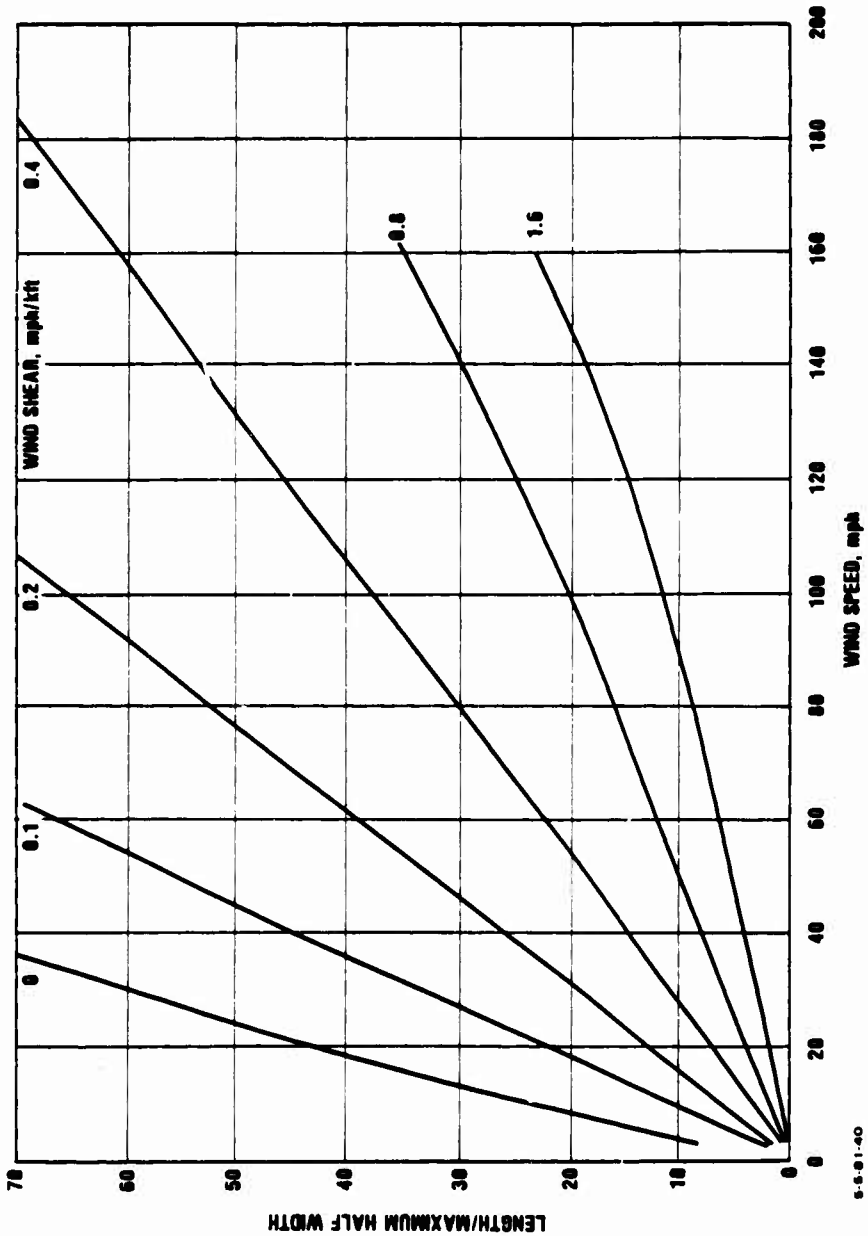
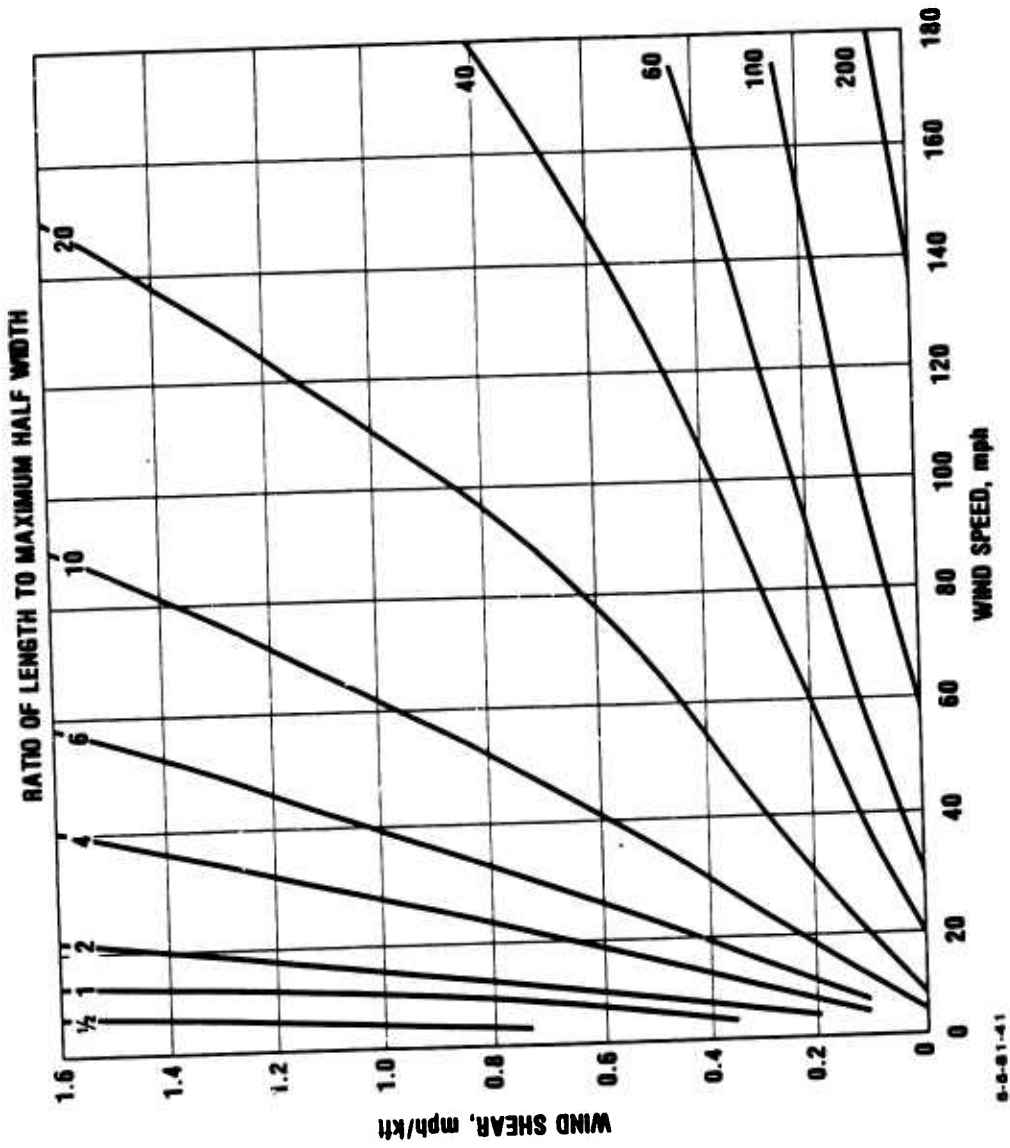


Figure II-30. RATIO OF LENGTH TO MAXIMUM HALF WIDTH AT A DOSE LEVEL OF 100 ROENTGENS AS A FUNCTION OF WIND SPEED FOR VARIOUS WIND SHEARS.



9-5-81-41

Figure II-31. CONTOURS OF CONSTANT RATIO OF LENGTH TO MAXIMUM HALF WIDTH AT 100 ROENTGENS DOSE FOR A 1 MT YIELD AS A FUNCTION OF WIND SPEED AND WIND SHEAR.

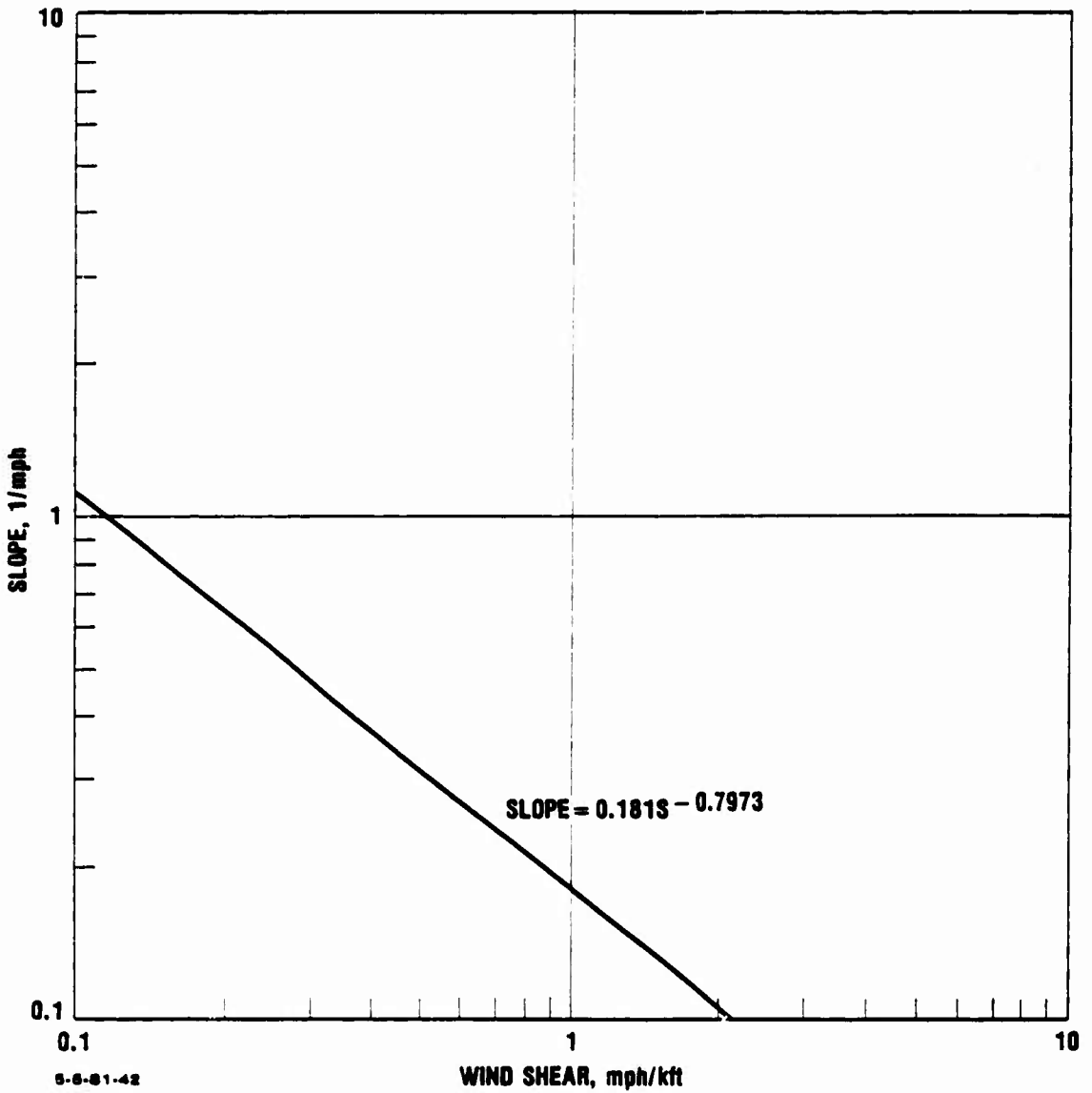


Figure II-32. SLOPE OF RATIO OF LENGTH TO MAXIMUM HALF WIDTH AS A FUNCTION OF WIND SHEAR FOR A 1 MT YIELD AT 100 ROENTGENS DOSAGE.

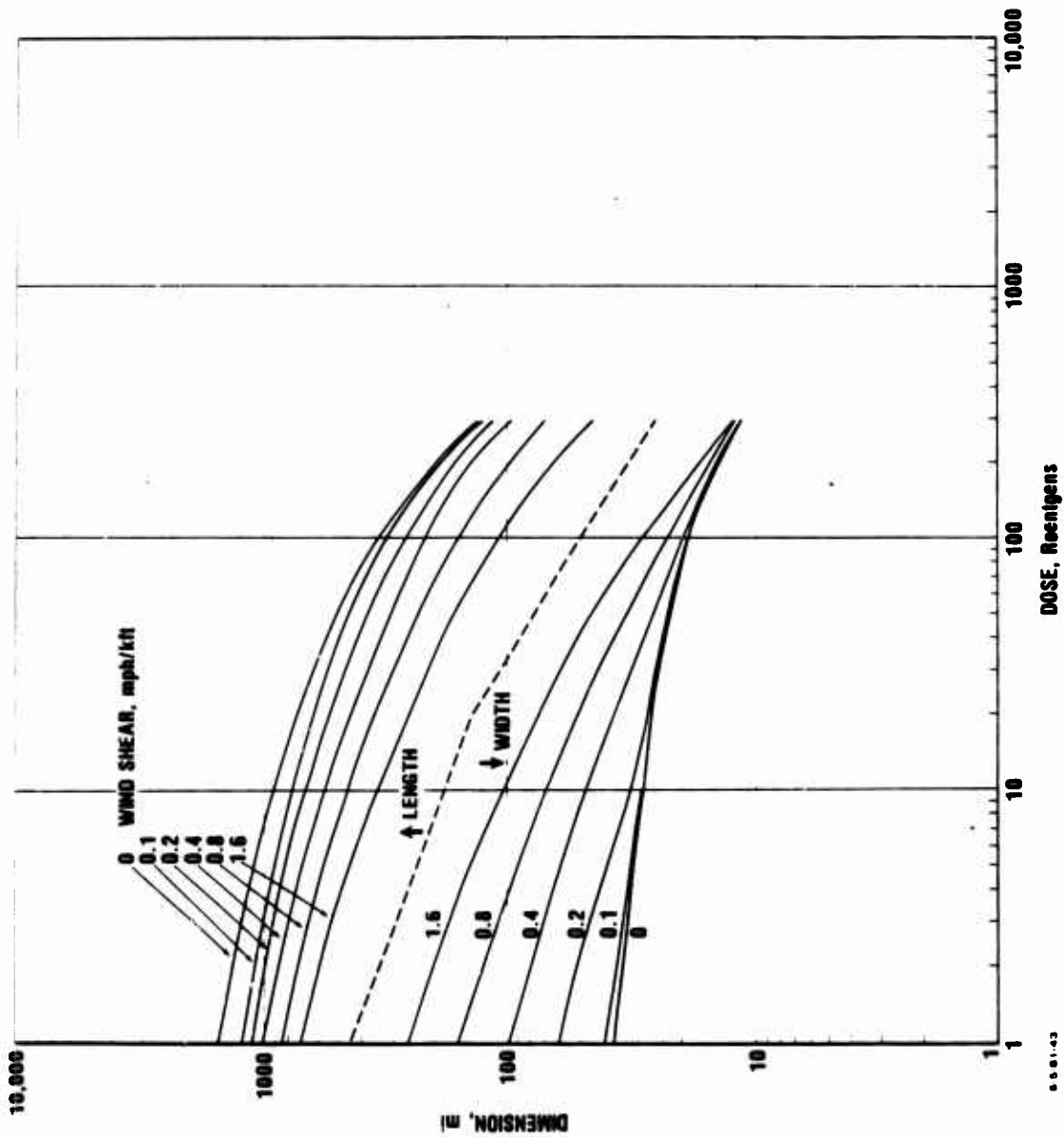


Figure II-33. PATTERN LENGTH AND WIDTH AS A FUNCTION OF DOSE FOR A 1 MT YIELD WITH A CLUSTER STANDARD DEVIATION OF 10 MILES FOR A 40 MPH WIND SPEED AND VARIOUS WIND SHEARS.

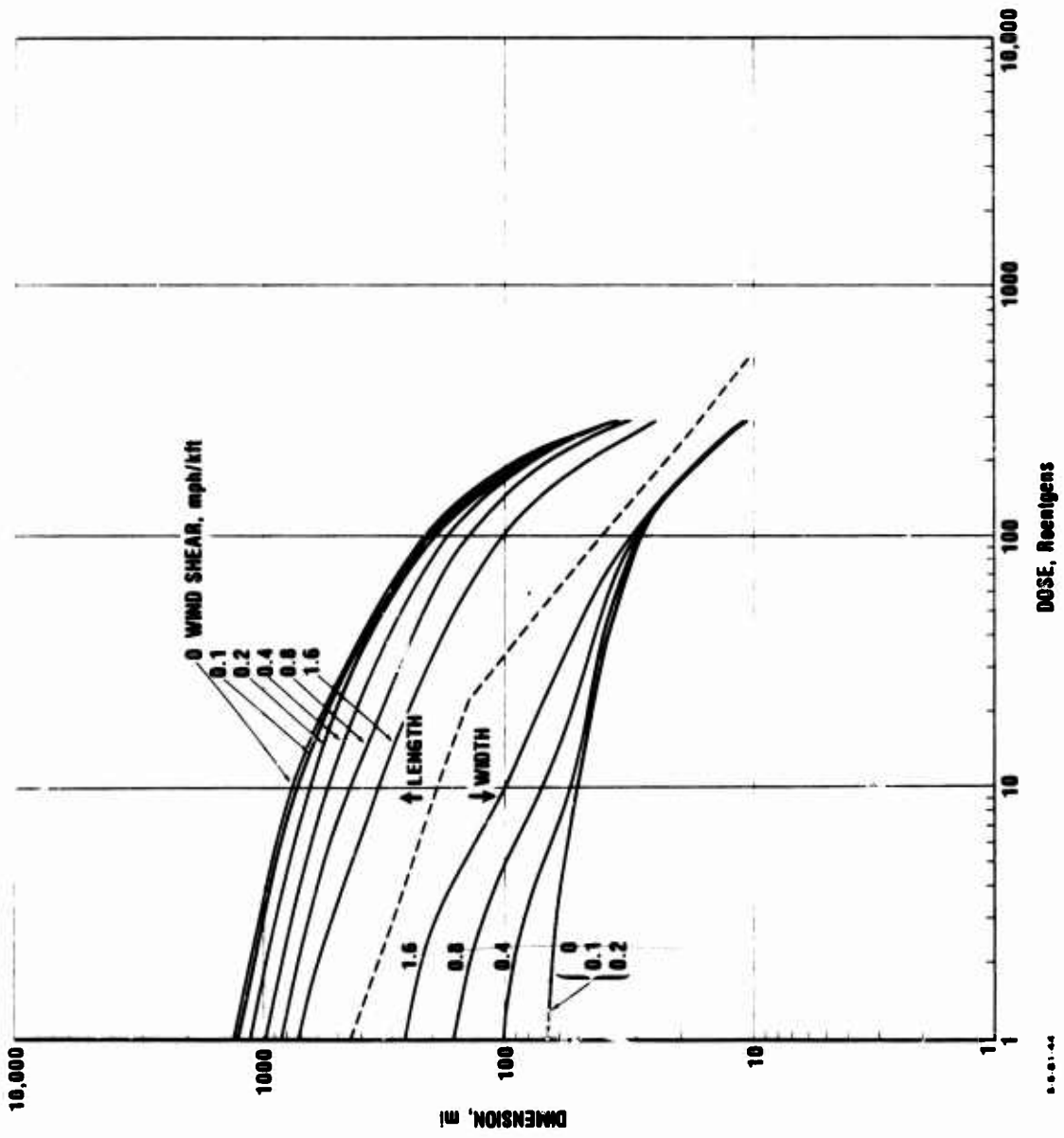


Figure II-34. PATTERN LENGTH AND WIDTH AS A FUNCTION OF DOSE FOR A 1 MT YIELD WITH A CLUSTER STANDARD DEVIATION OF 20 MILES FOR A 40 MPH WIND SPEED AND VARIOUS WIND SHEARS.

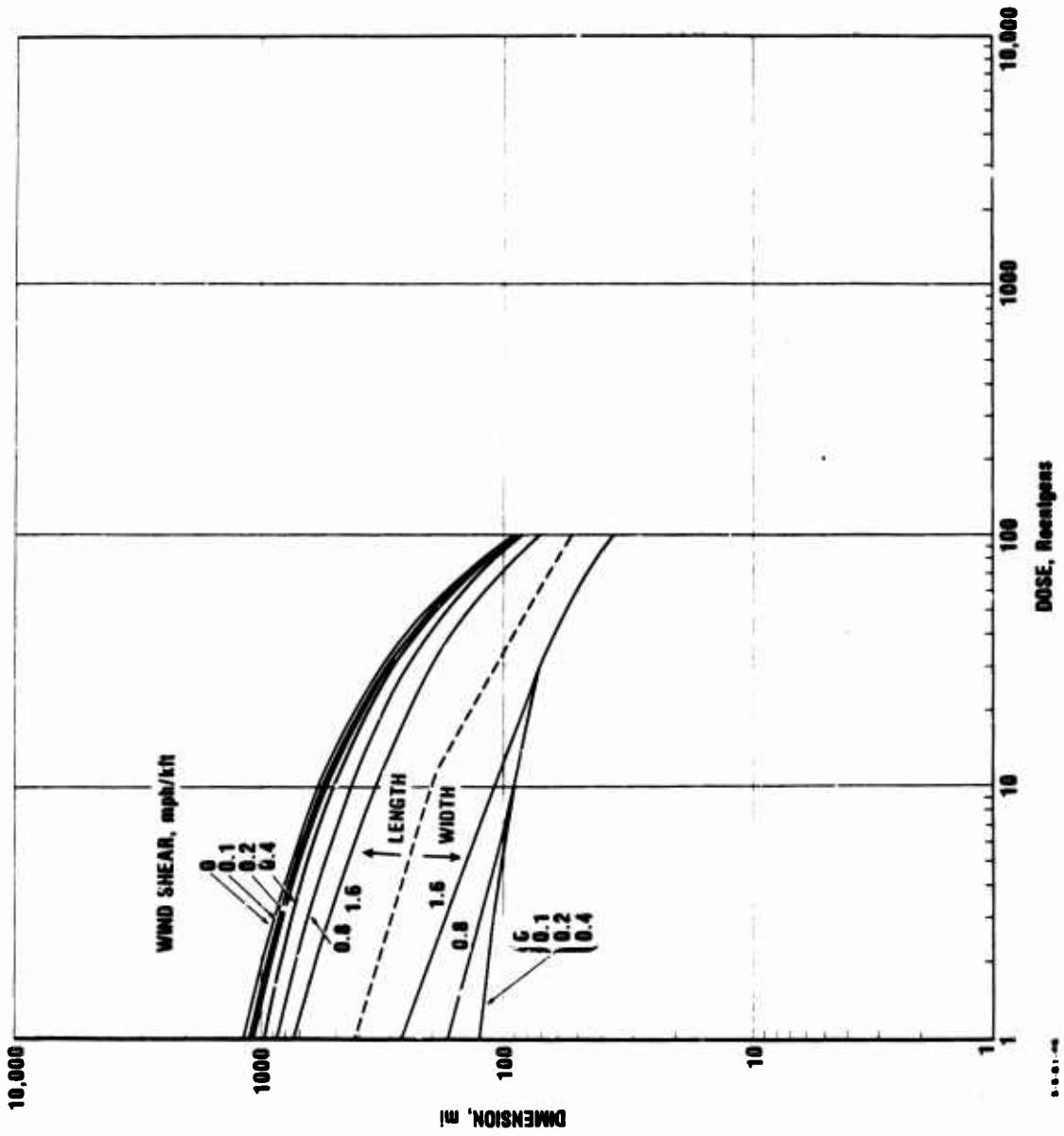


Figure II-35. PATTERN LENGTH AND WIDTH AS A FUNCTION OF DOSE FOR A 1 MT YIELD WITH A CLUSTER STANDARD DEVIATION OF 40 MILES FOR A 40 MPH WIND SPEED AND VARIOUS WIND SHEARS.

for shears from 0 to 0.4 mph/kilofoot are the same. These widths are the same since the cluster standard deviation dominates the spread due to wind shear. As the cluster standard deviation becomes larger, the mechanisms determining pattern length and width change (the width due to cluster standard deviation and the length due to the requirement to conserve the total amount of radioactivity), so that pattern length to width ratios become more dependent on dose level. Thus the simplification used with 0 standard deviation of considering pattern shape invariant with changes of dose level in the interesting ranges of doses cannot be applied here.

Finally, in Figure II-36 the effect of wind speed on pattern length and width is illustrated for a nominal 0.2 mph/kilofoot shear with a cluster standard deviation of 40 miles. The higher wind speeds show a more rapid decrease in pattern length, as would be expected since these higher speeds carry radioactivity at low dose levels further downwind at the expense of the higher levels. The pattern widths show a surprising degree of regularity. It is interesting to note that at a 1 Roentgen dose, the width ranges from about $2\frac{1}{2}$ to 4 cluster standard deviations, and that the pattern size begins to rapidly decrease at a pattern width which is about $1\frac{1}{2}$ to 2 cluster standard deviations.

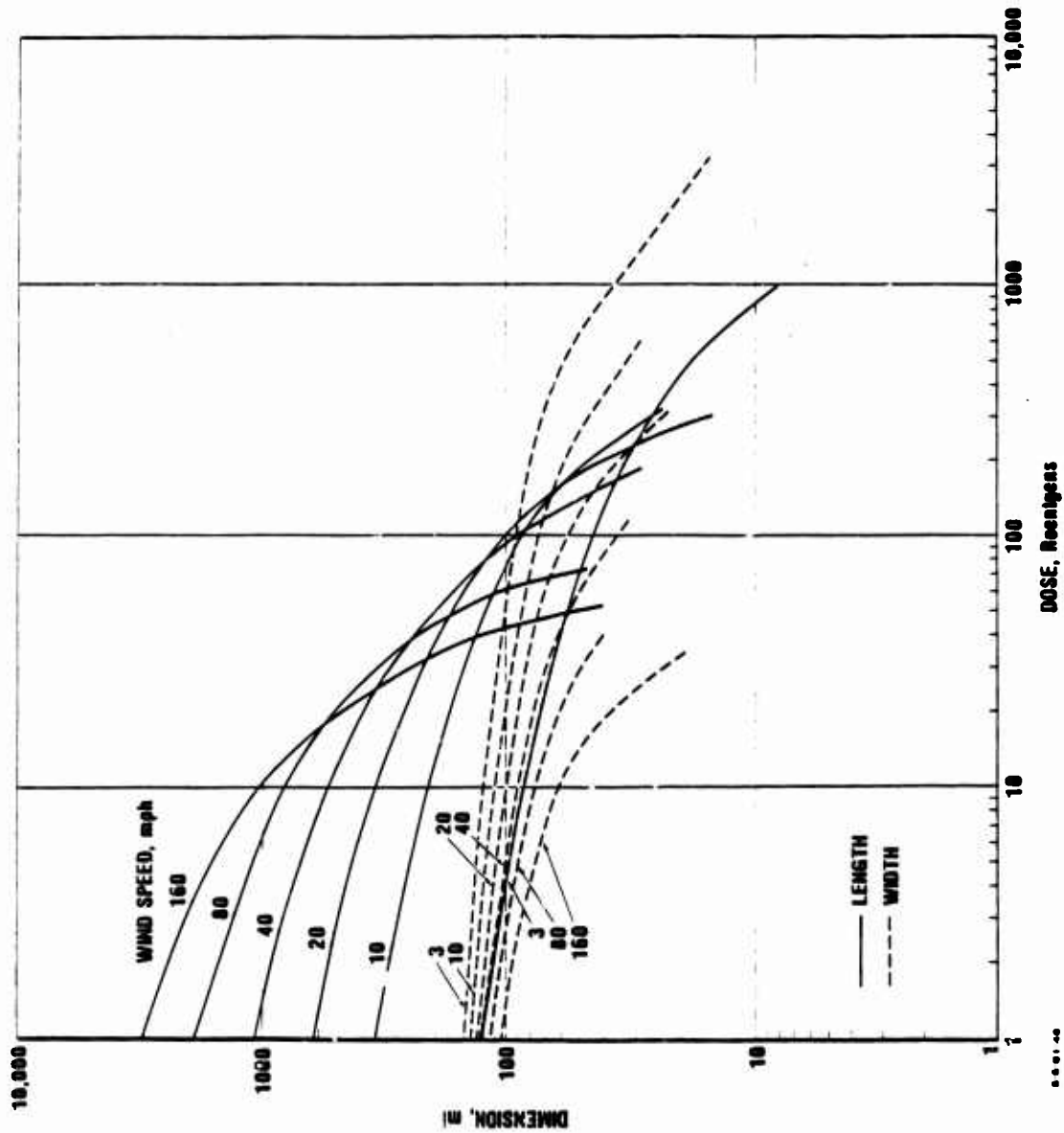


Figure II-36. PATTERN LENGTH AND WIDTH AS A FUNCTION OF DOSE FOR A 1 MT YIELD WITH A CLUSTER STANDARD DEVIATION OF 40 MILES FOR A 0.2 MPH/KILOFOOT WIND SHEAR AND VARIOUS WIND SPEEDS.

Chapter III

THE WINDS

A. GENERAL DESCRIPTION

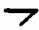




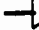

The effective fallout winds, one for each month of the year, used in this report to connect the fallout debris are from the twelve "most probable winds" of R. Mason, Command and Control Technical Center [Ref. 5]. The following quotation from [Ref. 5] describes these winds: "The fallout winds are calculated using the set of winds for a given day from each calendar month. Each set of winds was selected not because it represented a specific pattern most likely to be duplicated in the future, but rather because the characteristics most frequently observed for that month (locations of highs and lows and wind flow patterns) were present in that set. These winds are actual winds from a specific day, and since the atmosphere is a fluid, one should not expect the exact pattern to be duplicated at any time in the future. However, these "most probable" winds do represent the flow as it might be expected to occur, provided no unusual atmospheric conditions are present.

The twelve sets of winds are available with the data (five standard pressure surfaces) located on the SAC Weather Grid. When these data are treated mathematically, integrated fallout winds are obtained for each grid point."

The winds selected from [Ref. 5] are "level E" winds, which are to be used for yields of one megaton or greater (all references to winds in this study are effective

fallout winds, (winds averaged over a number of altitudes) not actual or "raw" winds.) Plots of these winds taken from [Ref. 5] are shown in Figures III-1a to III-1L.

The plots in [Ref. 4] are on a polar stereographic projection of the portion of the northern hemisphere extending from 10° latitude to 90° latitude. Figure III-1 shows that portion of the map covering the continental United States. The wind direction is given by the direction of the arrows. The length of each arrow gives the wind speed, with each inch representing 109 knots or 125 miles/hour. Wind speeds less than five miles/hour are represented by circles. The shape of the arrowhead represents the value of the wind shear,¹ in knots/kilofoot, according to the following legend:

Shape	Wind Shear Range
	0.00 - 0.05
	0.05 - 0.15
	0.15 - 0.20
	0.20 - 0.25
	0.25 - 0.30
	0.30 - 0.45
	0.45 - UP

The raw wind data were received on a magnetic tape from the Command and Control Technical Center and processed as described in [Ref. 4]. The effective fallout winds were calculated at the intersection of a two degree grid by interpolation from the polar stereographic grid. (The two degree spacing was chosen for convenience in the data processing.) The average distance between points in the United States for the original grid is about 190 miles, and for the new grid is about 140 miles in the North South direction and 110 miles in the East West direction. Thus the detail shown in the new

¹This is a "fallout wind shear" as defined in reference 1, not the usual meteorological wind shear.

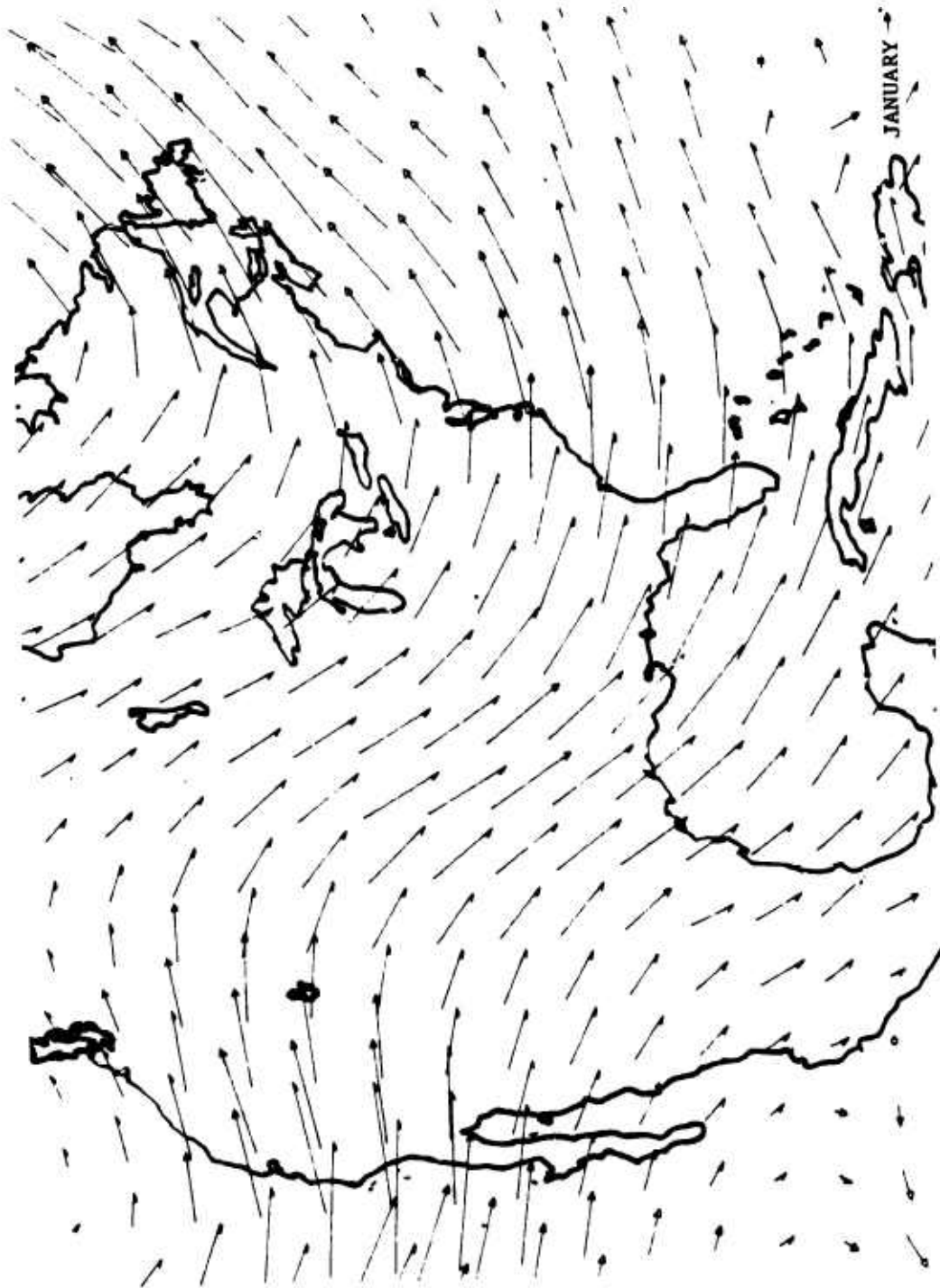


Figure III-1a . EFFECTIVE FALLOUT WIND VECTORS FOR THE MONTH OF JANUARY

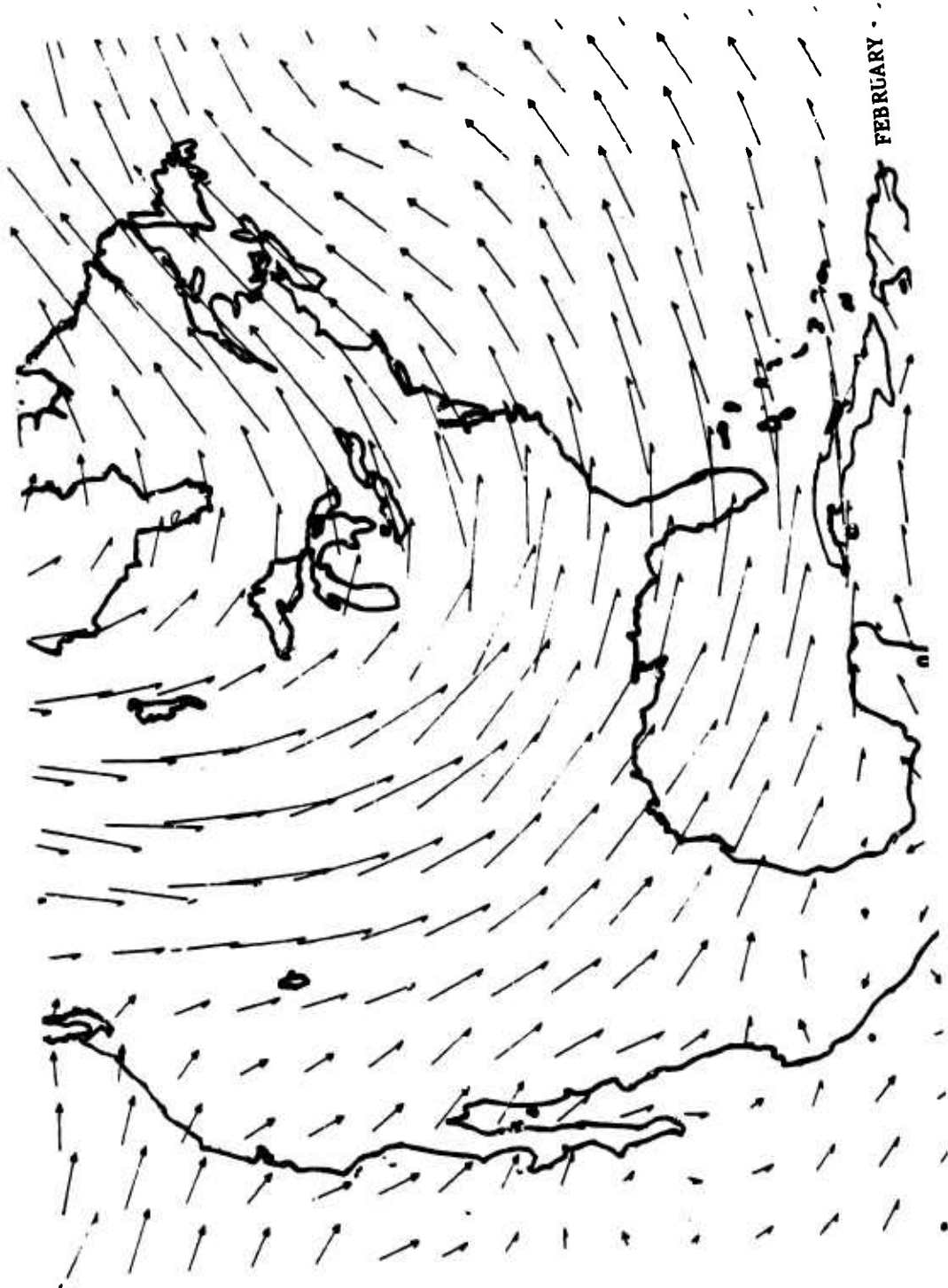


Figure III-1b. EFFECTIVE FALLOUT WIND VECTORS FOR THE MONTH OF FEBRUARY

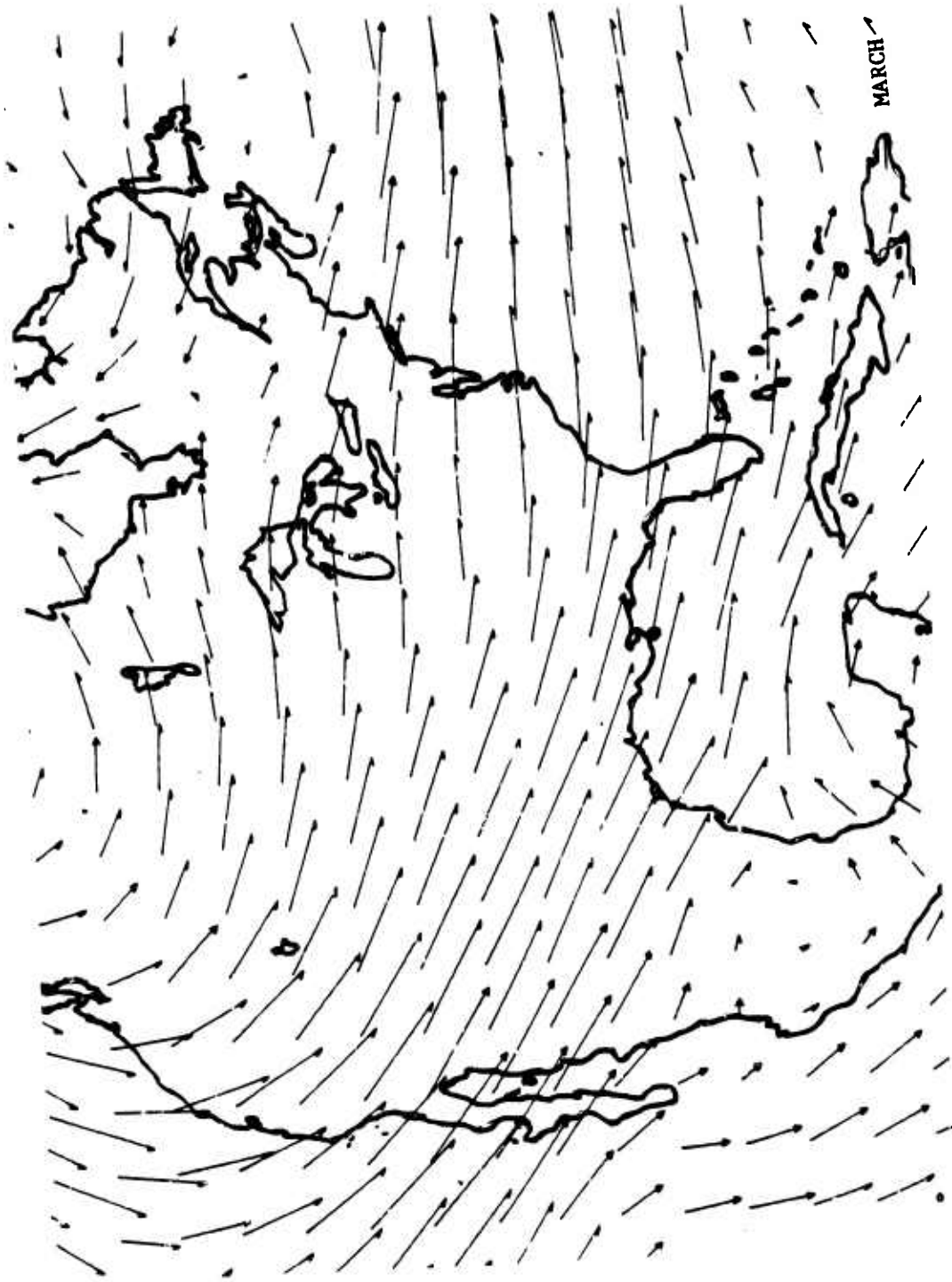


Figure III-1c. EFFECTIVE FALLOUT WIND VECTORS FOR THE MONTH OF MARCH

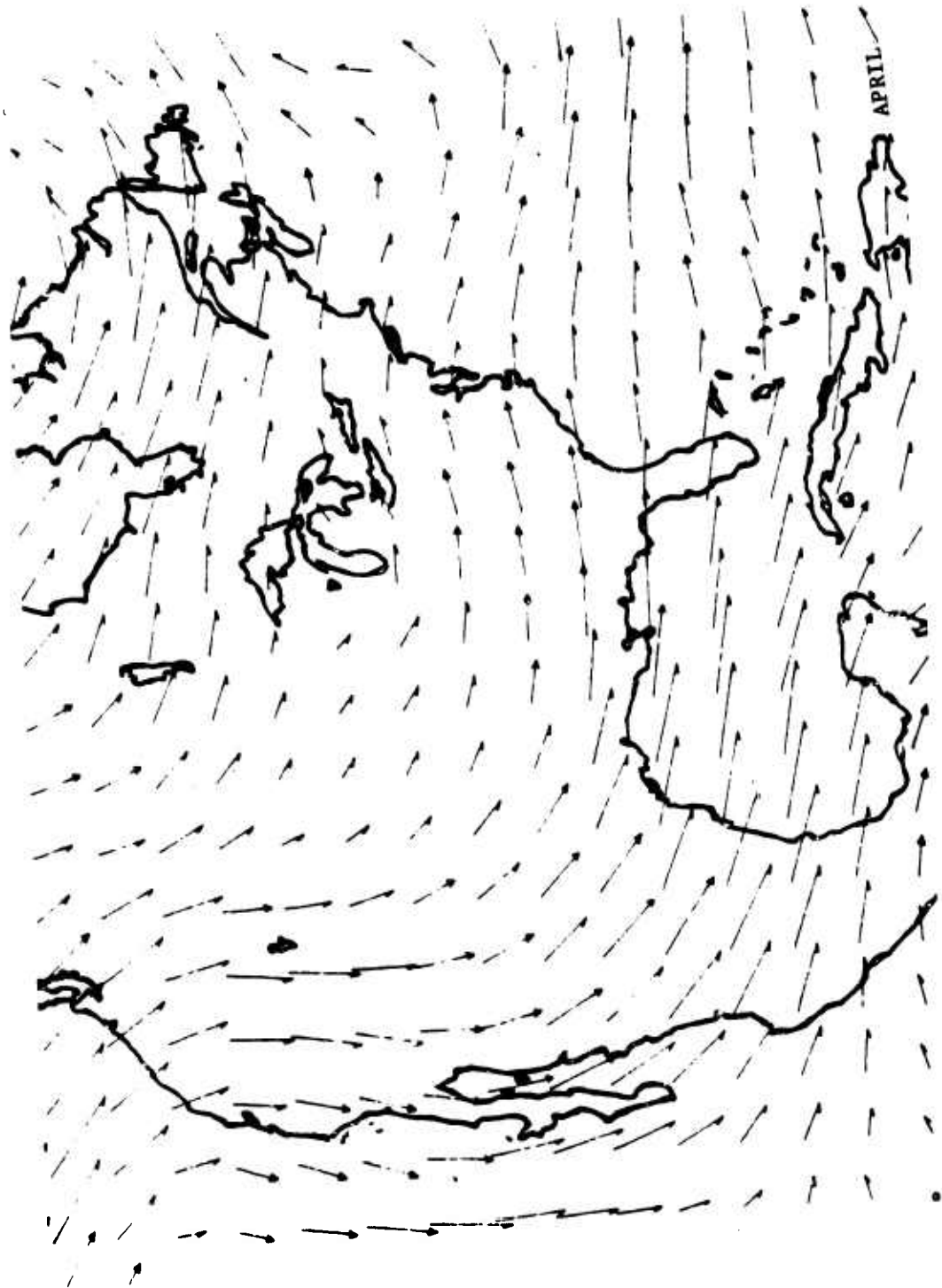


Figure III-1d. EFFECTIVE FALLOUT WIND VECTORS FOR THE MONTH OF APRIL

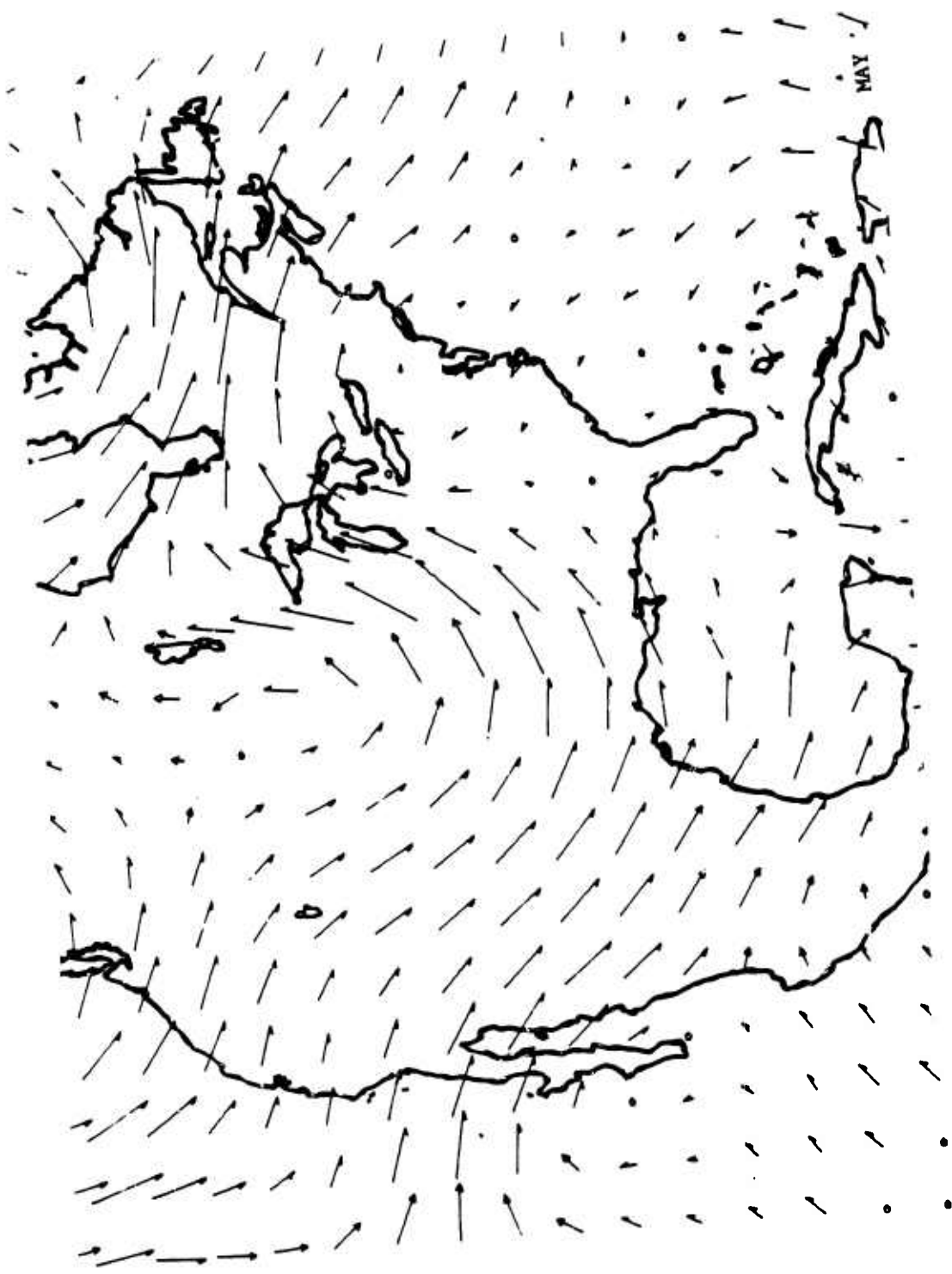


Figure III-le. EFFECTIVE FALLOUT WIND VECTORS FOR THE MONTH OF MAY

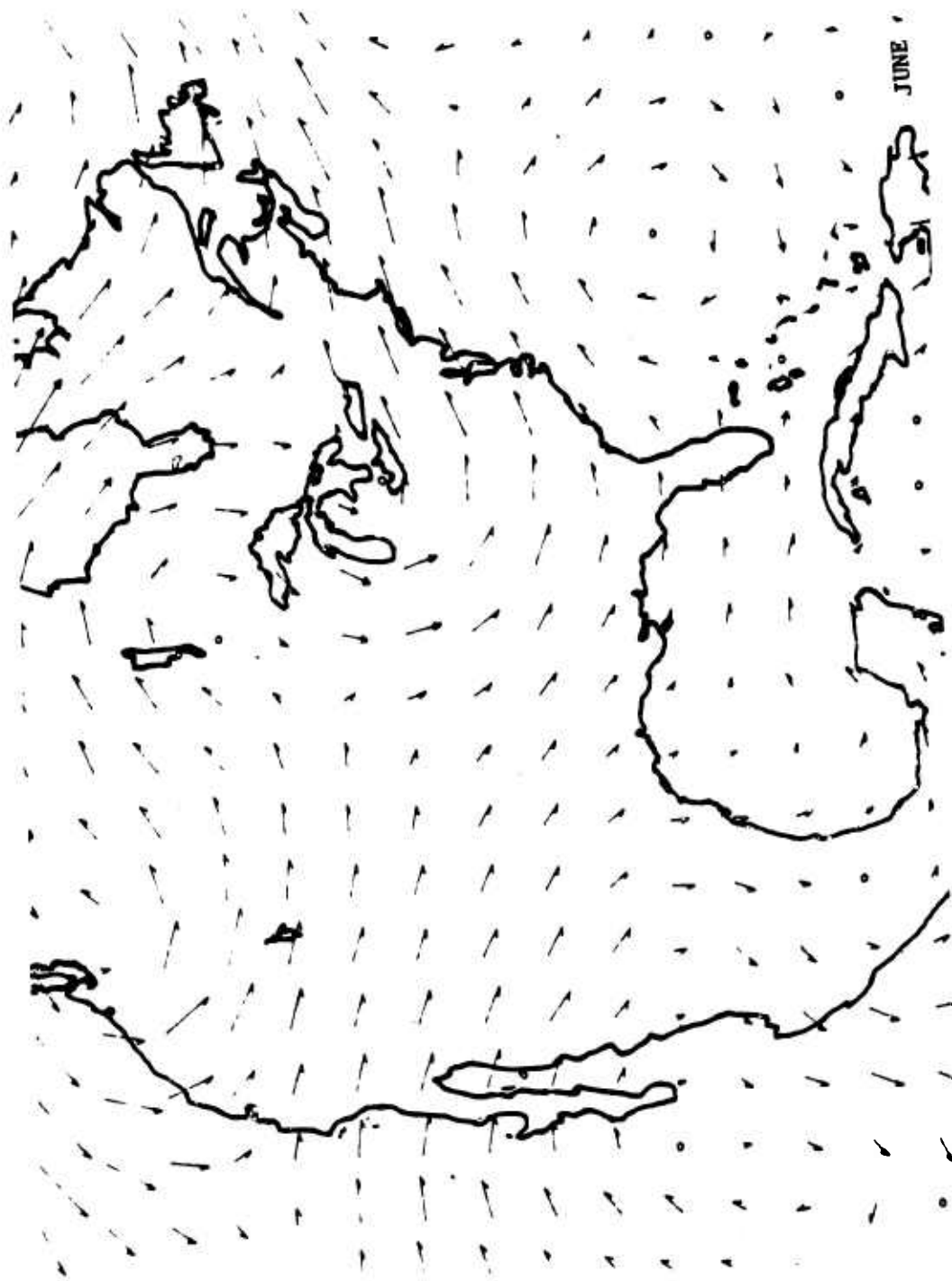


Figure III-1f. EFFECTIVE FALLOUT WIND VECTORS FOR THE MONTH OF JUNE

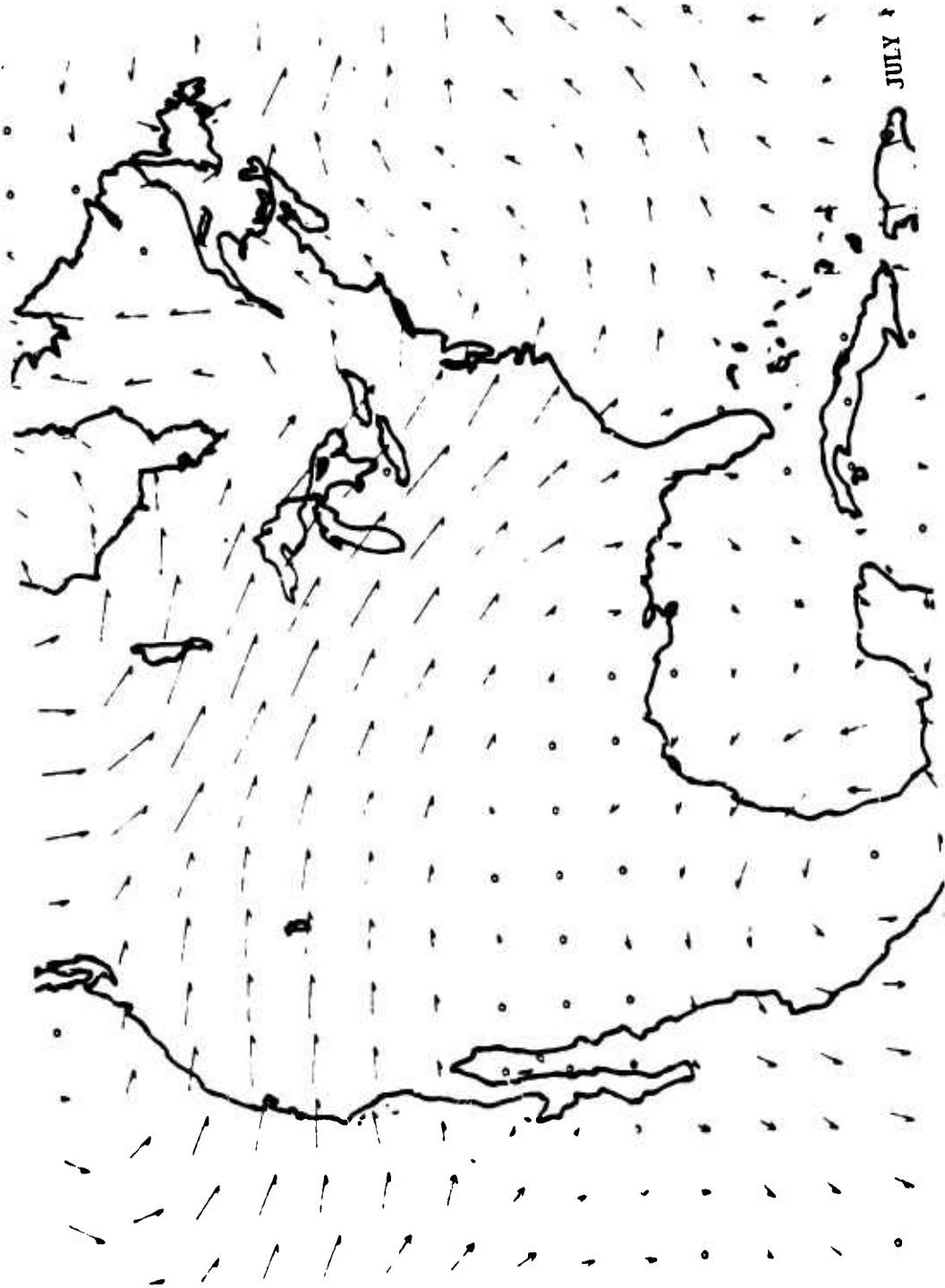


Figure III-19. EFFECTIVE FALLOUT WIND VECTORS FOR THE MONTH OF JULY

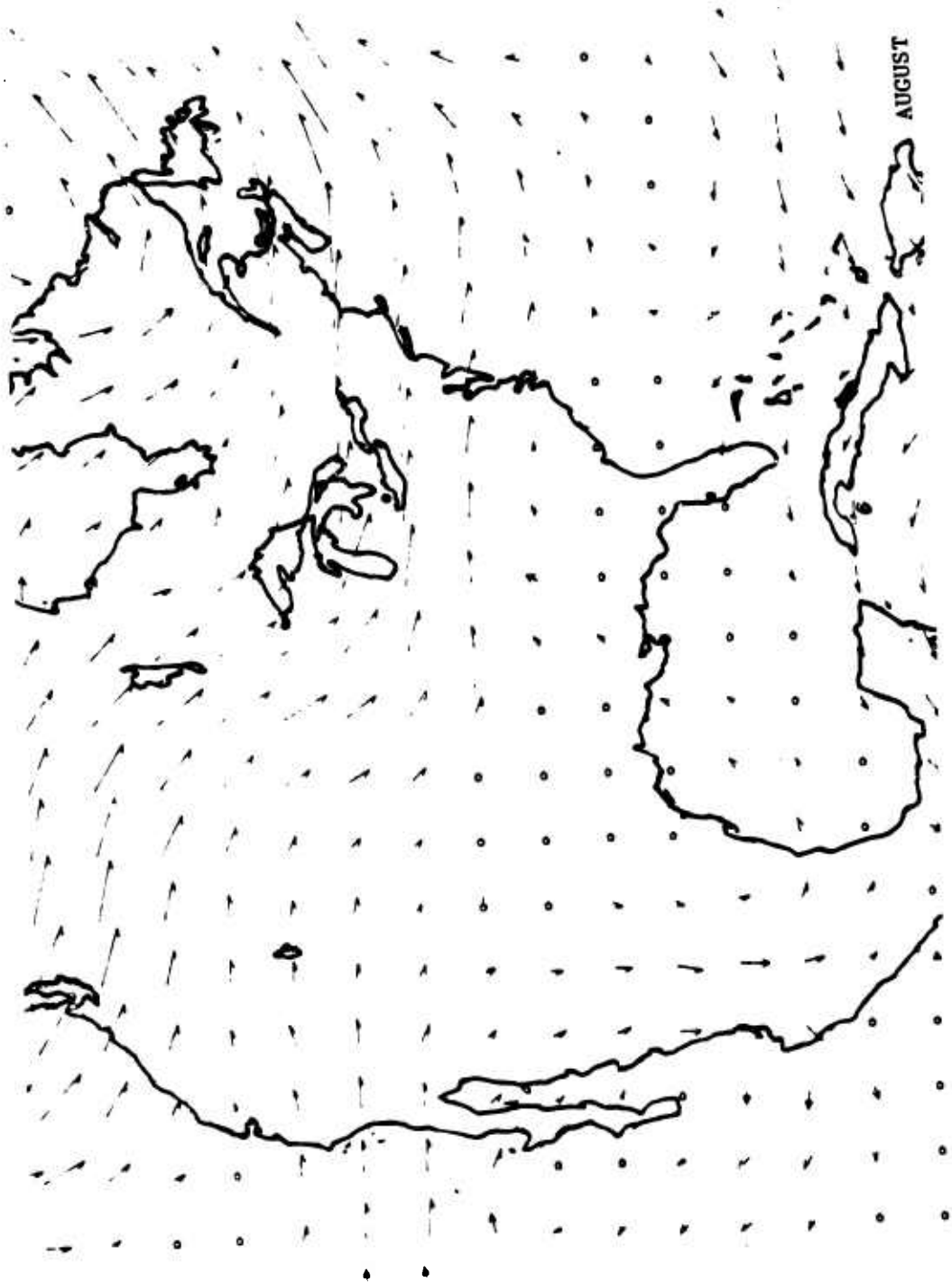


Figure III-1h. EFFECTIVE FALLOUT WIND VECTORS FOR THE MONTH OF AUGUST

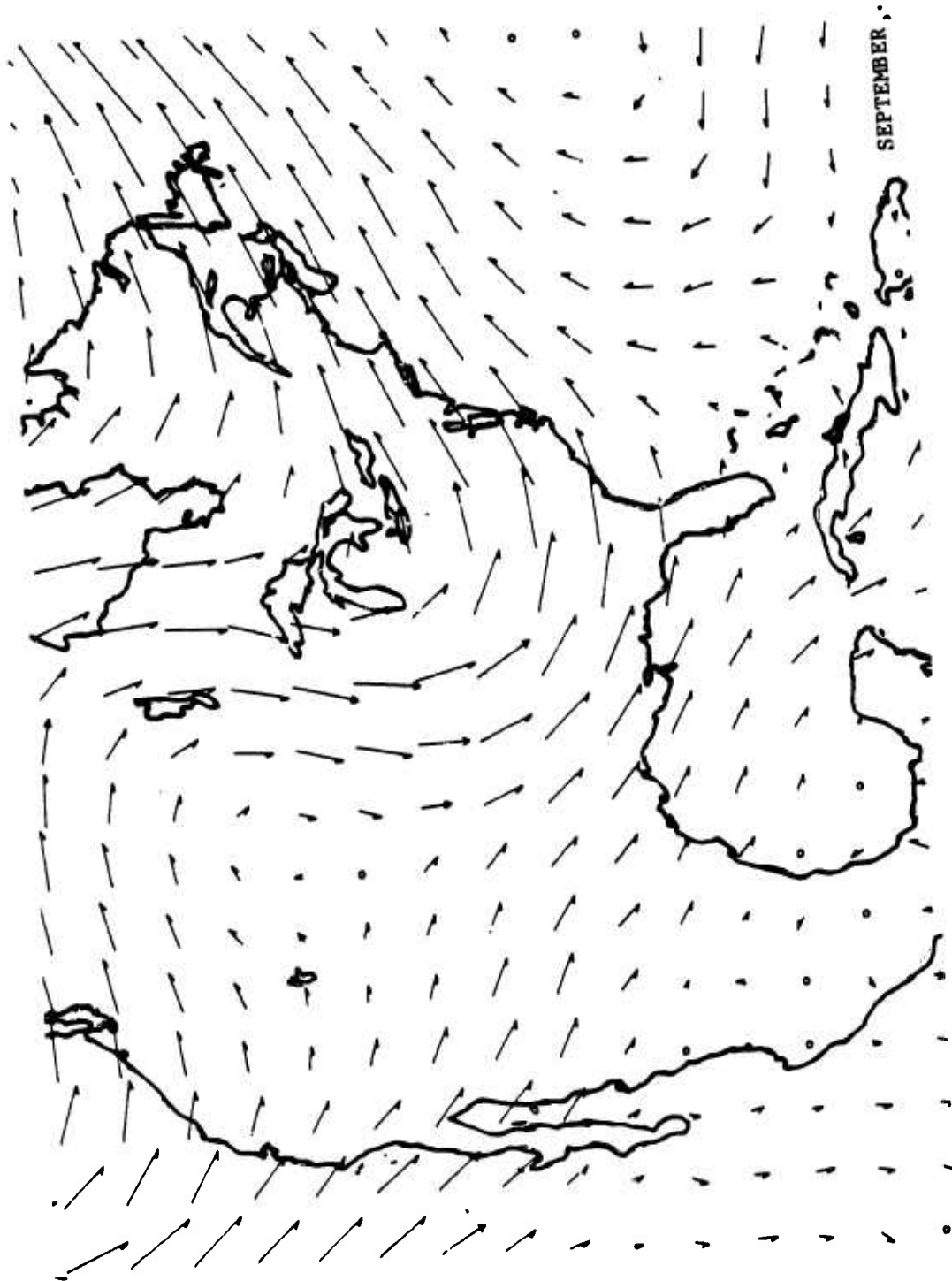


Figure III-1i. EFFECTIVE FALLOUT WIND VECTORS FOR THE MONTH OF SEPTEMBER

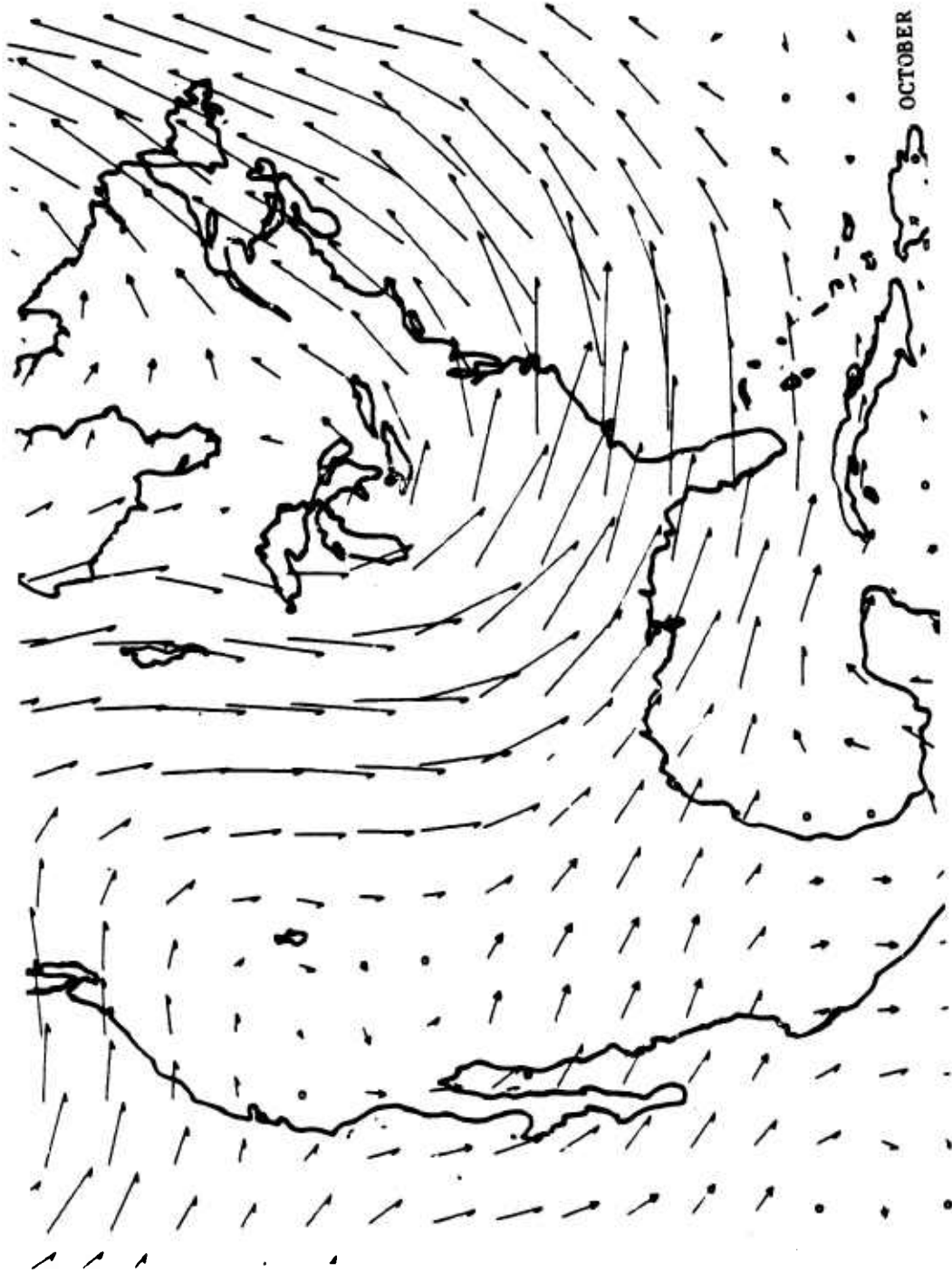


Figure III-1j. EFFECTIVE FALLOUT WIND VECTORS FOR THE MONTH OF OCTOBER

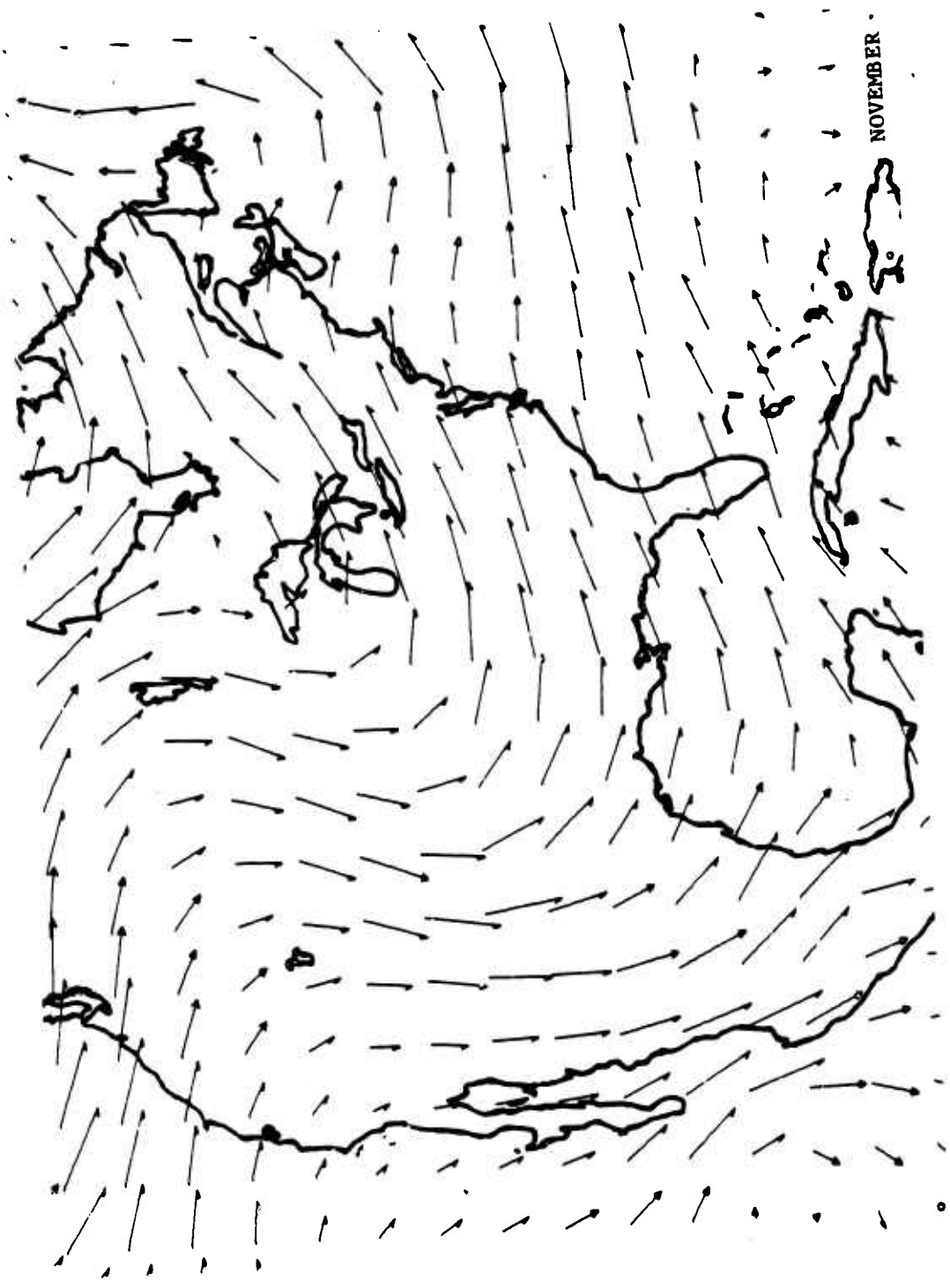


Figure III-1k. EFFECTIVE FOLLOW-UP WIND VECTORS FOR THE MONTH OF NOVEMBER

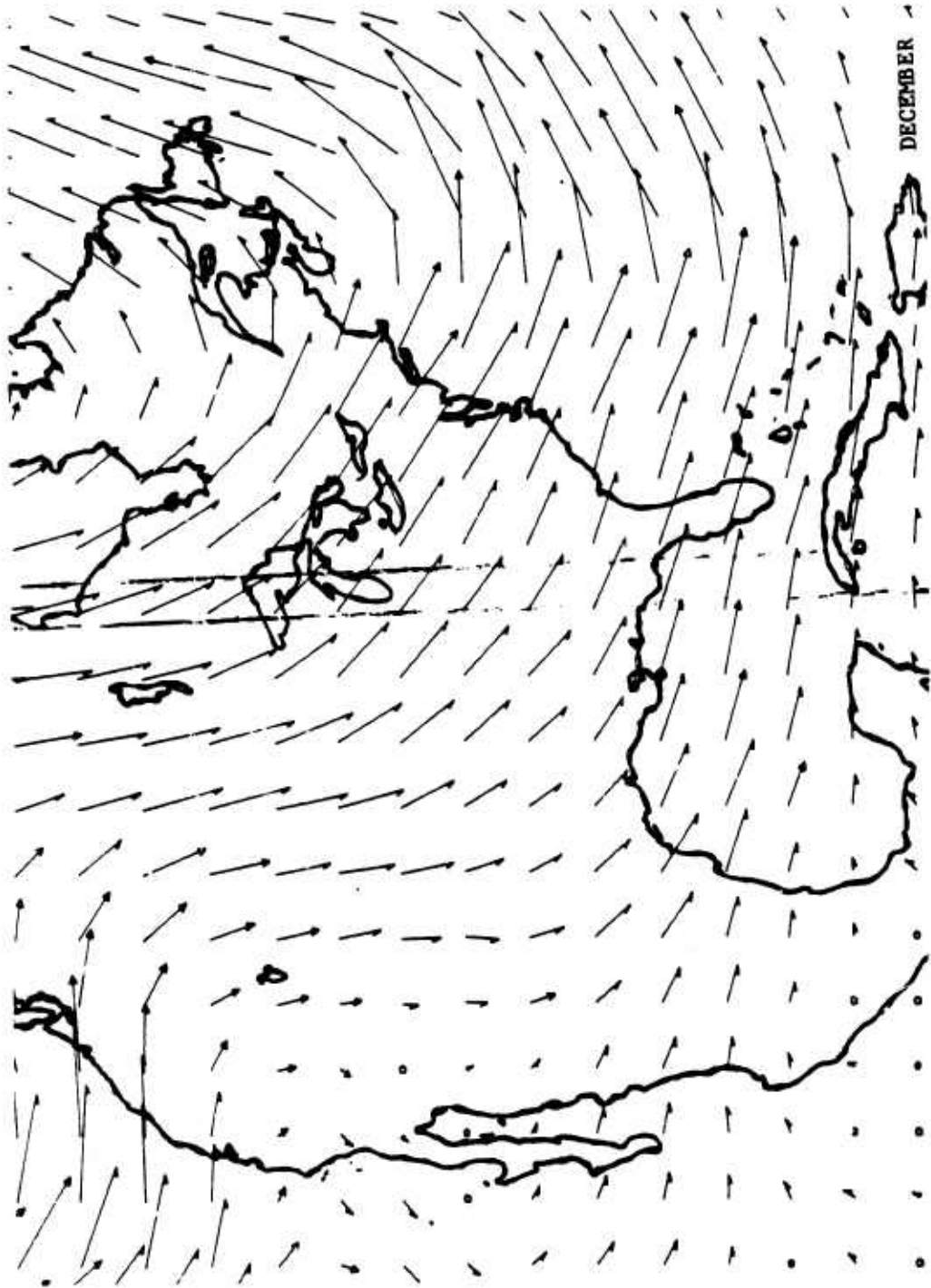


Figure III-11. EFFECTIVE FALLOUT WIND VECTORS FOR THE MONTH OF DECEMBER

grid is somewhat greater than the resolution of the original data. The two degree grid extends from 24° North latitude to 50° and from 65° West longitude to 125 degrees. All wind statistics discussed here refer to wind data on this two degree grid.

B. OVERALL WIND SPEED AND WIND SHEAR

The wind grid for each month has 434 points; for the 12 months there are a total of 5208 points. The mean wind speed for all these points is 40.8 mph, with a standard deviation for the wind speeds of 22.7 mph. The mean wind shear for these points is 0.126 mph/kilofoot, with a standard deviation of the wind shear of 0.107 mph/kilofoot. From a sample of this size there is about a 99 percent chance that due to sampling statistics alone, the true mean wind speed is within one mph of the calculated mean, and the true wind shear is within .005 mph/kilofoot of the calculated mean. It must be recalled; however, that these statistics were collected for winds on only 12 days, and there is partial, but not perfect, correlation between winds in different parts of the country. The limited sample of days will thus introduce a greater error into estimating the true mean effective fallout wind, but the magnitude of this error cannot be estimated from these limited data. However, for the purposes of explaining the characteristics of the fallout patterns in this report, we need only be concerned with the statistics of these 12 particular winds. Some percentile values for the wind speed and shear are:

	Minimum	10 Percentile	50 Percentile	90 Percentile	Maximum
Wind Speed	.3	7	36	68	118
Wind Shear	0.00	.005	.07	.23	.67

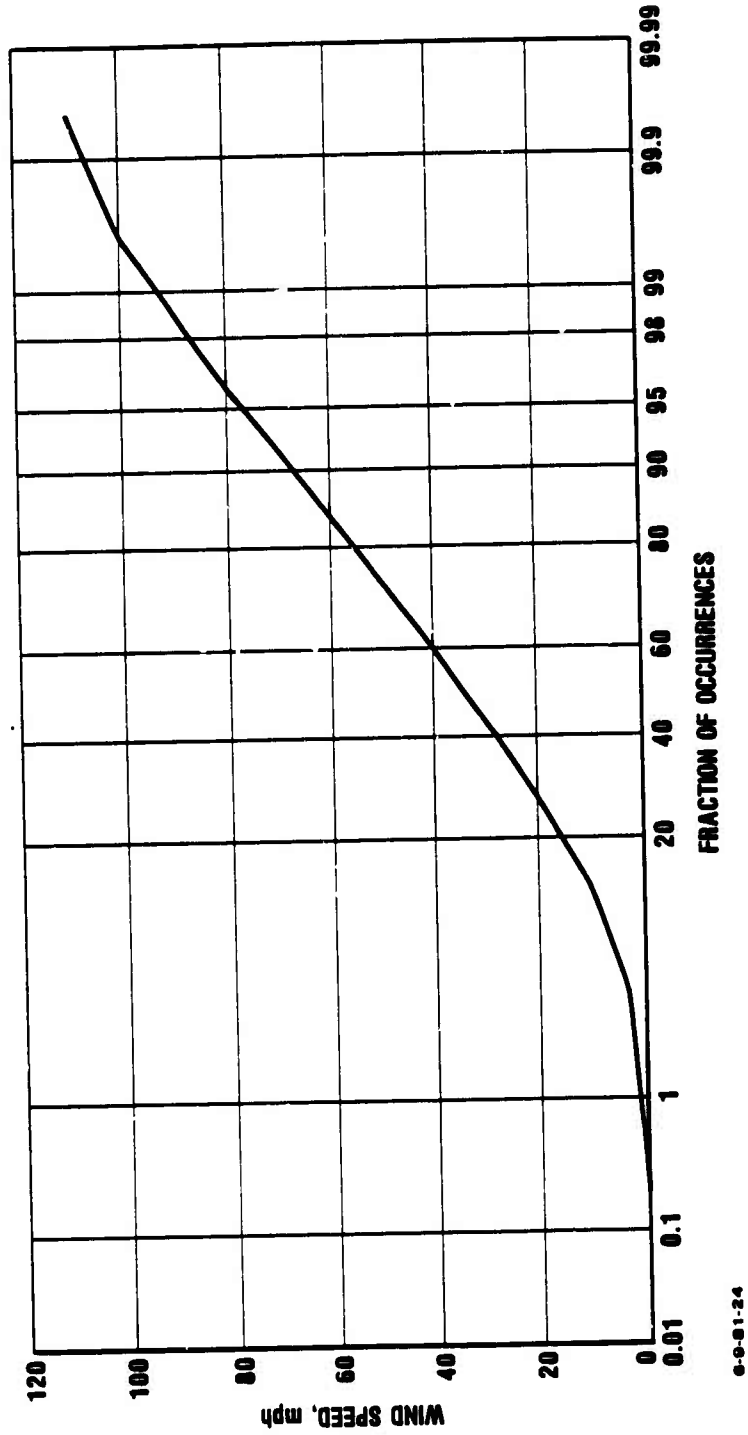
Both for the wind speed and wind shear, the median value is appreciably below the average.

Graphs of wind speed and wind shear versus cumulative fractions of occurrences are presented in Figures III-2 and III-3, plotted on normal probability paper. For wind speeds between 20 and 100 mph a reasonably straight line is obtained indicating an approximately normal distribution within range. The top curve in Figure III-3 is the direct cumulative histogram of the wind shear. Below values of about 0.2 the shear appears to depart seriously from a normal distribution. The bottom curve represents a distribution which has the shape of half a normal distribution. It begins at the 50 percent occurrence level. The number of occurrences are divided by 2 to preserve normalization. A straight line in this plot would indicate a normal distribution with mean zero, with the negative half of the distribution folded over and added to the positive half. As is seen, a better empirical approximation to such a distribution is obtained for low wind shear values.

In Figures III-4 and III-5, histograms of the wind speed and wind shear values are presented. Here the difference in behavior of the distributions for small values of the variables is clearly indicated. Very low wind speeds become less frequent while very low shear values are the most frequent. If this result seems counterintuitive it must be recalled that statistics of effective fallout winds, not surface winds, are being presented.

The histogram of wind speed in Figure III-4 has the appearance of a log normal distribution. In Figure III-6, the cumulative histogram for wind speed is plotted on probability paper using the logarithm of the wind speed as the ordinate. The continuous curving of the plot shows that a simple normal distribution does in fact give a better representation except at very low wind speeds.

The number of occurrences of wind speed and shear in different intervals is shown in a matrix in Table III-1. The



6-9-81-24

Figure III-2. CUMULATIVE HISTOGRAM OF WIND SPEED FOR ALL MONTHS ON A NORMAL PROBABILITY PLOT.

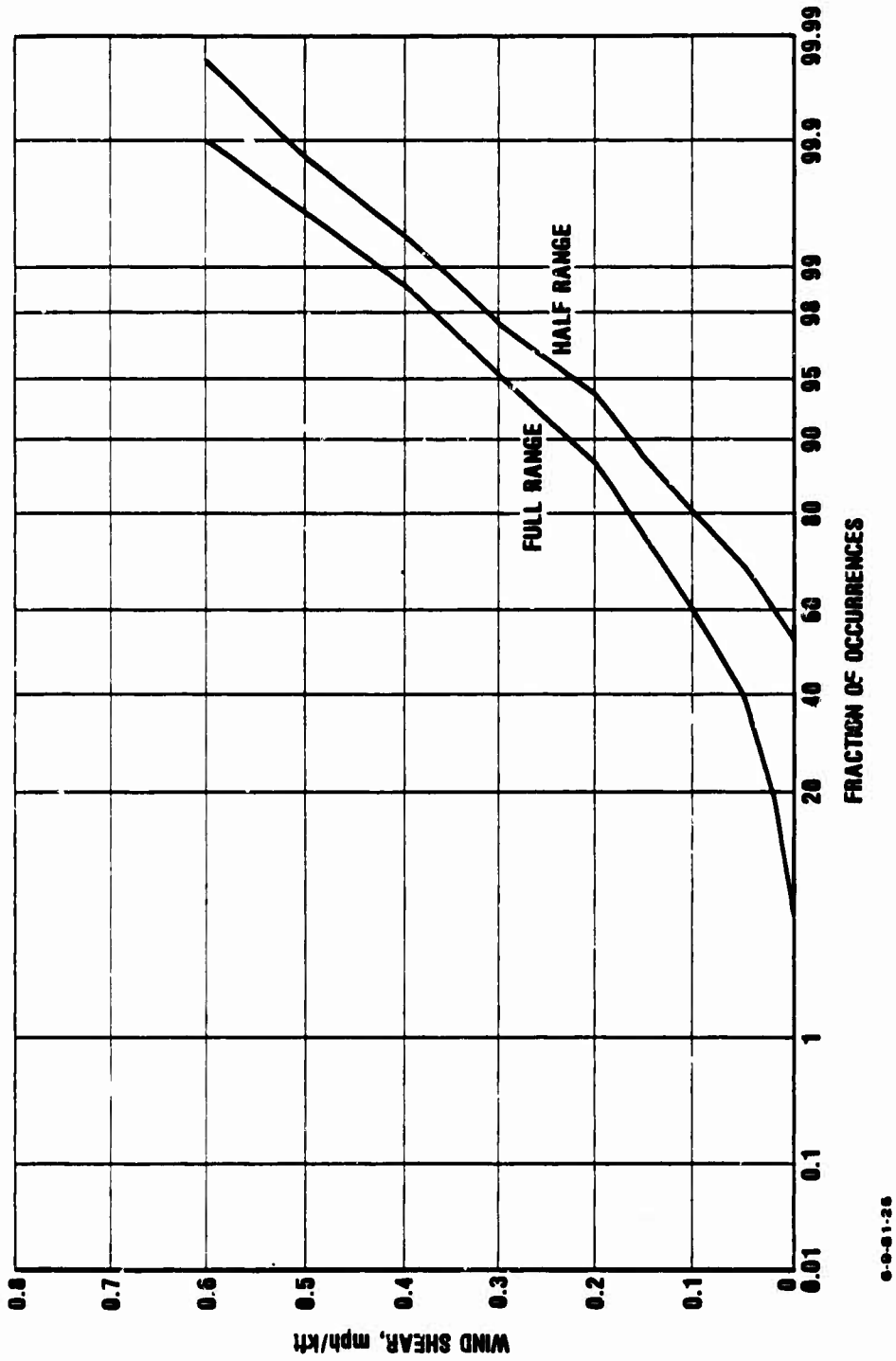
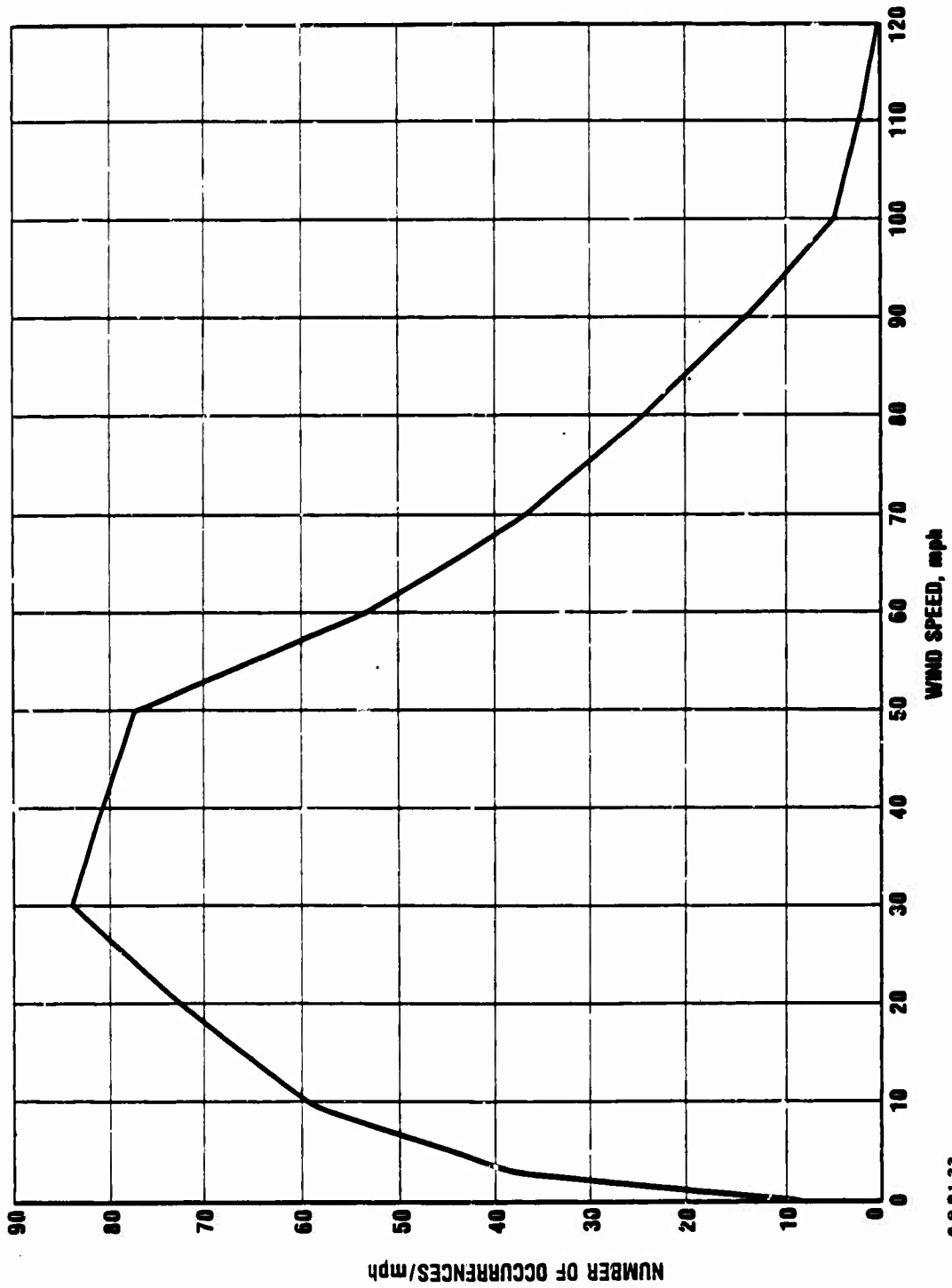
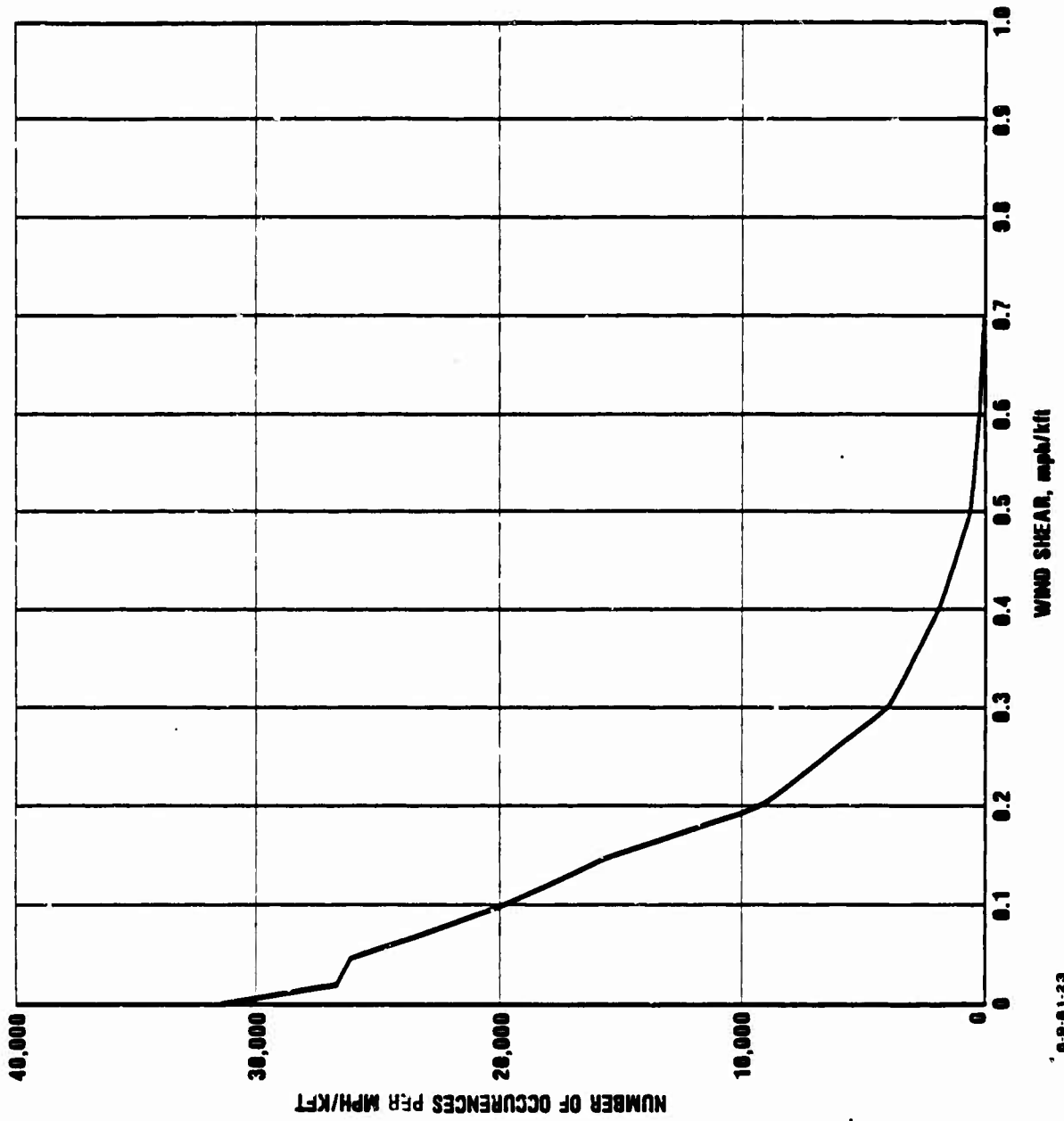


Figure III-3. CUMULATIVE HISTOGRAM OF WIND SHEAR FOR ALL MONTHS ON A NORMAL PROBABILITY PLOT.



0-0-01-22

Figure III-4. HISTOGRAM OF WIND SPEED FOR ALL MONTHS.



9-9-61-23

Figure III-5. HISTOGRAM OF WIND SHEAR FOR ALL MONTHS.

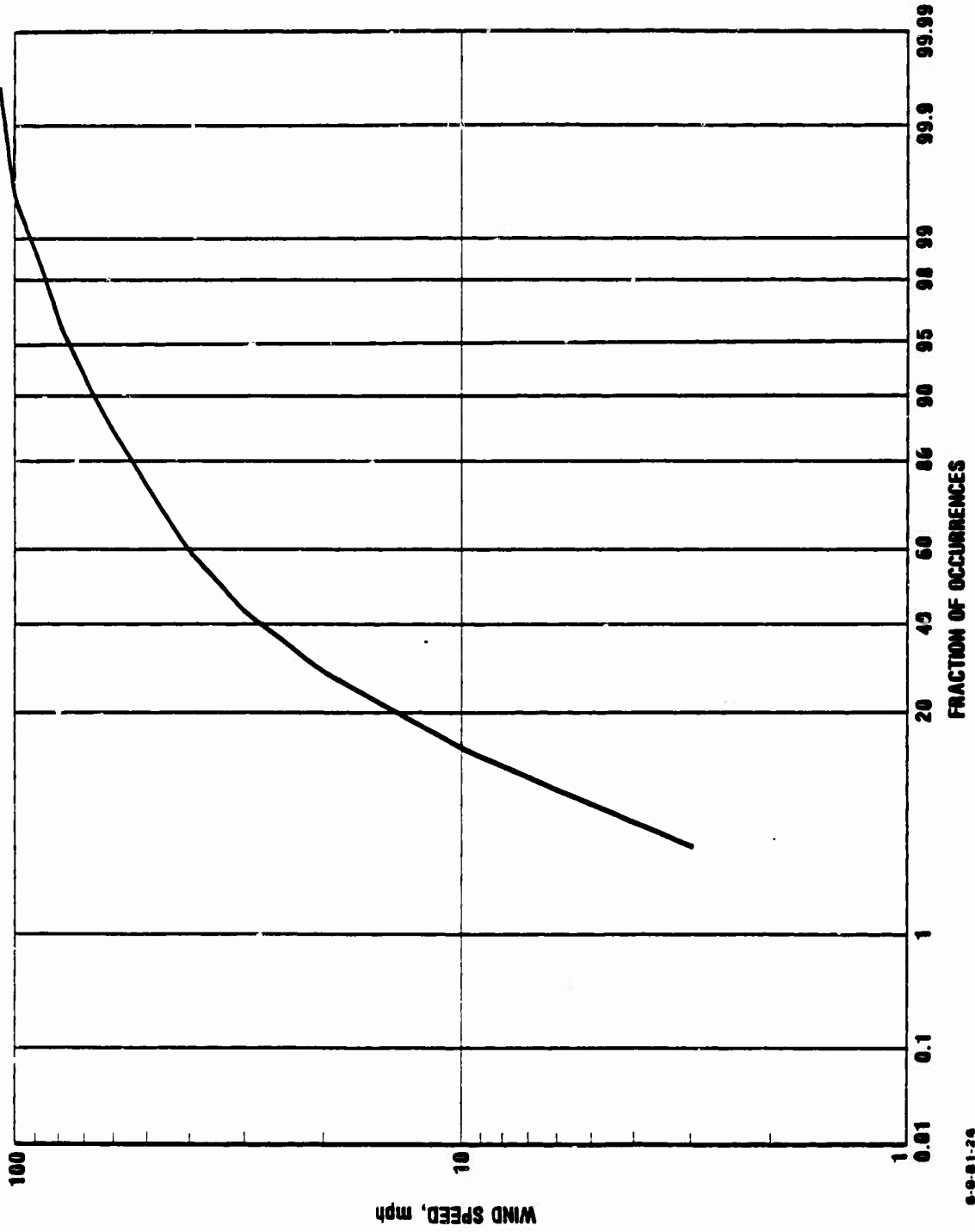


Figure III-6. CUMULATIVE HISTOGRAM OF WIND SPEED FOR ALL MONTHS ON A LOGAKITHMIC NORMAL PROBABILITY PLOT.

Table III-1. NUMBER OF OCCURRENCES OF WIND SPEED AND WIND SHEAR IN VARIOUS INTERVALS

Wind Shear mph/kilofoot	Wind Speed (mph)													
	0	3	10	20	30	40	50	60	70	80	90	100	110	120
0	2	16	36	43	63	51	39	27	17	16	2	2		
0.02	2	38	85	110	119	102	108	58	46	26	15	7	1	
0.05	2	44	123	150	163	172	157	87	69	47	19	11		
.1	4	38	80	161	147	140	176	124	78	46	24	3	5	
.15	1	25	77	105	121	127	120	86	38	38	33	6	1	
.2	1	21	72	86	112	119	97	66	50	26	17	7	5	2
.3	1	10	18	44	76	69	54	59	27	19	12	8	3	
.4		3	11	15	30	24	24	21	30	14	10	1	2	
.5			3	5	10	6	1	1	9	5	6		1	
.6				5		1		1		5		1	1	
.7							1				1			

dividing line for the intervals is midway between the value shown. A blank entry represents no occurrences. The lines on the Table are placed there as an aid to visualization and divide the Table into regions of 150 or more occurrences, 100-149, 50-99, 20-49 and less than 20 occurrences. These numbers add up to the total number so the fraction in each interval is readily obtained by dividing the listed value by 5208. From inspection of the Table there seems to be only a slight tendency for wind shear values to increase with wind speed. This is borne out by the low value of the correlation coefficient between wind speed and wind shear of 0.123. Thus to a first approximation the wind speed and wind shear may be taken as uncorrelated variables in the overall statistics.

C. MONTHLY AND REGIONAL WIND SPEED AND WIND SHEAR STATISTICS

Table III-2 presents selected wind statistics for each monthly wind. In Figure III-7 the mean wind speed and mean wind shear and the correlation coefficient between the two are plotted by month. The data for mean wind speed and mean wind shear indicate a definite annual trend. Assigning any rationale to the fluctuation of the correlation coefficient is problematical. Probably the best one can say is that these fluctuations may be due to the synoptic weather conditions on those particular days.

Figure III-8 presents the ratio of standard deviations, medians and maximum value of each month to the mean value for both wind speed and wind shear. In this Figure annual trends are not nearly as evident as in Figure III-7. Nevertheless, a definite increase in the ratio of standard deviation to mean wind speed for the summer months is apparent. This can be taken as an indication that wind speed variability is a trend, in part, to be a constant value rather than a constant fraction of the mean. The shear variability is almost twice as high a

Table III-2. SELECTED WIND STATISTICS FOR EACH MONTH

Month	Mean Speed	Standard Deviation of Speed Mean Speed	Median Speed	Maximum Speed	Mean Shear	Standard Deviation of Shear Mean Shear	Median Shear	Maximum Shear	Correlation Coefficient
January	59	.26	54	108	.19	.75	.13	.67	.45
February	58	.37	55	104	.16	.83	.10	.54	-.32
March	62	.31	57	100	.16	.86	.09	.66	-.32
April	42	.33	38	74	.15	.68	.11	.36	.11
May	30	.50	26	65	.13	.78	.08	.50	.14
June	22	.40	16	46	.09	.72	.06	.34	-.21
July	24	.57	18	53	.08	.74	.05	.24	-.21
August	22	.79	11	66	.07	1.10	.03	.41	-.16
September	32	.47	26	68	.09	.75	.05	.28	-.05
October	50	.58	39	118	.13	.66	.09	.42	-.12
November	40	.29	35	64	.12	.78	.08	.43	-.07
December	49	.43	45	97	.14	.74	.09	.42	-.15
All Months	41	.56	36	118	.13	.87	.07	.67	.12

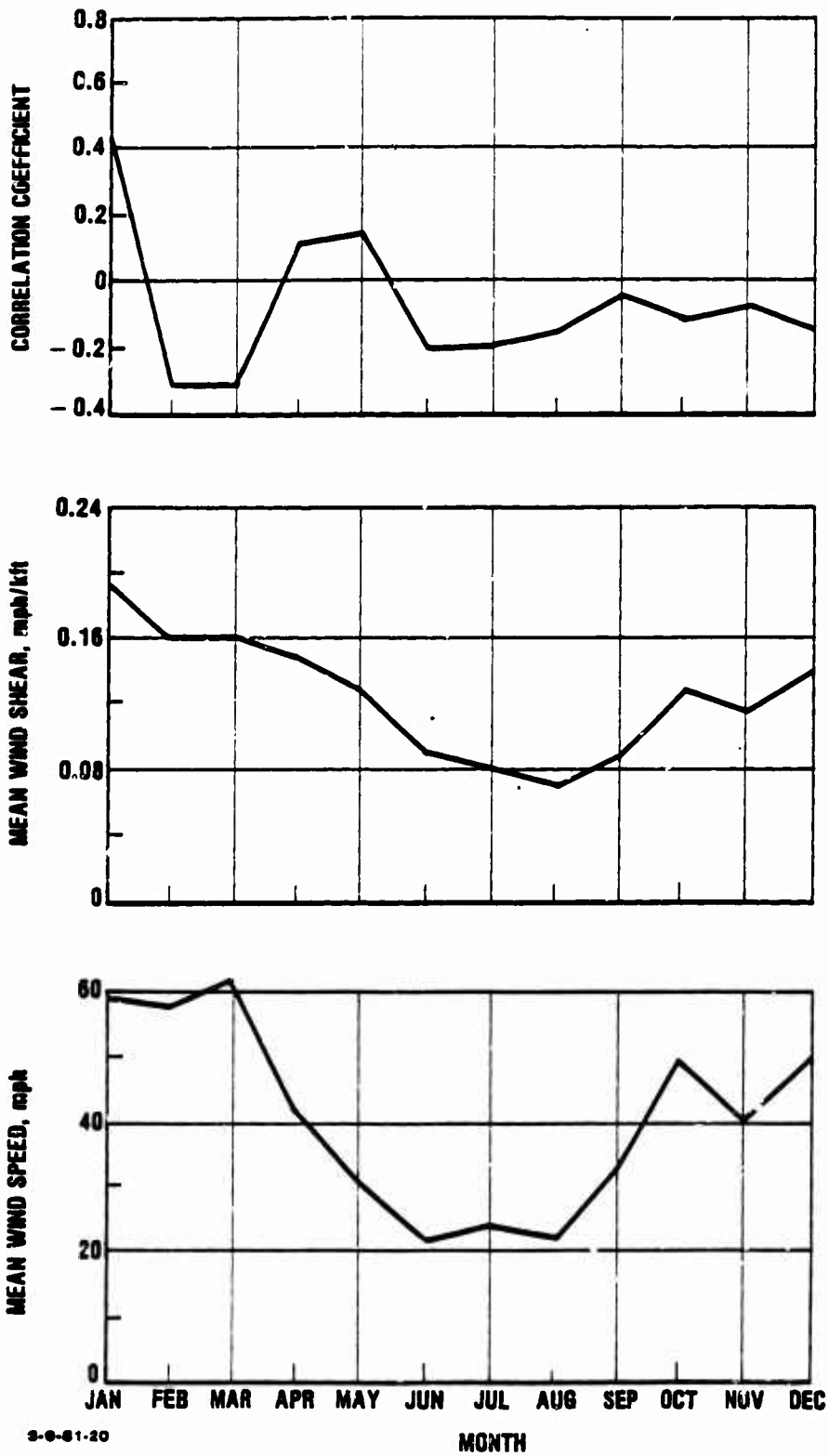
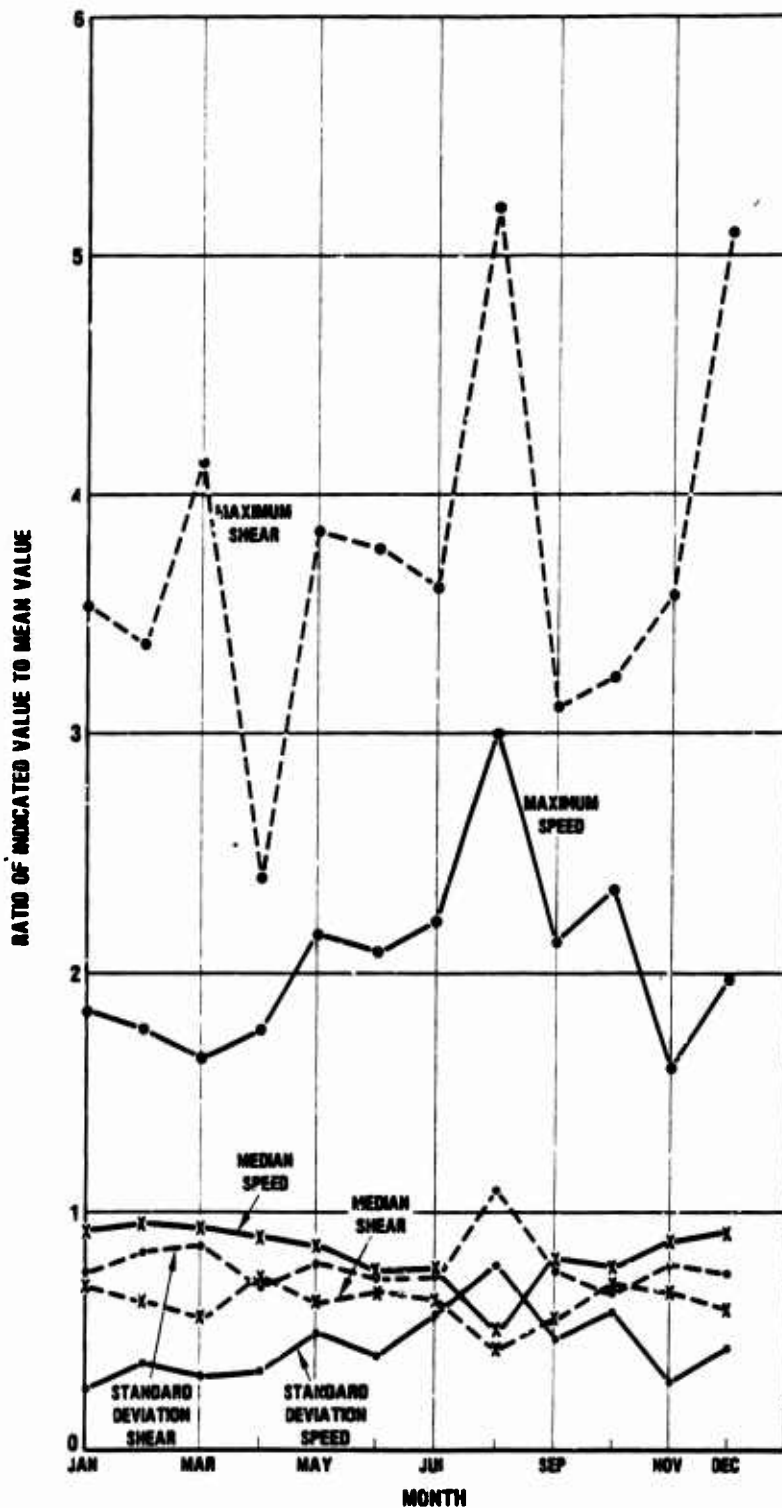


Figure III-7. MEAN WIND SPEED, MEAN WIND SHEAR AND CORRELATION COEFFICIENT BY MONTH.



6-6-61-19

Figure III-8. RATIO OF STANDARD DEVIATION, MEDIAN VALUE OR MAXIMUM VALUE OF WIND SPEED AS SHEAR TO MEAN VALUE FOR EACH MONTHLY WIND.

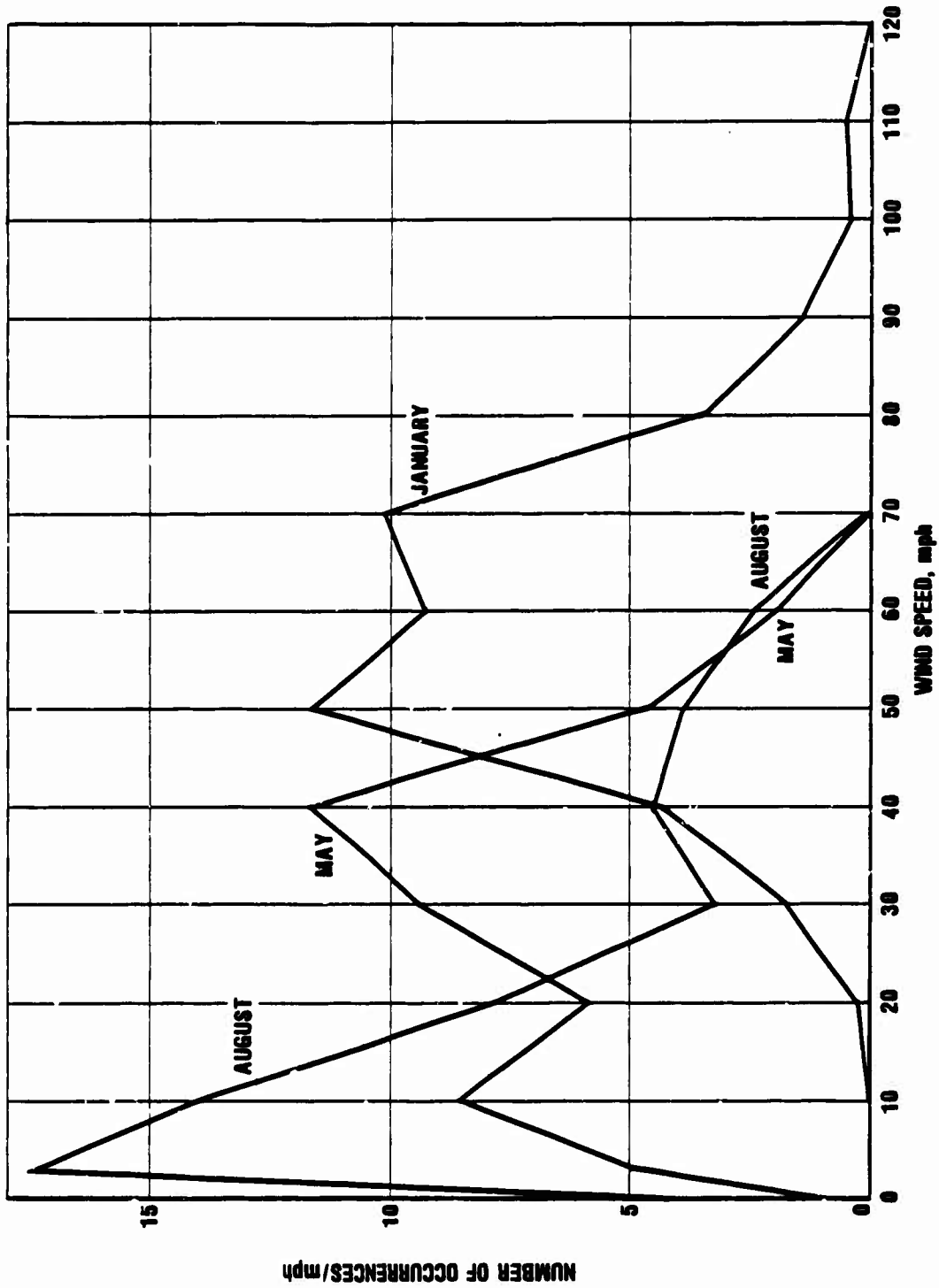
fraction of the mean as for speed, but the value seems to be more constant and shows less annual trend. The ratio of maximum wind speed to mean speed shows evidence of an annual variation with peaks at the minimum wind speed, as in the ratio of standard deviation to mean. The ratio of maximum to mean wind shear shows large fluctuation and little evidence of any non-random variations.

The ratio of median to standard deviation shows an indication of a dip in summer months for both wind speed and shear. A change in this ratio indicates changes in the detailed nature of the frequency distributions. Some of these changes are evident in Figure III-9 which presents histograms of wind speed distributions for the extreme months of January and August and the month of May, which is intermediate.

The differences in the distribution is evident. January could represent a normal distribution, while the distribution for August is very sharply truncated near zero values and that for May only somewhat so. Where the mean wind speed is high enough in January so there is no truncation of the distribution near zero values, a near normal distribution is obtained.

A set of four subregions were defined to determine whether there were any significant differences in the statistics between these regions. These regions included all points on the boundary and interior of the figures defined as follows:

Region Name	Minimum Latitude	Maximum Latitude	Minimum Longitude	Maximum Longitude	Number of Points
Northeast	38	44	65	89	52
Southeast	28	36	79	93	40
Southwest	30	38	105	119	40
Northwest	40	50	99	115	54



6-9-61:21

Figure III-9 HISTOGRAMS OF WIND SPEEDS FOR THE MONTH OF JANUARY, MAY AND AUGUST.

The regions were selected to represent different parts of the country, yet were made large enough to obtain a reasonably large number of points for depictions of wind statistics. Figure III-10 shows a map of these regions on the same projection as the wind illustrations of Figure III-1.

In Table III-3 the mean wind speed, mean wind shear, and correlation coefficient are shown for each month. The mean wind speed in the Northeast and Southeast for all months seems to be definitely higher than for the Southwest and Northwest. The wind shear for all months, however, appears to have little regional difference. The mean wind speeds for the individual months have larger individual variations between regions. January, for example, has rather low mean winds for all regions, while February shows high winds for three regions and a mean wind less than one-half this value for the Southwest. A strong tendency for the wind speeds in some regions to be independent of the rest is apparent. The same pattern is true for wind shear but the differences between regions seems even more accentuated. These differences are undoubtedly due to the fact that on any particular day, the meteorological conditions in different parts of the country can vary widely.

Wide variations in the correlation coefficient are also apparent. However, much larger values of correlation coefficient can be seen, the largest in absolute value being $-.86$. The mean value of the absolute value of these correlation coefficients is 0.34 ; the large values are well divided between positive and negative values. On a local basis for particular day there is a tendency for changes in wind speed to be related to changes in wind shear. If only positive correlation appeared, this could be readily explained since the wind shear is computed as the difference in absolute value of the sine of the wind angle difference at the two highest altitude levels of interest times the wind speed at the next to the highest

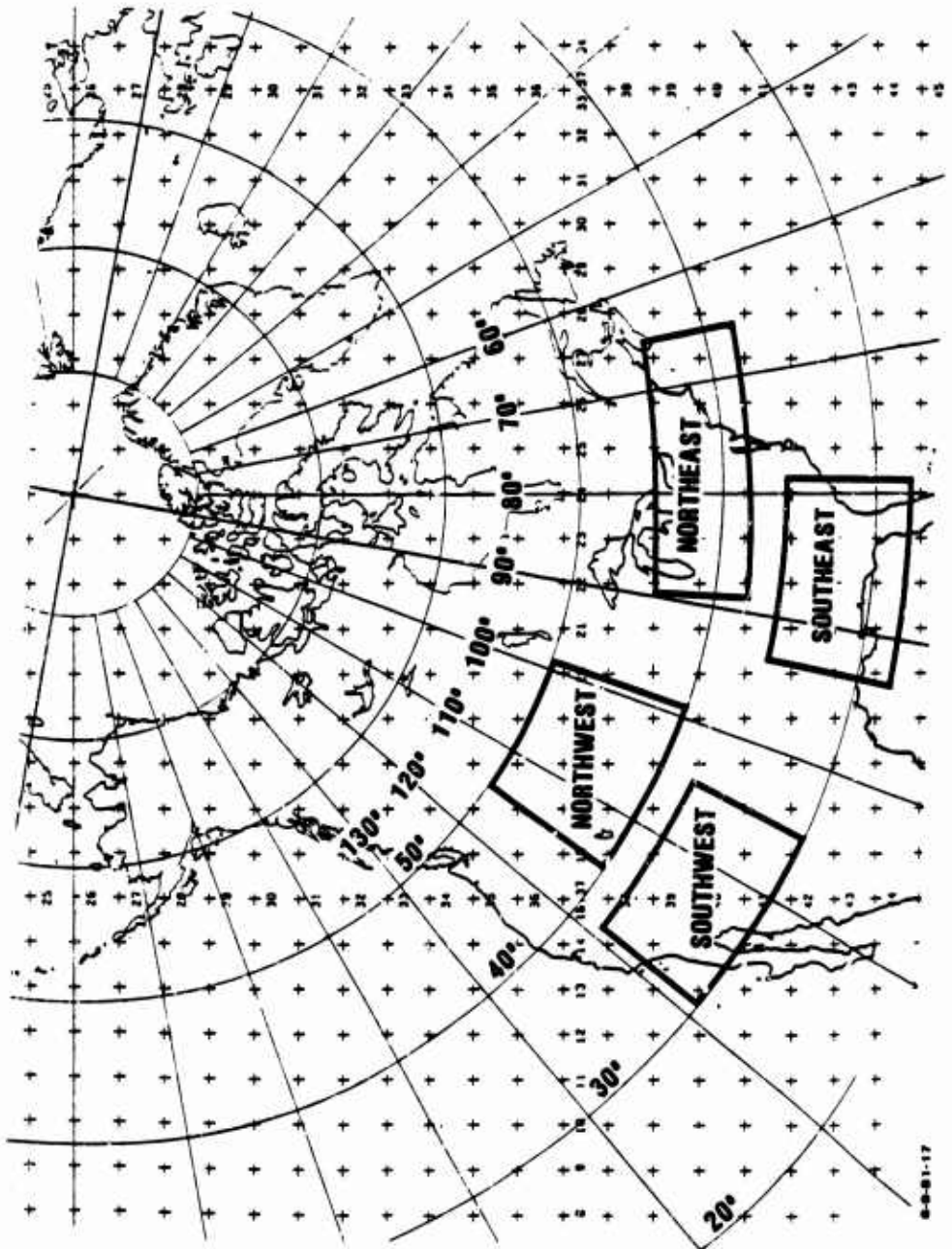


Figure III-10. LOCATION OF SUB AREAS.

Table III-3. SELECTED WIND STATISTICS BY MONTH AND REGION

	Mean Wind Speed (mph)				Mean Wind Shear (mph/kilofoot)				Correlation Coefficient			
	North- east	South- east	South- west	North- west	North- east	South- east	South- west	North- west	North- east	South- east	South- west	North- west
January	63	71	60	51	.28	.15	.13	.11	.75	.00	.50	.08
February	73	73	30	69	.18	.07	.15	.04	-.52	-.63	-.72	.04
March	54	71	89	39	.26	.08	.12	.12	.59	.03	.69	-.72
April	29	47	47	33	.18	.25	.24	.10	.10	-.04	.14	.57
May	26	21	39	22	.10	.05	.09	.22	.17	.23	-.01	-.22
June	31	20	25	24	.14	.11	.04	.06	-.57	-.26	.20	-.71
July	39	16	14	37	.09	.05	.08	.05	.19	.32	-.34	-.15
August	43	6	12	23	.07	.10	.05	.02	-.01	.19	.63	.07
September	51	43	26	17	.09	.06	.08	.14	-.48	.53	.20	-.30
October	73	91*	19	44	.11	.15	.21	.11	.37	.34	-.06	-.21
November	44	47	36	39	.12	.08	.07	.13	-.67	-.40	.50	.04
December	65	57	16	47	.12	.09	.17	.18	.48	.35	-.12	-.86
All Months	49	47	35	39	.14	.10	.12	.11	.12	.20	.14	-.18

level. The large negative correlations require a little deeper explanation.

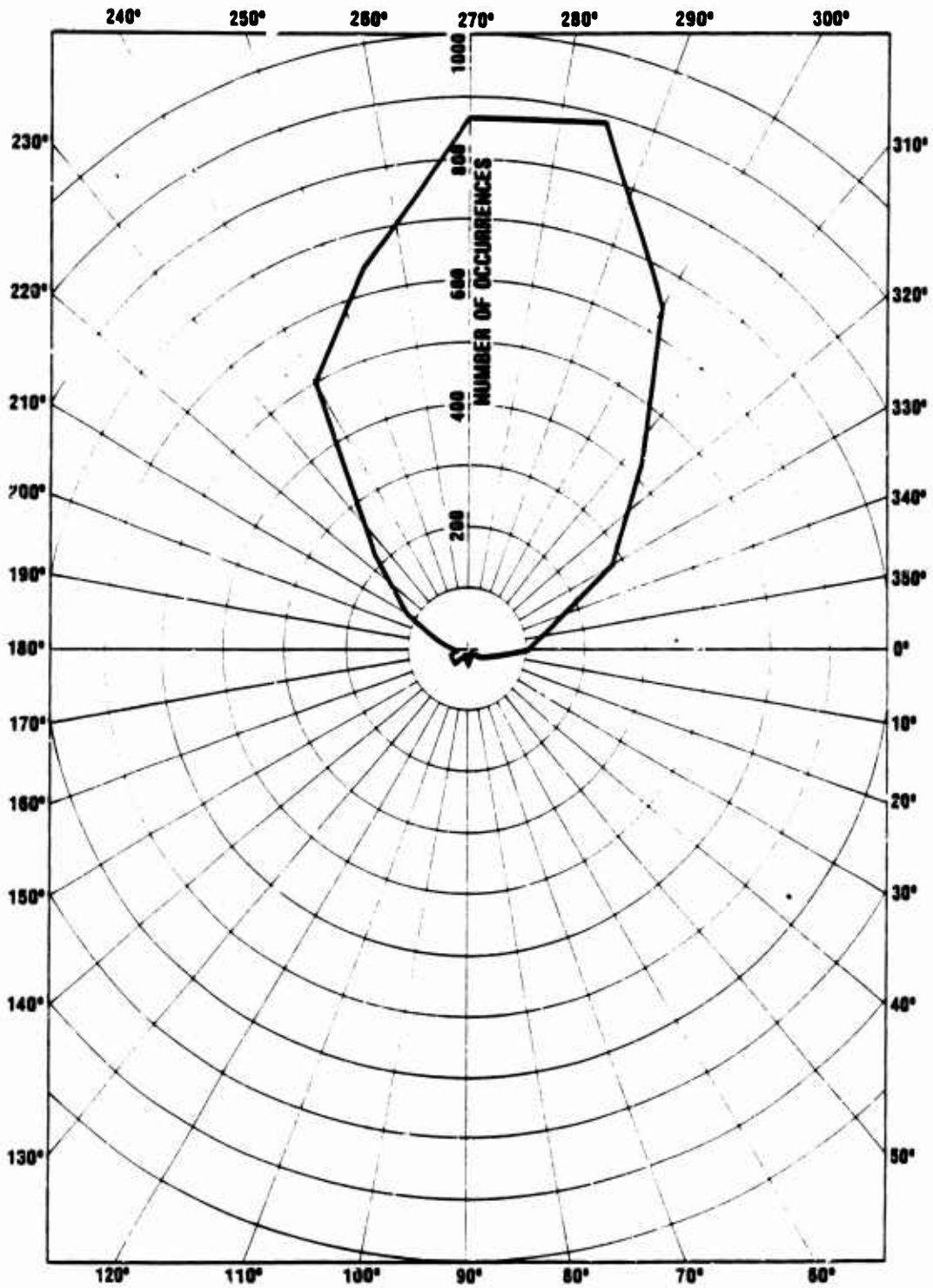
The variability of the winds on a particular day within a region is illustrated in Table III-4 where the ratio of standard deviation of wind speed and shear to the mean value is presented for each month and region. In Table III-2 the ratio of standard deviation to mean wind speed was somewhat lower for each month than for all months averaged together, but not drastically so. When considered by region, however, this ratio is generally lower and often drastically reduced. Occasionally, when conditions are varying rapidly over a region, this ratio is increased. For example, the reason for the value of 0.77 in the Southeast region in May is readily apparent by glancing at the flow pattern for May in Figure III-1.

The variations of the shear within regions for a particular day are not as drastically reduced. The mechanisms causing variability in shear values seem still effective over areas of this size.

D. OVERALL WIND DIRECTION STATISTICS

The analysis of wind direction here will be limited to studying frequencies of winds in different directions and the correlation of wind direction with wind speed.¹ In Figure III-11, a polar histogram of the number of wind occurrences in 15 degree intervals for all locations for all twelve winds is blowing from, measured in degrees counterclockwise from the North. Thus, for example, a wind direction of 270 degrees represents a wind blowing from West to East, and a wind direction of 225 degrees represents a wind blowing from Southwest to Northeast. Since there are 5208 total data points, the average number of data points per interval is 217. The observed number of data points per interval ranged from a

¹The interesting question of correlation of wind direction with position is left for the future.



6-6-61-28

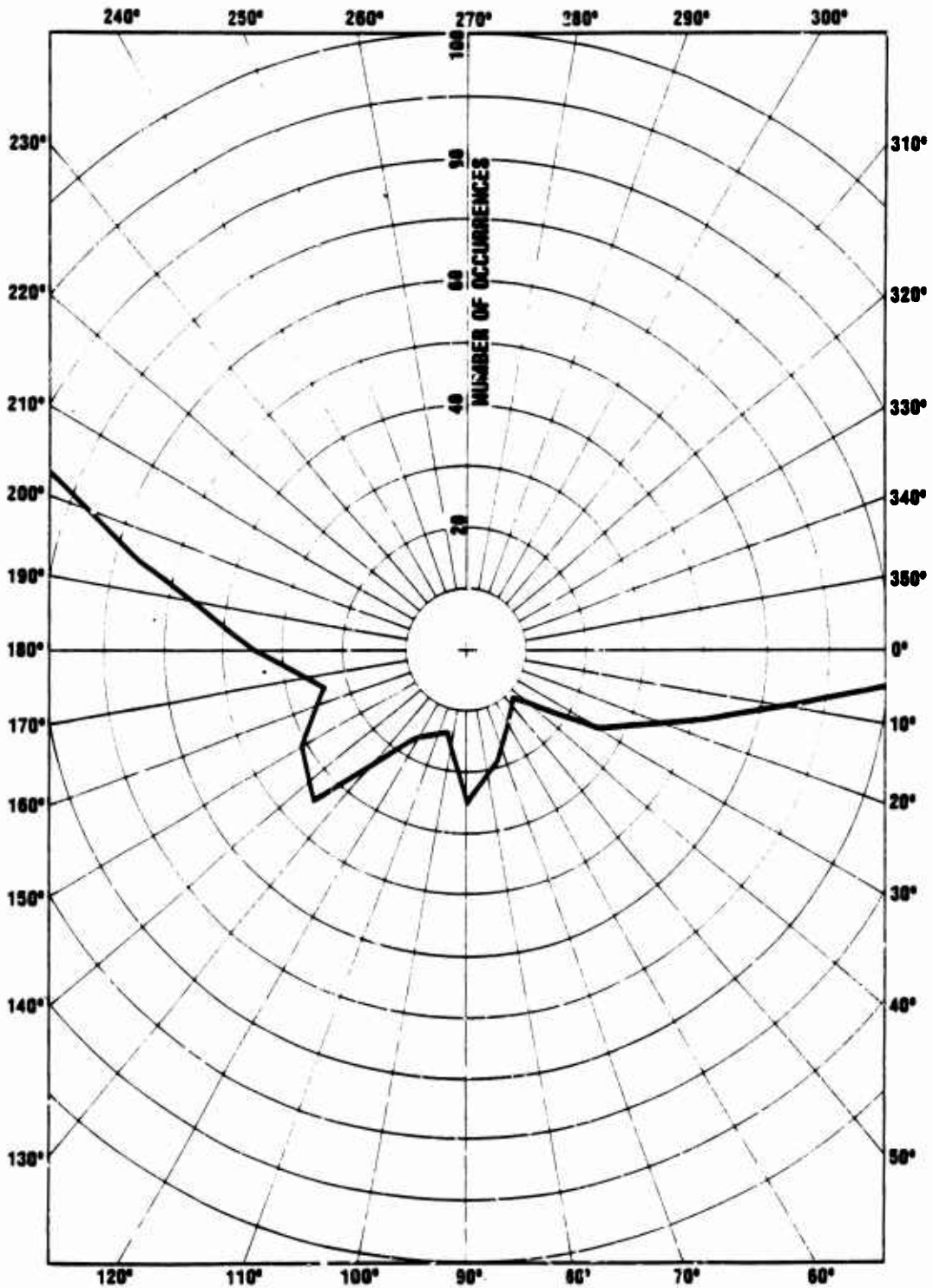
Figure III-11. POLAR HISTOGRAM OF NUMBER OF WIND ANGLE OCCURRENCES IN 15° INTERVALS.

minimum of 11 to a maximum of 888. In Figure III-12, the same histogram is presented with the occurrences scale expanded by a factor of 10 to better illustrate the region where winds are blowing toward the West.

Figure III-11 illustrates that the interval with the most frequent winds is 15 degrees South of due East. The mean wind direction is 277° , and the standard deviation for the mean wind direction is 42 degrees. Thus 68 percent of the time the wind is blowing between 235 degrees and 320 degrees, a relatively restricted angle.

Figure III-13 presents a polar plot of the mean wind speed at different angles for all months. For example, the mean wind speed at 270° represents the average speed of all winds blowing between angles of 262.5 and 277.5 degrees. A strong variation of wind speed with angle is evident. A comparison with Figure III-11 shows that the mean wind speed is highly correlated with the number of occurrences, with the high mean wind speeds occurring in the more frequent directions. This is further illustrated in Figure III-14 where the number of occurrences in each 15 degree interval is presented as a function of the mean wind speed in that interval. A possible curve fitting the plotted points is presented in the Figure. The pure statistical fluctuation expected about an average curve (at the mean number of occurrences of 217) if a binomial probability distribution is assumed gives a standard deviation of 15 occurrences. Thus a good deal of the observed fluctuation from a hypothetical mean curve could be explained by purely random phenomena.

In Table III-5, the observed number of occurrences for various combinations of velocities and winds are presented. Two elements are immediately evident, the larger number of occurrences of wind blowing to the East, and their higher values. The distribution of velocities at angles near 270



6-6-81-28

Figure III-12. POLAR HISTOGRAM OF NUMBER OF WIND ANGLE OCCURRENCES IN 15 DEGREE INTERVALS - WITH EXPANDED SCALE.

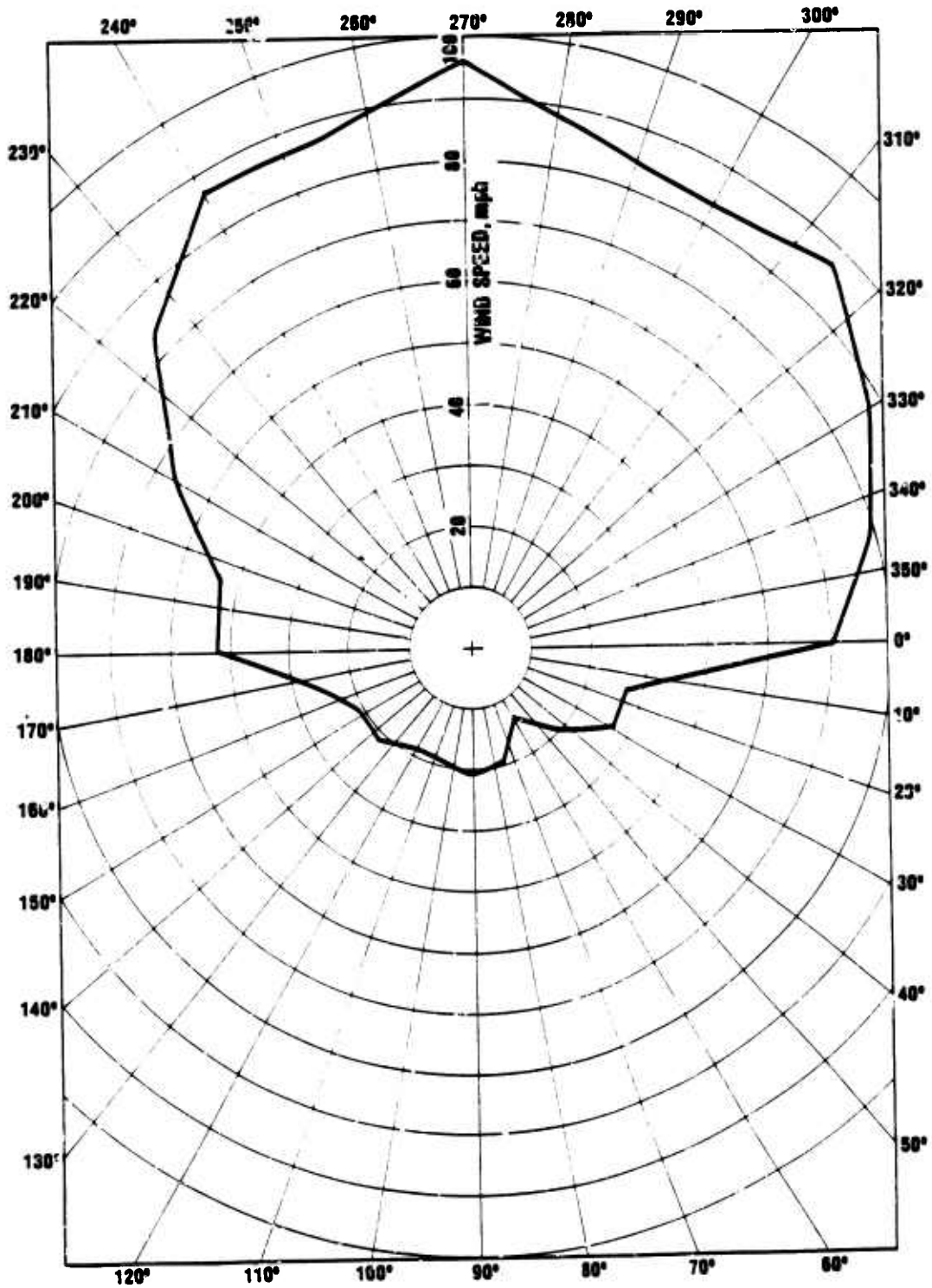
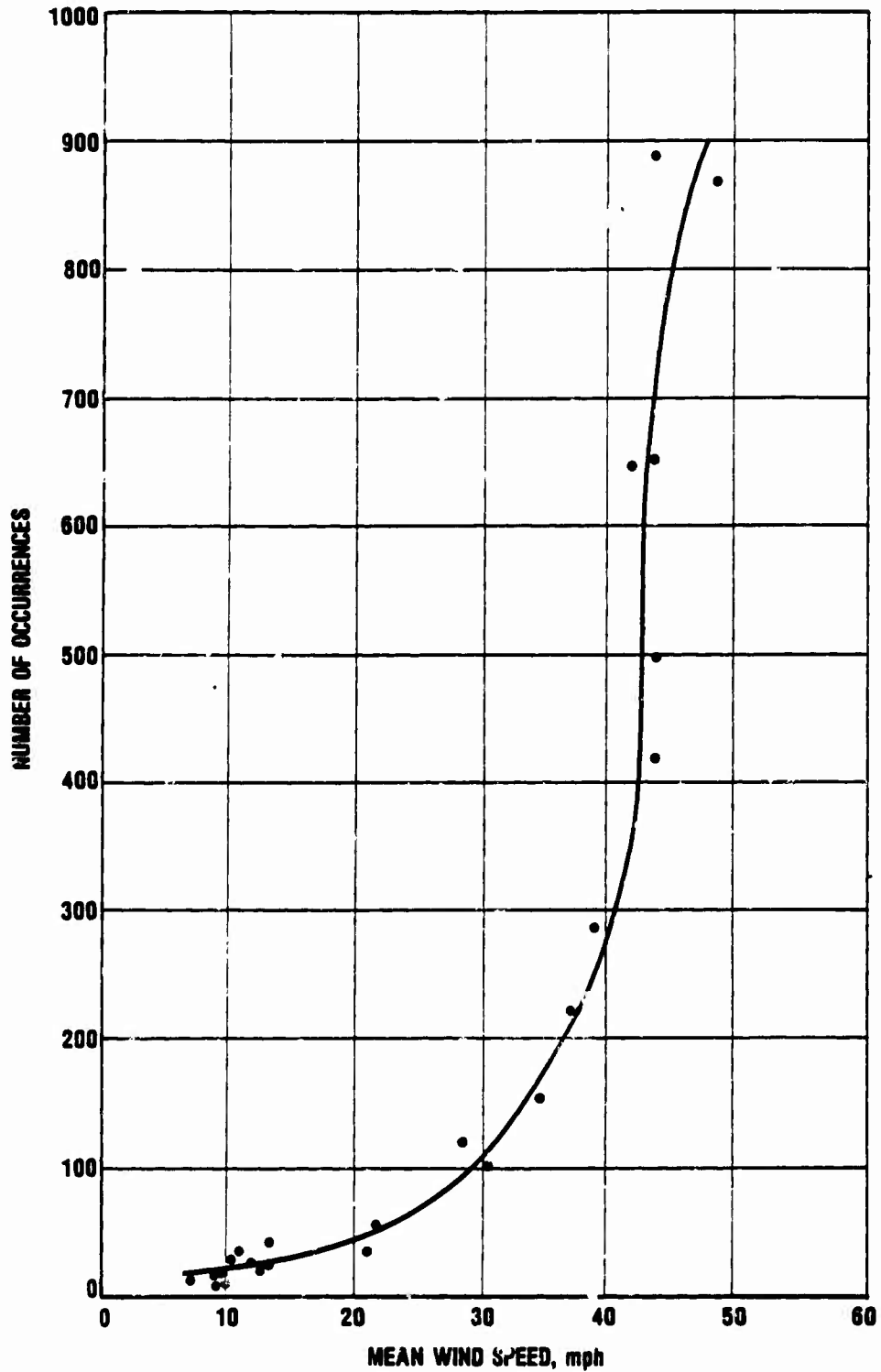


Figure III-13. MEAN WIND SPEED FOR WINDS AT DIFFERENT ANGLES FOR ALL MONTHS.



6-8-81-18

Figure III-14. NUMBER OF OCCURRENCES OF WIND IN A 15 DEGREE INTERVAL AS A FUNCTION OF MEAN WIND SPEED IN THAT INTERVAL.

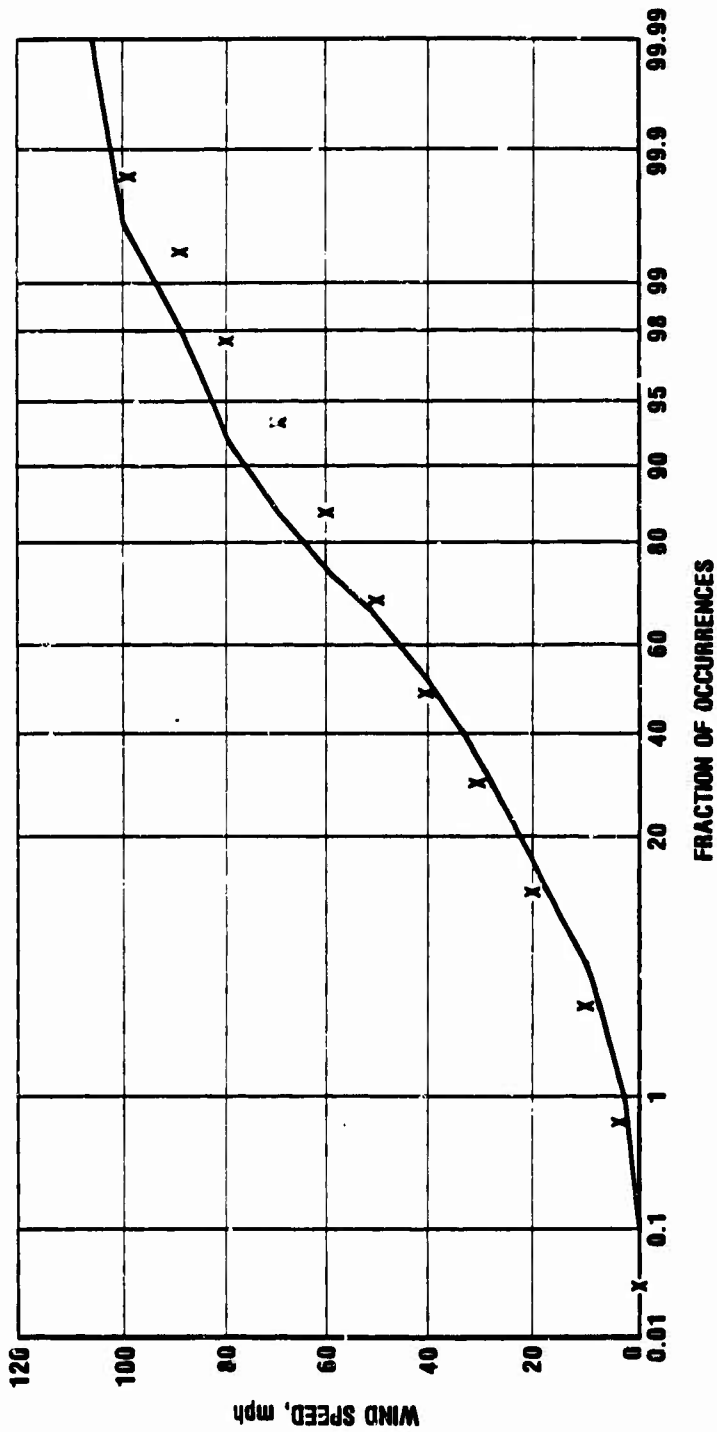
Table III-5. NUMBER OF OCCURRENCES OF VARIOUS WIND SPEEDS AND DIRECTIONS FOR ALL MONTHS

Angle (Degrees)	VELOCITY (MILES/HOUR)													
	0	3	10	20	30	40	50	60	70	80	90	100	110	120
360		6	21	14	18	13	24	2	3					
15	2	7	18	11	4									
30		5	10	10										
45		3	7	1										
60	1	6	7											
75		2	16	1										
90	1	5	9	10										
105		3	9	2										
120	1	7	6	2	1									
135	1	8	18	7	1									
150	1	11	12	6	1									
165	1	8	6	6	2	1								
180		8	8	9	1	5	3	1						
195		14	13	9	6	5	4	5						
210	1	10	13	36	29	13	8	4	4	1	2			
225	2	7	25	46	53	18	21	15	14	13	7	3		
240		7	39	77	94	67	78	44	27	21	29	11	5	
255		13	47	79	94	131	87	98	46	28	18	6	4	
270	1	10	39	84	151	165	119	79	87	67	50	13	3	
285		8	51	127	152	151	141	104	84	46	10	6	6	2
300	1	16	41	86	114	100	121	90	43	23	7	6	1	
315		8	30	31	67	75	95	51	34	16	11	1		
330		10	32	44	39	41	63	27	10	16	3			
345		13	28	26	14	26	13	10	12	11	2			

degrees has an approximately normal appearance. This is illustrated by Figure III-15 where the solid curve shows a cumulative histogram for winds at 270 degrees on a normal probability plot. (The meaning of the x's on the Figure will be discussed shortly.) In the range from 20 mph to 100 mph, reasonable straight lines can be fitted to the histogram, indicating an approximately normal distribution. For winds blowing towards the West, the number of samples is too small to say much about distributions, but at least for some angles, 30 to 90 degrees, a highly skewed distribution is indicated.

One method of describing climatological wind statistics at a particular location, is to imagine that a sample wind vector at any particular time may be drawn from a statistical distribution the sum of two vectors, a mean wind vector, \bar{S} , and a random wind vector, \bar{W} . The random wind vector is taken from an elliptical normal distribution. The wind statistics then are described by the magnitude and direction of the mean wind vector and the two standard deviations of the elliptical normal distribution. For many uses a circular normal distribution of the random wind vector can be assumed; the single standard deviation is taken as the geometrical mean of the two elliptical standard deviations.

A Monte Carlo simulation was written which generated wind vectors drawn from a circular normal distribution as described in the previous paragraph. These wind vectors then were treated as observed wind vectors and similar statistics were observed. An effort was then made to find a mean wind vector and a standard deviation which could produce statistics close to the observed values of nationwide statistics for all twelve winds. This method of describing actual wind values at any particular location is well established. However, here we are using fallout winds, not actual winds, and applying the method over the entire nation, not just at a point. Thus while one might



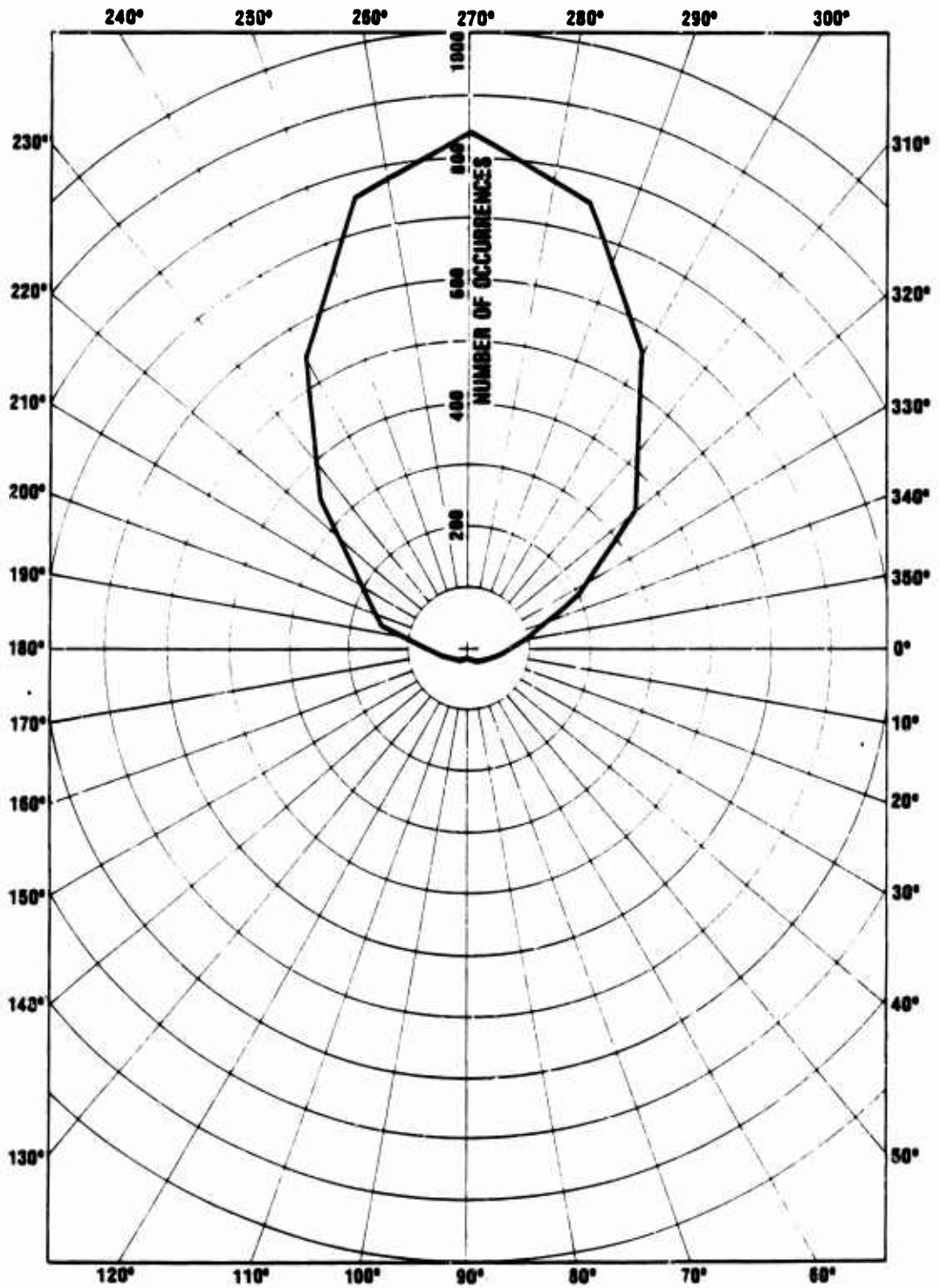
6-0-01-27

Figure III-15. CUMULATIVE HISTOGRAM OF WIND SPEED FOR ALL MONTHS FOR WINDS AT AN ANGLE OF 270° ON A NORMAL PROBABILITY PLOT.

hope this method will work well, there is no a priori justification for using it in this fashion. In the first case shown,¹ the conditions were chosen (1) to match the average speed of all trials to the observed mean wind speed of 40.8 mph, and (2) to match the number of occurrences of the observed wind in the Easterly Direction, namely 393 occurrences between 0 and 180 degrees.

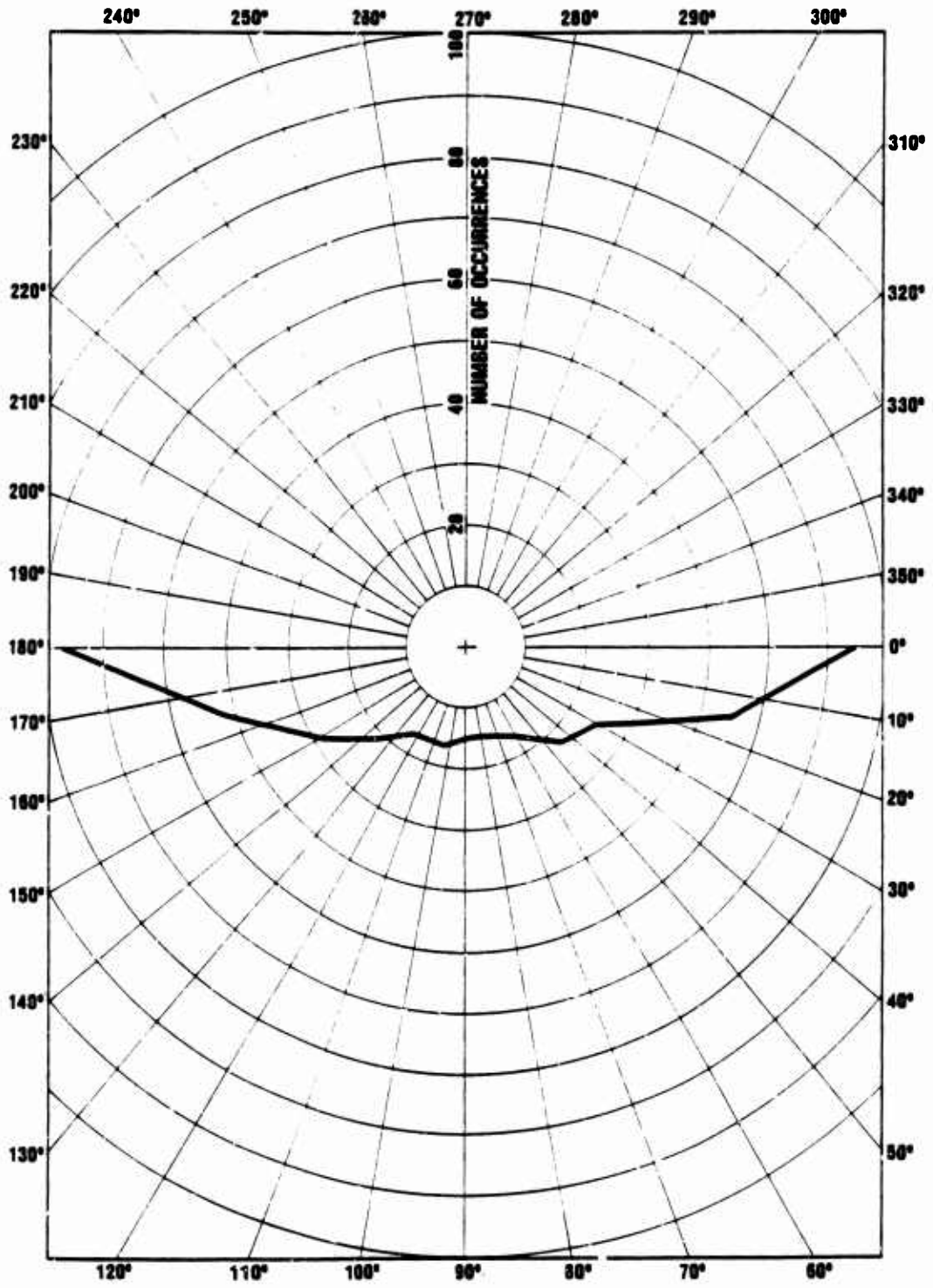
The simulation run used the speed of the mean wind vector, $|S|$, of 32.9 miles/hour and a standard deviation of 21.6 mile/hour. Since the mean wind direction of the observed winds was only -7° from 270° , for convenience the direction of the mean wind vector in the simulation was taken at 270° . A large number of trials (500,000) was used in order to obtain adequate statistics for the winds blowing toward the West. The average wind speed for all trials was 40.86 mph and there were 399 adjusted occurrences between 0 and 180 degrees. (The number of occurrences from the simulation was adjusted by multiplying the actual number for the simulation by the ratio of number of trials, i.e. 5208/500,000.) Figure III-16 shows a histogram of the number of adjusted occurrences, which compares quite well with Figure III-11. Figure III-17 shows the region from 0 to 180° with an expanded scale which should compare with Figure III-12. The mean wind speed as a function of angle is shown in Figure III-18. For wind blowing toward the East the agreement is quite good, but for winds blowing toward the West the simulation gives wind speeds about twice as high as observed. This discrepancy apparently is due to mechanisms different from the simple one used in the simulation dominating the values for the wind blowing to the West. However, if the magnitude of this discrepancy is not thought too large, the simulation offers a simple mechanism for describing nationwide winds.

¹Two cases are shown here.



6-7-61-31

Figure III-16. POLAR HISTOGRAM OF NUMBER OF WIND ANGLE OCCURRENCES IN 15 DEGREE INTERVALS FOR THE FIRST SIMULATION.



6-8-81-33

Figure III-17. POLAR HISTOGRAM WITH EXPANDED SCALE OF NUMBER OF WIND ANGLE OCCURRENCES IN 15 DEGREE INTERVALS FOR THE FIRST SIMULATION.

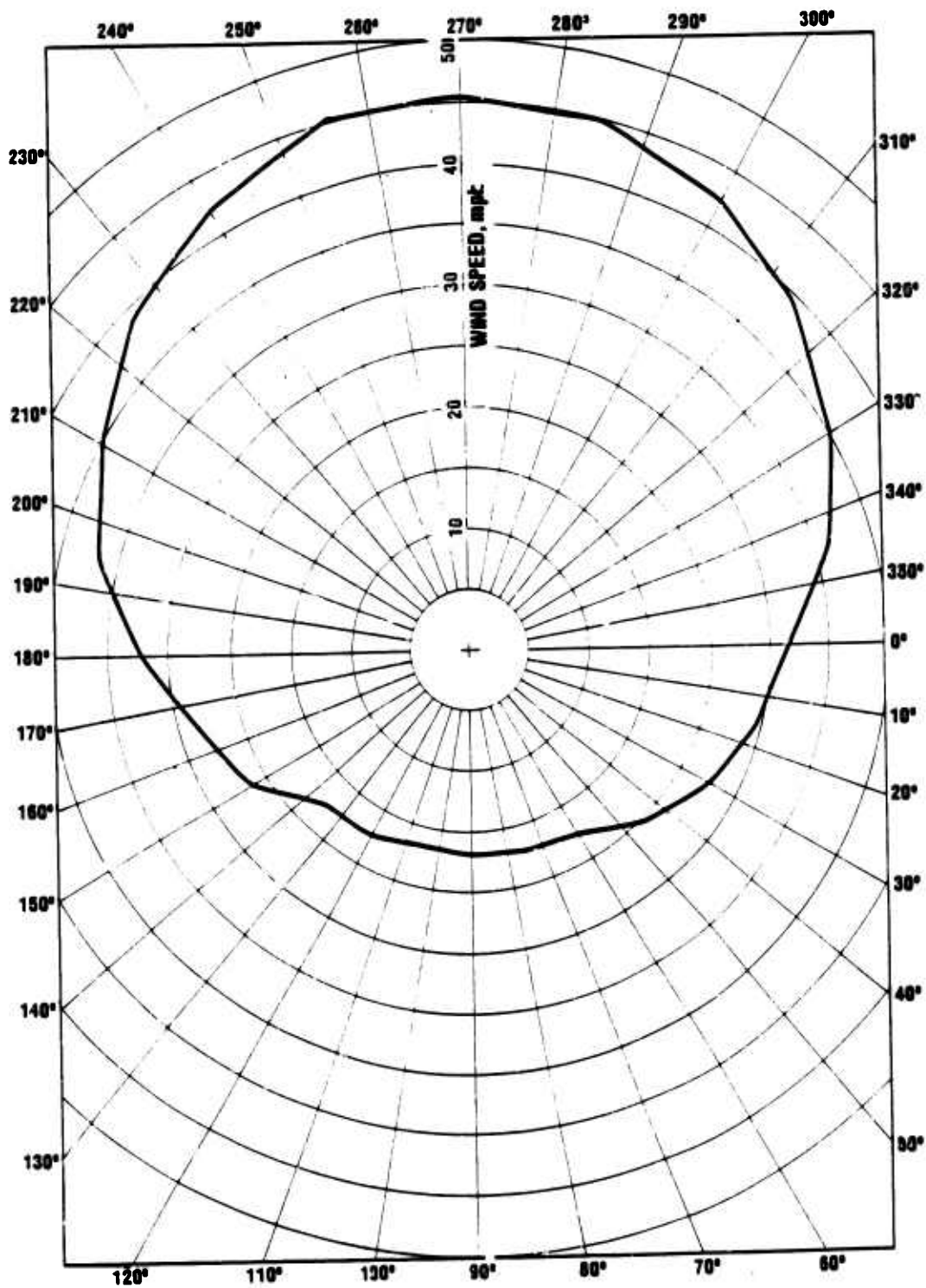


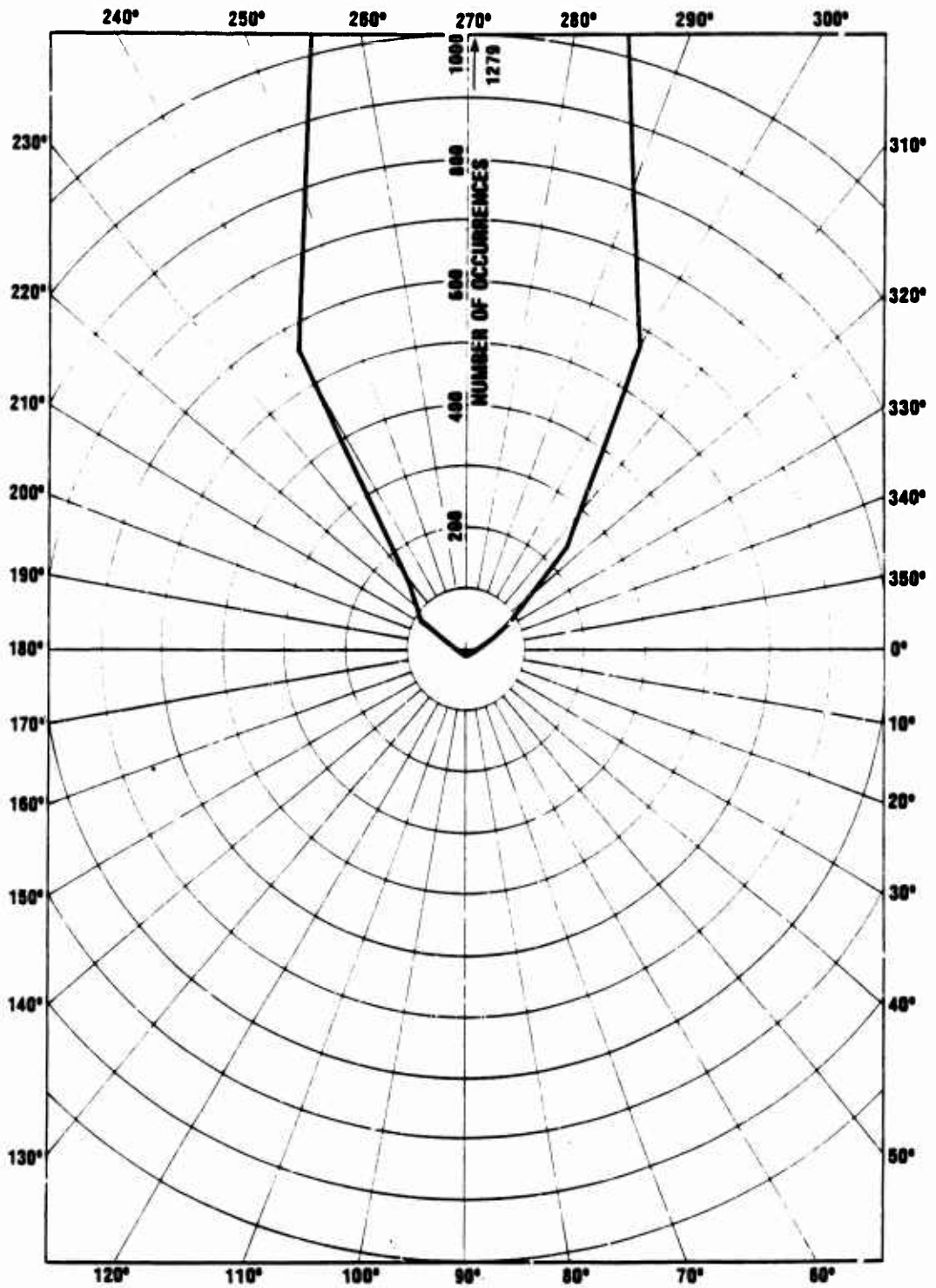
Figure III-18. MEAN WIND SPEED FOR WINDS AT DIFFERENT ANGLES FOR THE FIRST SIMULATION.

Table III-6 shows the number of adjusted occurrences at different velocity levels and angles. The number of occurrences has been adjusted, as with Figure III-16, to be comparable with Table III-5. Where the number of occurrences is greater than zero, but rounds to zero, a dash is indicated. A fairly good agreement is seen between the two Tables for wind blowing toward the East. The maximum number of observed occurrences for the observed winds is 165 at a wind direction of 270 degrees and wind speed of 40 mph. For the simulation, the maximum value is 172 occurring at the same wind speeds and angles. The x's on Figure III-15 represent the cumulative frequency distribution at 270° from the simulation. As should be expected, once the velocity is substantially above 0 miles/hour, the x's form nearly a straight line, giving a close fit to a normal frequency distribution. Except for the range from 60 to 90 miles/hour, they are also quite close to the observed distribution. In the range from 60 to 90 mile/hour, the observed distribution shows somewhat higher numbers of occurrences than from a normal distribution; that is, the distribution is skewed toward high wind values.

A second simulation was run where the objective was to match the mean wind speeds from winds blowing toward the West, rather than the number of occurrences for these winds. In this simulation the speed of the mean wind vector was 37.19 mile/hour and the standard deviation of the random wind vector was 15.80 miles/hour. This gives a ratio of standard deviation to mean wind speed of 0.425, compared to 0.657 for the first simulation. Again 500,000 trials were used. The overall average wind speed from the simulation was 40.9 miles/hour, close to the observed value of 40.8 miles/hour. Figure III-19 presents a polar histogram of the number of occurrences as a function of wind angle, and Figure III-20 presents the same histogram with an expanded scale. As before, the number of occurrences have been scaled to be comparable with the observed data in Figures III-11 and III-12. Figure III-21 presents the

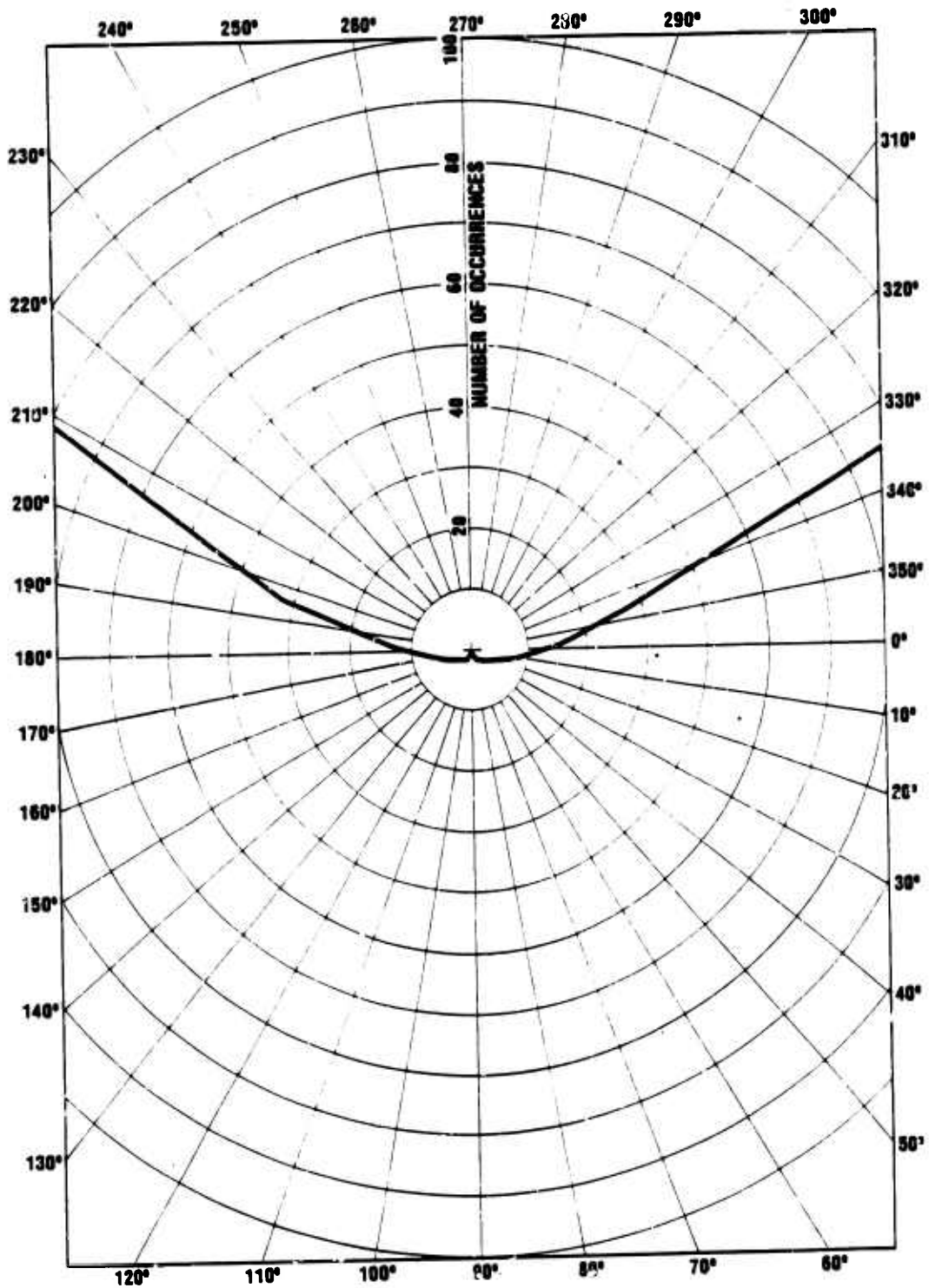
Table III-6. NUMBER OF OCCURRENCES OF VARIOUS WIND SPEEDS AND DIRECTIONS FROM MONTE CARLO SIMULATION.

VELOCITY (MILES/HOUR)														
Angle (Degrees)	0	3	10	20	30	40	50	60	70	80	90	100	110	120
0		2	11	19	15	11	4	2	1		-			
15	-	2	10	14	10	7	2	1	-					
30	0	1	7	7	6	2	1	-	-					
45	-	2	6	7	4	1	1	-	-					
60	-	3	5	6	3	1	-	-						
75	-	2	4	6	2	1	-							
90	-	2	5	4	2	1	-							
105	-	2	6	5	2	1	-	-						
120	-	1	7	5	3	1	-							
135		2	7	7	3	1	-	-						
150	-	2	8	9	7	2	1	-	-					
165	-	2	11	11	9	5	2	1	-					
180	-	3	11	18	18	10	5	1	1					
195	-	4	13	26	31	23	17	6	2	1	-	-		
210		4	16	38	47	40	29	13	9	2	-	-		
225	-	5	22	54	73	75	64	37	17	7	2	1	-	
240	-	5	23	65	105	122	106	70	37	16	5	3	1	-
255		4	27	73	122	157	156	107	66	29	12	3	1	
270	-	5	24	78	139	172	166	123	77	33	15	3	1	-
285	-	4	25	73	132	143	156	110	64	30	8	4	1	
300	-	4	22	64	107	118	108	71	41	17	5	1		
315	-	4	19	53	76	76	61	37	20	6	2	1	-	
330	-	2	17	39	48	38	29	15	6	2	1	-		
345	-	2	14	27	30	21	13	6	1	1	-			



6-8-81-34

Figure III-19. POLAR HISTOGRAM OF NUMBER OF WIND ANGLE OCCURRENCES IN 15 DEGREE INTERVALS FOR THE SECOND SIMULATION.



6-8-61-38

Figure III-20. POLAR HISTOGRAM WITH EXPANDED SCALE OF NUMBER OF WIND ANGLE OCCURRENCES IN 15 DEGREE INTERVALS FOR SECOND SIMULATION.

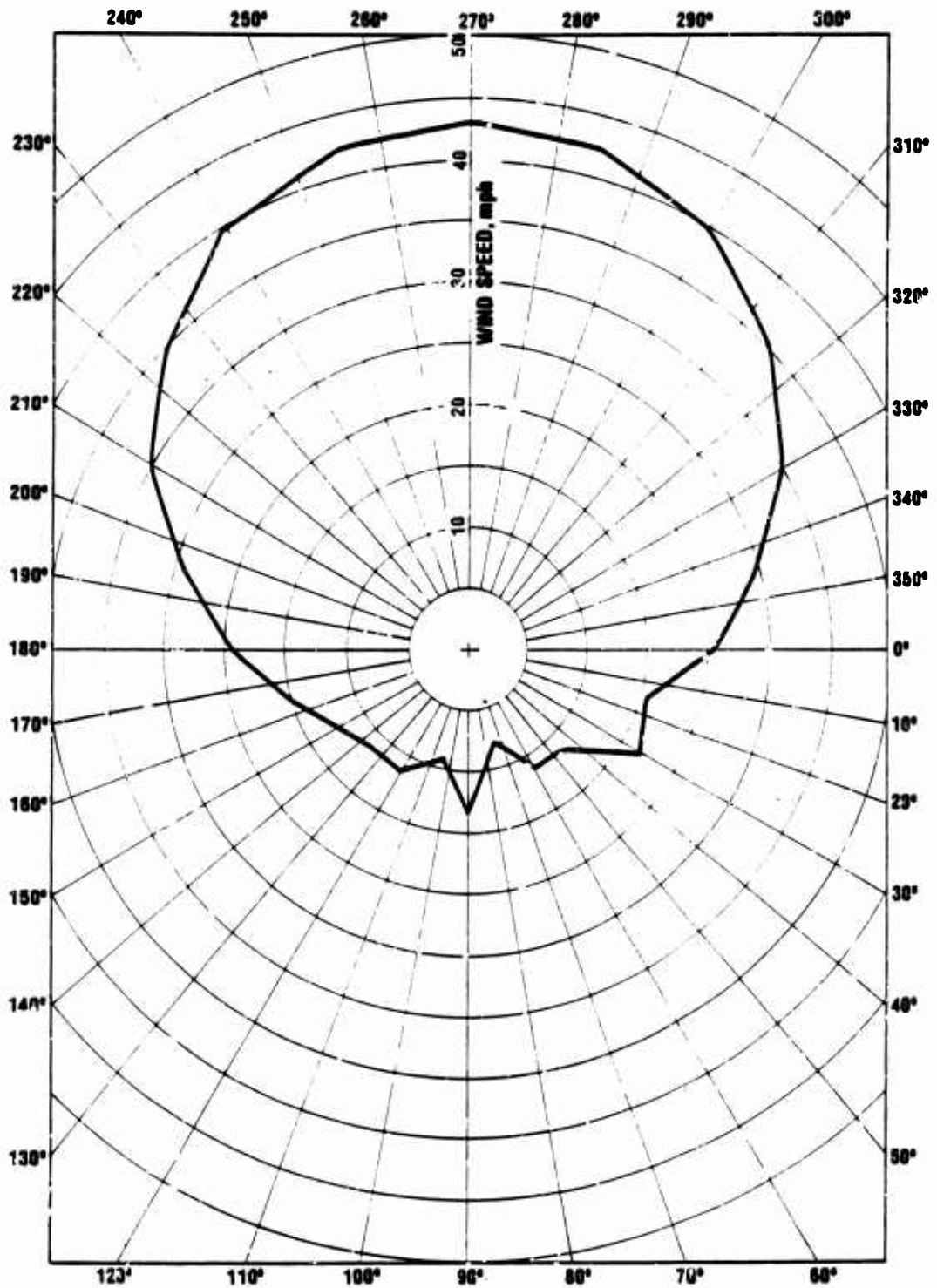


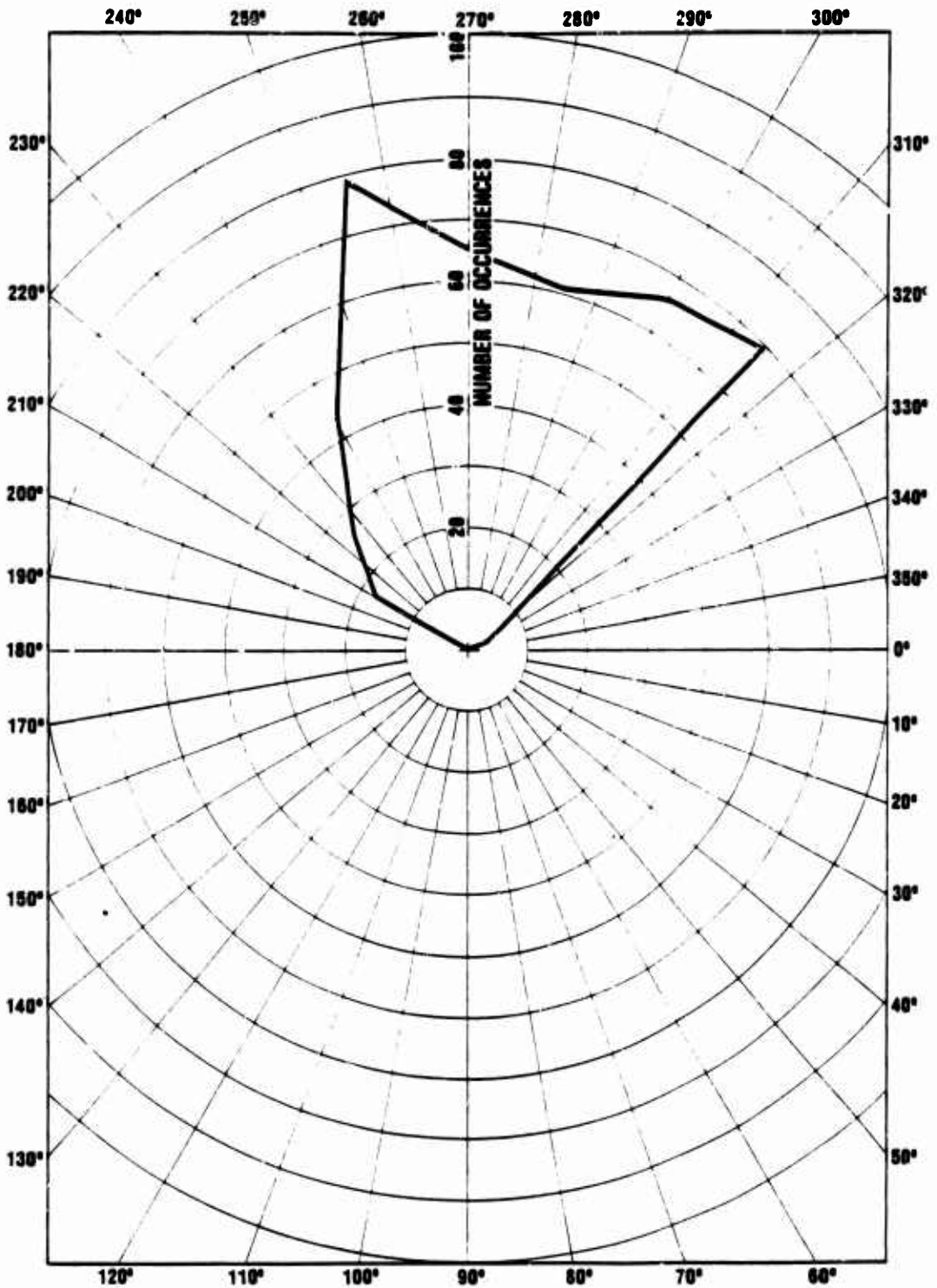
Figure III-21. MEAN WIND SPEED FOR WIND AT DIFFERENT ANGLES FOR THE SECOND SIMULATION.

mean wind speed as a function of angle. A comparison with the observed values presented in Figure III-13 shows quite good agreement for all angles. However, the number of occurrences of the winds blowing toward the West is considerably smaller. The cumulative scaled number of winds between 0 and 180 degrees is only 63.6, less than 1/6 of the observed value of 393. This second simulation shows that it is possible to match either the observed number of occurrences of winds blowing to the West or their observed mean speeds by this method, but not both simultaneously. For many uses a match of one of these statistics might be adequate, while for other more complex procedures might be necessary.

E. MONTHLY AND REGIONAL WIND DIRECTION STATISTICS

In Figures III-22 through III-27, polar histograms of numbers of occurrences and mean wind speeds are shown for the months of January, April, and August. The number of occurrences is not scaled here, it should be multiplied by 12 to be comparable to those for all months added together. The three months were selected to illustrate the statistics for a variety of wind patterns. For both January and April the wind is restricted to a relatively narrow angle, but for August some winds in almost every direction are seen. The wind direction for January has almost a constant number of occurrences over some 60 degrees, whereas for April it is strongly peaked at one angle. Although the number of occurrences for April is sharply peaked, the shape of the mean wind speed pattern for both April and August is similar. The mean wind speed for August shows a pattern somewhat similar in shape as for the nationwide winds, although the speeds are appreciably decreased. In all these patterns, the total number of events is small enough so that an appreciable random scatter appears in the patterns.

In Figures III-28 through III-35 polar histograms of number of occurrences and mean wind speeds are presented for



6-6-81-37

Figure III-22. POLAR HISTOGRAM OF THE NUMBER OF WIND OCCURRENCES IN 15 DEGREE INTERVALS FOR JANUARY.

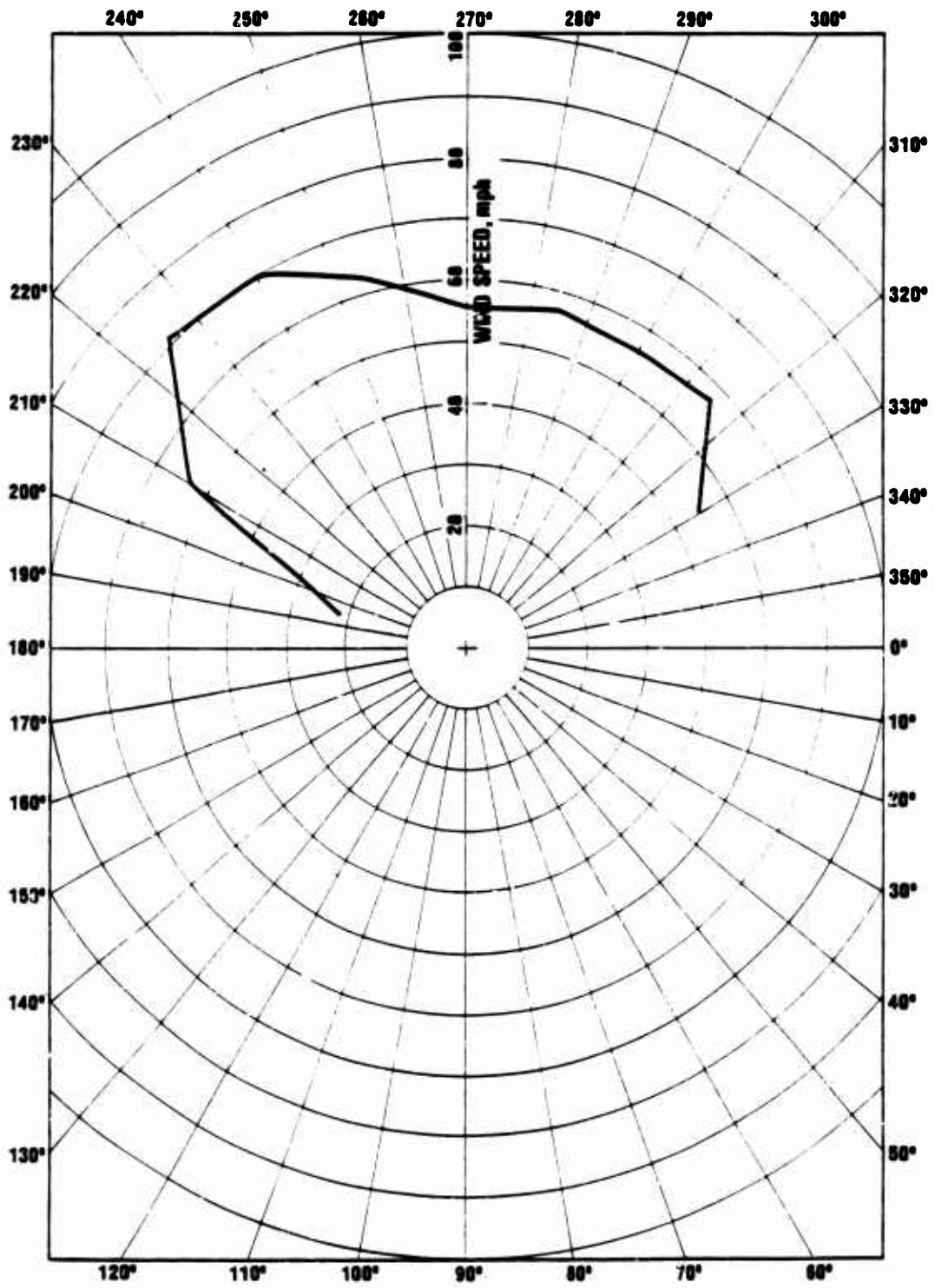
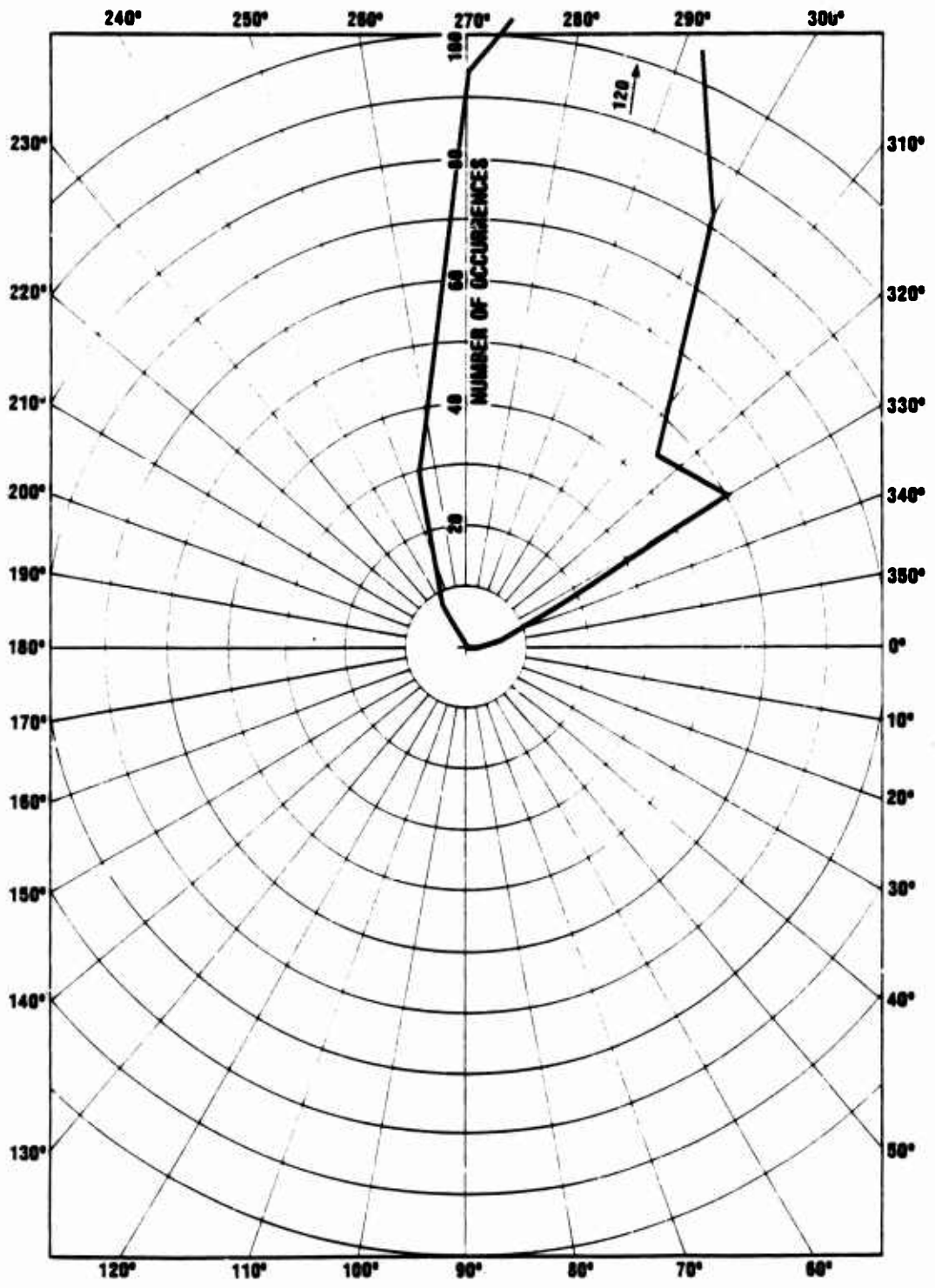


Figure III-23. MEAN WIND SPEED FOR WINDS AT DIFFERENT ANGLES FOR JANUARY.



6-6-61-30

Figure III-24. POLAR HISTOGRAM OF THE NUMBER OF WIND OCCURRENCES IN 15 DEGREE INTERVALS FOR APRIL.

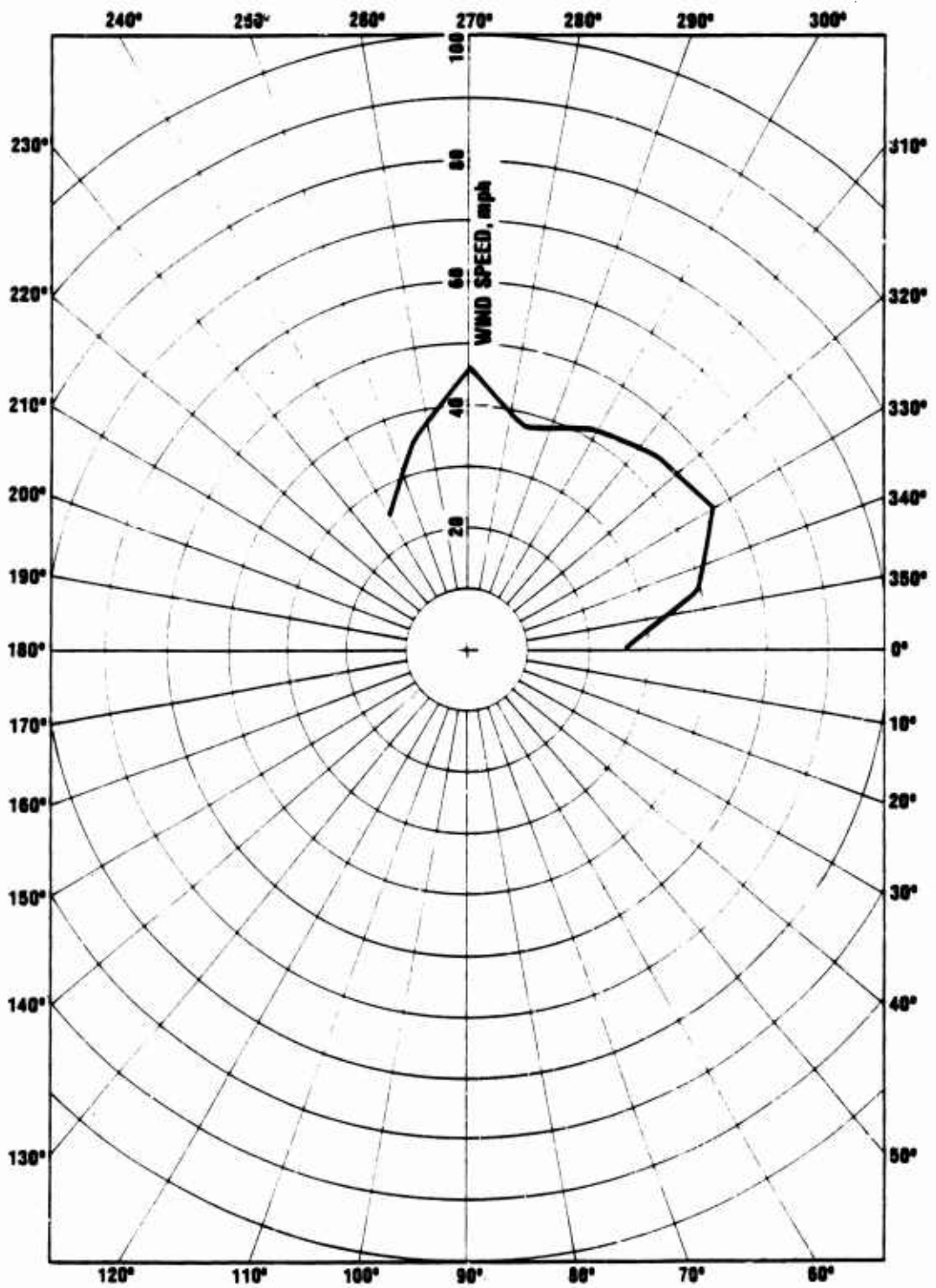
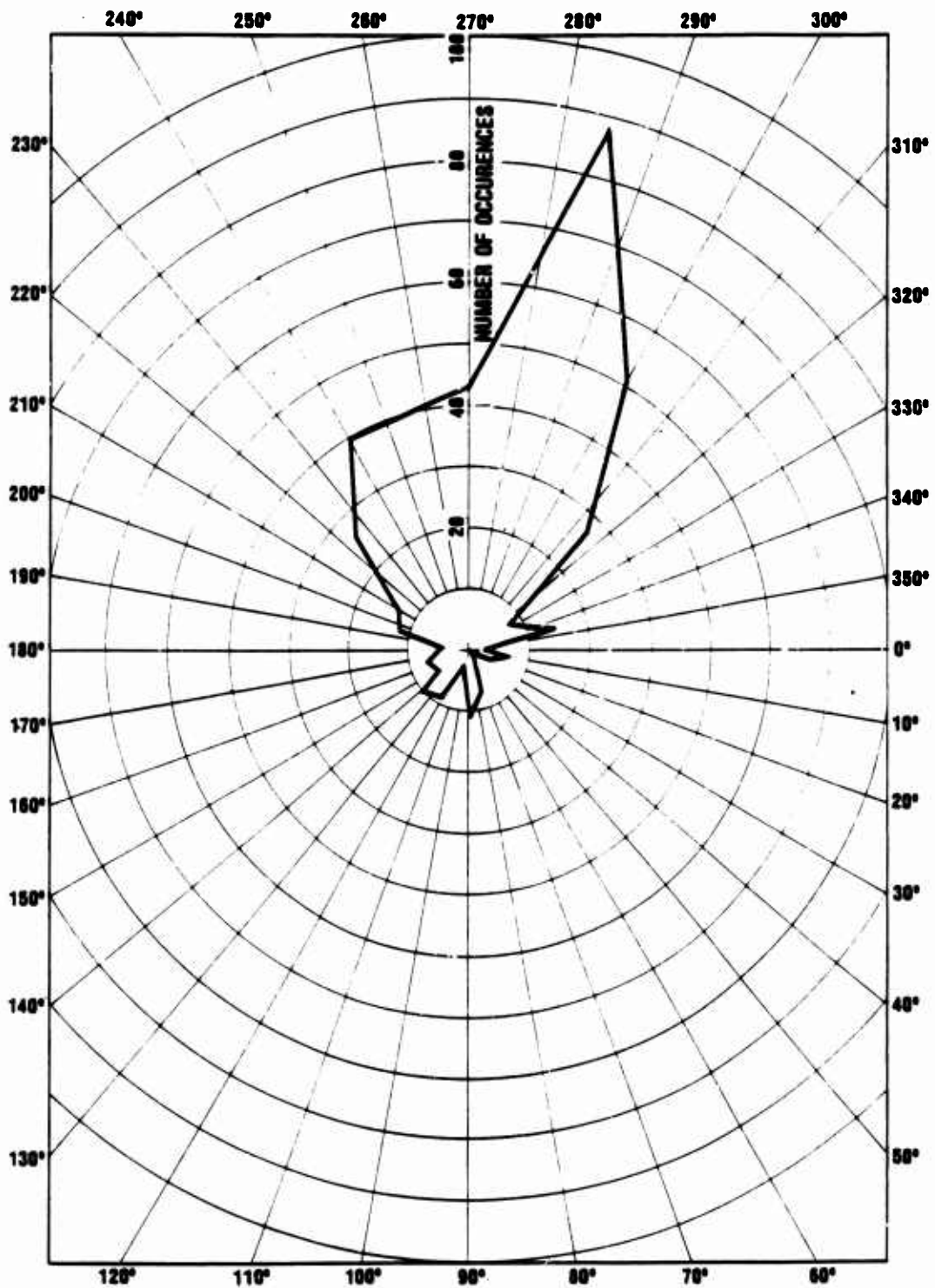
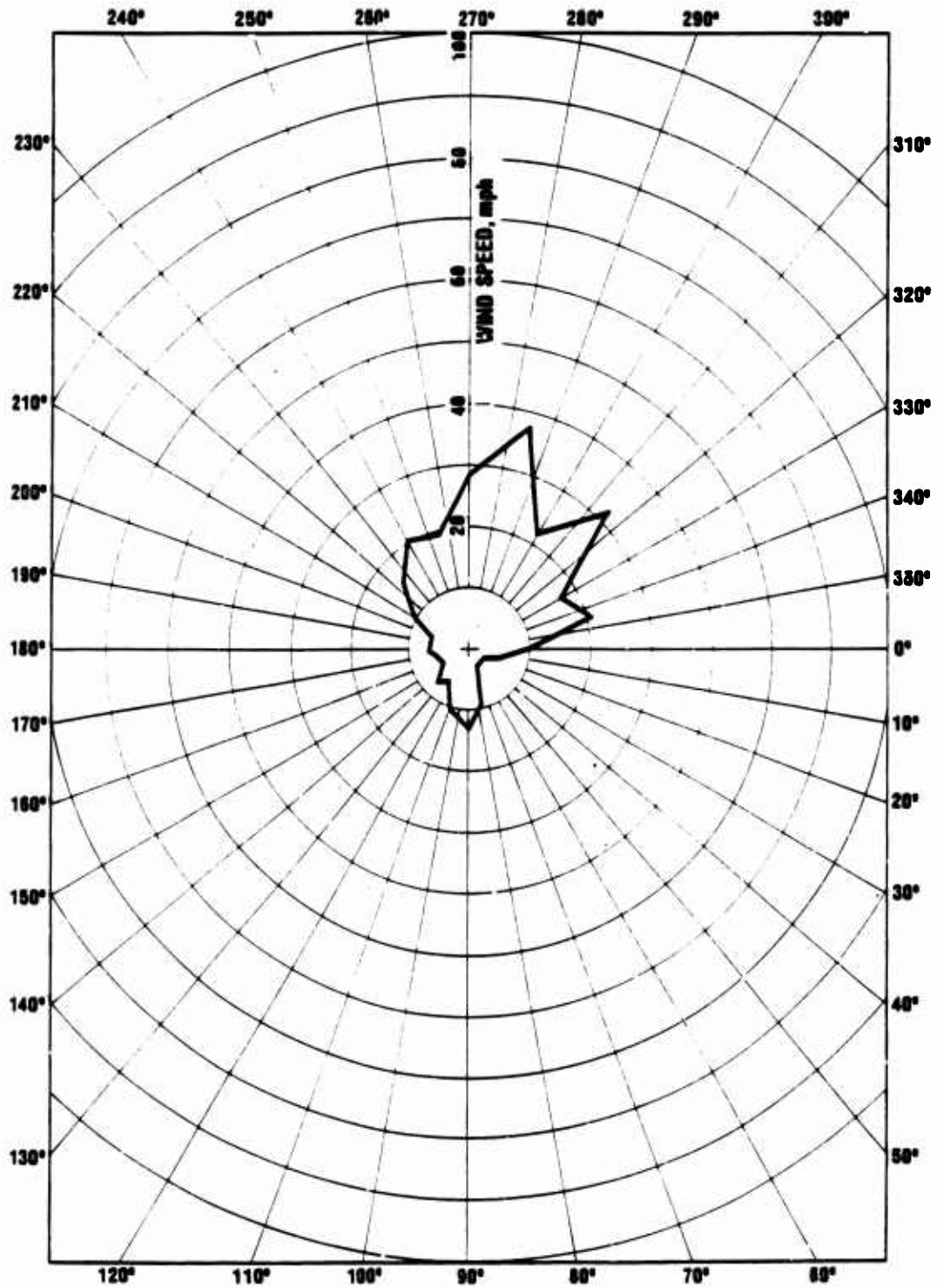


Figure III-25. MEAN WIND SPEED FOR WIND AT DIFFERENT ANGLES FOR APRIL.



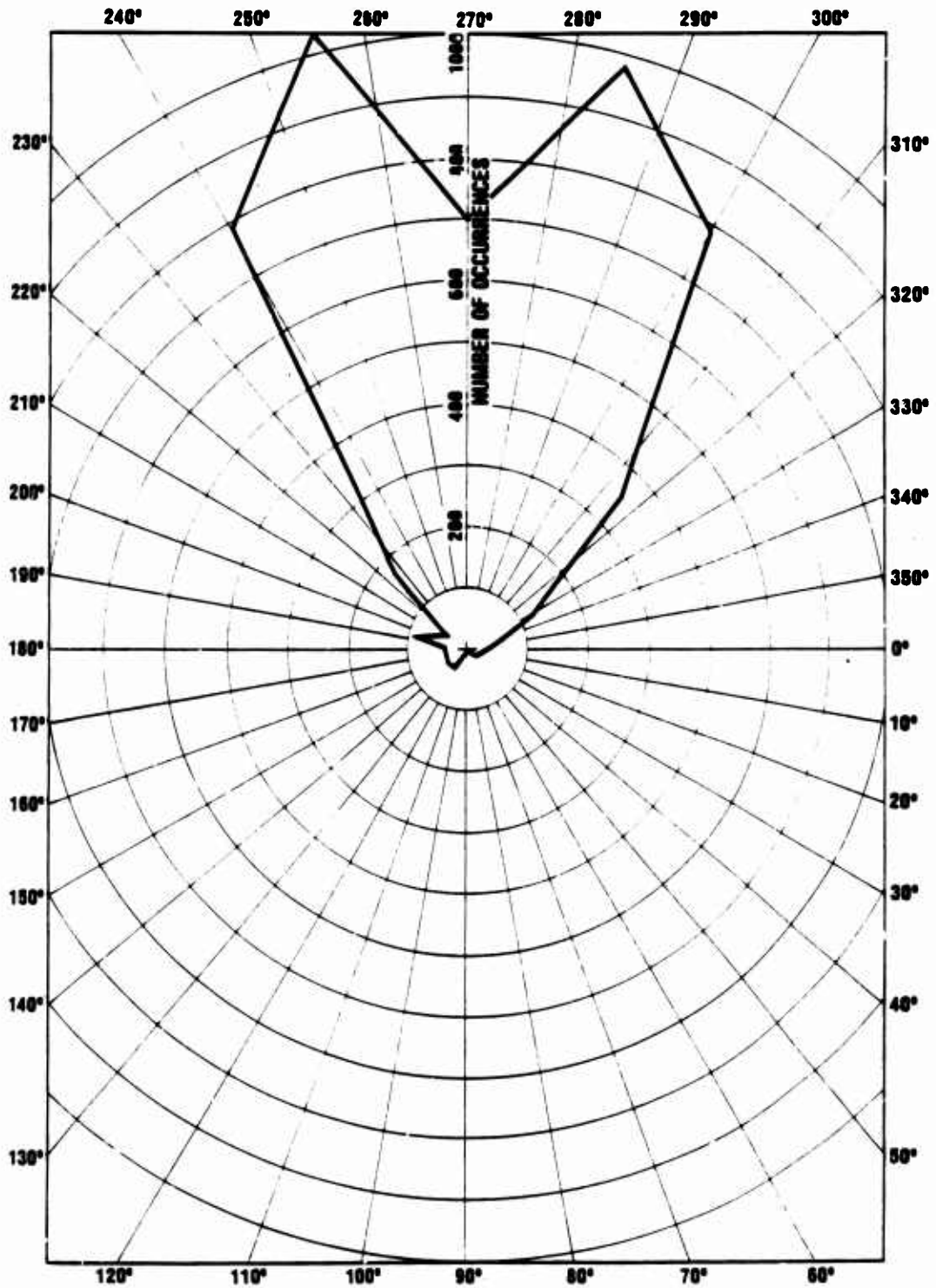
6-81-41

Figure III-26. POLAR HISTOGRAM OF THE NUMBER OF WIND OCCURRENCES IN 15 DEGREE INTERVALS FOR AUGUST.



6-9-61-42

Figure III-27. MEAN WIND SPEED FOR WINDS AT DIFFERENT ANGLES FOR AUGUST.



6-9-61-43

Figure III-28. POLAR HISTOGRAM OF THE NUMBER OF WIND OCCURRENCES IN 15 DEGREE INTERVALS FOR THE NORTHEAST.

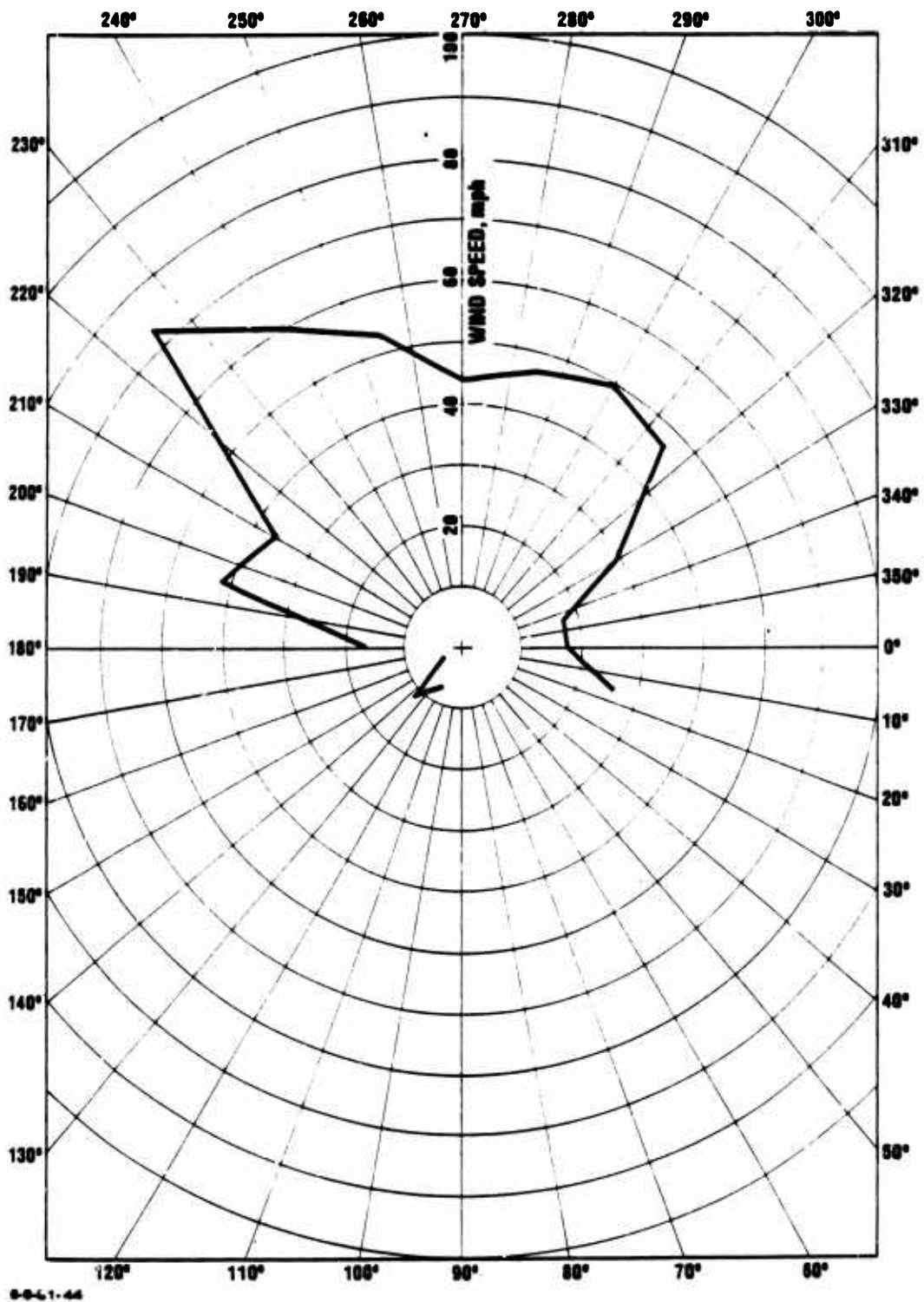
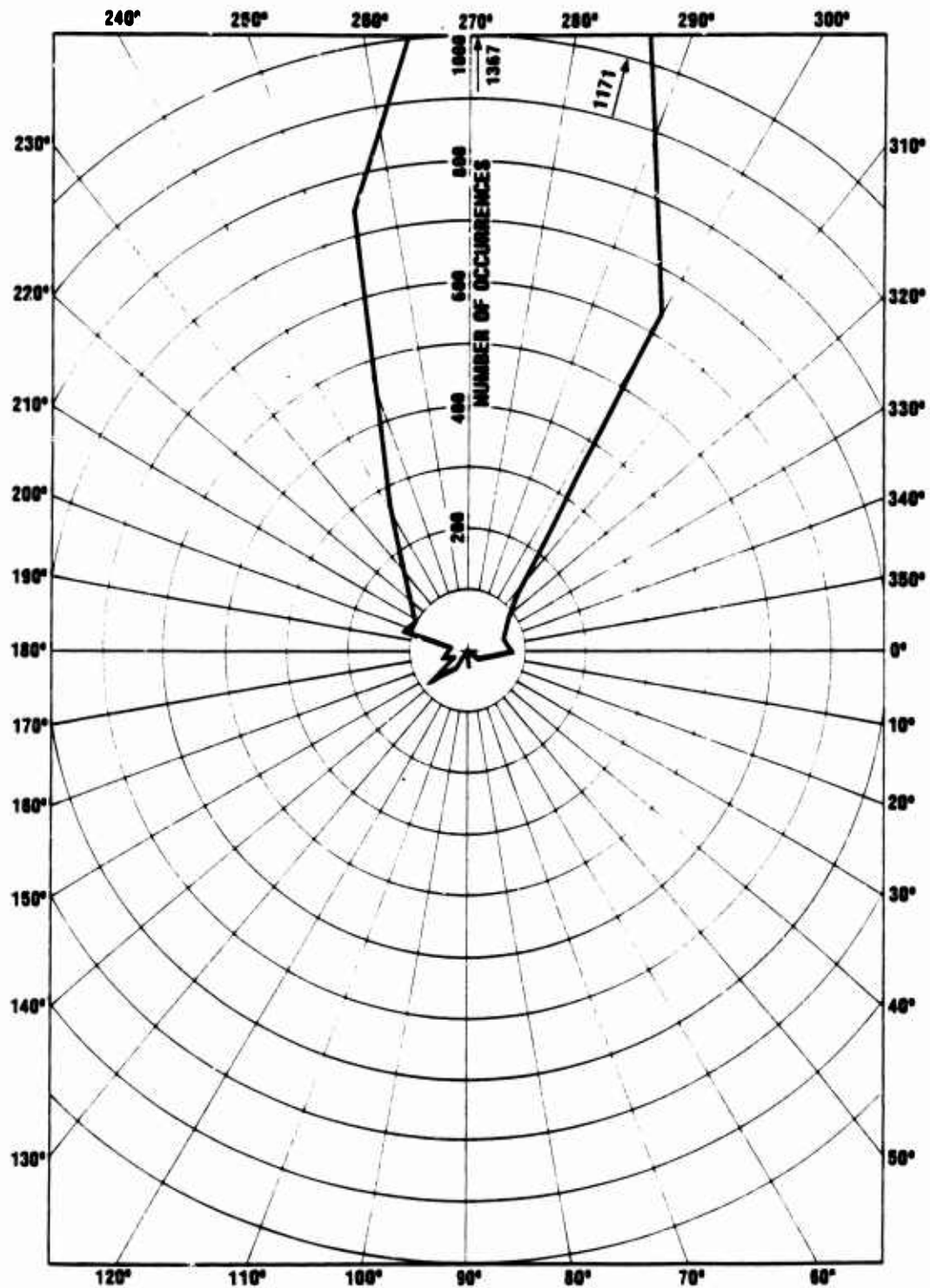


Figure III-29. MEAN WIND SPEED FOR WINDS AT DIFFERENT ANGLES FOR THE NORTHEAST.



6-9-81-46

Figure III-30. POLAR HISTOGRAM OF THE NUMBER OF WIND OCCURRENCES IN 15 DEGREE INTERVALS FOR THE SOUTHEAST.

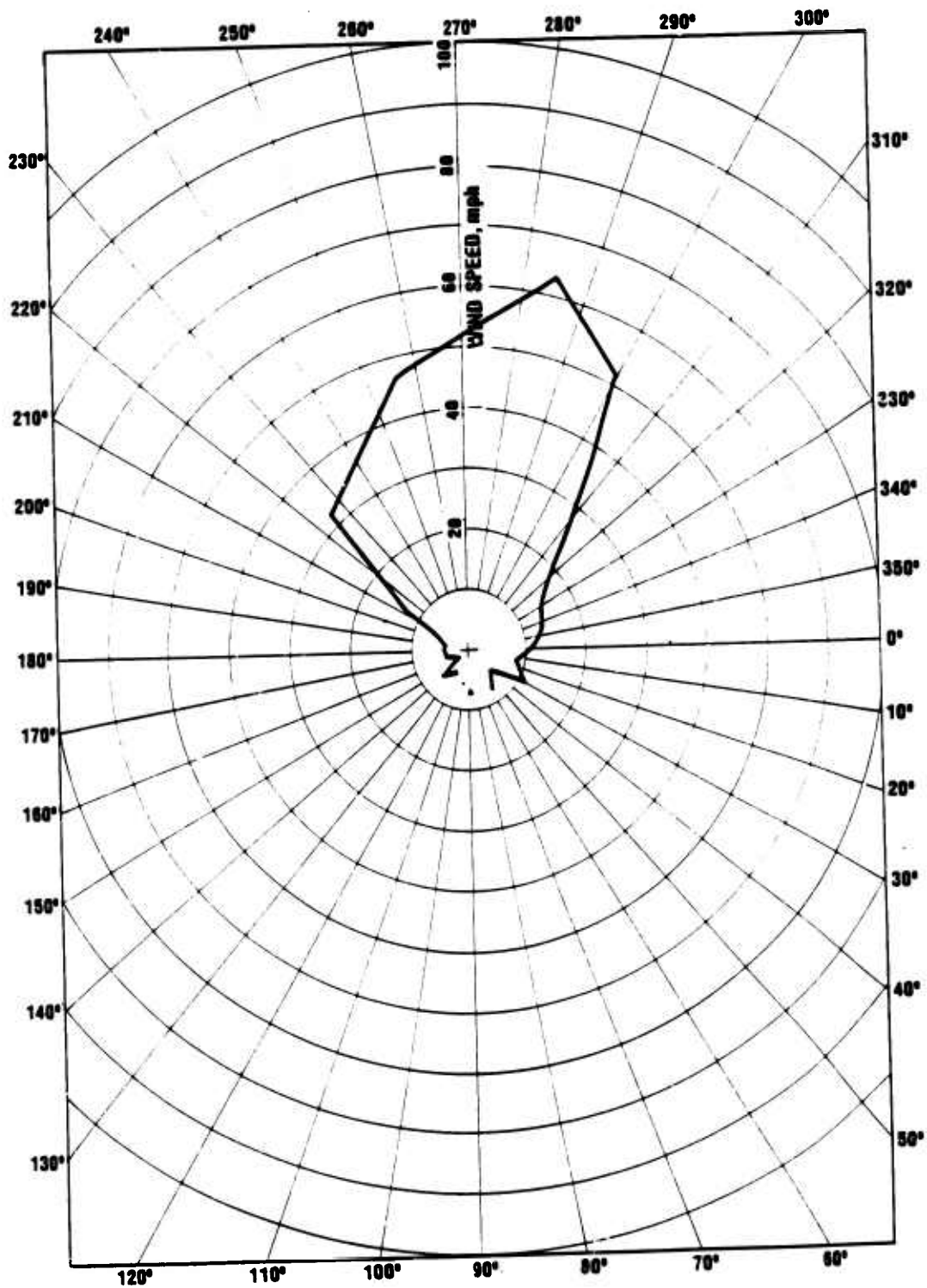
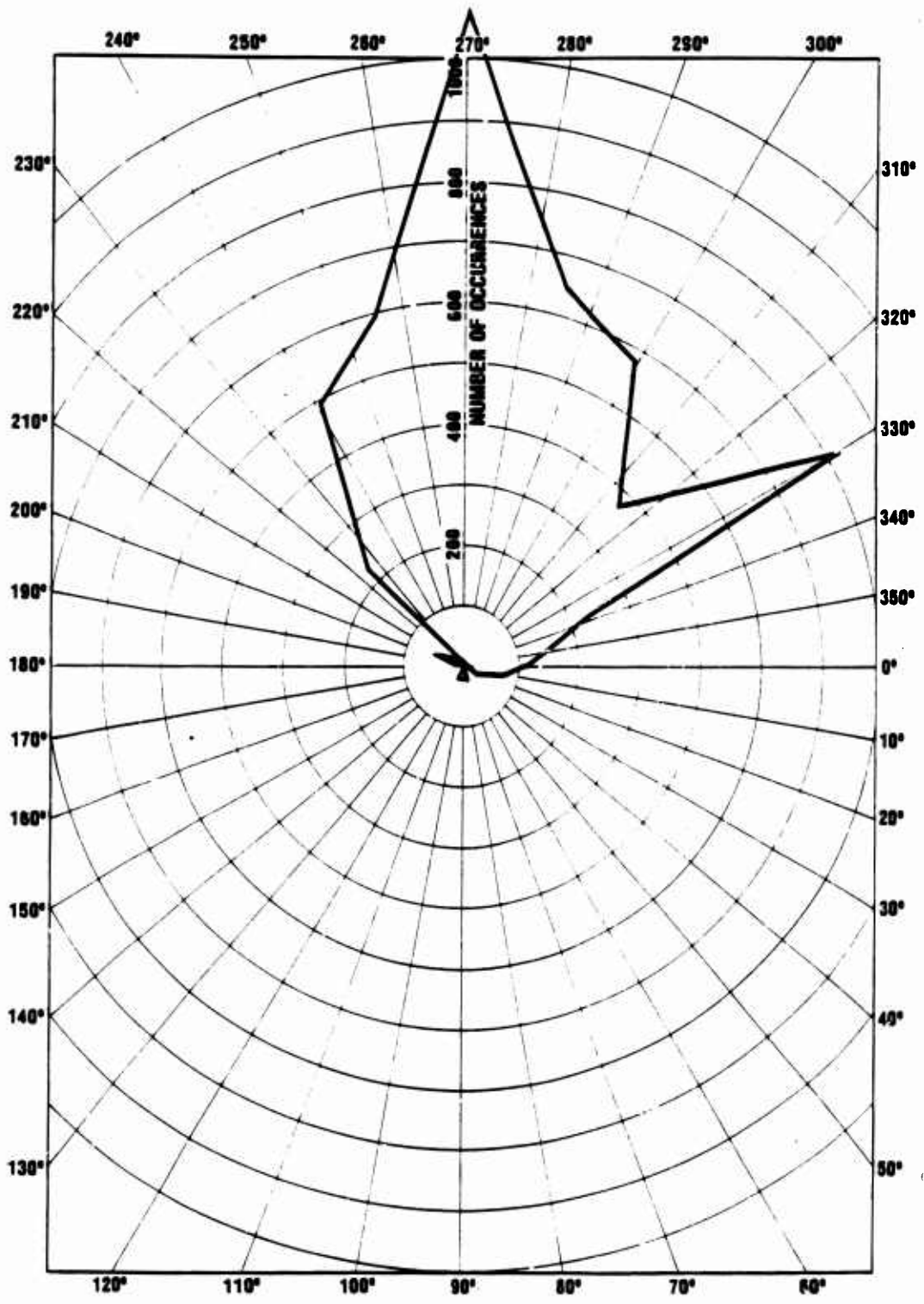


Figure III-31. MEAN WIND SPEED FOR WINDS AT DIFFERENT ANGLES FOR THE SOUTHEAST.



0-0-01-47

Figure III-32. POLAR HISTOGRAM OF THE NUMBER OF WIND OCCURRENCES IN 15 DEGREE INTERVALS FOR THE SOUTHWEST.

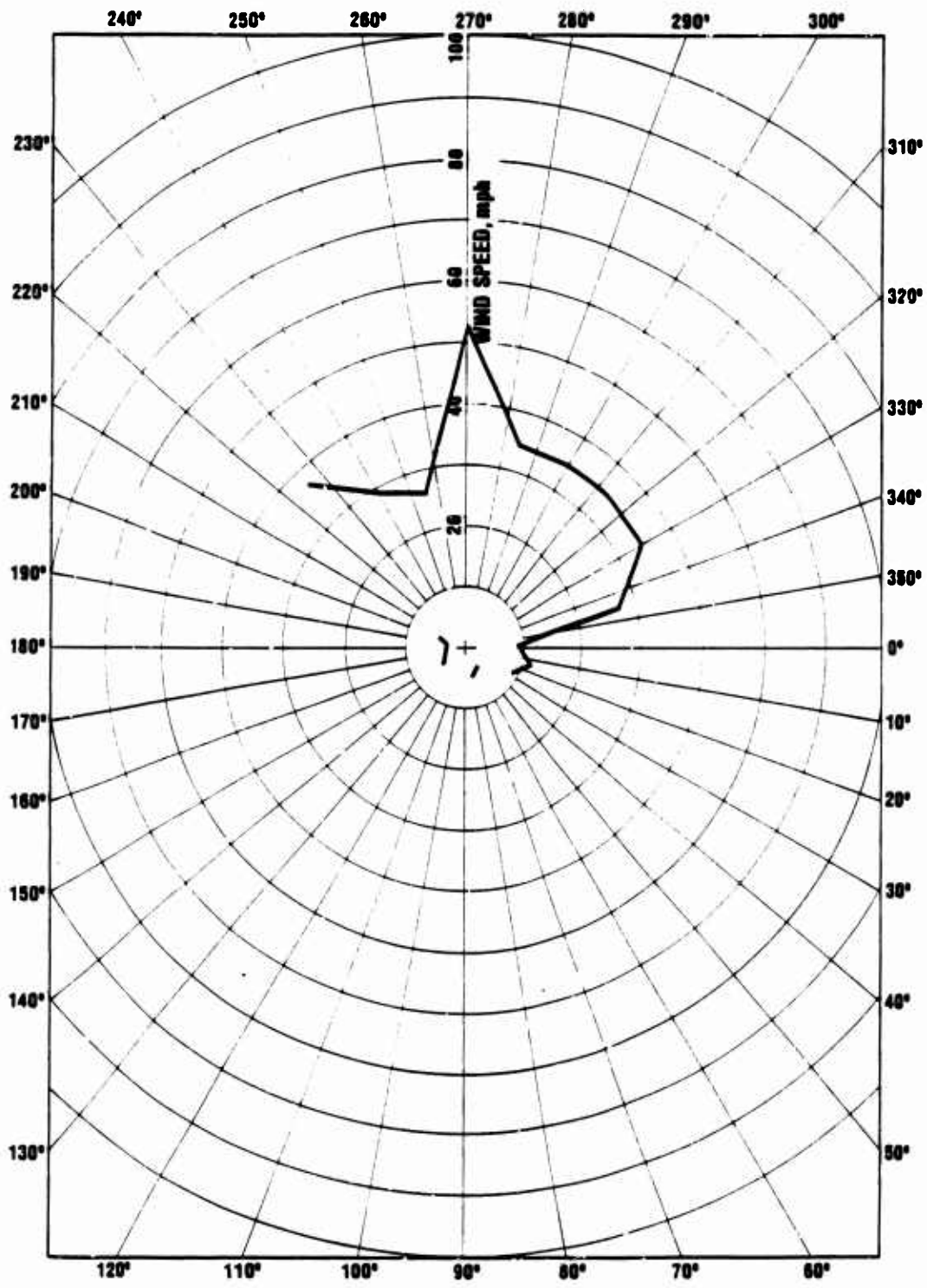
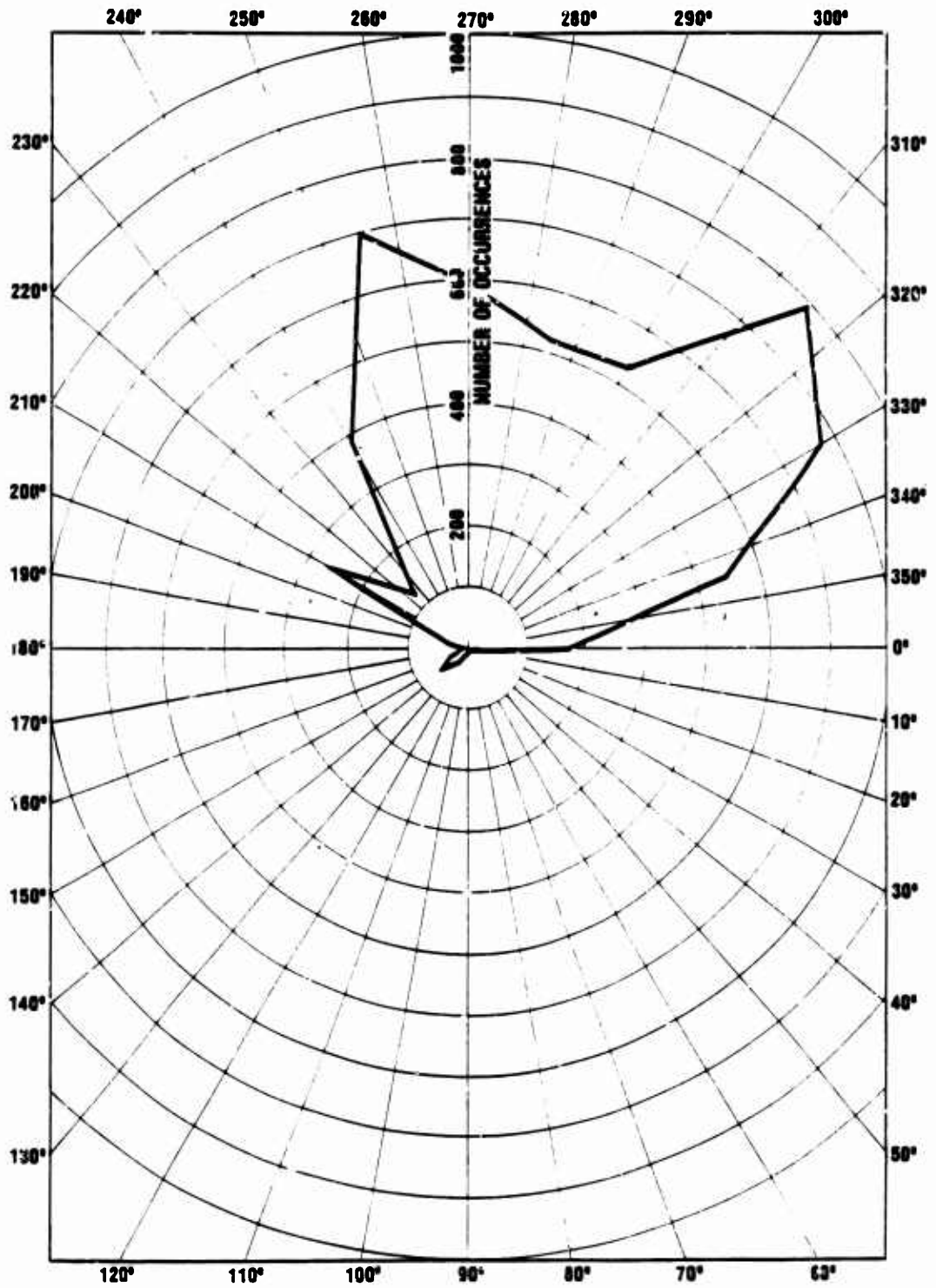


Figure III-33. MEAN WIND SPEED FOR WINDS AT DIFFERENT ANGLES FOR THE SOUTHWEST.



0-0-01-40

Figure III-34. POLAR HISTOGRAM OF THE NUMBER OF WIND OCCURRENCES IN 15 DEGREE ANGLES FOR THE NORTHWEST.

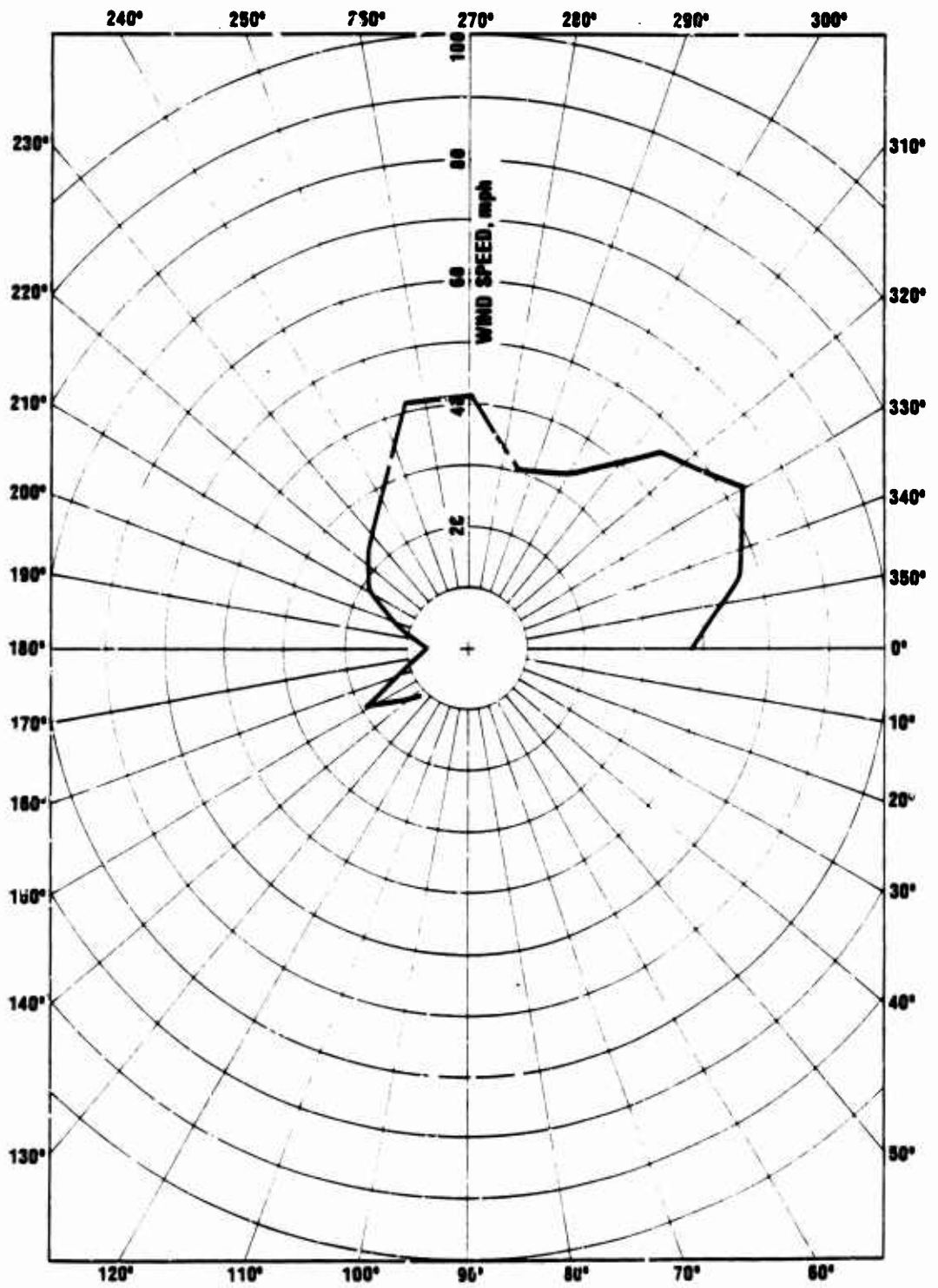


Figure III-35. MEAN WIND SPEED FOR WINDS AT DIFFERENT ANGLES FOR THE NORTHWEST.

the four regions discussed earlier. The number of occurrences are scaled in these Figures to be comparable with the nationwide values. The mean wind direction is near 270 degrees except for the Northwest where it skewed about 20 degrees to the South. Both the Northeast and Southwest show a bimodal distribution, although this might come from the limited sample of winds. The Southeast shows a peaked distribution, as does the Southwest if the one point at 330 degrees is neglected. The mean wind speeds for the Northeast and Northwest show a bimodal tendency, as does the histogram, whereas for the Southeast and Southwest more unimodal distribution occurs. These effects may be due to statistical fluctuations in the limited sample of 12 winds, or may be real. The patterns are not amenable to duplication by the simulation method used for the nationwide calculation, although for smaller regions (or a single location) the climatological description of a wind sample consisting of a mean wind vector plus a random vector drawn from a normal distribution should be applicable.

Chapter IV

THE ATTACK

A. DESCRIPTION

The attack used in this study is an unclassified attack developed by FEMA which was used in defining risk areas for crises relocation studies. The attack is directed against time-urgent strategic offensive delivery forces (counterforce targets), other military targets, industry and population. The attack has at least one weapon delivered upon each urbanized area in the United States. The full attack consists of the following weapons:

Yield	Number of Weapons
1 Megaton	843
2 Megatons	185
3 Megatons	176
20 Megatons	240

The total attack consists of 1444 weapons with a total yield of 6541 megatons. All weapons are assumed to be surface burst with a fission fraction of 0.5. The full attack is called Attack A.

Attack B is used against only "counterforce" targets and consists of the following weapons selected from Attack A:

Yield	Number of Weapons
1 Megaton	50
20 Megatons	126

Attack B consists of 176 weapons with a total yield of 2570 megatons. The 1 megaton weapons are primarily used against airfields and the 20 megaton weapons are all used against missile fields.

In both Attacks A and B the 126 twenty megaton weapons used against missile fields are an artifice. A single 20 megaton weapon represents 20 one megaton weapons targeted against 20 separate launching silos. This artifice was introduced when the attack was first developed to avoid identifying locations of individual missile silo locations and, for computational efficiency, to keep the total number of weapons smaller but still give adequate input for civil defense damage assessment (as opposed to adequate damage assessment for the strategic delivery forces themselves).

These two attacks are taken here as representative, for civil defense purposes, of the total intensity and distribution of weapons in two strategic war scenarios often used in defense planning. The total yield of Attack A is compatible with SALT II limitations. If the reader wishes to modify certain assumptions, for example the weapon fission fractions or heights of burst, this can be done by modifying the interpretation of the dose ranges. In most locations the doses due to attacks on missile fields are identifiable and separable from those due to attacks on cities and separate modifications can be made for these two types of weapons. Finally, since the resolution of the fallout patterns is ten miles square and since the fallout pattern covers large areas, the patterns obtained are insensitive to the details of attack within cities. Thus, whether industry or population is the principle intended victim of an attack upon a particular city should have an insignificant effect upon the overall result. For the remainder of this chapter the attack will be taken as a given phenomena, and the distribution of the weapons will be the subject of study.

A map of the weapon locations for Attack A is presented in Figure IV-1 (this map is on the same scale as the fallout maps in the appendices). The figures on the map give the total yield for all weapons in a ten mile square (which is the resolution of the map). The numerals 1 through 9 indicate yields of the same values; the letters have values as follows:

Letter	Yield Range, Megatons
A	10-19
B	20-29
C	30-39
D	40-49
E	50-59
...	...

The clusters of B's on the map are the 20 megaton weapons detonated on the missile fields. Immediately evident are the clusters of weapons over large urban areas. Another immediate feature is the higher density of individual weapons or small weapon concentrations in the Eastern portion of the county as compared to the Western portion. Most points in the East are within, say, 50 miles of a weapon detonation, while large stretches of the West have no weapons within one or two hundred miles.

In Figure IV-2 weapon locations are presented for Attack B. Here one sees 9 clusters of 20 megaton weapons on the missile fields and a rather wide dispersion of the one megaton weapons. Clearly in this attack the fallout patterns will be dominated by the winds from the missile fields.

A somewhat different method of presenting Attack A is given in Figure IV-3. Here the weapons are grouped into clusters and the total yield in each cluster is given. The clustering, in general, associates together all weapons which are linked by having the two psi blast overpressure contours from adjacent weapons crossing. A different cluster is

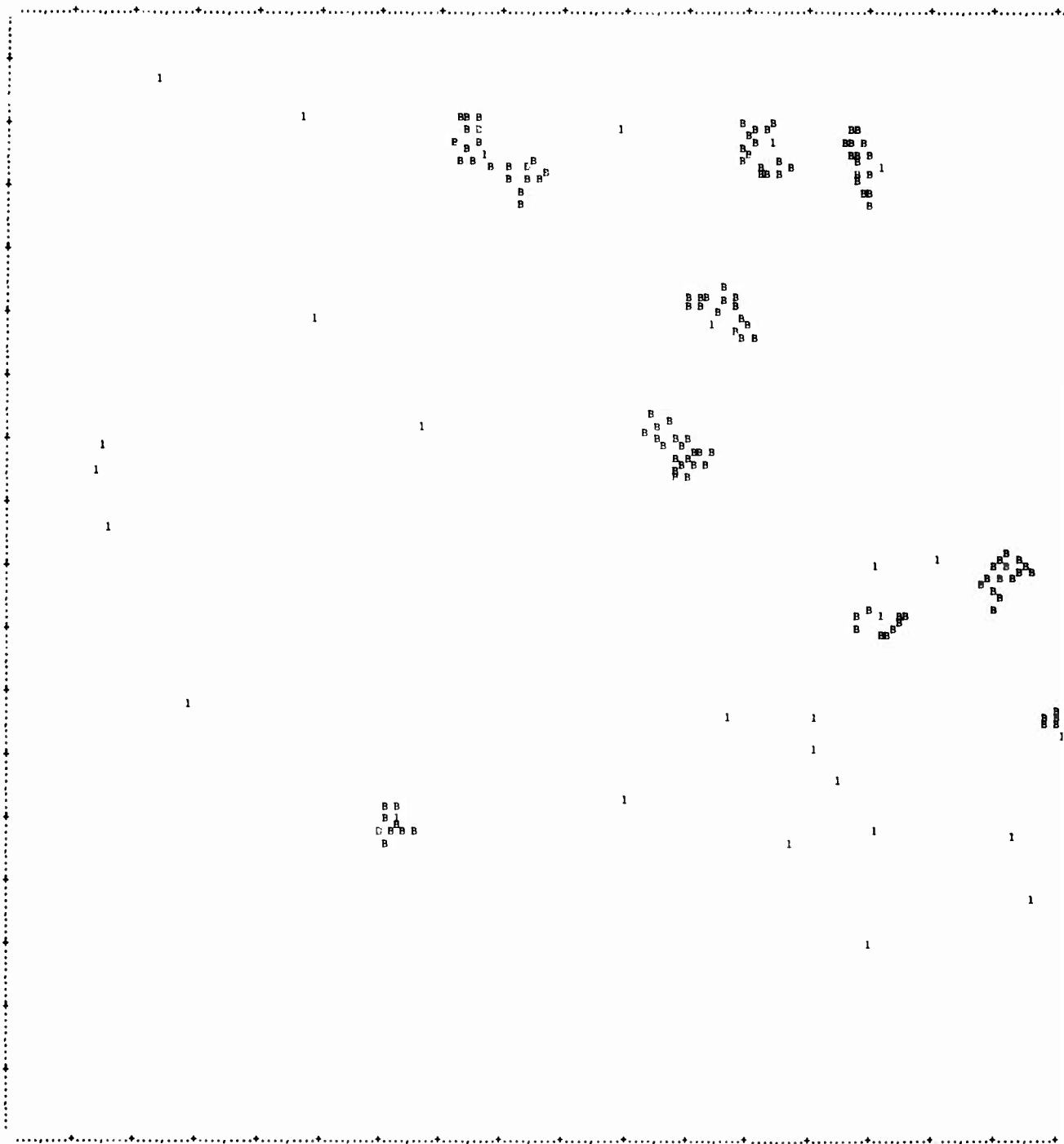
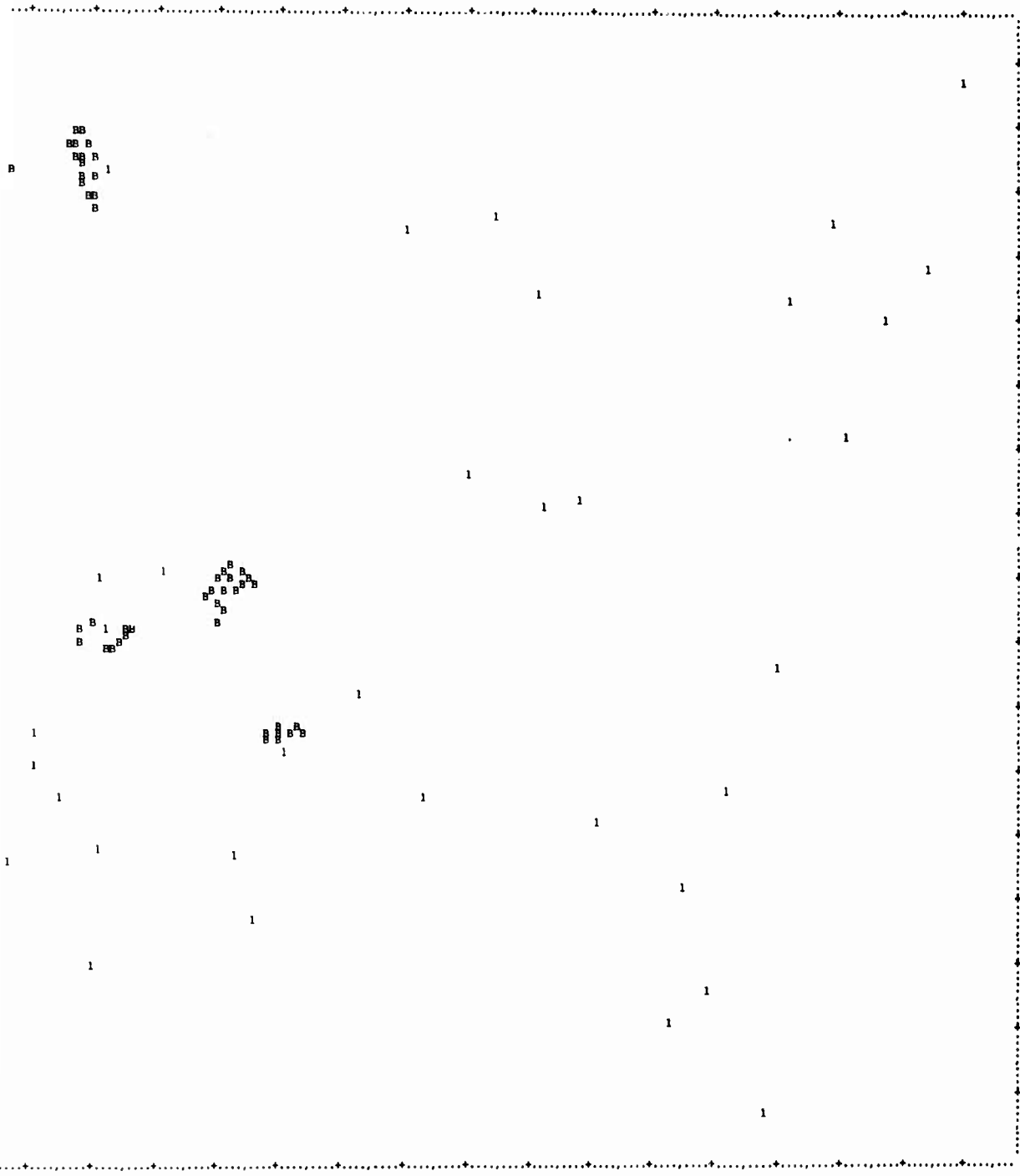


Figure IV-2. MAP OF WEAPON LOCATIONS FOR ATTACK



LOCATIONS FOR ATTACK B (COUNTERFORCE ONLY).

defined for each urbanized area, even if the two psi contours cross some weapons from adjacent urbanized areas. A plus sign on the map indicates the ten mile square which contains the centroid of the cluster, while the yield of the cluster is given to the right of it. In a few cases there are adjacent clusters. The yield given is the yield of the Eastern most cluster, the yield of the Western most cluster is not presented.

In Figure IV-4 the cluster locations for Attack B are presented. Again the predominance of the large yields delivered to the missile fields, compared with any other elements of the attack, is evident.

B. DEPICTION

The mass of detail in Figures IV-1 through IV-4 is difficult to follow and, from the fallout maps in the Appendices, seems to have more detail than is really necessary to adequately define the patterns. A defocusing of these detailed pictures might allow more ready comprehension. A method of accomplishing this is to compute smoothed weapon densities on a grid of monitor points and plot weapon density contours using these points.

Consider a monitor point P, one element of a grid. Let R_1 be the distance of the L'th weapon from the monitor point P, and let Y_1 be the yield of that weapon. Then the density at P, $D(P)$, is defined as

$$D(P) = \sum_1 \frac{Y_1 e^{-(R_1^2/2\sigma^2)}}{2\pi\sigma^2}$$

where:

the summation is taken over all weapons, and σ is a constant defining how rapidly weapon influence diminishes with distance.

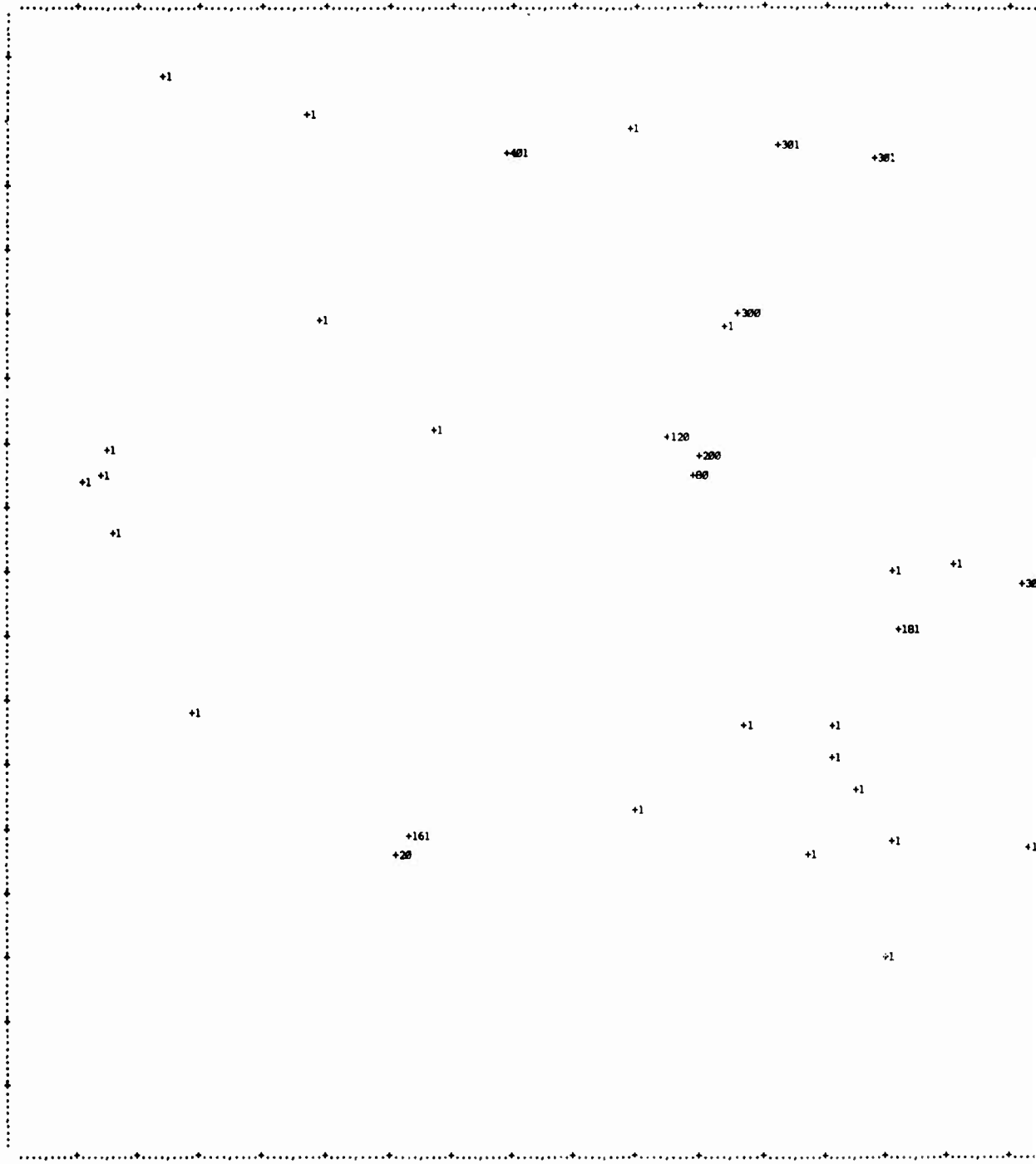
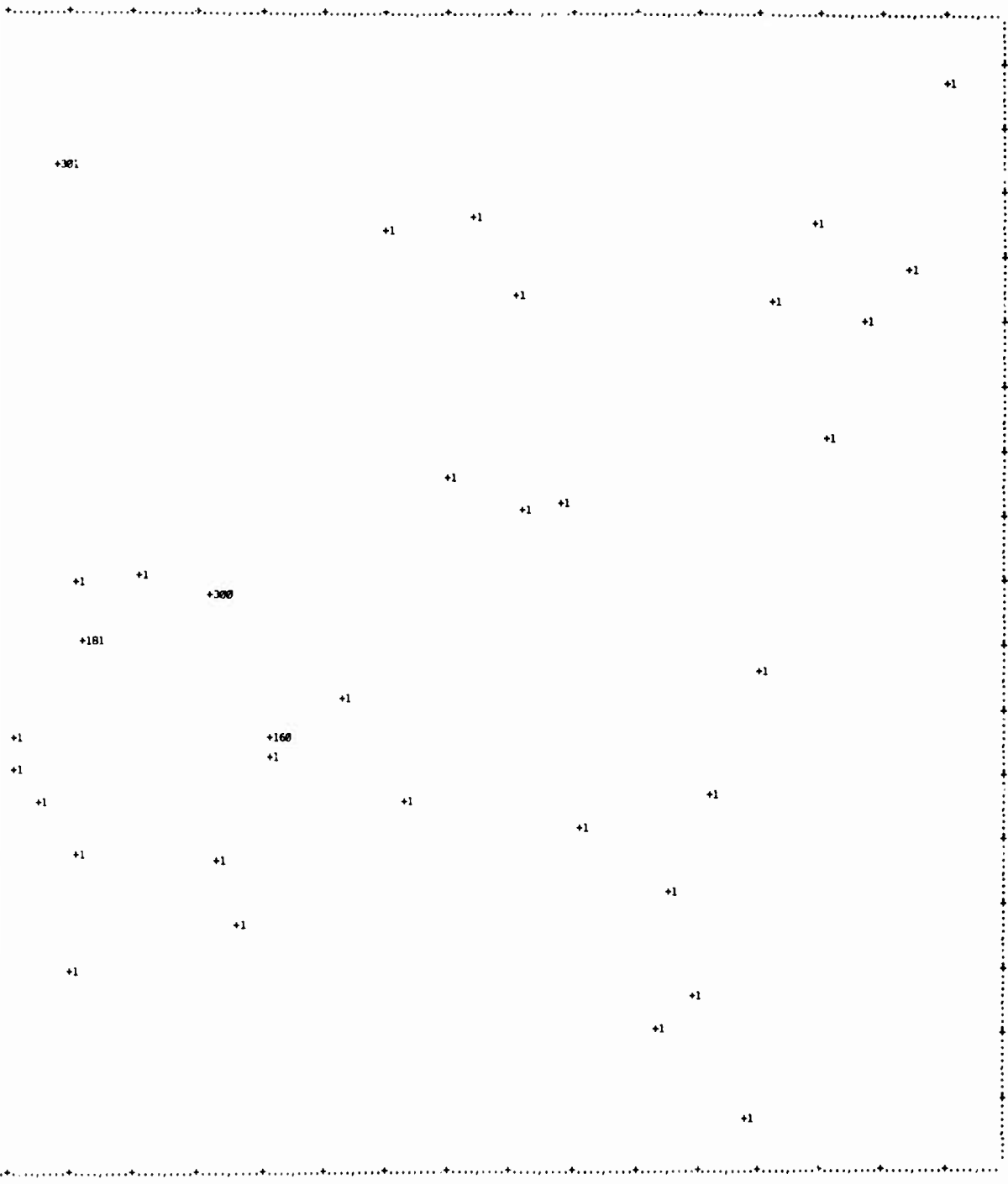


Figure IV-4. MAP OF CLUSTER LOCATIONS FOR

1

2



LOCATIONS FOR ATTACK B (COUNTERFORCE ONLY).

For example, suppose σ is 100 miles. A weapon at the monitor point might be given relative weight 1. Compared to this weapon a weapon at a 50 mile distance would have a relative weight of 0.88, at 100 miles at relative weight of .60, at 150 miles of a relative weight of 0.32, at 200 miles a relative weight of 0.13, and at 300 miles a relative weight of 0.01.

The sum is normalized by the normalization factor $2\pi\sigma^2$ so that if each square mile had a weapon of 1 megaton yield, the density computed would be 1 MT/mile².

Figure IV-5 shows weapon density contours with σ equal to 100 miles for Attack A for the same area as covered by the fallout maps in the Appendices. The contours were generated by computing weapon densities at the intersections of a 20 x 30 grid of monitor points, with the grid spacing 100 miles, and drawing contours at various density intervals. The contour values give weapon densities in kilotons of total yield per square mile.

In Figure IV-6 the attack on the missile fields is immediately evident, producing peak weapon densities, with this weighting, of 6 kilotons/mile². The attacks on San Francisco and Los Angeles produce a single 2 kiloton/mile² contour covering both cities. The peak weapon density at San Francisco is 3 kilotons/mile² and at Los Angeles 5 kilotons/mile². The Washington-New York-Boston corridor on the East Coast is completely covered by high weapon densities; the pattern extends Westward at somewhat lower intensities but is still over 3 kilotons/mile² as far west as Chicago.

The features of the attack are defocused still more where weapon density contours for the full attack are presented for a value of sigma of 200 miles. Here the attack features merge into several fairly smooth areas of high density in the San Francisco area, in the Western missile fields and in the Northeast. Some former separated peaks have been eroded into spurs of larger high density regions. The peak density in

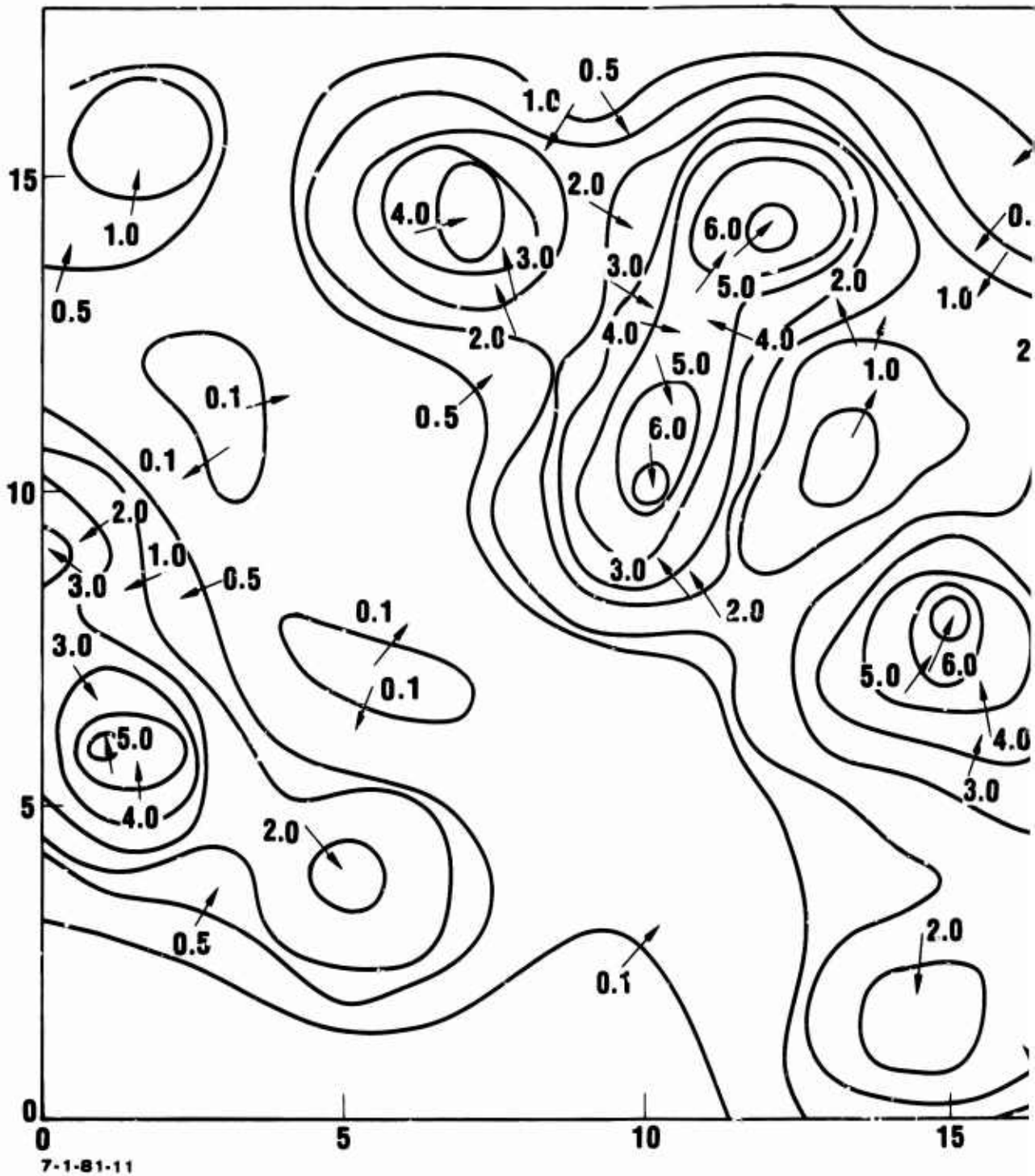
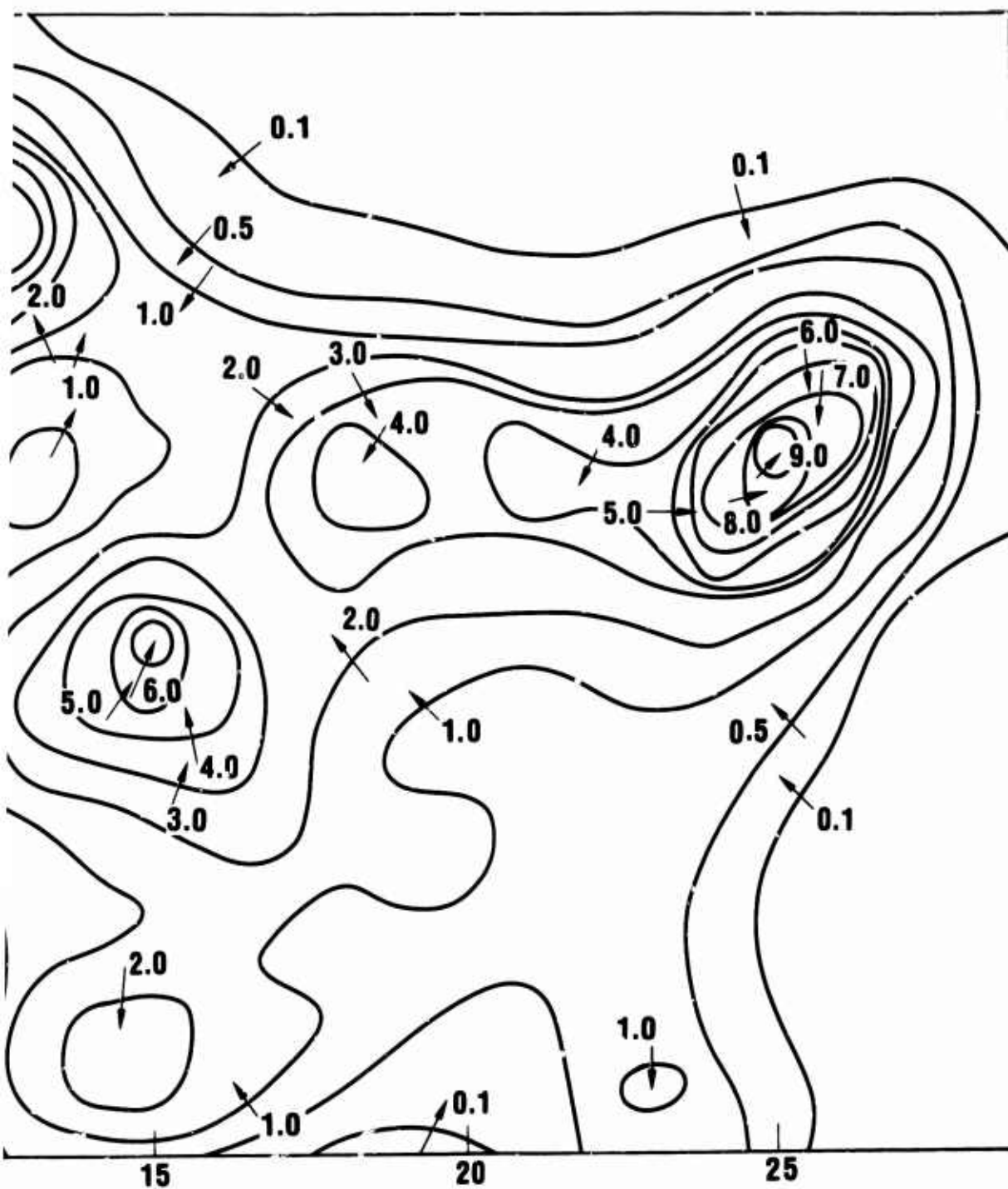


Figure IV-5. WEAPON DENSITY CONTOURS FOR ATTACK SIGMA OF 100 MILES.



CONTOURS FOR ATTACK A WITH GAUSSIAN WEIGHTING AND ES.

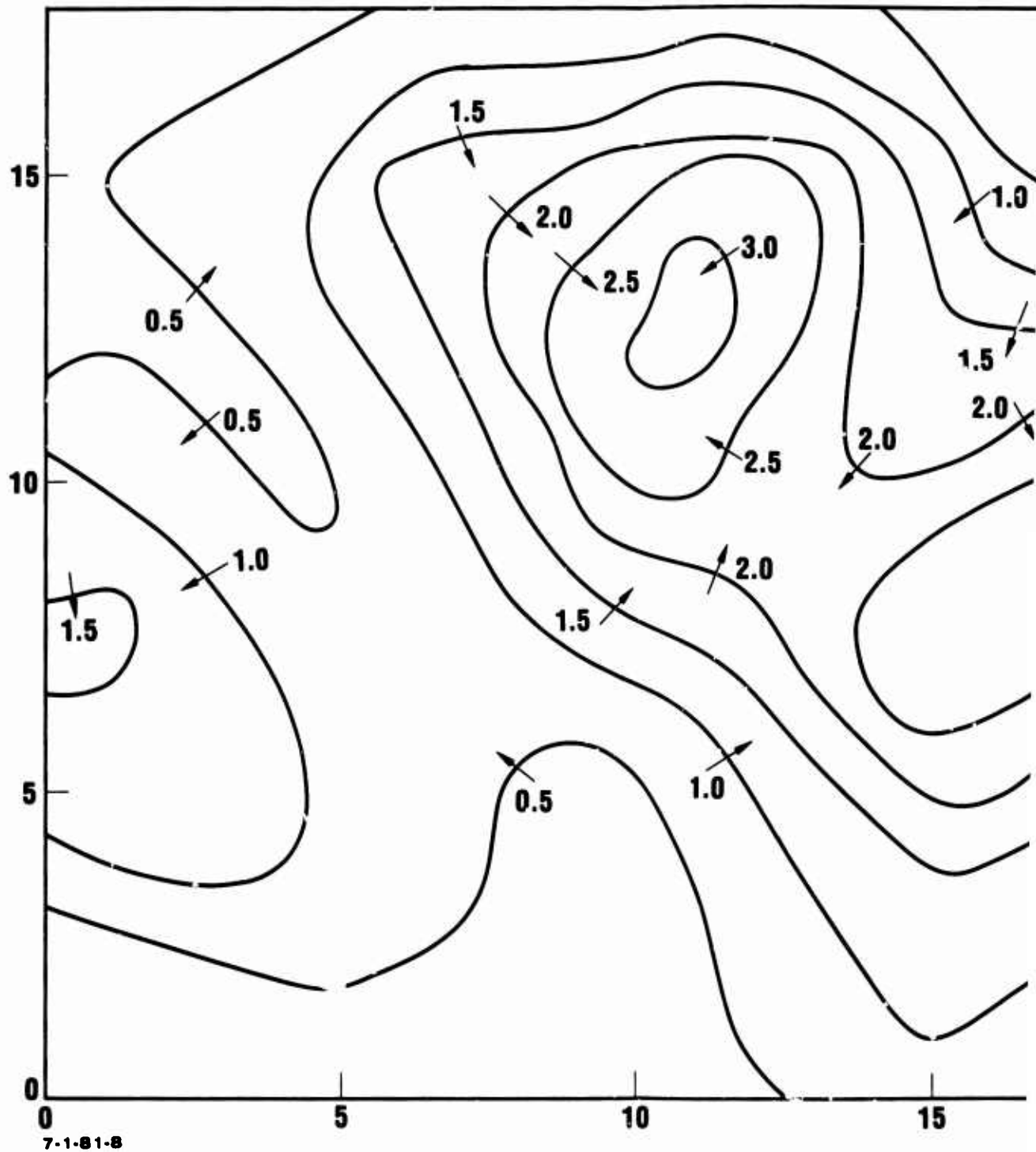
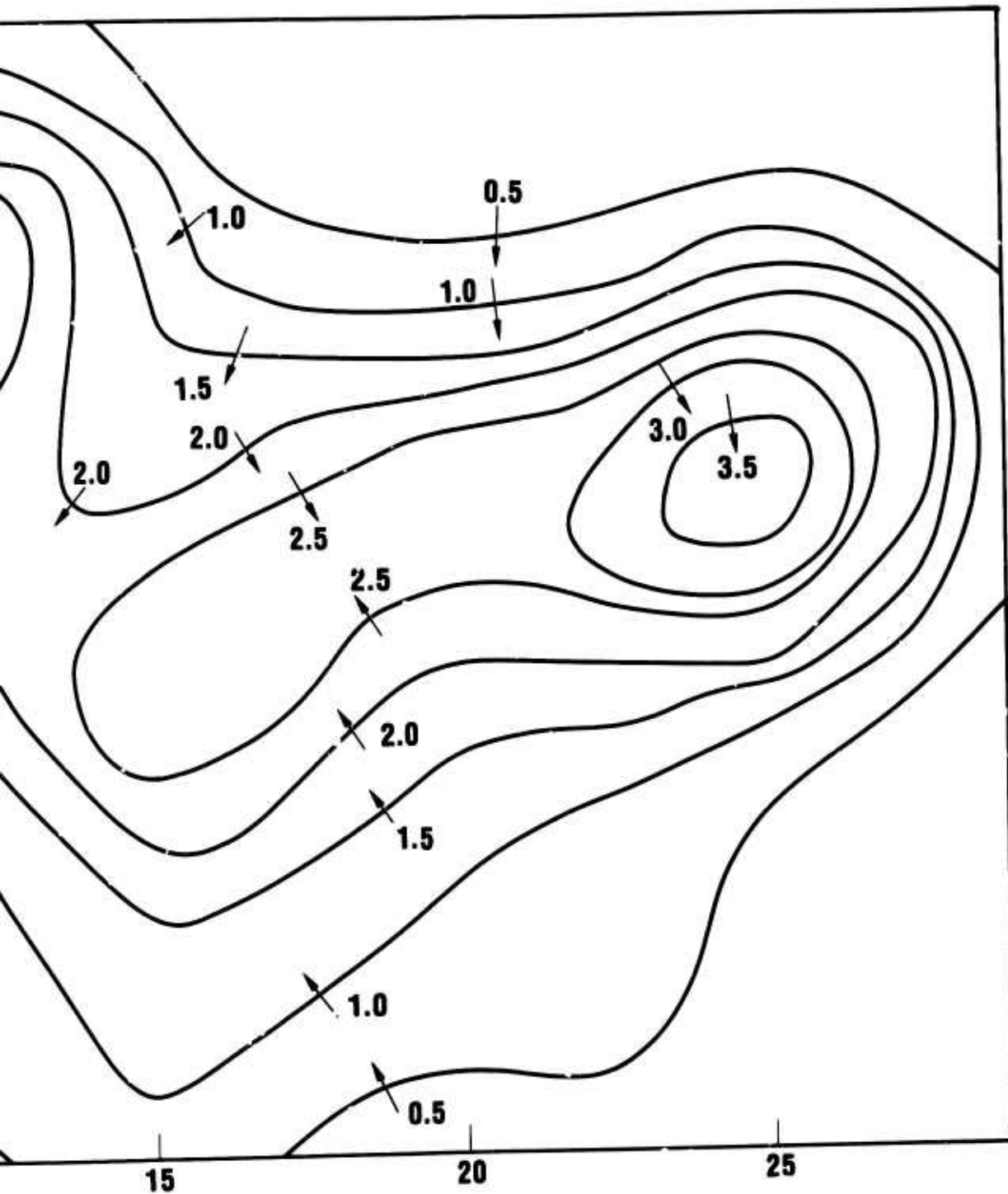


Figure IV-6. WEAPON DENSITY CONTOURS FOR AT
SIGMA OF 200 MILES.



TY CONTOURS FOR ATTACK A WITH GAUSSIAN WEIGHTING AND
MILES.

the Northeast has decreased from 9 kilotons/mile² to 3.5 kilotons/mile². A decrease in peak density is to be expected as sigma is increased, since the density is dispersed further out.

In Figure IV-7 the weapon density is computed using a different weighting function. Here the density is computed by

$$D(P) = \sum_1 \frac{Y_1 e^{-(R_1/\sigma)}}{2\pi\sigma^2} .$$

The normalization factor still gives unit density of the plane uniformly covered by weapons with 1 megaton of yield in each square mile. The exponential weighting of this formula, compared with the Gaussian weighting of the previous formula, gives less weight to weapons out to a distance of R/σ approximately 2, and greater weight to more distant weapons. The normalization factor has the same value for the two weightings. The value of σ used in Figure IV-7 is 200 miles. The figures show that the type of weighting factor gives still more defocusing of the weapon pattern and a slower descent in weapon density from the peaks.

Figure IV-8 shows weapon densities for the counterforce only attack with exponential weighting and sigma of 200 miles. Here the peak due to the missile field is the main feature showing. This peak is fairly regular at the 2.0 kiloton/mile² level, but shows spurs due to other missile fields at lower levels. The isolated one megaton weapons which are also in the attack will contribute a peak density of only 0.004 kilotons/mile² with this weighting and would not be noticed on this presentation.

Since fallout is blown downwind, it would be interesting to determine the effect of having weapons in the upwind direction from a monitor point receiving more weight than weapons

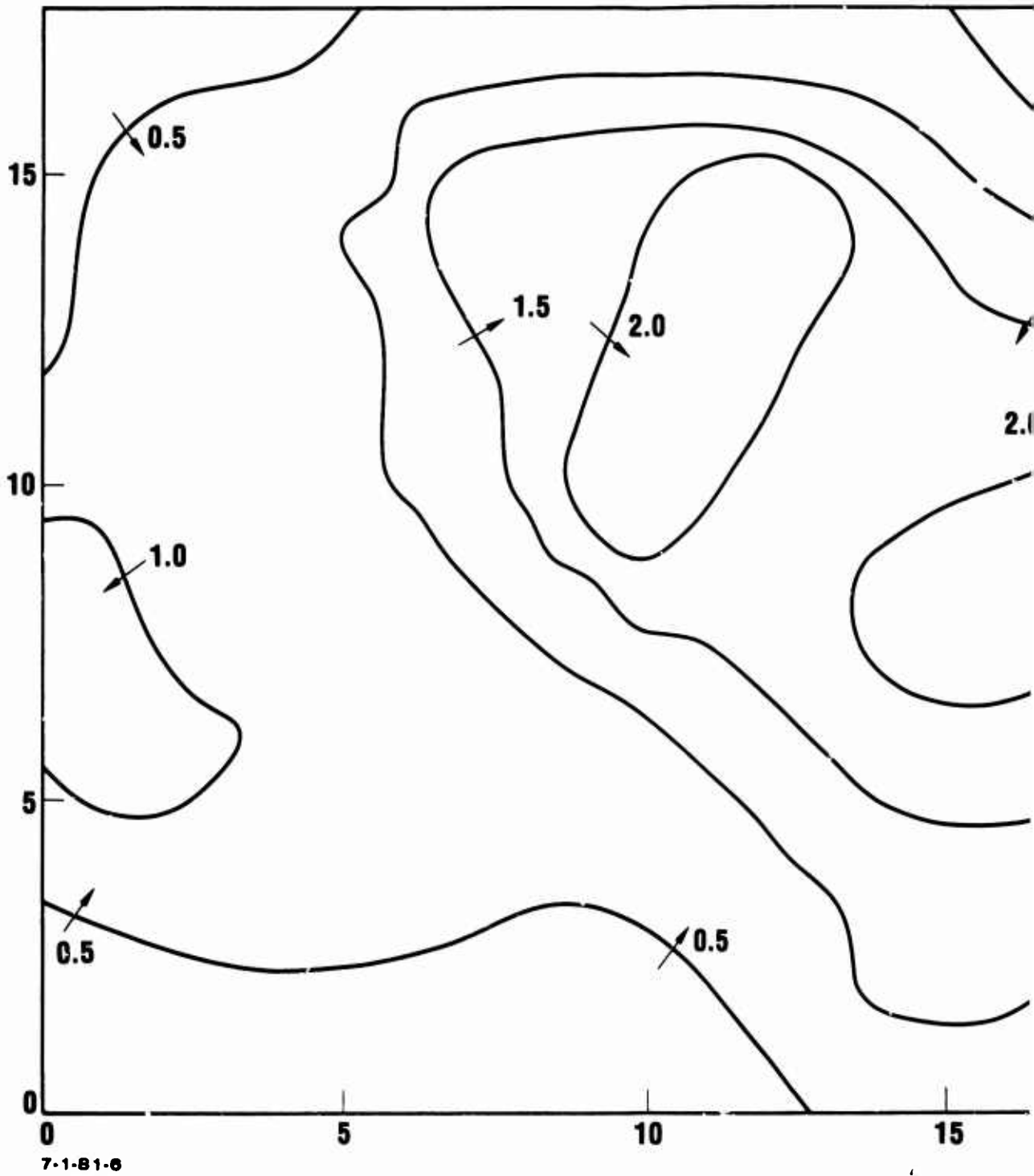
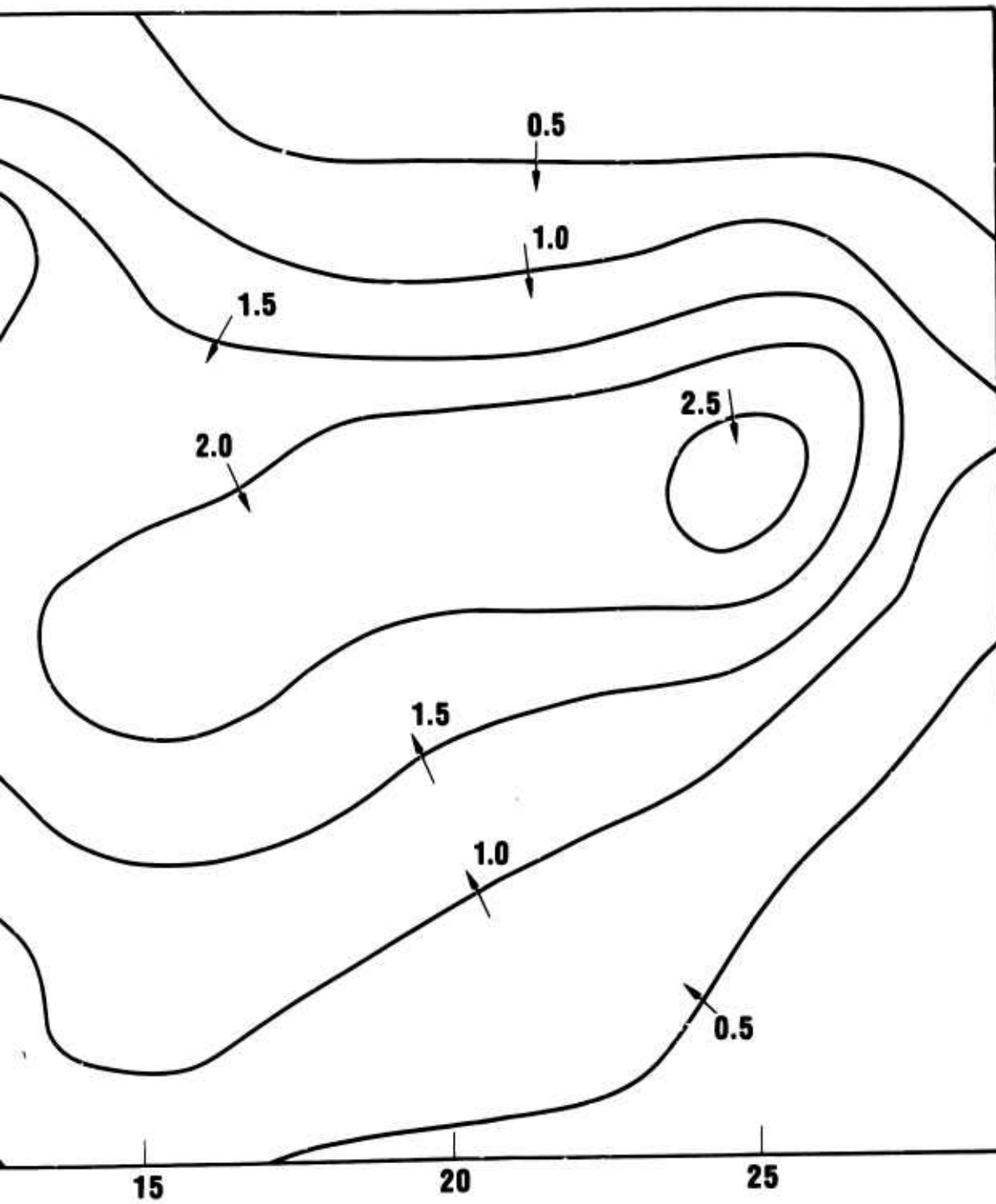


Figure IV-7. WEAPON DENSITY CONTOURS FOR ATTACK A AND SIGMA OF 200 MILES.



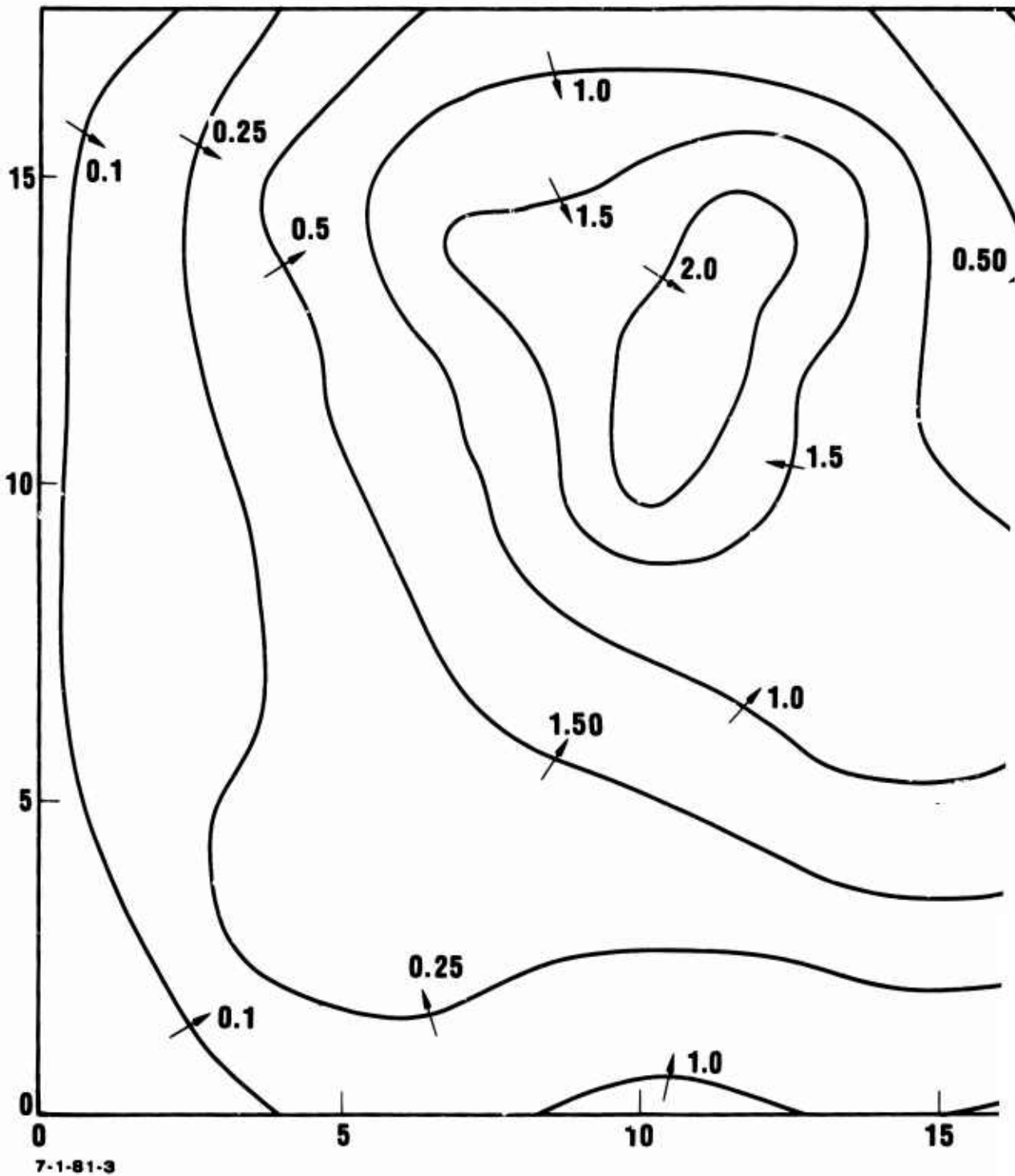
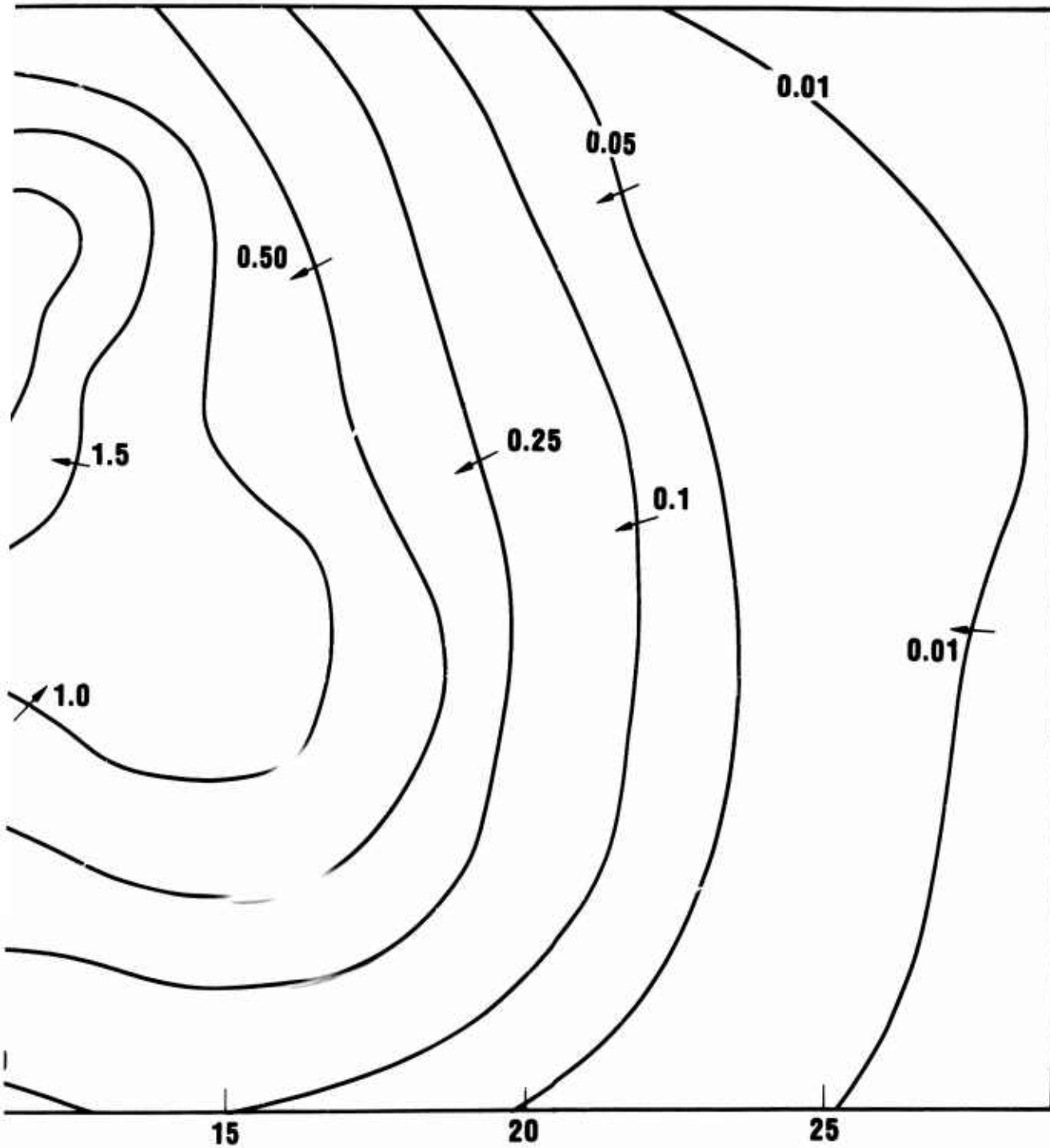


Figure IV-8. WEAPON DENSITY CONTOURS FOR A AND SIGMA OF 200 MILES.



DENSITY CONTOURS FOR ATTACK B WITH EXPONENTIAL WEIGHTING OF 200 MILES.

in the downwind direction. This was achieved by making σ a function of direction. Since the wind blows predominately from West to East, the value of σ should be larger in the westerly direction. Contours of constant sigma were taken to be ellipses with the monitor point at the downwind focus of the ellipse. The normalization factor was computed numerically to ensure a one megaton weapon density when the weapons are uniformly dispersed with one megaton in each square mile¹.

Figure IV-9 shows weapon density contours with Gaussian weighting for Attack A with semi major and semi minor axis of the ellipse of 200 and 100 miles. The width of a single pattern is usually small compared to its length, which would mean that the semi minor axis of the weighting ellipse should be small compared to the semi major axis. However winds are quite likely over an angle of, say, plus or minus 45 degrees from due West. To reflect this wind variability and to attempt to define the fallout risk the semi minor axis is taken as one half the semi major axis in the example shown. The complexity of the contours is intermediate between those of centered contour with sigmas of 100 and 200 miles. An inspection of the patterns in the Appendices and Chapter II shows pattern lengths for the high intensity part of the contour of several hundred miles, and of significant doses of possibly 1000 miles. Figure IV-10 shows density contours with the same weighting but for semi major and semi minor axis twice as large, namely 400 and 200 miles. Here, not only significant smoothing, but also significant translation of features of the pattern downwind is observed.

A still further smoothing is observed in Figure IV-11 which has the same elliptical weighting factor as the previous

¹For the cases considered the normalization factor was not too far from $2\pi ab$, where a is the semi major and b the semi minor axis of the ellipse. Of course when $a \rightarrow b$, the $a \rightarrow \sigma$ and $b \rightarrow \sigma$ and one would expect the normalization constant to approach $2\pi\sigma^2$.

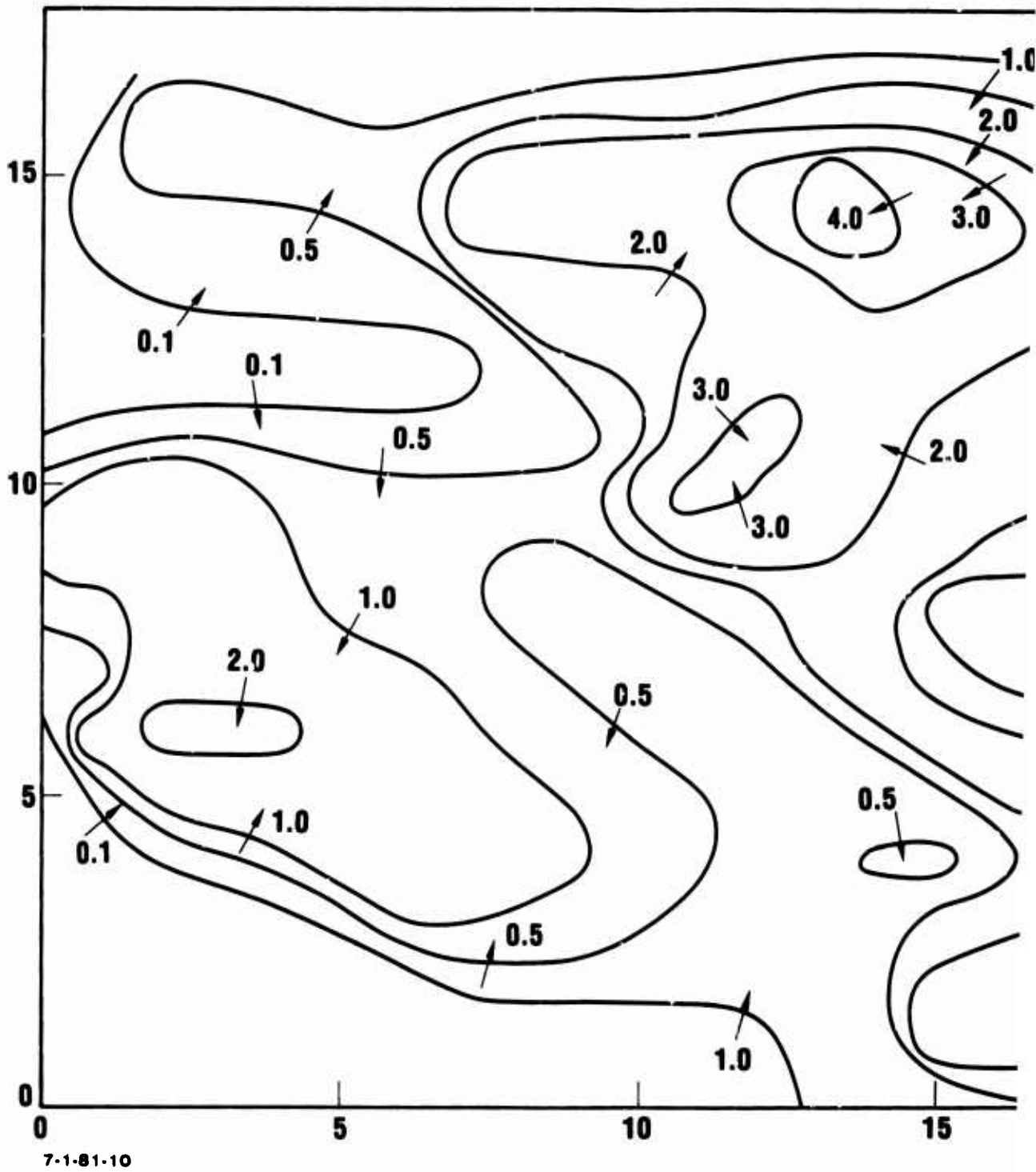
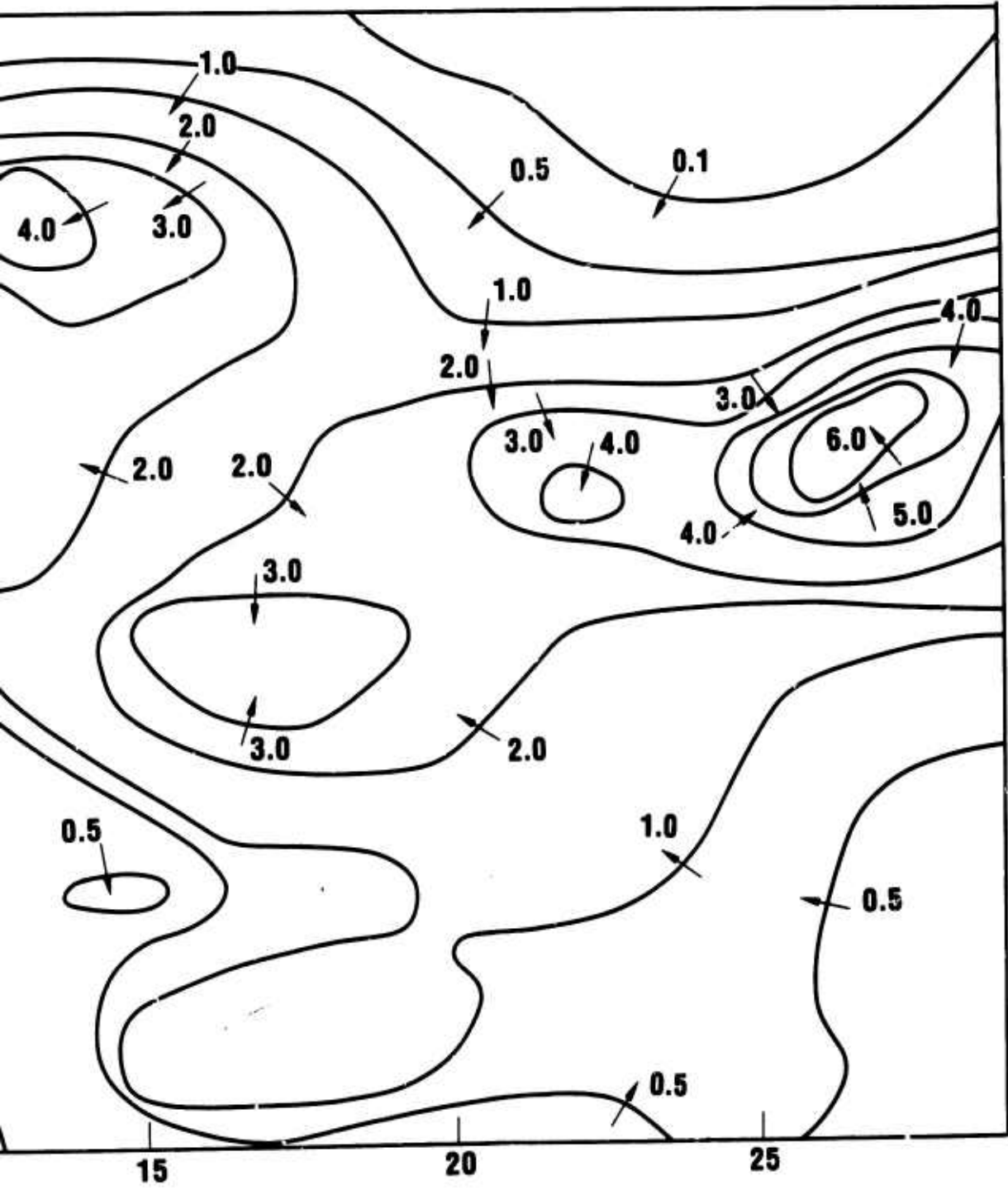


Figure IV-9. WEAPON DENSITY CONTOURS FOR AT WEIGHTING AND SEMI MAJOR AND S



CONTOURS FOR ATTACK A WITH ELLIPTICAL GAUSSIAN
SEMI MAJOR AND SEMI MINOR AXIS OF 200 AND 100 MILES.

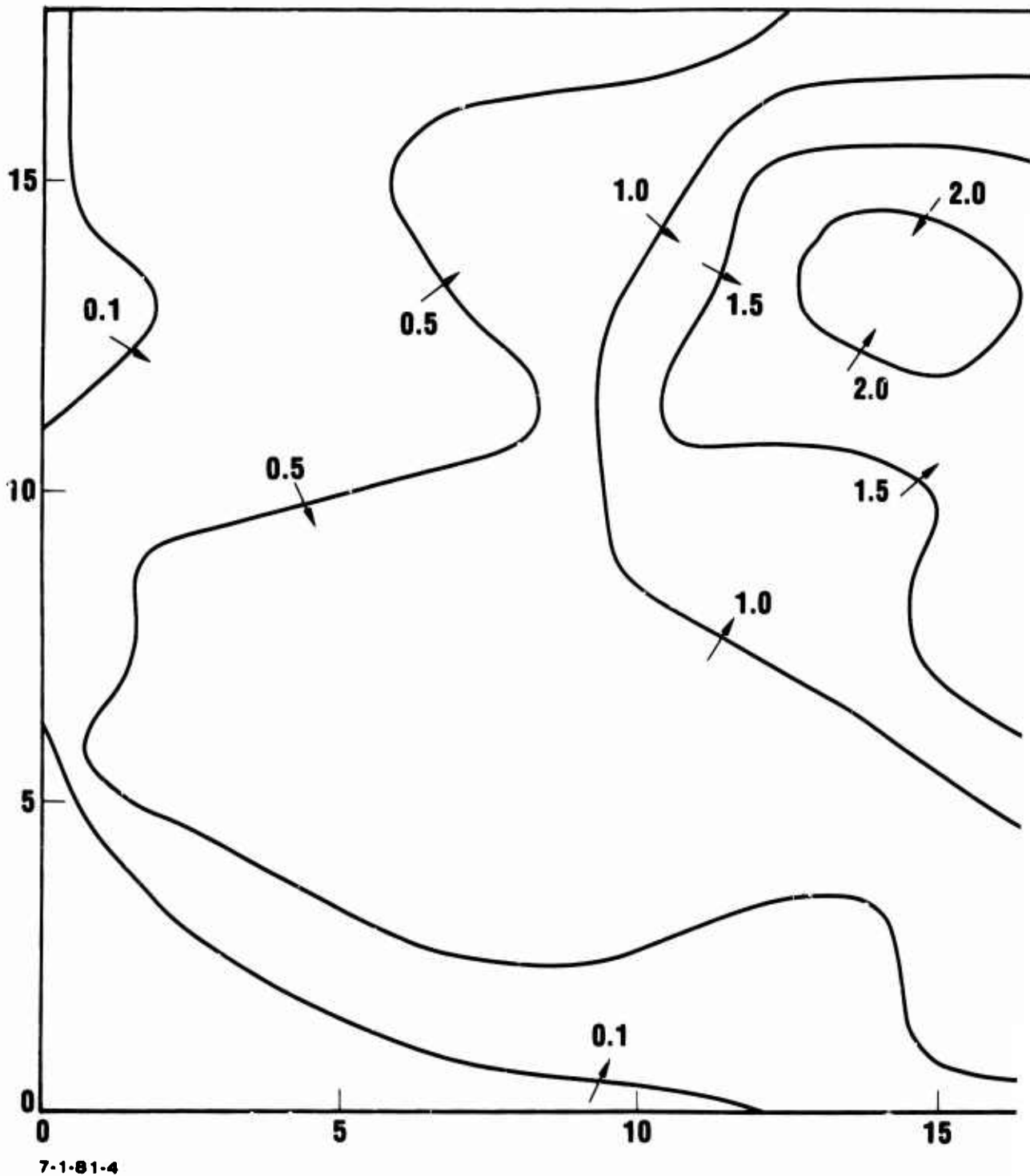
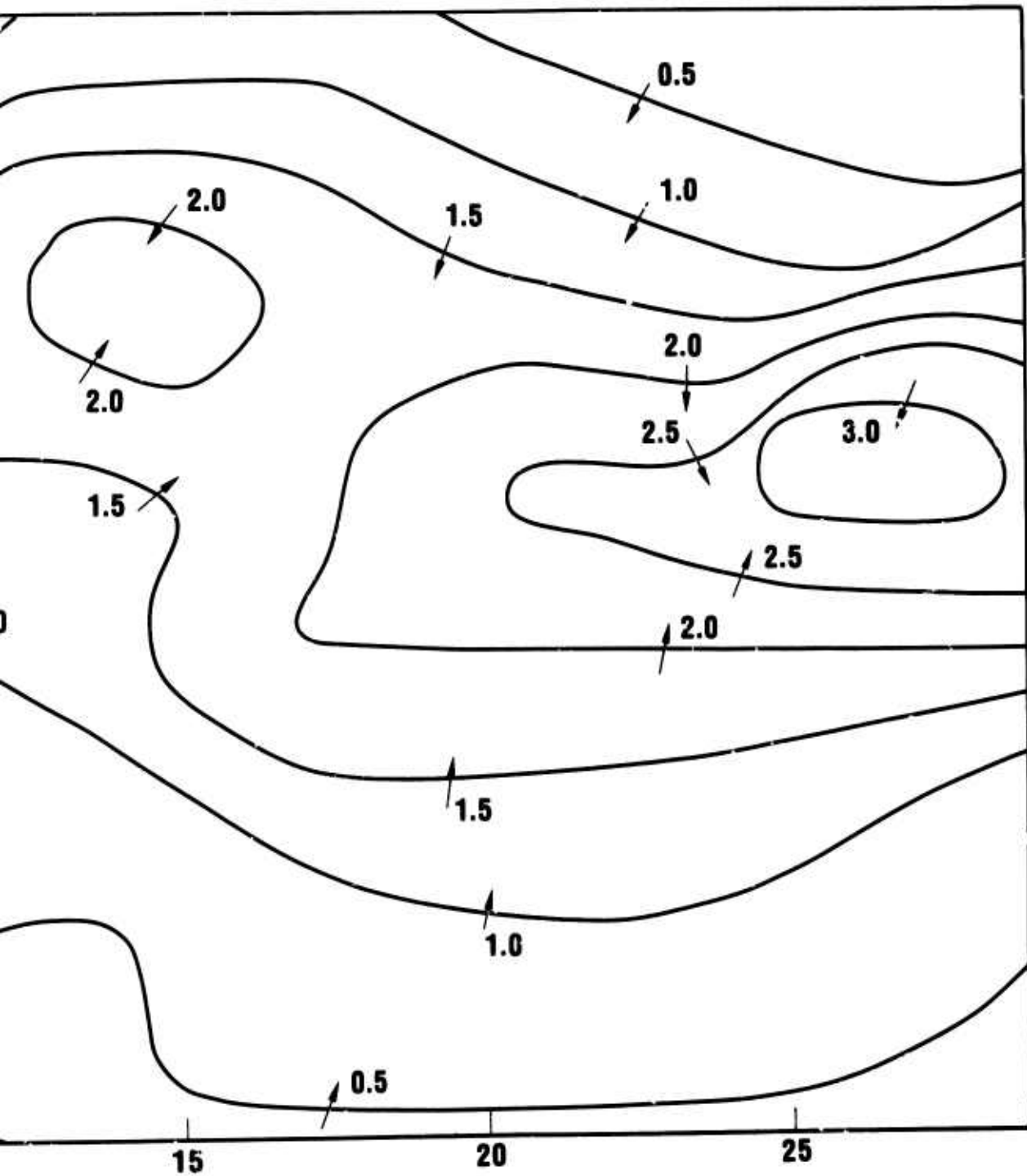


Figure IV-10. WEAPON DENSITY CONTOURS FOR AT WEIGHTING AND SEMI MAJOR AND S



TY CONTOURS FOR ATTACK A WITH ELLIPTICAL GAUSSIAN
D SEMI MAJOR AND SEMI MINOR AXIS OF 400 AND 200 MILES.

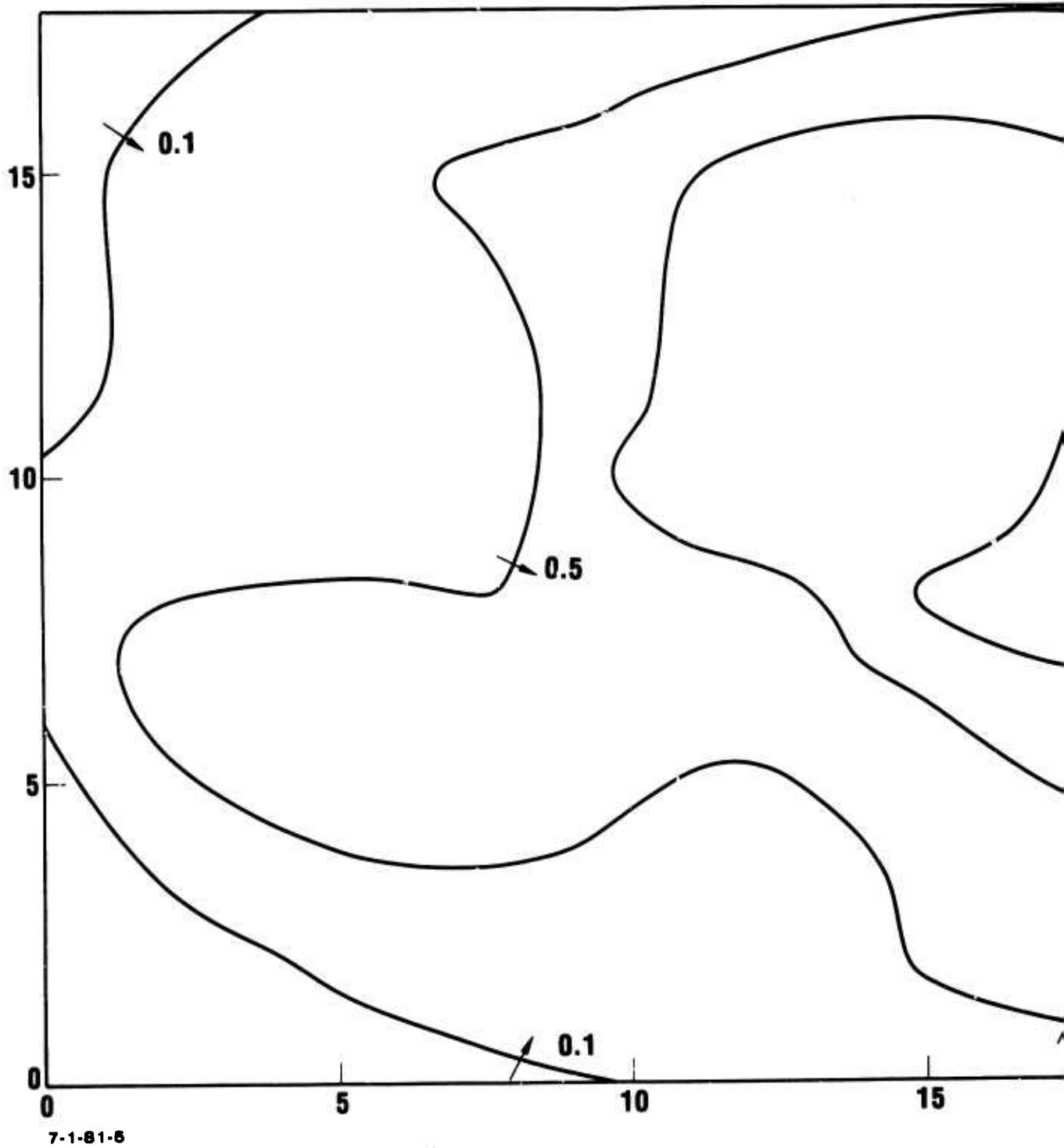
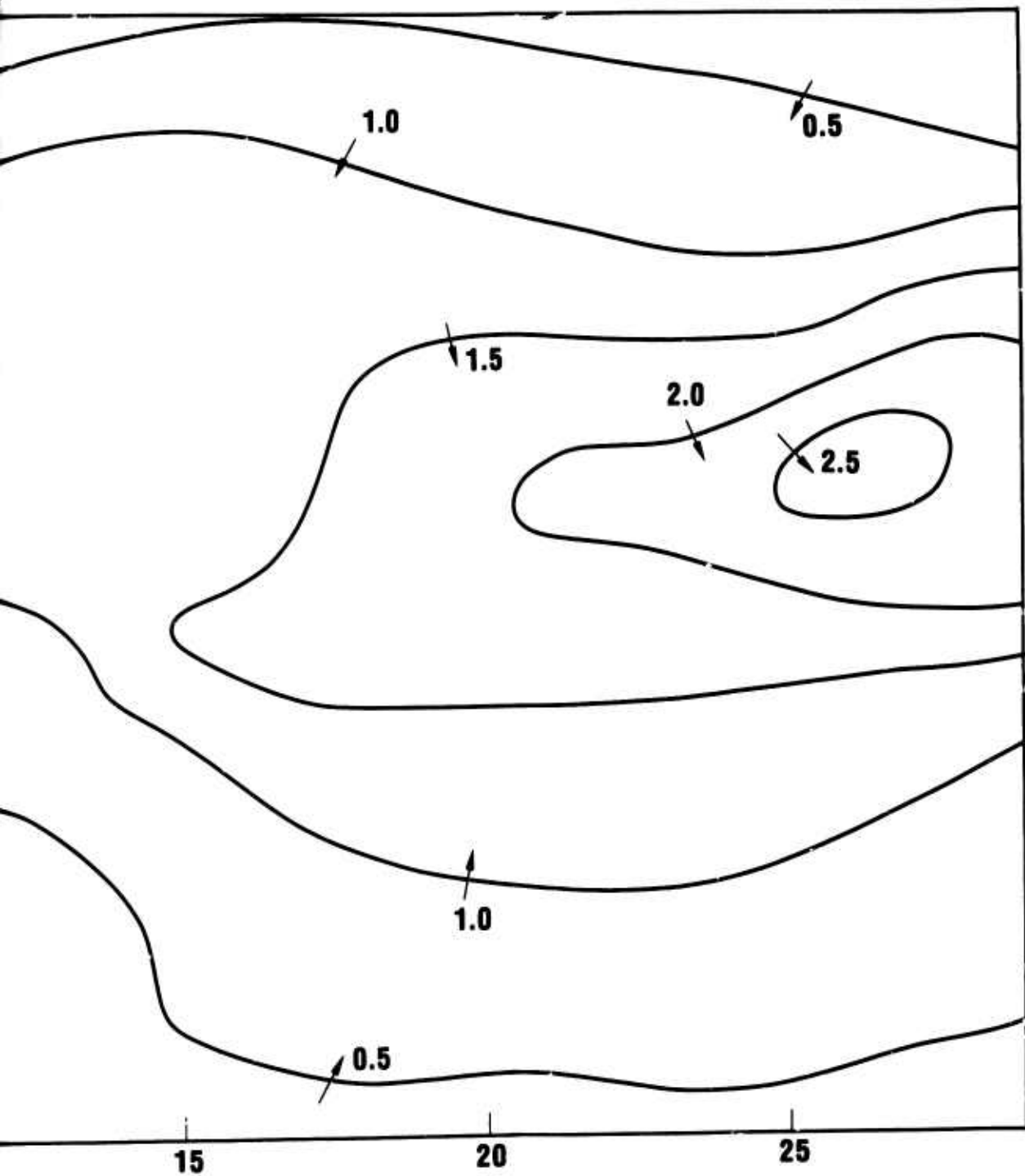


Figure IV-11. WEAPON DENSITY CONTOURS FOR ATTACK WEIGHTING AND SEMI MAJOR AND SEMI M



CONTOUR LINES FOR ATTACK A WITH ELLIPTICAL EXPONENTIAL
SEMI MAJOR AND SEMI MINOR AXIS OF 400 AND 200 MILES.

Figure, but has exponential weighting. In this Figure a good portion of the high density contours along the Eastern seaboard are displaced out of the picture.

Figure IV-12 shows density contours for Attack B with elliptical exponential weighting, and semi major and semi minor axis of 400 and 200 miles. The density contours clearly identify what could be considered as risk contours extending across most of the county.

Attack B has a total yield of 2570 megaton. The total area covered by the 600 grid squares of dimension 100 x 100 miles is 6×10^6 square miles. The average yield, if spread uniformly over the analysis grid, is $2570 \times 10^3 / 6 \times 10^6 = 0.428$ kilotons/mile². If the yield densities for the case with Gaussian weighting and a sigma of 200 are summed over all grid points (using yields in kilotons), a value of 255.8 is obtained. Dividing this by the number of grid points, 600, gives an average yield per grid point of 0.426 kilotons/mile². The good agreement of this number with the average yield spread over the area of 0.428 indicates that the summing procedure is an adequate integrator of total yield and that not much effect is lost outside of the boundry of the summing.

The total yield for Attack A is 6541 megaton, yielding an average yield over the area of 1.09 kilotons/mile². For the Gaussian weighting with sigma of 200, the average value of the density sums is 1.035 kilotons/mile². This lesser value indicates that for this attack, with more weapons near the boundry, and with the relatively large value of sigma, about 5 percent of the yield is lost beyond the grid.

The area of the continental United States is 3×10^6 mile², half of the area of the grid. Thus average weapon densities over the continental United States, where all the

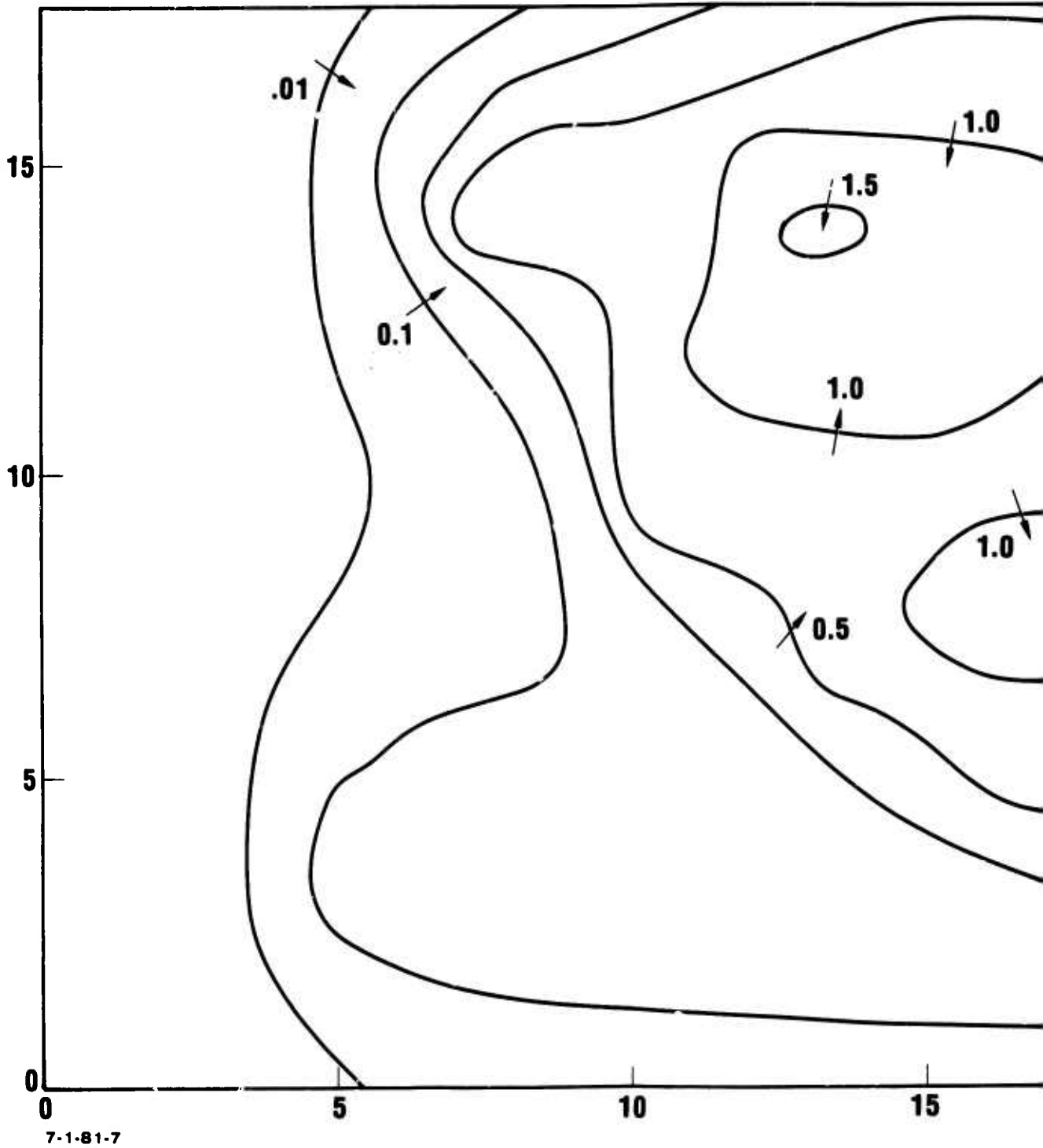
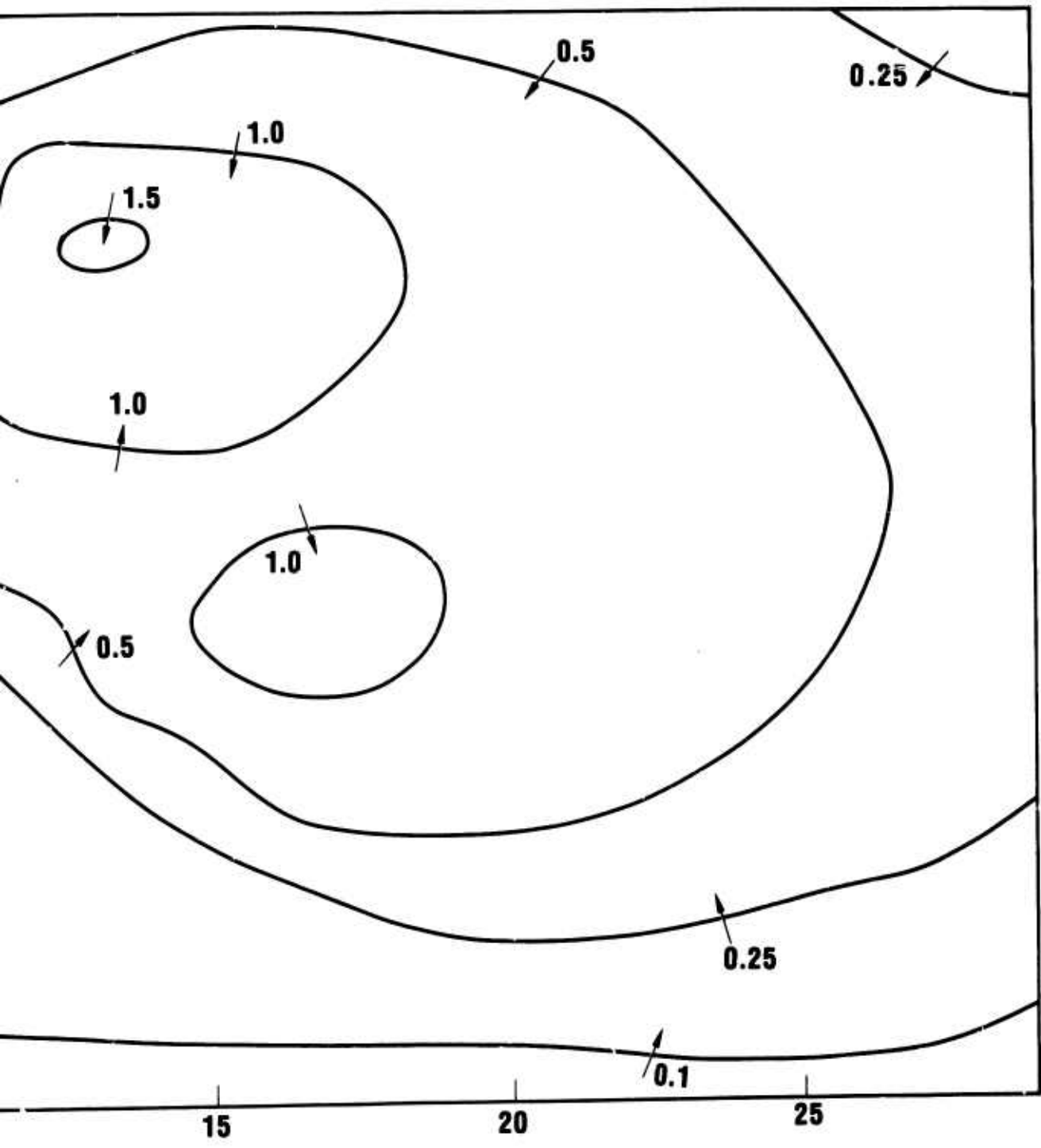


Figure IV-12. WEAPON DENSITY CONTOURS FOR ATTACK WEIGHTING AND SEMI MAJOR AND SEMI



DENSITY CONTOURS FOR ATTACK B WITH ELLIPTICAL EXPONENTIAL
AND SEMI MAJOR AND SEMI MINOR AXIS OF 400 AND 200 MILES.

weapons land, are twice those for the grid. These average densities are 2.18 kilotons/mile² for Attack A and 0.856 kilotons/mile² for Attack B.

For the elliptically weighted weapons some of the weapon density will be displaced out of the grid area. This can be considered as equivalent to having some of the fallout blown away from the United States. The fractions of density lost give an estimate of the fraction of the fallout which is blown away from the United States into the ocean. The fraction lost is composed of two parts, that outside of the grid area (which is almost all displaced from the Eastern edge of the grid), and that between the Eastern seaboard of the United States and the Eastern edge of the grid. The following Table presents the fractions lost for four cases.

Types of Weighting	Ellipse, Semi Major and Semi Minor Axis	Percent out of Grid	Percent from Seaboard to Grid	Total Percent Lost
Exponential	200,100	15.8	8.3	24.1
Gaussian	200,100	6.1	8.6	14.7
Exponential	400,200	32.2	8.6	40.8
Gaussian	400,200	18.7	9.8	28.5

From the Table one could estimate that on the average from 15 to 40 percent of the fallout generated is ineffective because it is blown over the Eastern seaboard due to the prevailing winds. Since the smaller ellipses, with 200 miles semi major axis, probably represent the fallout deposition better, the percent of fallout blown eastward to the ocean might best be estimated at about 20 to 25 percent.

In the previous weapon density contour, the ellipse semi minor axis has been kept small to large to represent risk which might come from winds over a variety of angles. If a small semi minor axis were chosen, the contours could be considered

to represent a single wind. Since the ellipses are always oriented along the x axis in the ten mile grid used for the maps, the wind represented would be a wind everywhere blowing from West to East (since the East-West direction on the map changes due to the map projection, the wind is actually blowing East by North at the left end of the map and East by South at the right end of the map). Figure IV-13 shows weapon density contours with elliptical Gaussian weighting for a semi major axis of 400 miles and a semi minor axis of 40 miles. This might be representative of a high wind speed, low wind shear condition. The fallout winds for March are most nearly in a due West to East direction. These density contours show many of the same general features as the fallout map for March for Attack A (see Appendix A). The length and widths of the high intensity region match rather well, but the density contours are more extended in the low intensity regions. Figure IV-14 had elliptical Gaussian weighting for a semi-major axis of 200 miles, and retaining a semi minor axis of 40 miles. Here the contours appear to better represent the low density region. To try to achieve a better match efforts could be made to adjust the weighting factors based on the dose distance relations presented in Chapter II. Such an effort, however, would eventually lead to a new fallout model which attempts to duplicate the WSEG-10 model results. If very significant improvement in some model features could be expected from this course, such an effort might be desirable. No such improvement is foreseen, so the use of this weighting procedure is limited here to the examples already presented of different ways to illustrate some of the features of the attack.

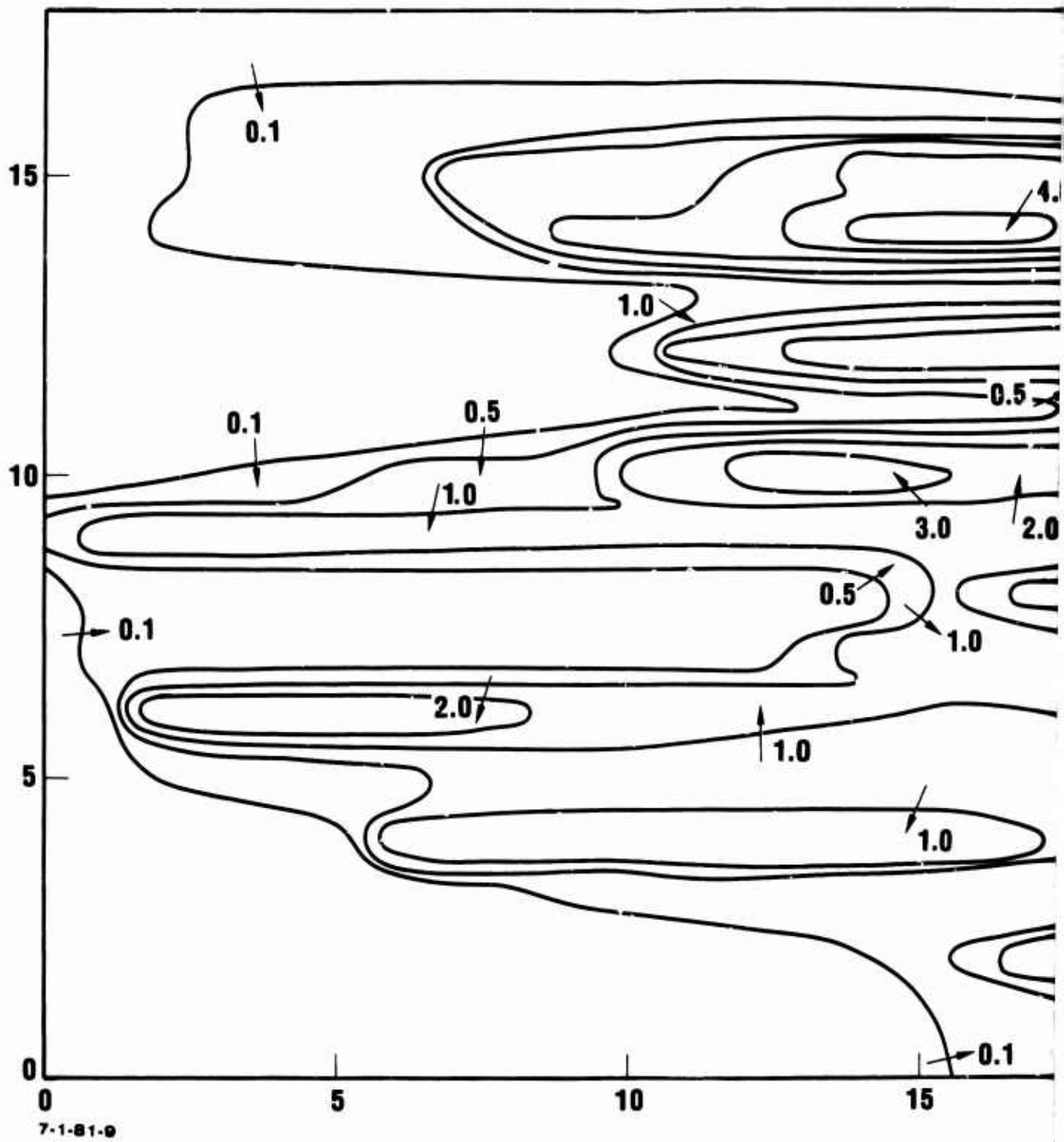
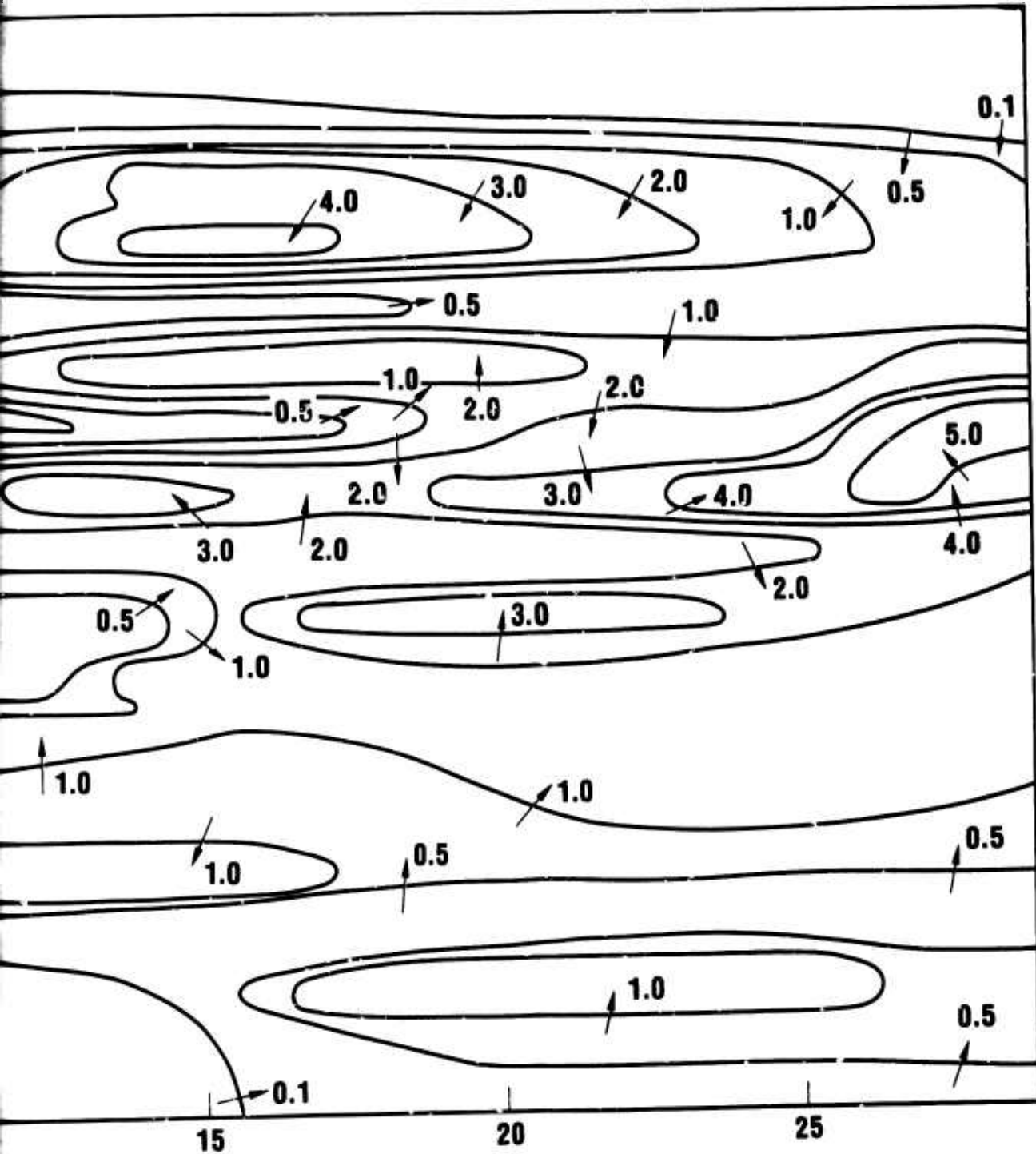
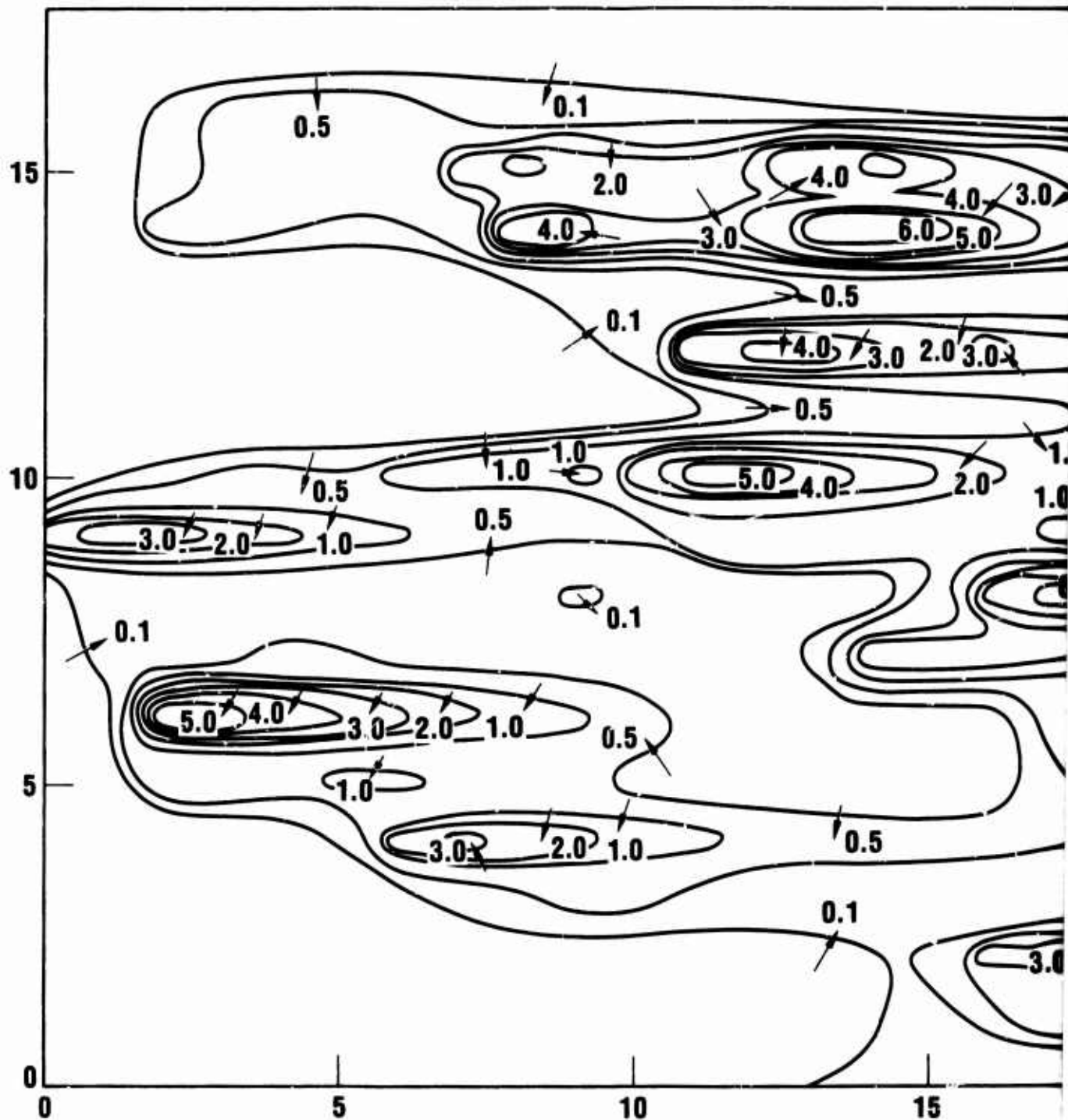


Figure IV-13. WEAPON DENSITY CONTOURS FOR ATTACK /
WEIGHTING AND WITH SEMI MAJOR AND S
40 MILES.

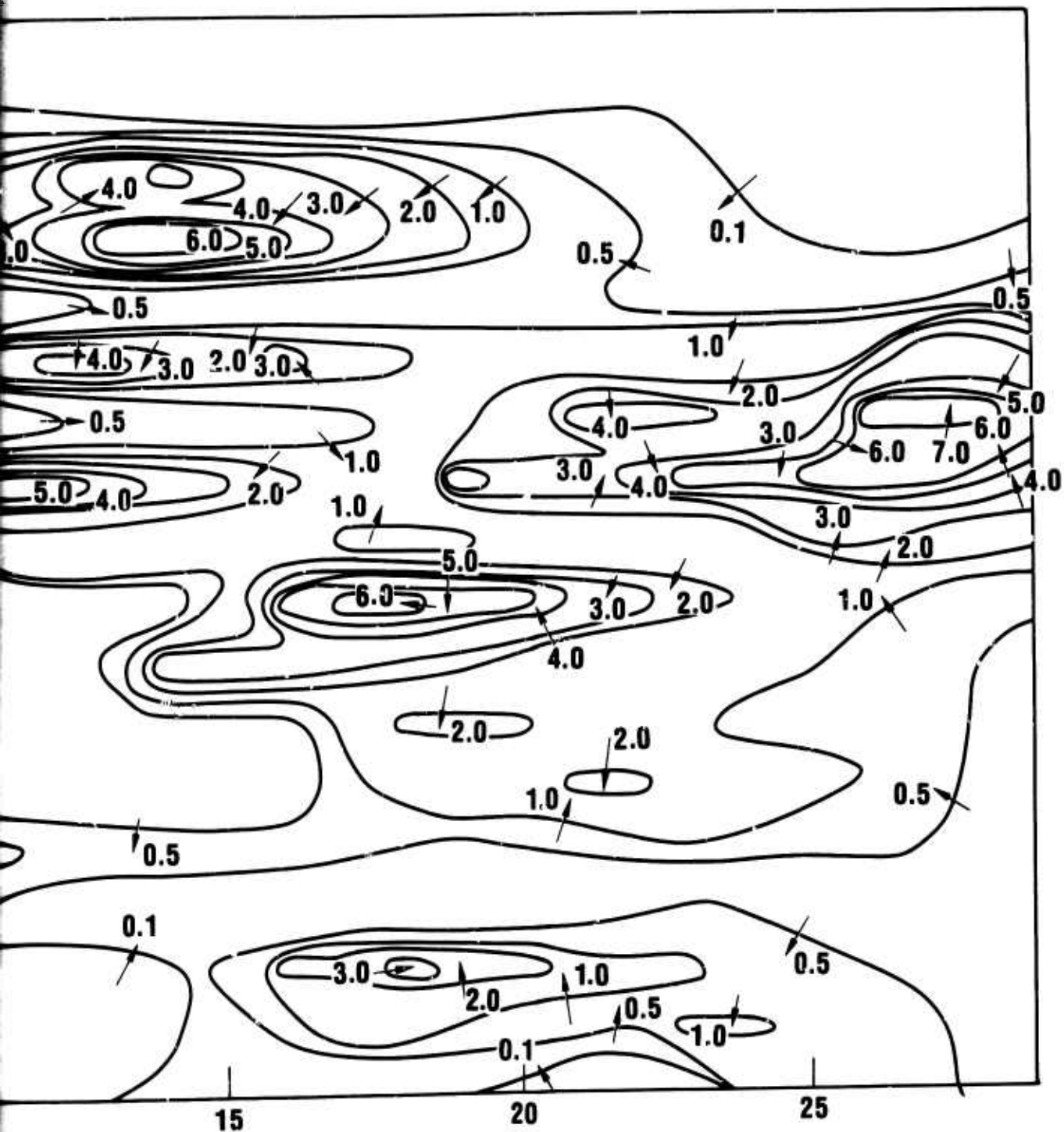


...ITY CONTOURS FOR ATTACK A WITH ELLIPTICAL GAUSSIAN
...ND WITH SEMI MAJOR AND SEMI MINOR AXIS EQUAL 400 AND



7-1-21-16

Figure IV-14. WEAPON DENSITY CONTOURS FOR ATTACK A WITH WEIGHTING AND WITH SEMI MAJOR AND SEMI MINOR AXES.



TY CONTOURS FOR ATTACK A WITH ELLIPTICAL GAUSSIAN
 WITH SEMI MAJOR AND SEMI MINOR AXIS EQUAL 200 AND 40

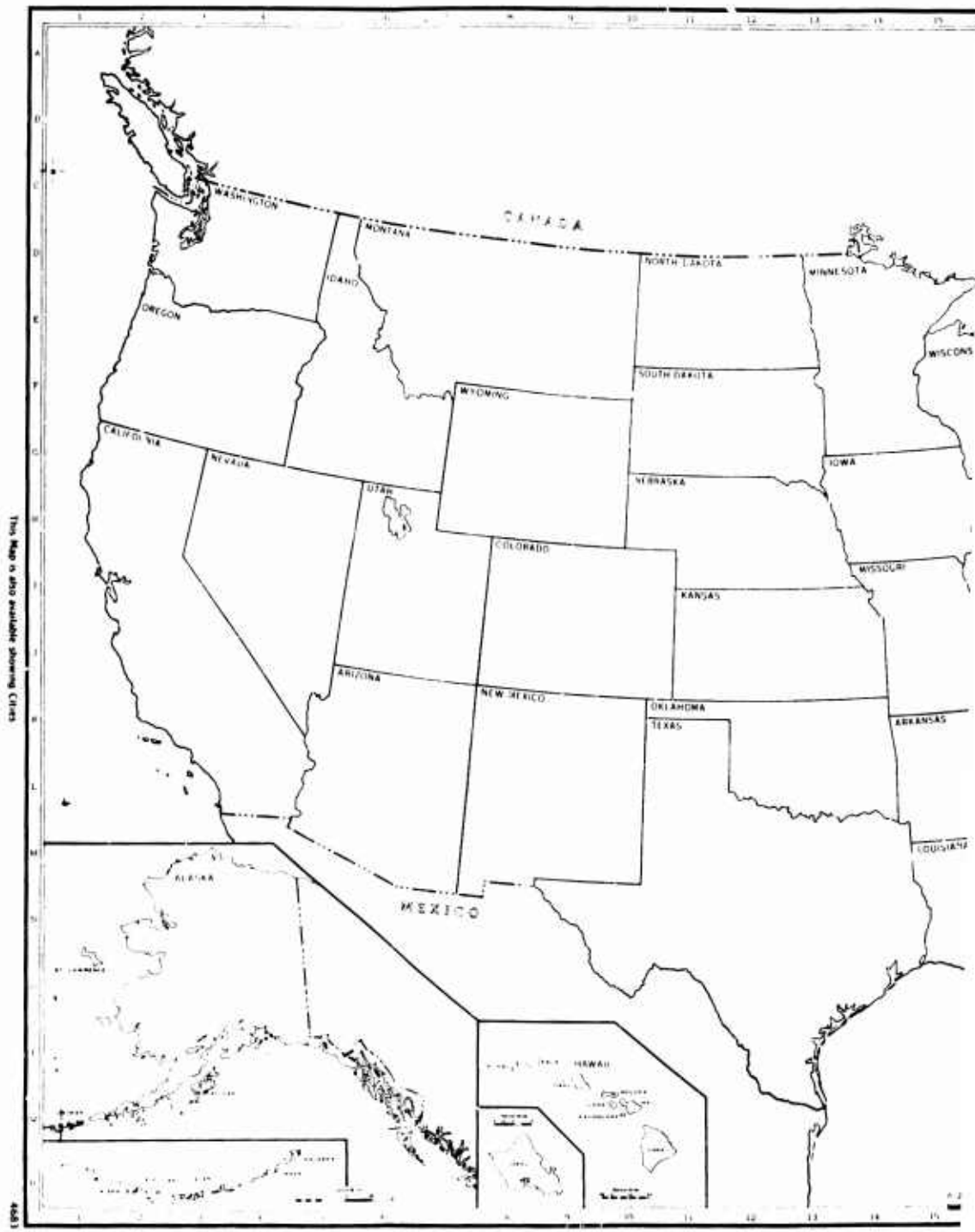
CHAPTER V THE RESULTS

A. PRESENTATION OF FALLOUT MAPS

The fallout doses in this report were produced by the GUISTO fallout damage assessment program [Ref. 5] using the WSEG-10 fallout model described in Chapter II. The WSEG-10 maximum biological dose is given here; this is the maximum dose obtained assuming 10 percent of the dose is irreparable and 90 percent of the dose is repairable with a repair constant of one month. It is almost the same as the total dose accumulated in four days assuming the total dose is irreparable.

This GUISTO program computes fallout doses on a 10 mile rectangular grid covering the Continental United States. The grid is a rectangular grid in a plain which is an Albers Equal Area projection of the United States. Thus a map of the United States which would overlay the grid would be a familiar Albers Equal Area Projection Map. The grid has 178 squares in the North-South direction and 289 in the East-West direction. The latitudes and longitudes of the corners of the grid are 23.35 and 119.33 degrees, 98.18 and 128.22 degrees, 48.07 and 65.28 degrees, and 23.27 and 74.30 degrees.

Figure V-1 is a state outline map of the United States (an Albers Equal Area Projection); Figure V-2 is a map of all the urbanized areas in the United States prepared by the same plotting program as that which produced the fallout doses. Figure V-1 also is provided as a plastic overlay to assist in finding dose levels at specific locations from the fallout maps in the appendices.



V-1. OUTLINE MAP OF THE UNITED STATES WITH AN AL

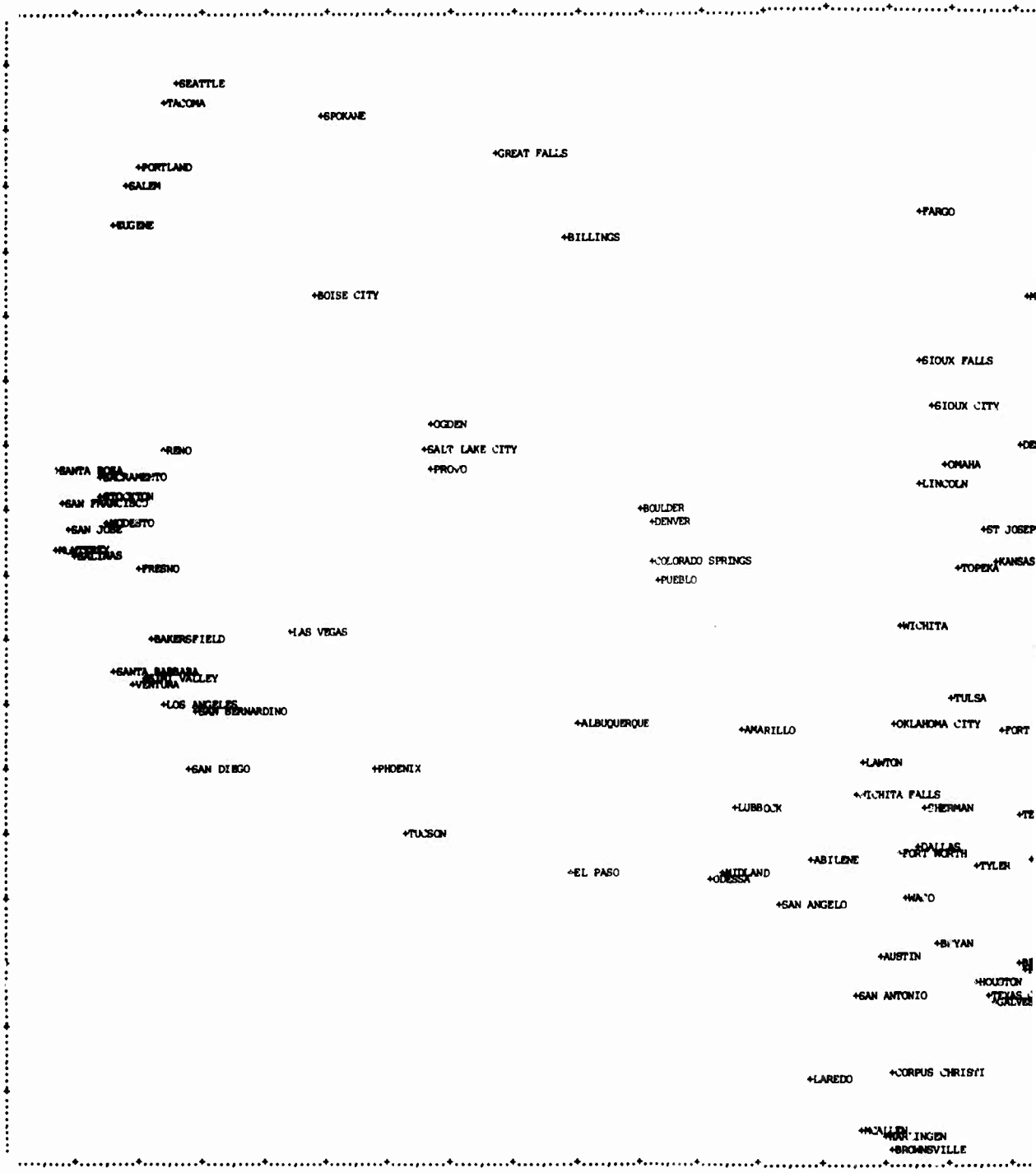


RAND McNALLY
STATE OUTLINE MAP

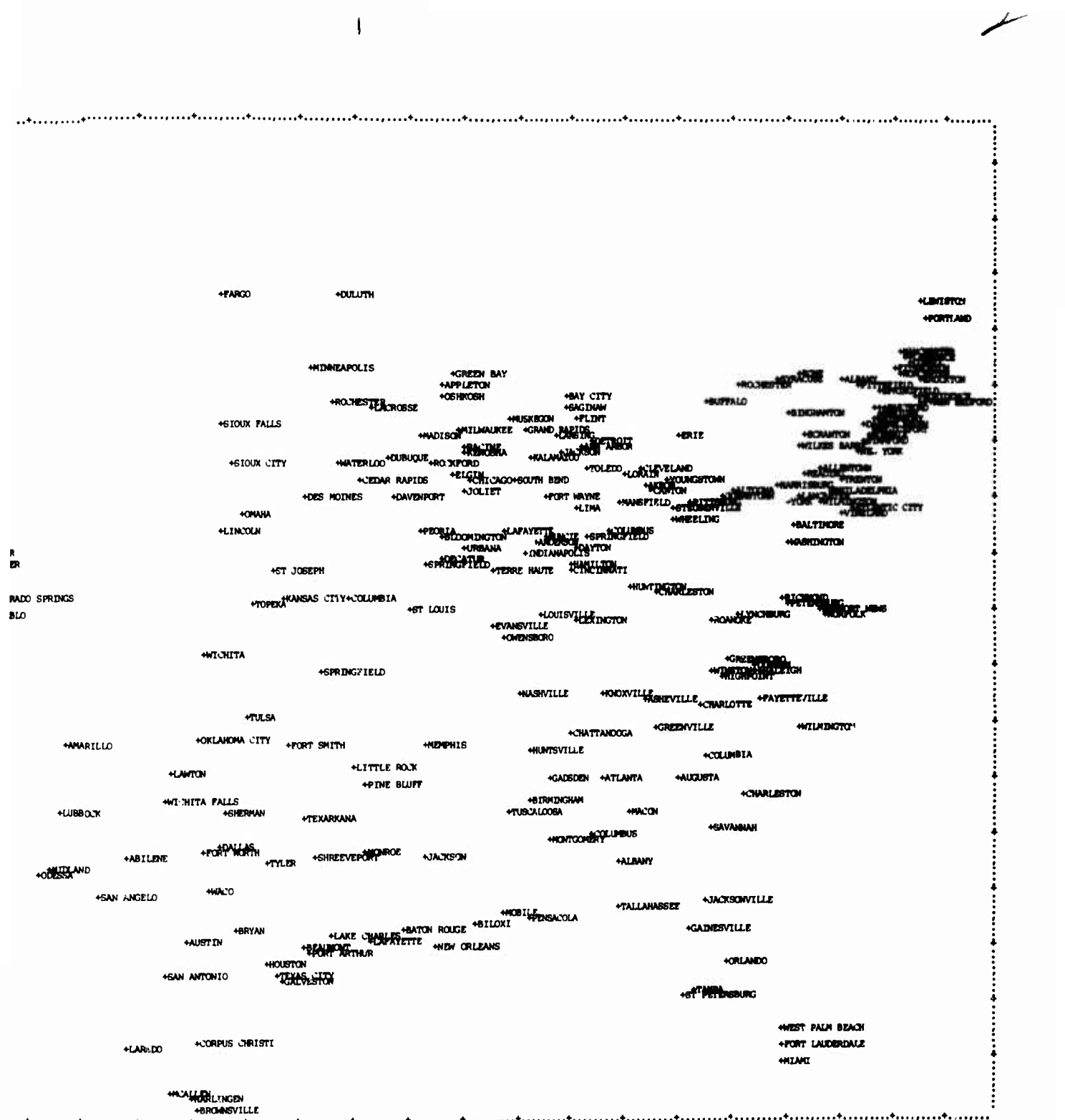
UNITED STATES
SIZE 11/12

UNITED STATES WITH AN ALBERS EQUAL AREA PROJECTION.

197/198



V-2. MAJOR URBANIZED AREA IN UNITED STATES ON



AREA IN UNITED STATES ON AN ALBERS EQUAL AREA PROJECTION

Two types of plots are presented, accenting doses at different levels. For the low level plots in Appendix B for Attack A and Appendix D for Attack B, the following Table indicates the dose level, in Roentgens, associated with each character plotted.

Blank	Dose < 0.1
.	$0.1 \leq \text{Dose} < 0.3$
+	$0.3 \leq \text{Dose} < 1$
1	$1 \leq \text{Dose} < 3$
2	$3 \leq \text{Dose} < 10$
3	$10 \leq \text{Dose} < 30$
4	$30 \leq \text{Dose} < 100$
5	$100 \leq \text{Dose} < 300$
6	$300 \leq \text{Dose} < 1,000$
7	$1,000 \leq \text{Dose} < 3,000$
8	$3,000 \leq \text{Dose} < 10,000$
9	$10,000 \leq \text{Dose} < 30,000$
0	$30,000 \leq \text{Dose}$

This set of plotting characters enables the dose to be determined within a factor of about 3. The second type of plot is in Appendix A for Attack A and Appendix C for Attack B accenting a higher dose range as given by the following table:

Blank	Dose < 500
+	$500 \leq \text{Dose} < 1,000$
A	$1,000 \leq \text{Dose} < 2,500$
B	$2,500 \leq \text{Dose} < 5,000$
C	$5,000 \leq \text{Dose} < 10,000$
D	$10,000 \leq \text{Dose} < 30,000$
E	$30,000 \leq \text{Dose}$

Various factors not considered in this analysis could reduce the dose levels below those predicted. These would

include terrain shielding, weathering of fallout particles, the influence of trees and buildings, small (but not zero) heights of burst, and enemy selection of small (but not zero) heights of burst to simplify attack planning. On the other hand a fission fraction of 0.5 is assumed, while values much closer to one are possible.

The reader should place his own estimate of the importance of those factors before interpreting the significance of the various dose levels. For example, if it is thought that the presented levels represent a best guess, then the following interpretation could be used. In this interpretation 100 Roentgens is taken as the onset level for sickness. The likelihood of sickness increases to one with doses of 300 Roentgens. Three hundred Roentgens is taken as the onset level of death with the likelihood of death increasing to one at 600 Roentgens. Even with no shelter, a protection factor of 2 is assumed due to terrain irregularities. Home shelter, even without basements, is assigned a protection factor of 5, with basements of 10, Fallout Shelter Survey (NFSS) shelter is given a protection factor of 40, high grade shelter a protection factor of 100, and very high grade shelter a protection factor of at least 500.

Blank	No fatalities. Sickness possible without shelter. Home shelter is adequate to prevent sickness.
+	Sickness likely without shelter, fatalities possible. Home shelter is adequate to prevent fatalities but sickness possible without basements. NFSS shelter adequate.
A	Death almost certain without shelter and likely in home shelter without basement. Sickness almost certain in home shelters without basements, possible in home shelters with basements. NFSS shelter adequate.
B	Death almost certain in home shelters without basements, likely with basements. NFSS shelter adequate.

- C Death certain in home shelter. Sickness likely in NFSS shelter, but not death. High grade shelter adequate.
- D Death likely in NFSS shelter, and sickness likely in high grade shelter. Very high grade shelter adequate.
- E Death certain in NFSS shelter, sickness likely in high grade shelter. Very high grade shelter adequate.

B. COMBINED STATISTICS

This section presents statistics for all twelve months combined. Although a sample of 12 is not large for reducing statistical fluctuations to a low value, this sample appears to give generally regular appearing results and is adequate to show gross trends.

The mean doses for the full attack, Attack A, are shown in Figure V-3 and for the counterforce attack, Attack B, in Figure V-4. These maps are presented to the same scale as the individual fallout plots in the appendices. The mesh square numbers, in tens, are indicated along the side of the plots. The contours were produced through an averaging process over a mesh with a 100 mile spacing. For each square of the mesh, all doses for each of the 100 ten-by-ten-mile-squares, and for each month of the year, were added together and divided by the number of values added (i.e., 1200 except at the boundry of the mesh). The values for each square were plotted at the lower left hand corner of the mesh. Then smooth contour lines were drawn. This process causes an effective displacement of the contours 50 miles to the South and to the West of the center of the square which normally would be the point chosen. This may be adjusted by displacement of these maps slightly from other presentations given in this study. The contour intervals are the same as in the high level monthly fallout plots except that a 100 Roentgen contour is added at the lowest end.

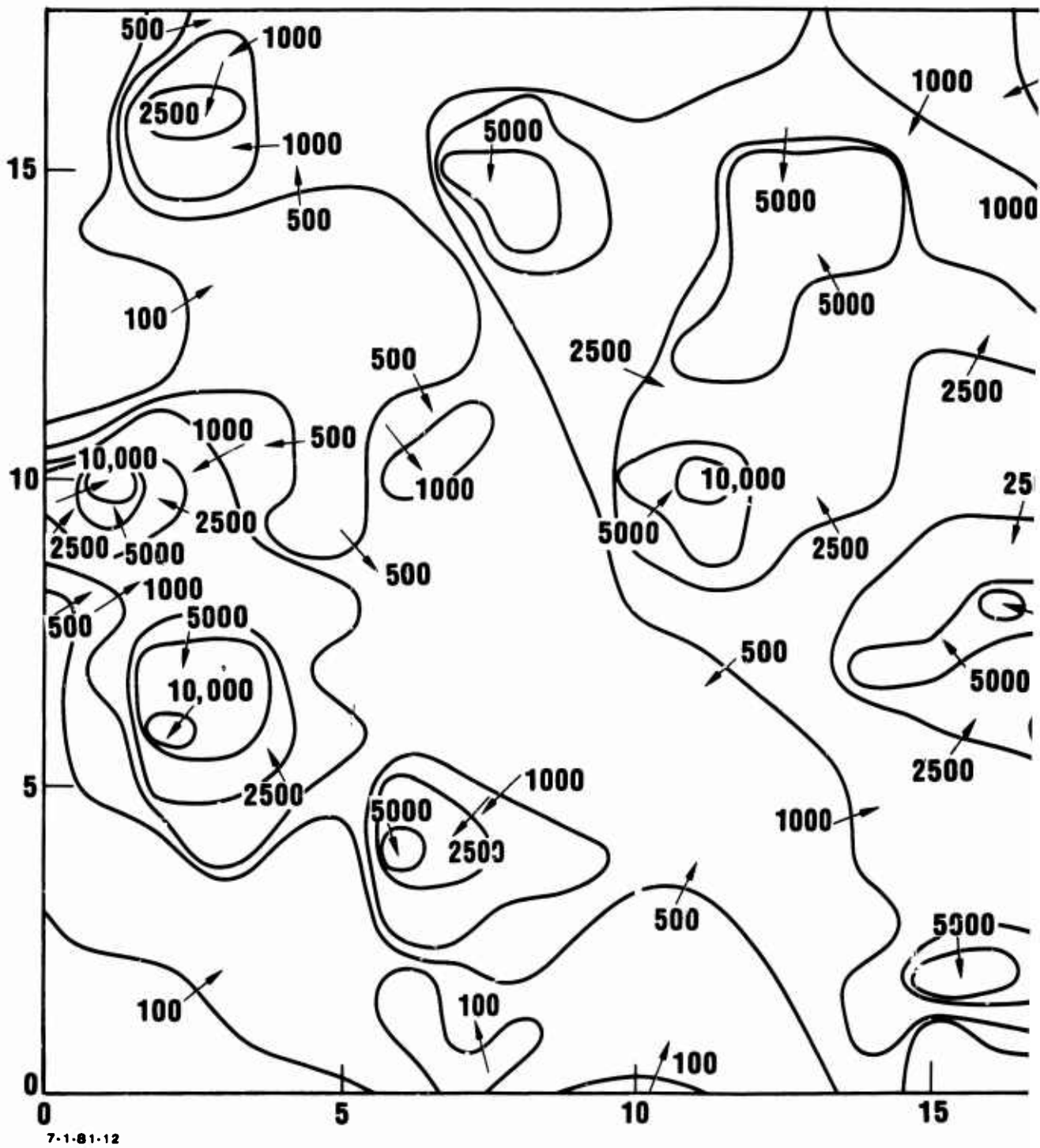
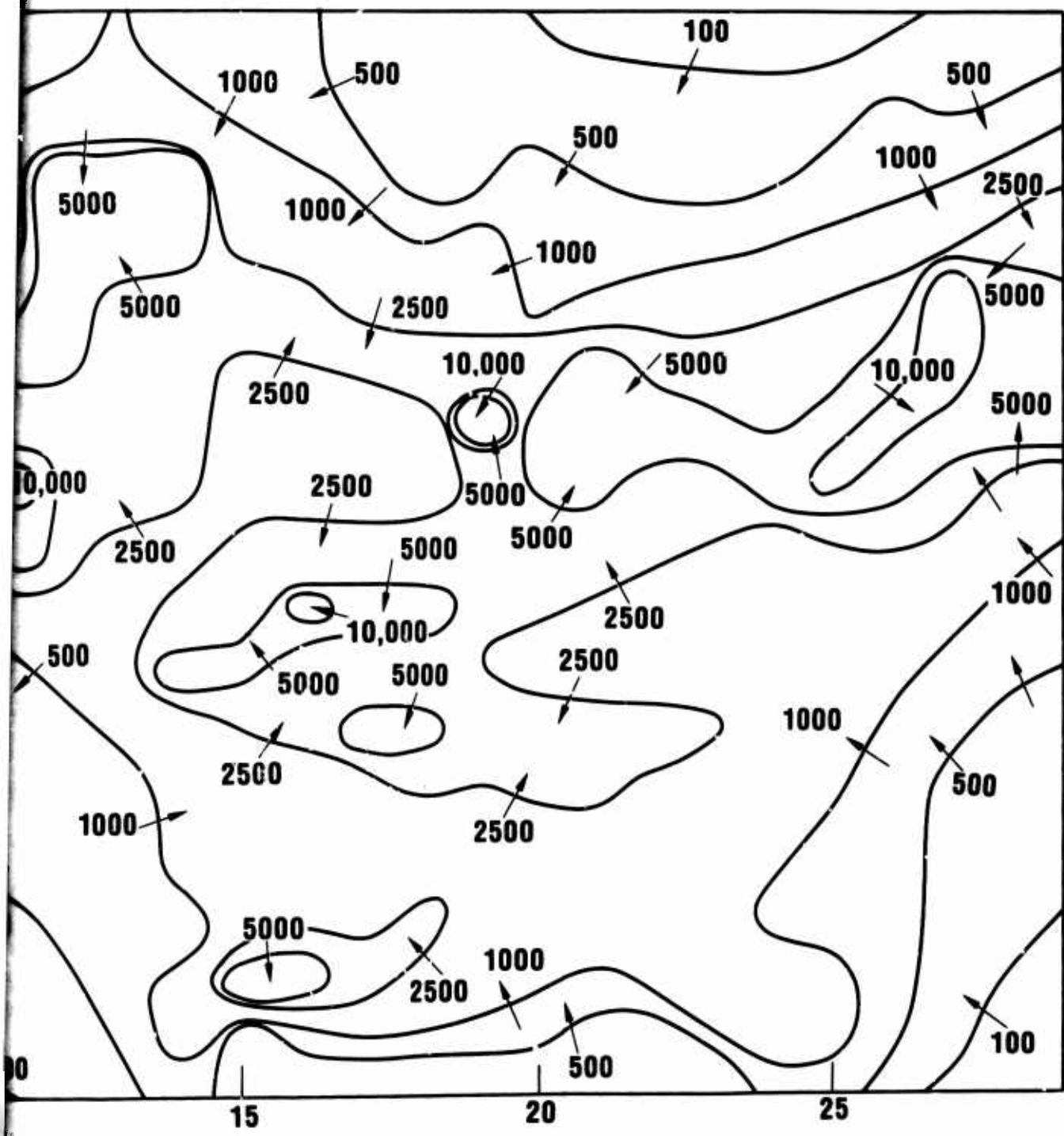
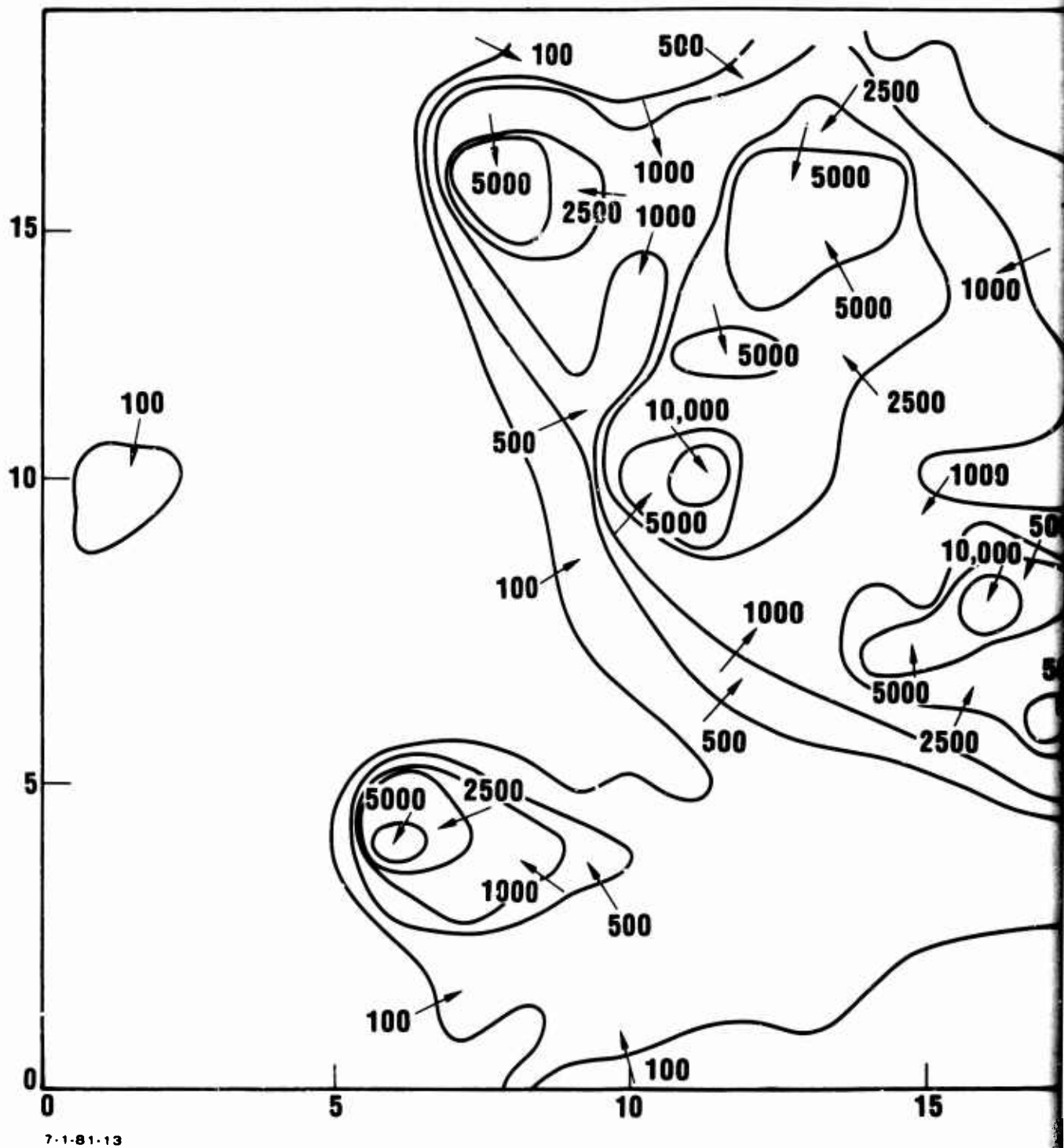


Figure V-3. MEAN BIOLOGICAL DOSES

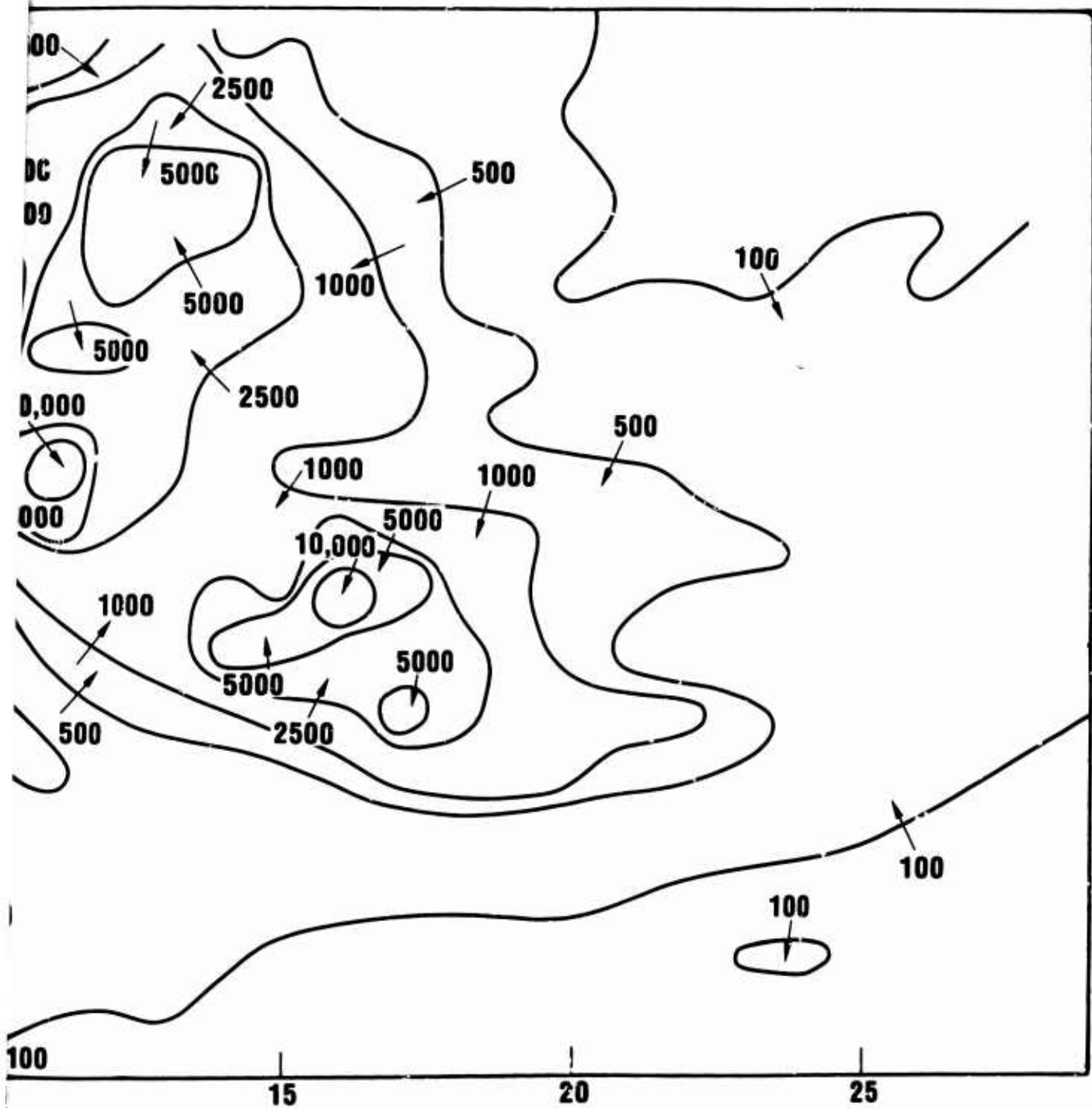


MEAN BIOLOGICAL DOSES FOR ATTACK A.



7-1-81-13

Figure V-4. MEAN BIOLOGICAL DOSES FOR



MEAN BIOLOGICAL DOSES FOR ATTACK B.

In Figure V-4 the primary feature is obviously the attack on the individual missile fields. At the 5000 Roentgen level and above, the shapes are dominated by the attack pattern on a particular field, but at the lower levels, say 1000 Roentgen, the interactions between the various fields produce more complex geometrys. The effect of the generally West to East winds is shown by the general displacement downwind of the contours, however, the contours generally flow downwind over a rather wide angle.

The contours in Figure V-4 show a surprising degree of smoothness, although the fluctuation of some contours, e.g., the downwind 500 Roentgen contour between North-South distance values of 500 to 1500 miles, is probably due to the particular sample of winds drawn. Due to the averaging process over the 100 mile grids, the hot spots from individual weapons do not appear. Deleting the averaging to include these hot spots would give a much more mottled and difficult to interpret set of contours. The plot for the full attack shows the same general features as for the missile fields, with the addition of the contributions to the attack on large urban areas, and the general increase in background levels from individual weapons spread across the country. The principal feature added by these contours is the high intensity ridge in the Eastern part of the country which peaks along the Washington-Boston corridor and extends Westward to Chicago. Added to that are individual concentrations for other heavily attacked areas, e.g., San Francisco, Los Angeles, and Houston.

The standard deviation of the dose about the mean value was also computed. Due to the variability of the doses these standard deviations were large, almost always greater than the value of the mean dose. Because of these large values a different means of representing the dose variability, i.e. histograms, was chosen.

Figure V-5 shows nationwide histograms of biological doses for Attack A, and Figure V-6 shows histogram for Attack B. The dose intervals used are the same as for the high range fallout plots as given earlier in this Chapter. The ordinate represents the percentage of time a dose falls in the interval represented. The values are all values for all months in the same 100 x 100 mile squares used for computing mean doses. To keep the number of histograms presented fairly small, they are presented only for every fourth 100 mile square in the East-West direction, and every third square in the North-South direction. The coordinates of the square for which the histogram is presented is given by the coordinates of the lower left hand corner of the histogram. Thus, for example, the lower left histogram represents all events in the square from 0 to 100 miles in both the North-South and East-West directions. The histogram illustrates the variability in fallout doses which may be expected, and the different types of risk exposure. Both unimodal and bimodal distribution are observed and distributions either spread or not spread over a range of values.

Figure V-7 shows histograms for all 100 mile squares in the Northeast for Attack A. Some of the histograms repeat those presented in Figure V-5, for example, histograms with coordinates 24 and 9 are presented on both Figures. To assist in identifying positions, the locations of some cities in the Northeast are given. For example, Washington, D.C. is located near the South-Western corner of the square with coordinates 24, 10. The high values of mean dose exhibited in Figure V-3 for the Northeast corridor is reflected here in the high chance of high exposure ranges shown in the histograms for this region.

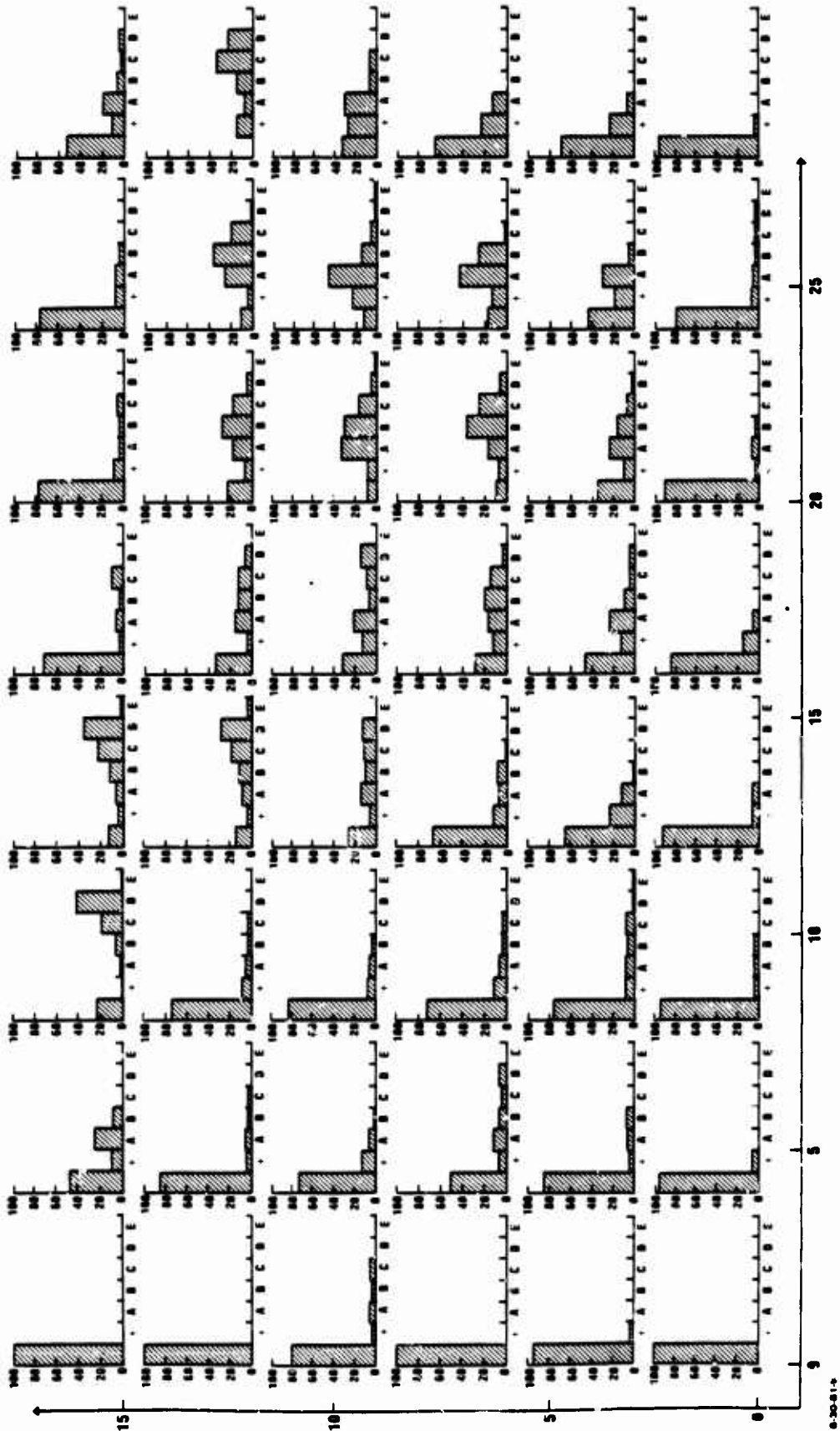


Figure V-5. NATIONWIDE HISTOGRAMS OF BIOLOGICAL DOSES FOR ATTACK A.

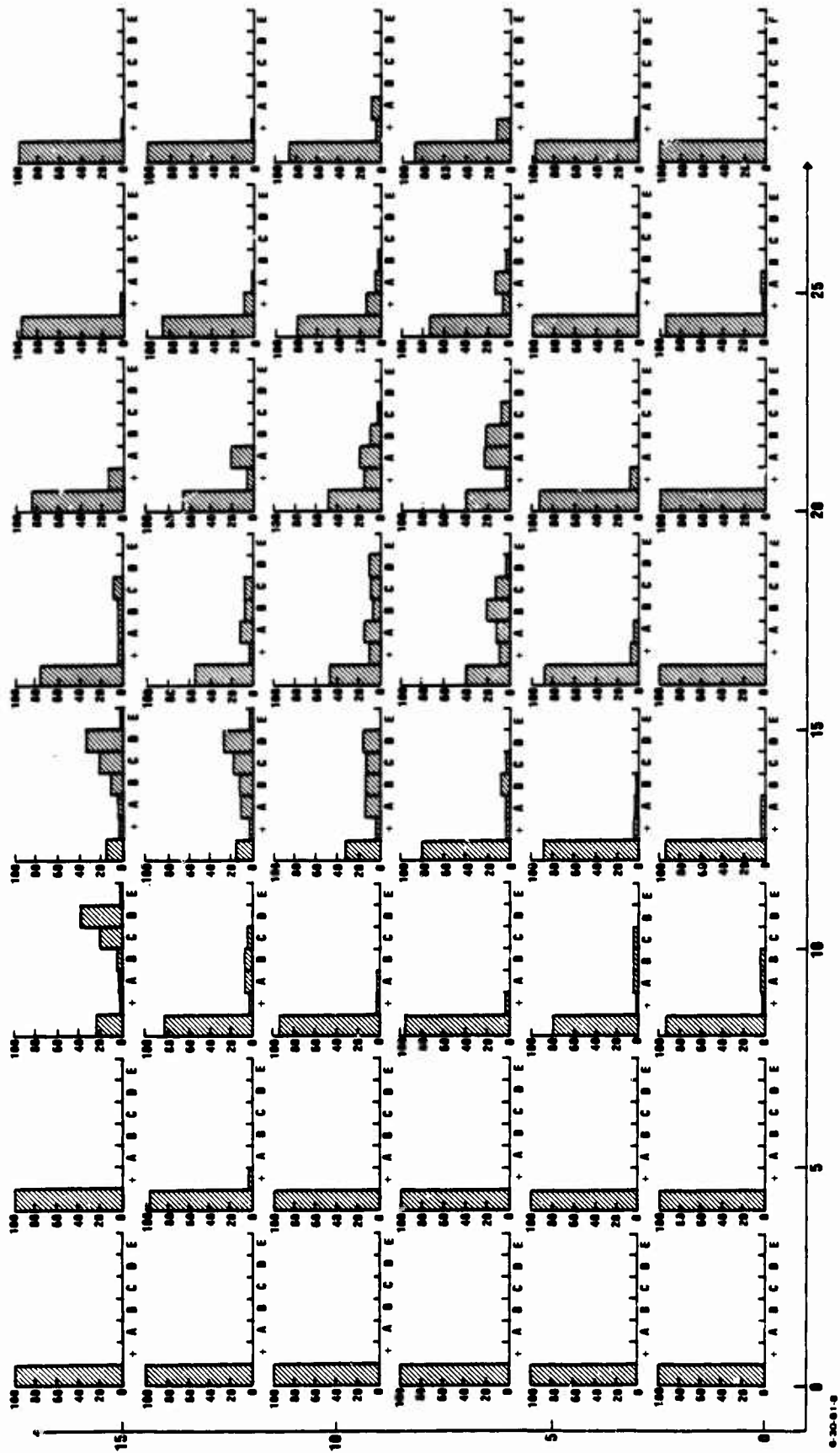


Figure V-6. NATIONWIDE HISTOGRAMS OF BIOLOGICAL DOSES FOR ATTACK B.

Another way of illustrating the risk is through contour maps where the contours represent the chance that doses are in a certain range. Figure V-8 presents contours of the probability that the dose is less than 500 Roentgens for Attack A and Figure V-9 presents comparable contours for Attack B. The intervals are 0 to 10 percent, 10 to 30 percent, 30 to 50 percent, 50 to 70 percent and over 90 percent. The regions on the map between contour lines are indicated by the change at the lower end of the range, for example, an arrow crossing a contour line labeled 50 indicated the contour is the boundary between the 30 to 50 percent region and the 50 to 70 percent region, and the head of the arrow is in the latter region. The changes are averaged over 100 mile squares as done for the mean doses. These chances are the same as the chances of being at the lowest level as presented in the histograms. The contours run in the opposite direction as for the mean doses. Here a ridge represents a high chance of low dose level, i.e., a safer region, where for the mean dose a ridge indicates a high mean dose level, i.e., a less safe region. The ridge of mean doses over 5000 Roentgens for the Northeast seen in Figure V-3 corresponds to small chances (less than 10 percent) of doses under 500 Roentgen.

In Figures V-10 and V-11 similar contours are presented for Attacks A and B except that here the critical dose level is raised to 2500 Roentgens. These are the regions denoted by Blank, + and A on the fallout maps of the Appendices. The previous contours indicate the chance that minimal fallout protection will be adequate, while these indicate the chance that less than National Fallout Shelter Survey standards will be adequate.

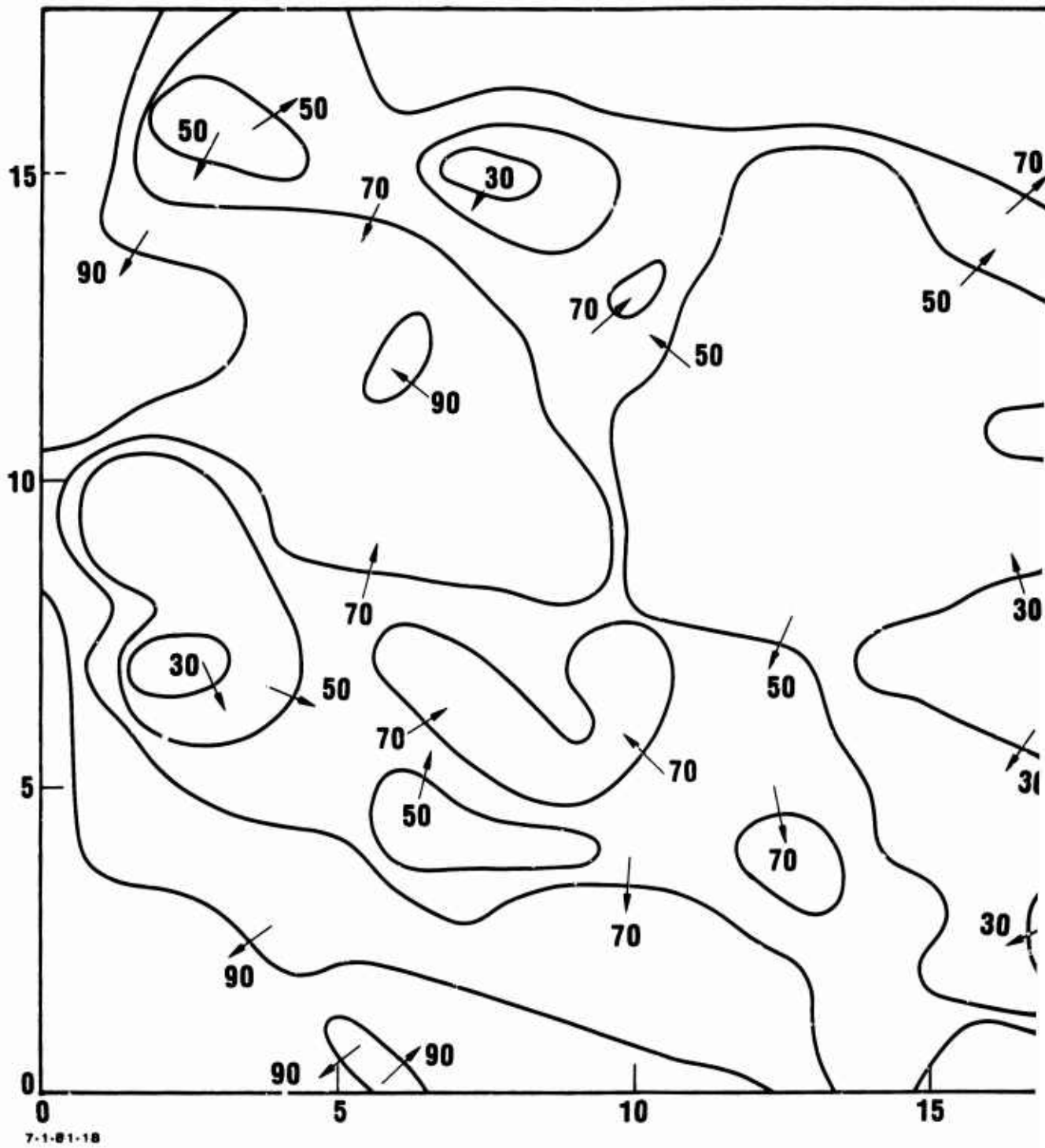
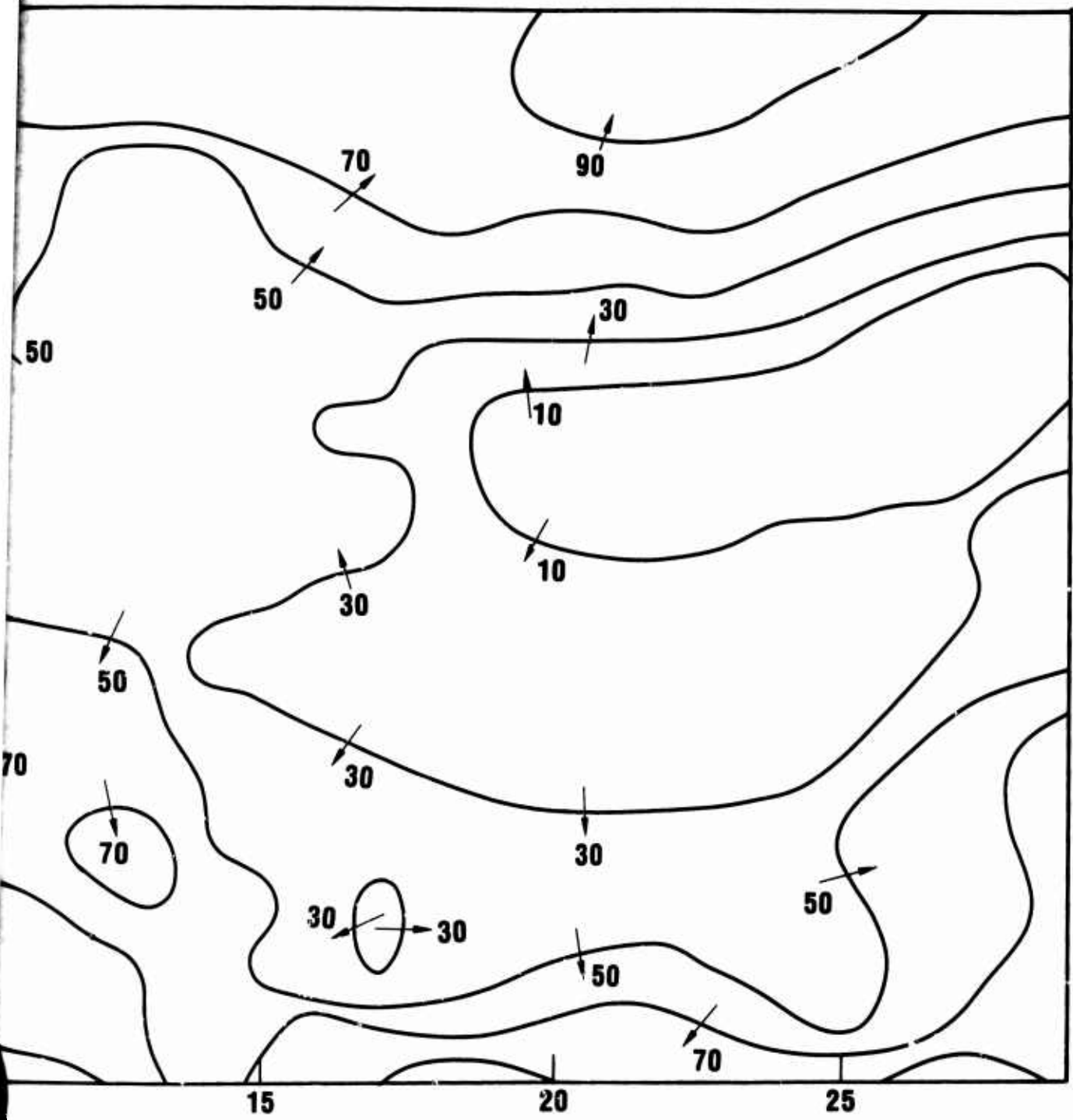


Figure V-8. CONTOURS OF LIKELIHOOD OF DOSE BEI



OF LIKELIHOOD OF DOSE BEING BELOW 500R FOR ATTACK A.

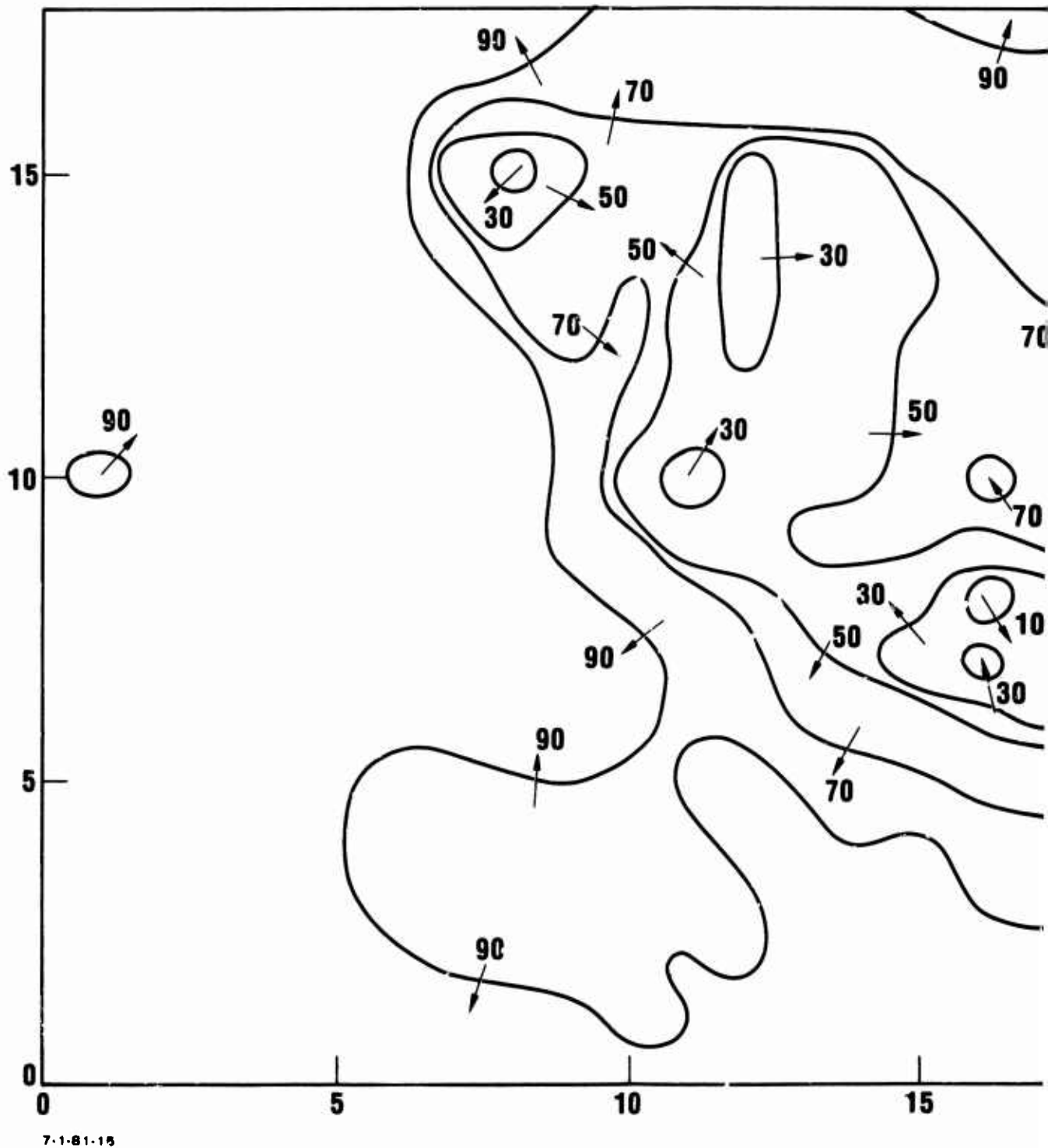
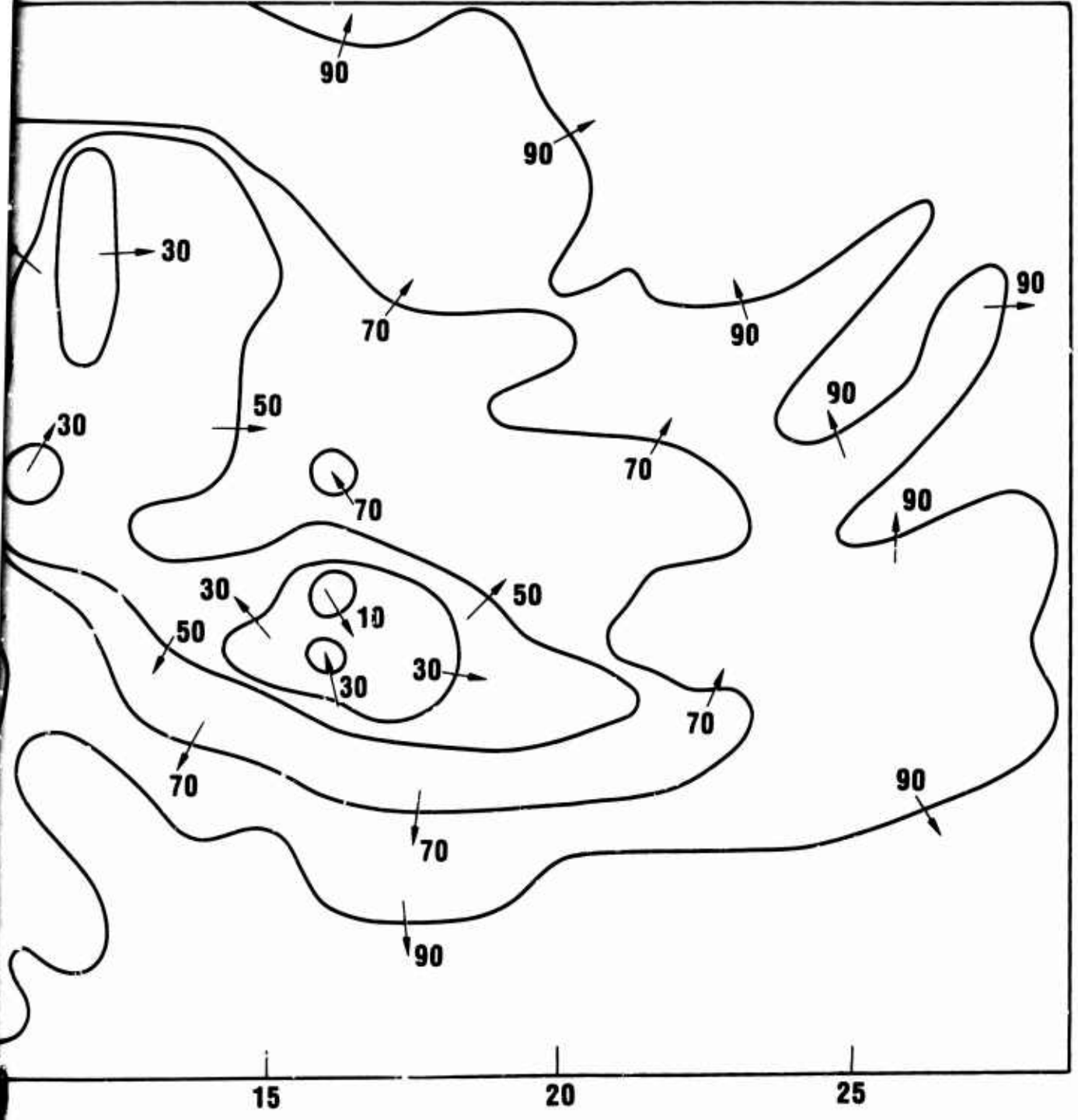


Figure V-9. CONTOURS OF LIKELIHOOD OF DOSE BEI



PROBABILITY OF LIKELIHOOD OF DOSE BEING BELOW 500R FOR ATTACK B.

217/218

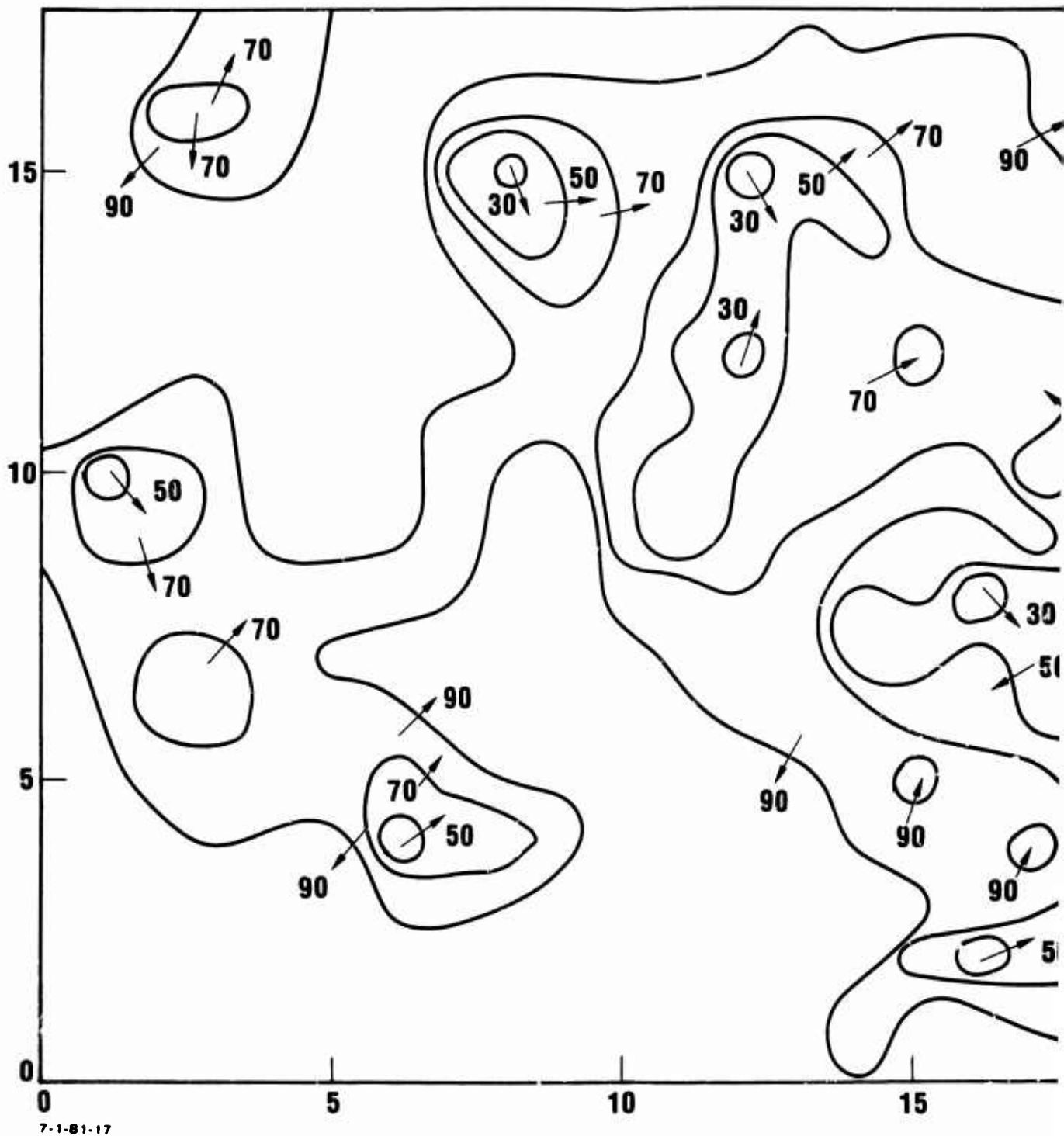
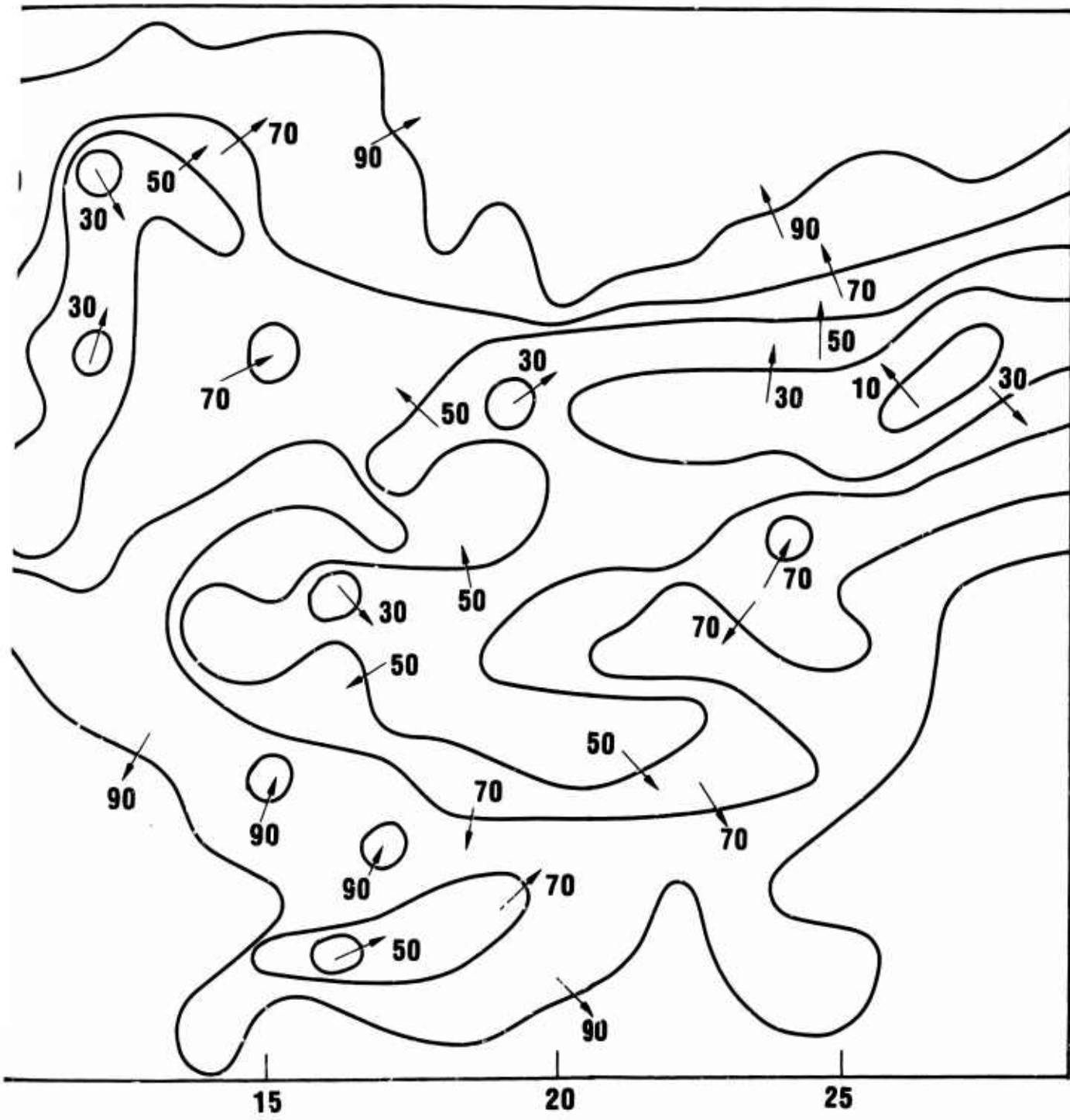


Figure V-10. CONTOURS OF LIKELIHOOD OF DOSE BEING BELOW



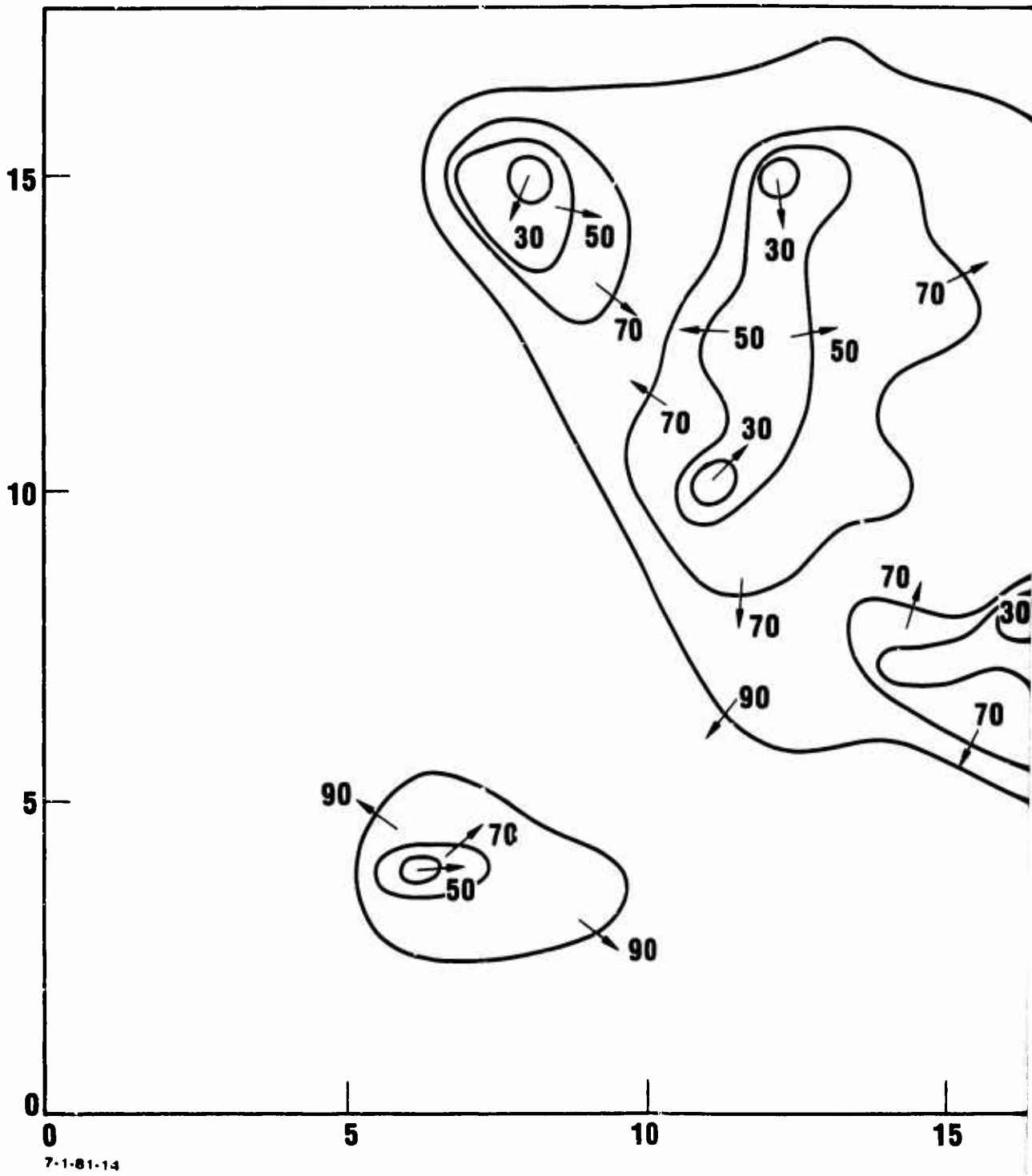
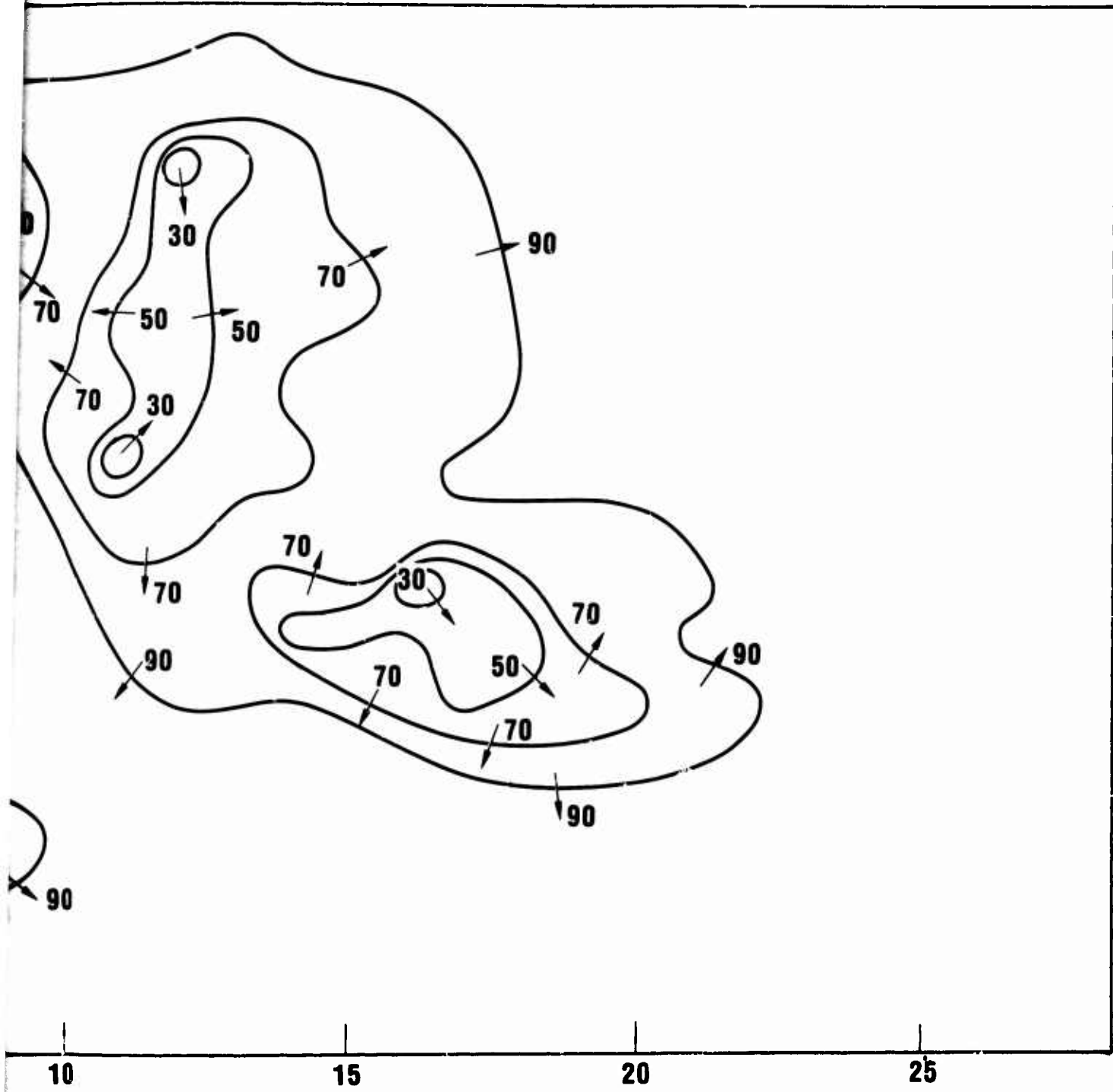


Figure V-11. CONTOURS OF LIKELIHOOD OF DOSE BEING



OURS OF LIKELIHOOD OF DOSE BEING BELOW 2500R FOR ATTACK B.

221/222

REFERENCES

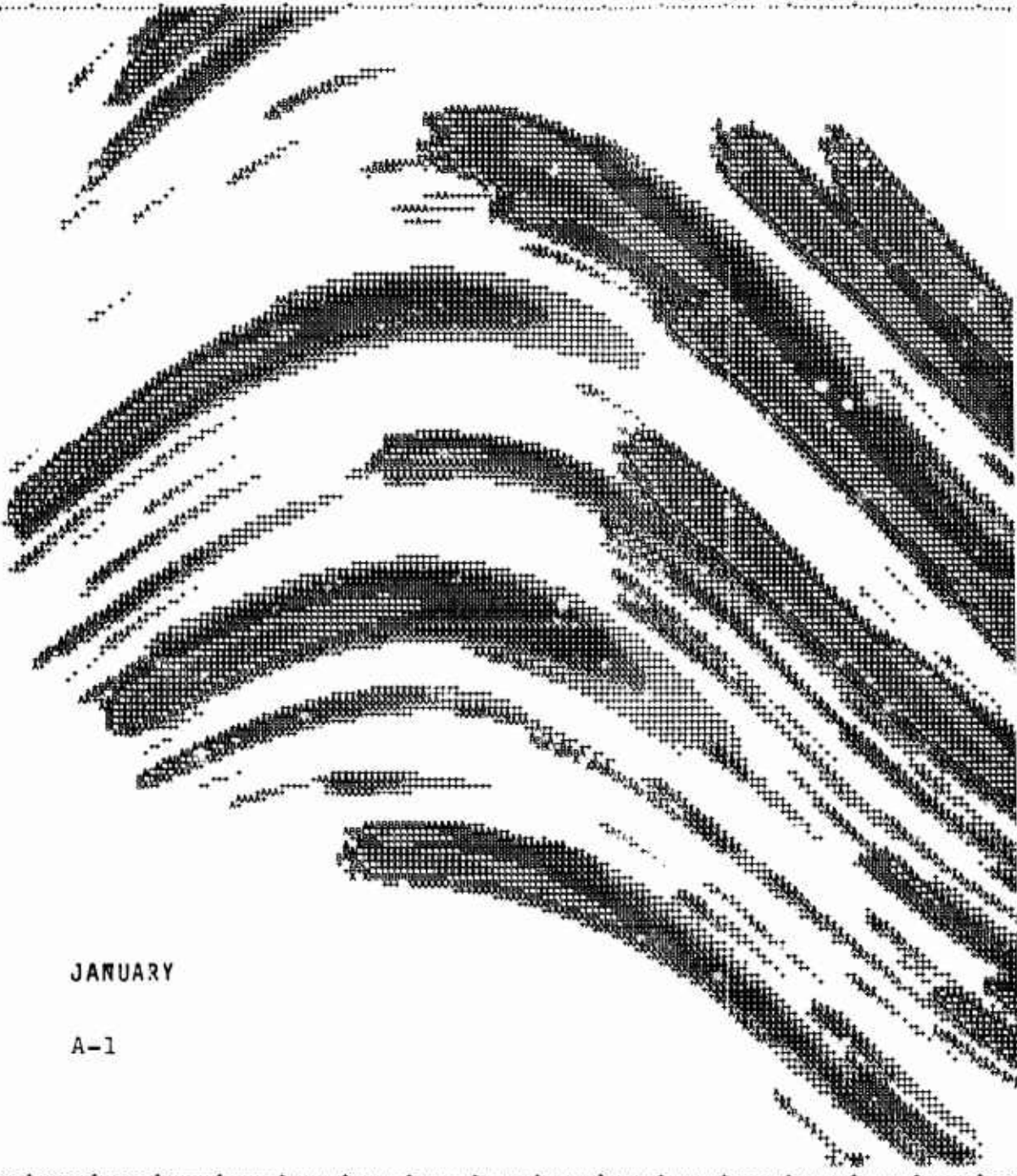
- [1] Pugh, George E. and Galiano, Robert J. "An Analytic Model of Close-In Deposition of Fallout for Use in Operational-Type Studies," WSEG Research Memorandum No. 10, Weapons System Evaluation Group, 15 October 1959, Revised October 1960. UNCLASSIFIED.
- [2] Polan, M. "An Analysis of the Fallout Prediction Models Presented at the USNRDL-DASA Fallout Symposium of September 1962, Volume 1: Analyses, Comparisons, and Classification of Models," U.S. Naval Radiological Defense Laboratory, USNRDL-TRC-68, September, 1966. UNCLASSIFIED.
- [3] Schmidt, Leo A. "Methodology of Fallout-Risk Assessment" IDA Paper P-1065, January, 1975. UNCLASSIFIED.
- [4] Allan, Julian E. "'Most Probable' Fallout Wind Illustration," Technical Memorandum Draft, National Military Command System Support Center, August 30, 1974. UNCLASSIFIED.
- [5] Schmidt, Leo A. "Development of Civil Defense Damage Assessment Programs," IDA Paper P-1526, November, 1980. UNCLASSIFIED.

Appendix A
FULL ATTACK, HIGH DOSE RANGE

FALLOUT MAPS FOR ATTACK A (FULL ATTACK)
IN THE HIGH DOSE RANGE

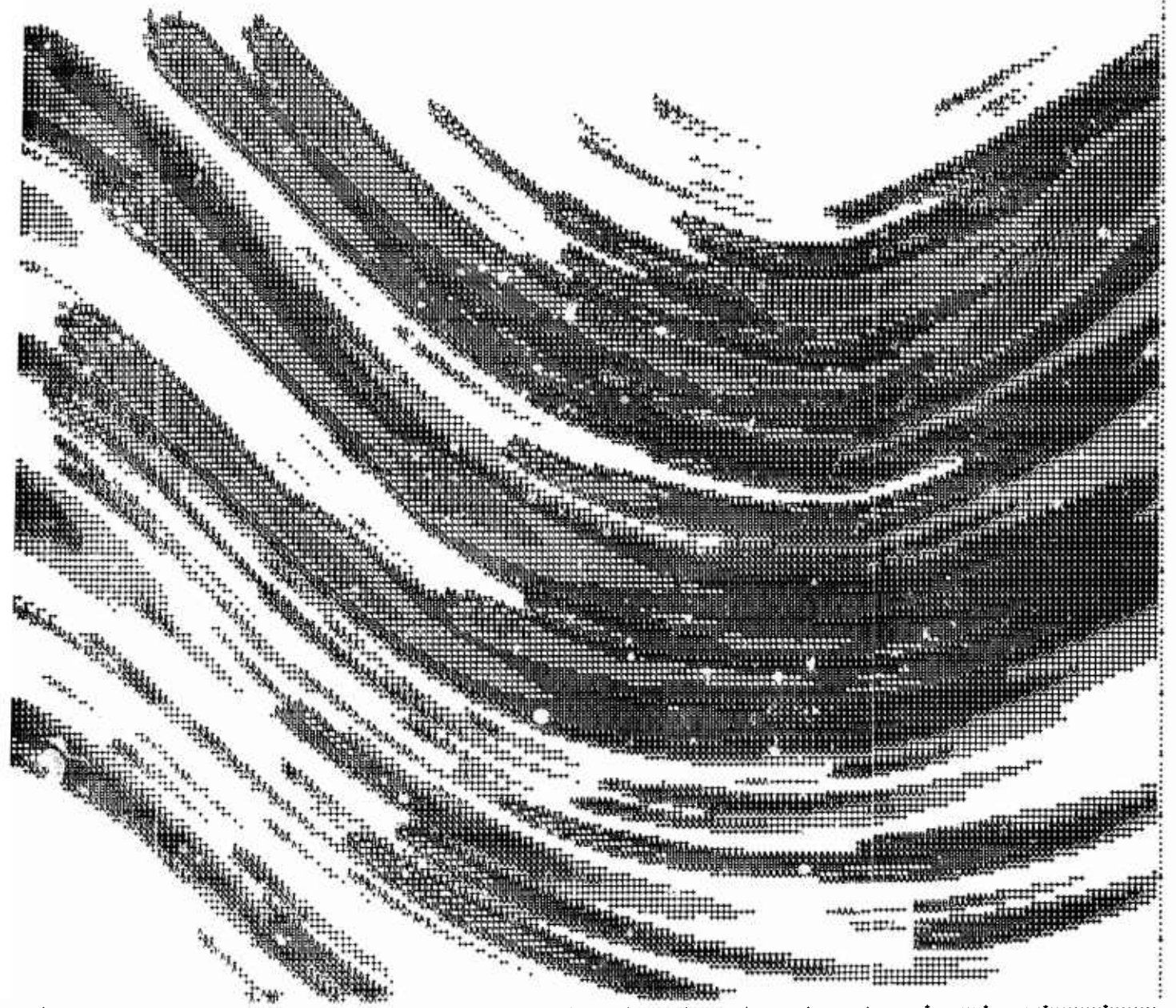
Figures A-1 through A-12 present maps of biological fall-out dose deposition for Attack A (the full attack) for each month of the year. The dose ranges chosen emphasize sheltering requirements. The symbol definitions are:

Symbol	Dose Range (Roentgens)
Blank	Dose < 500
+	$500 \leq \text{Dose} < 1,000$
A	$1,000 \leq \text{Dose} < 2,500$
B	$2,500 \leq \text{Dose} < 5,000$
C	$5,000 \leq \text{Dose} < 10,000$
D	$10,000 \leq \text{Dose} < 30,000$
E	$30,000 \leq \text{Dose}$



JANUARY

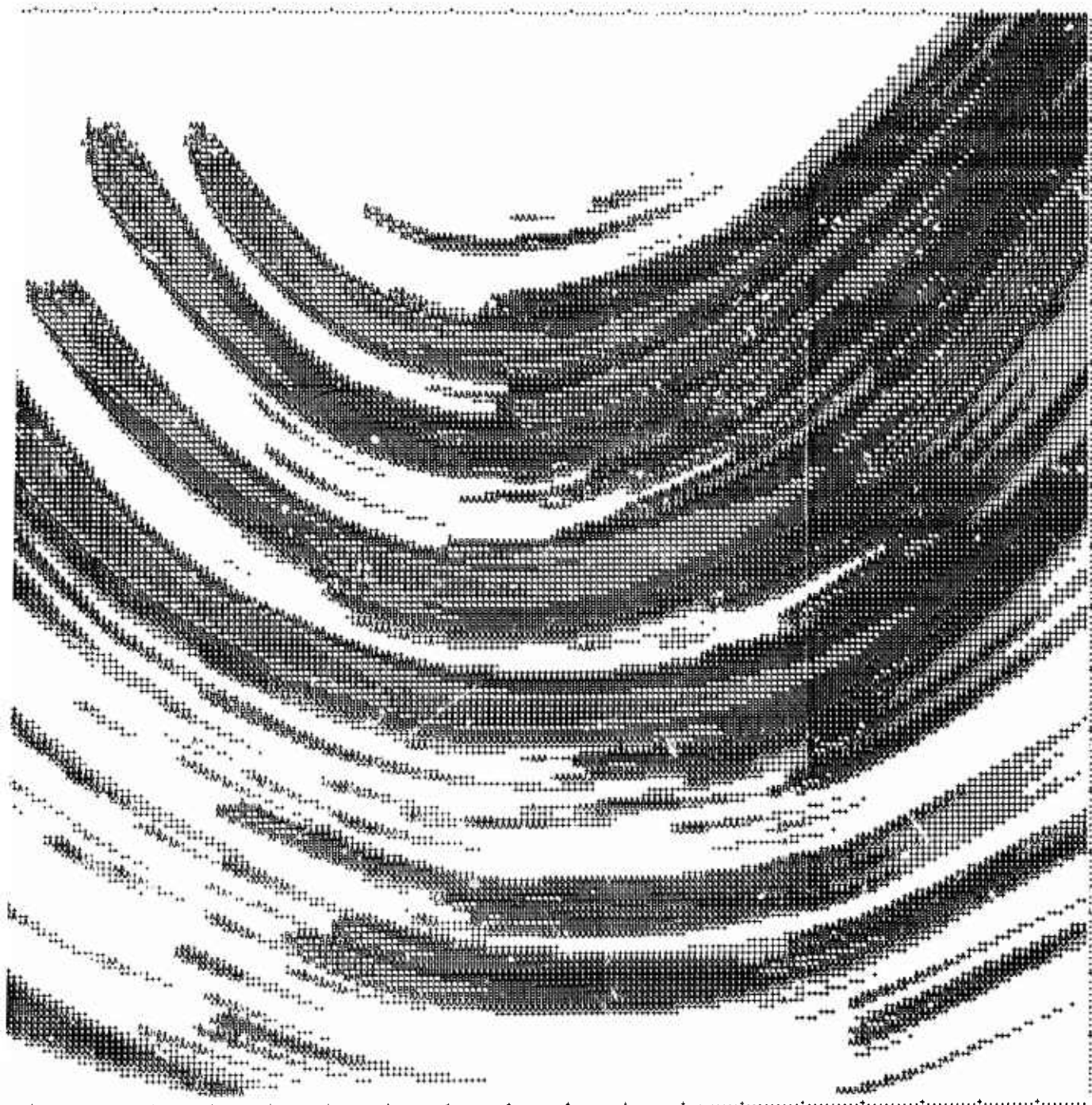
A-1





FEBRUARY

A-2





MARCH

A-3

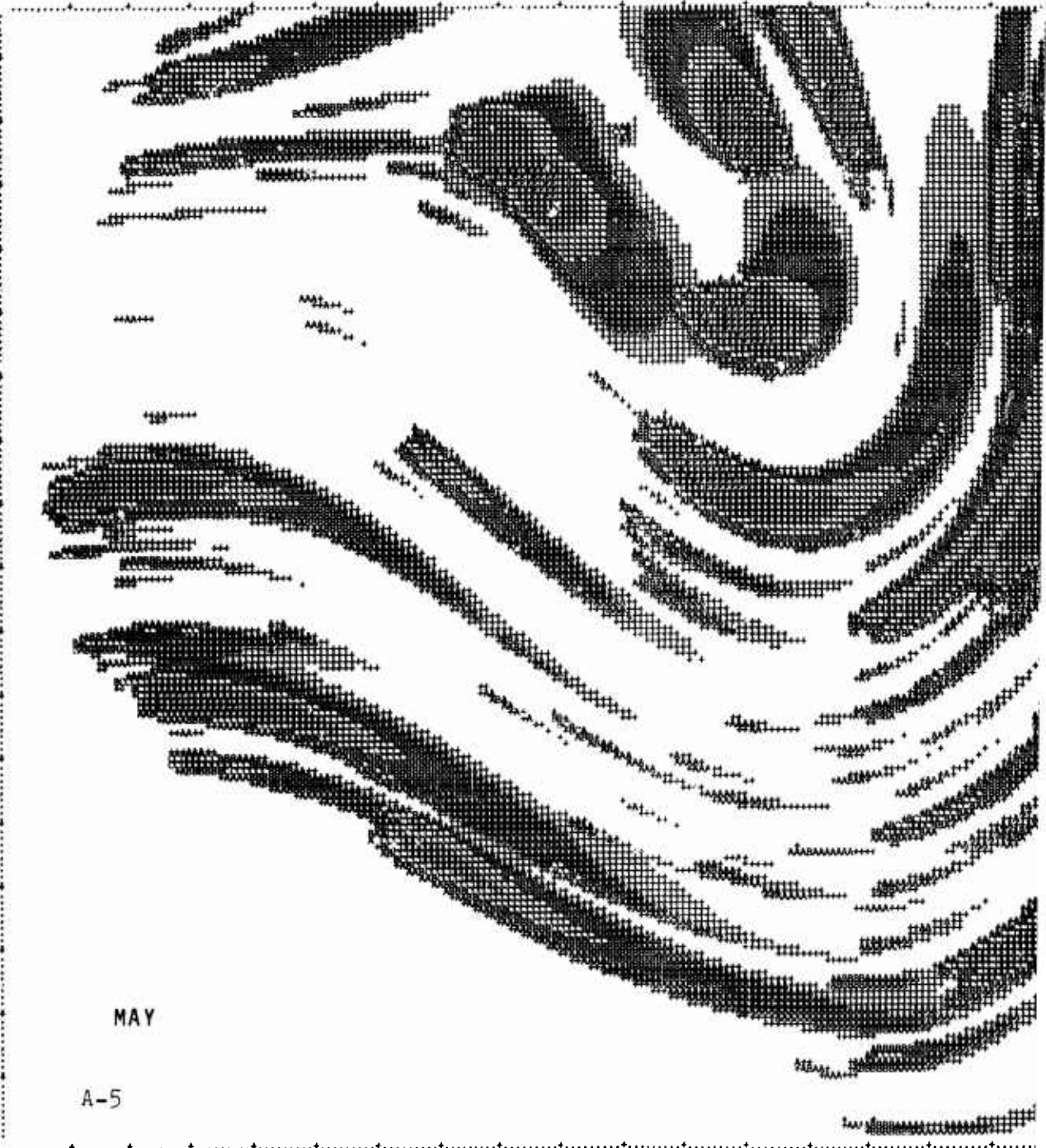




APRIL

A-4

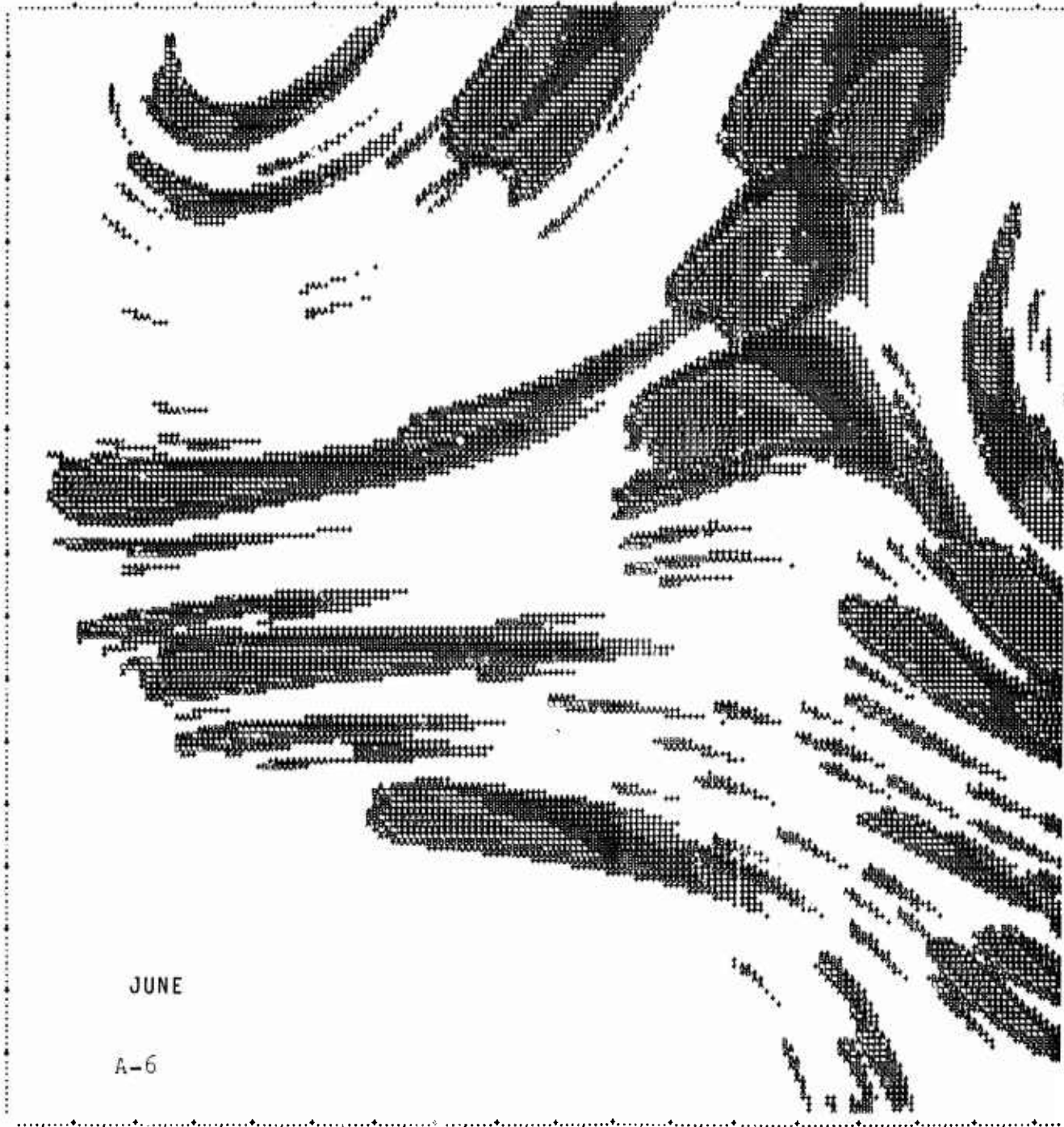




MAY

A-5





JUNE

A-6



2

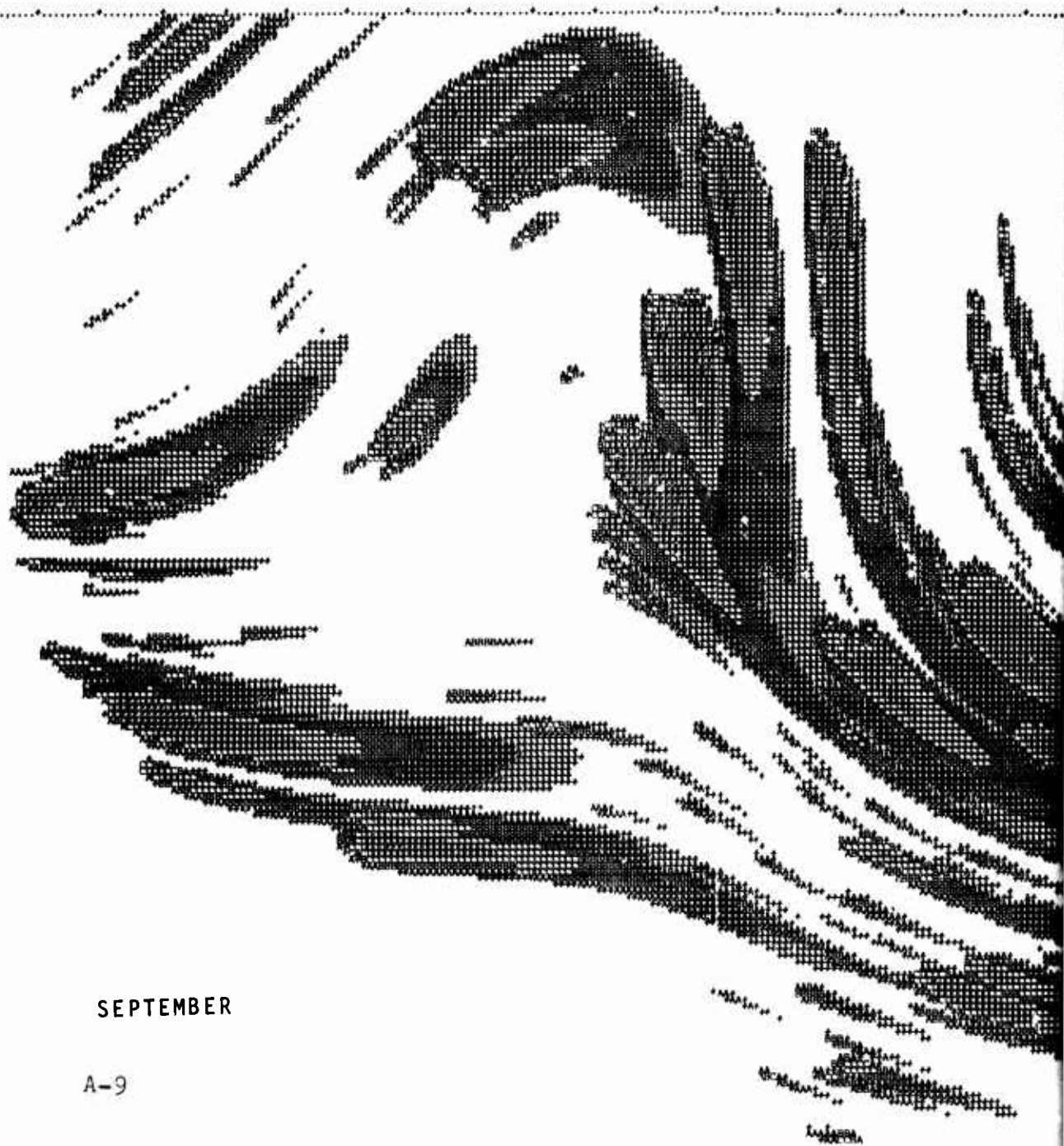




AUGUST

A-8

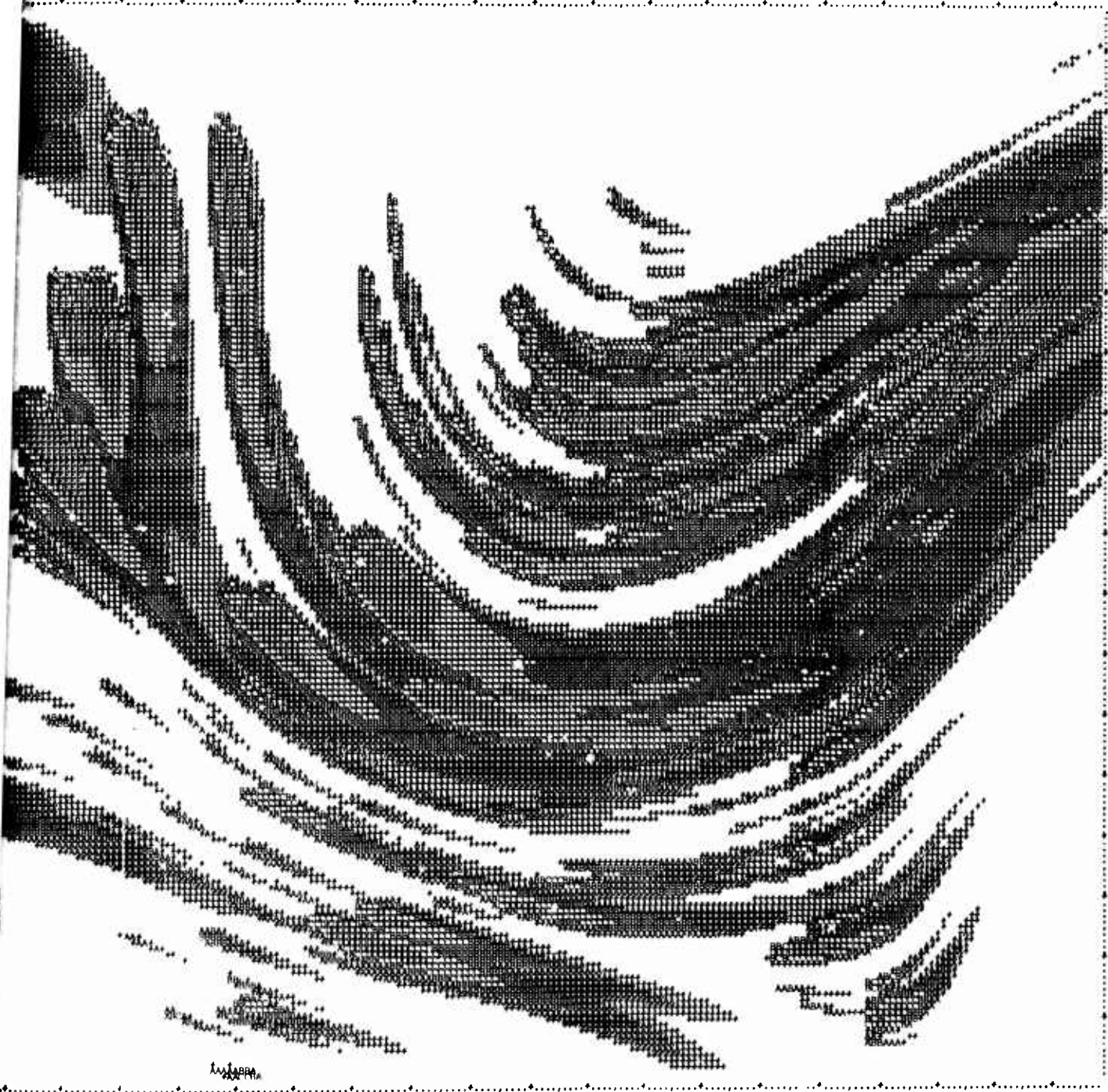




SEPTEMBER

A-9

2

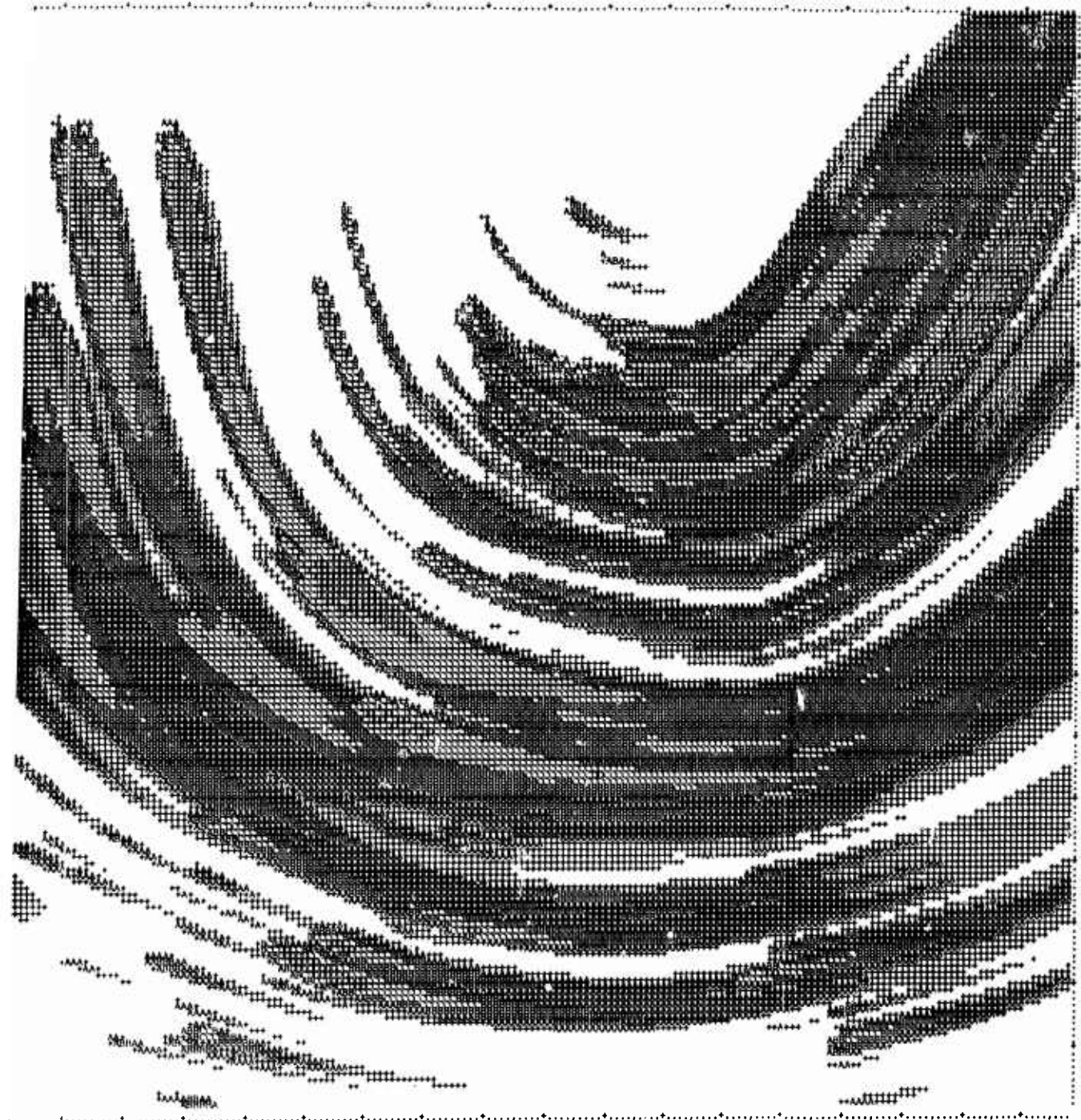


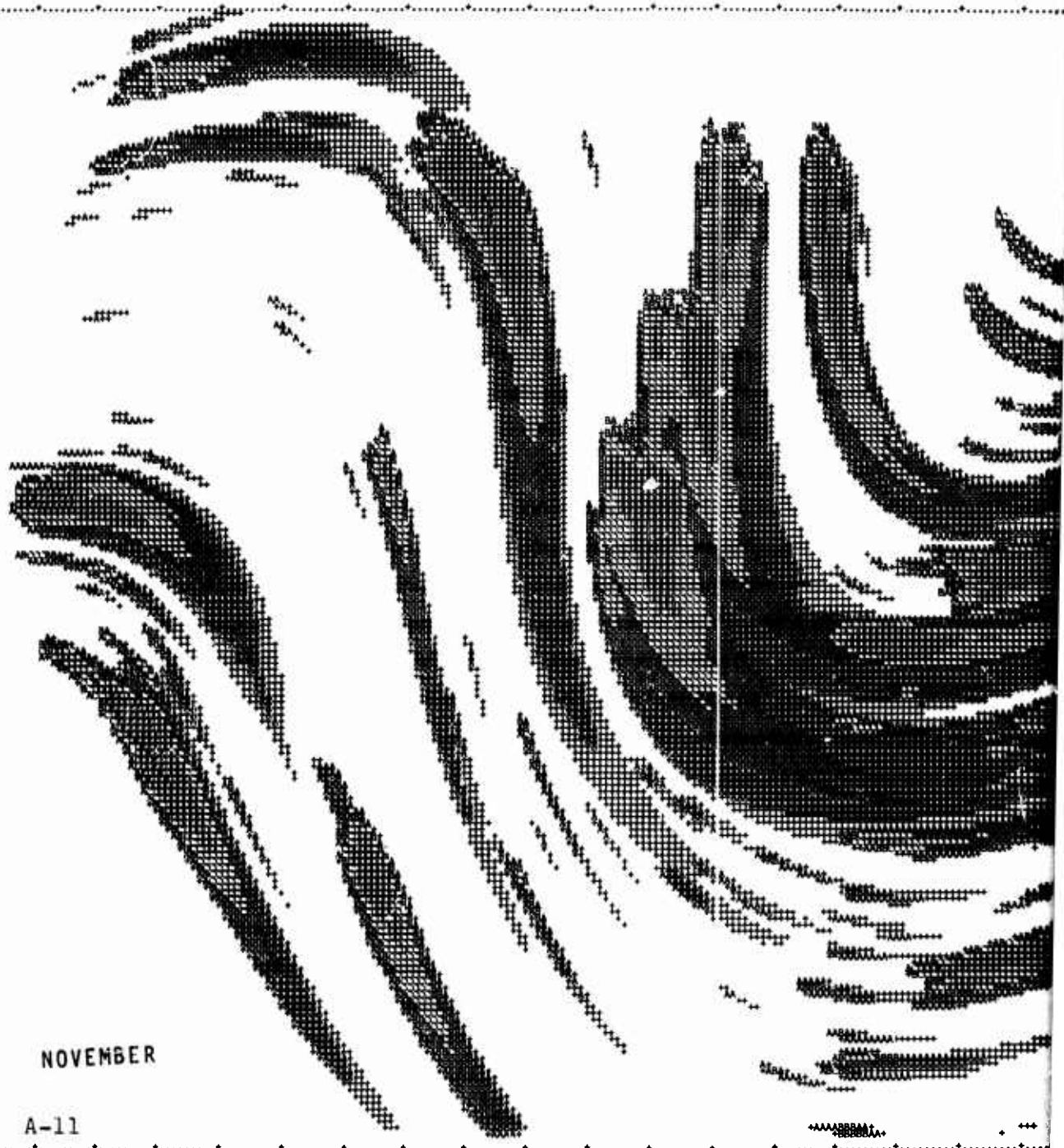
LAPPA



OCTOBER

A-10





NOVEMBER

A-11





DECEMBER

A-12

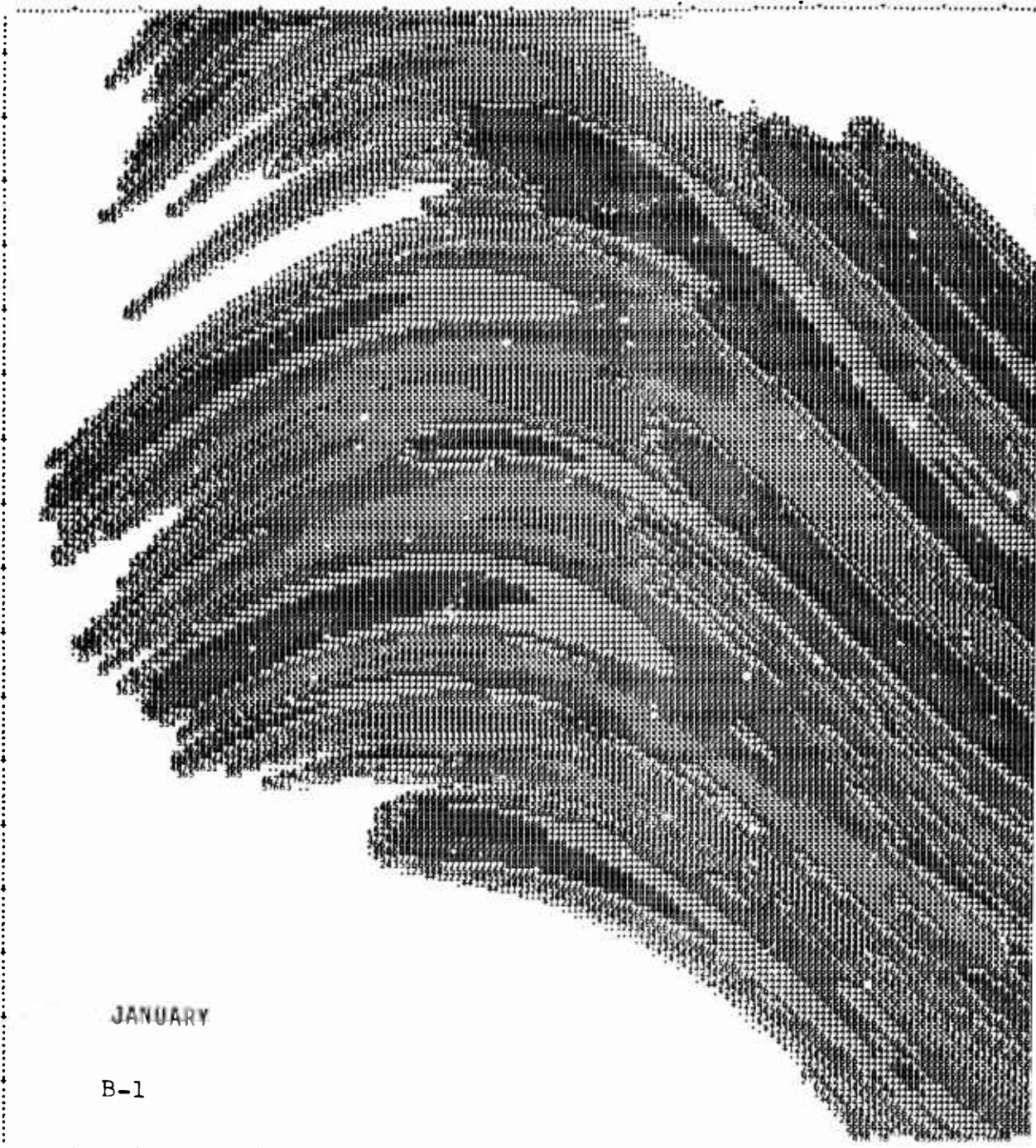


Appendix B
FULL ATTACK, LOW DOSE RANGE

FALLOUT MAPS FOR ATTACK A (FULL ATTACK)
IN THE LOW DOSE RANGE

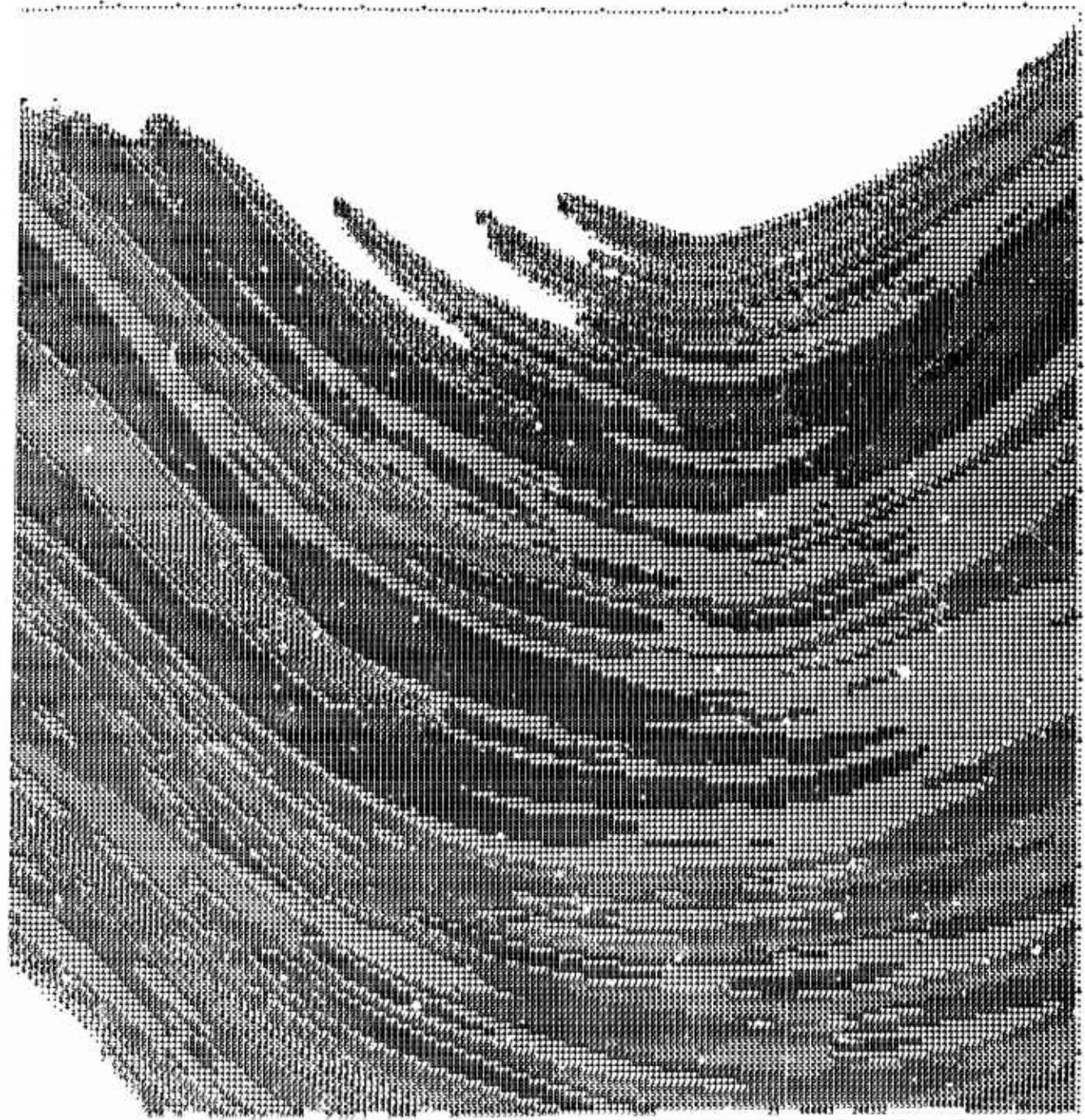
Figures B-1 through B-12 present maps of biological fall-out dose deposition for attack A (the full attack) for each month of the year. The dose ranges chosen allow estimating dose level within a factor of about 3. The symbol definitions are:

Symbol	Dose Range (Roentgens)
Blank	Dose < 0.1
o	$0.1 \leq \text{Dose} < 0.3$
+	$0.3 \leq \text{Dose} < 1$
1	$1 \leq \text{Dose} < 3$
2	$3 \leq \text{Dose} < 10$
3	$10 \leq \text{Dose} < 30$
4	$30 \leq \text{Dose} < 100$
5	$100 \leq \text{Dose} < 300$
6	$300 \leq \text{Dose} < 1000$
7	$1000 \leq \text{Dose} < 3000$
8	$3000 \leq \text{Dose} < 10,000$
9	$10,000 \leq \text{Dose} < 30,000$
0	$30,000 \leq \text{Dose}$

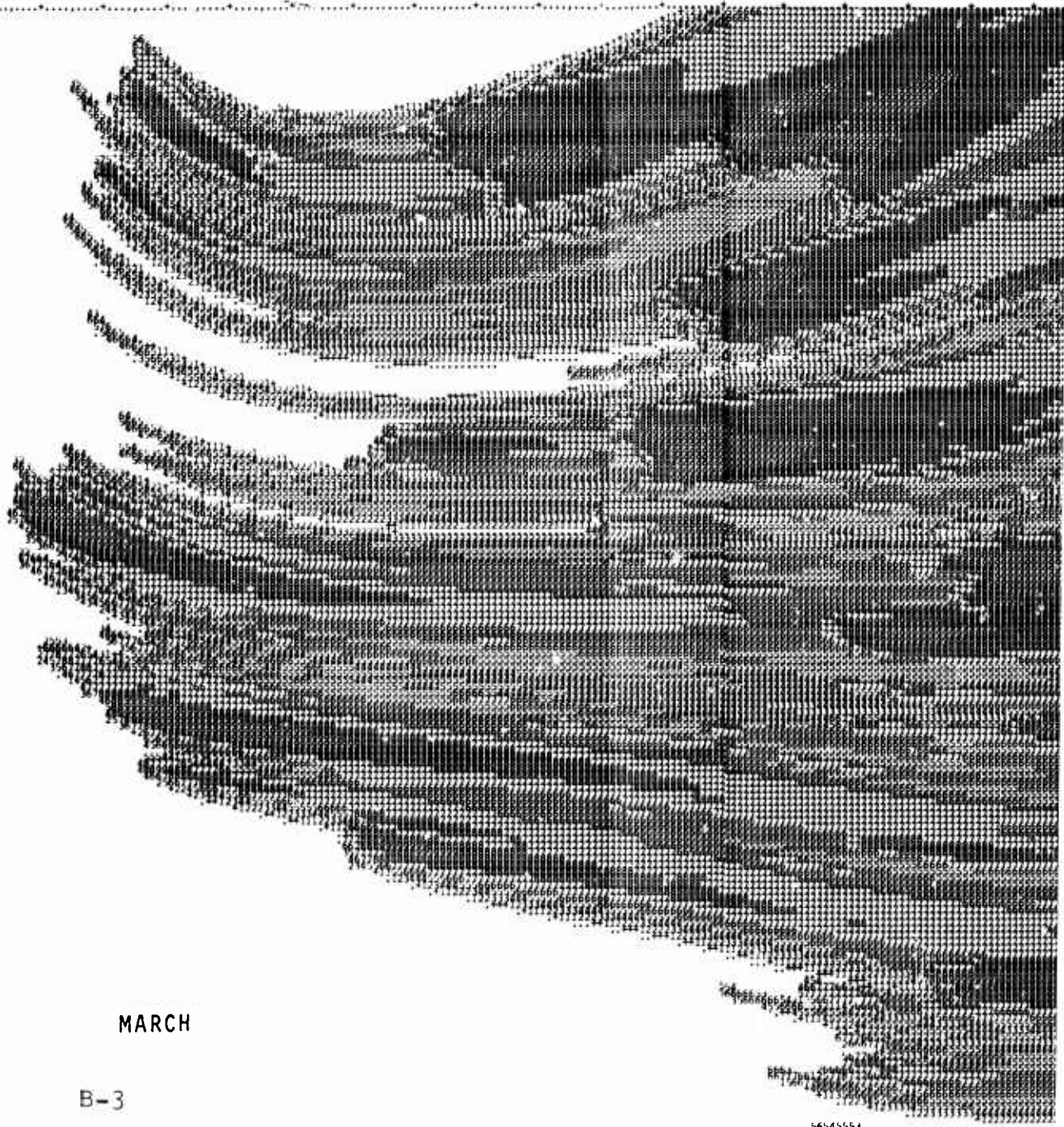


JANUARY

B-1



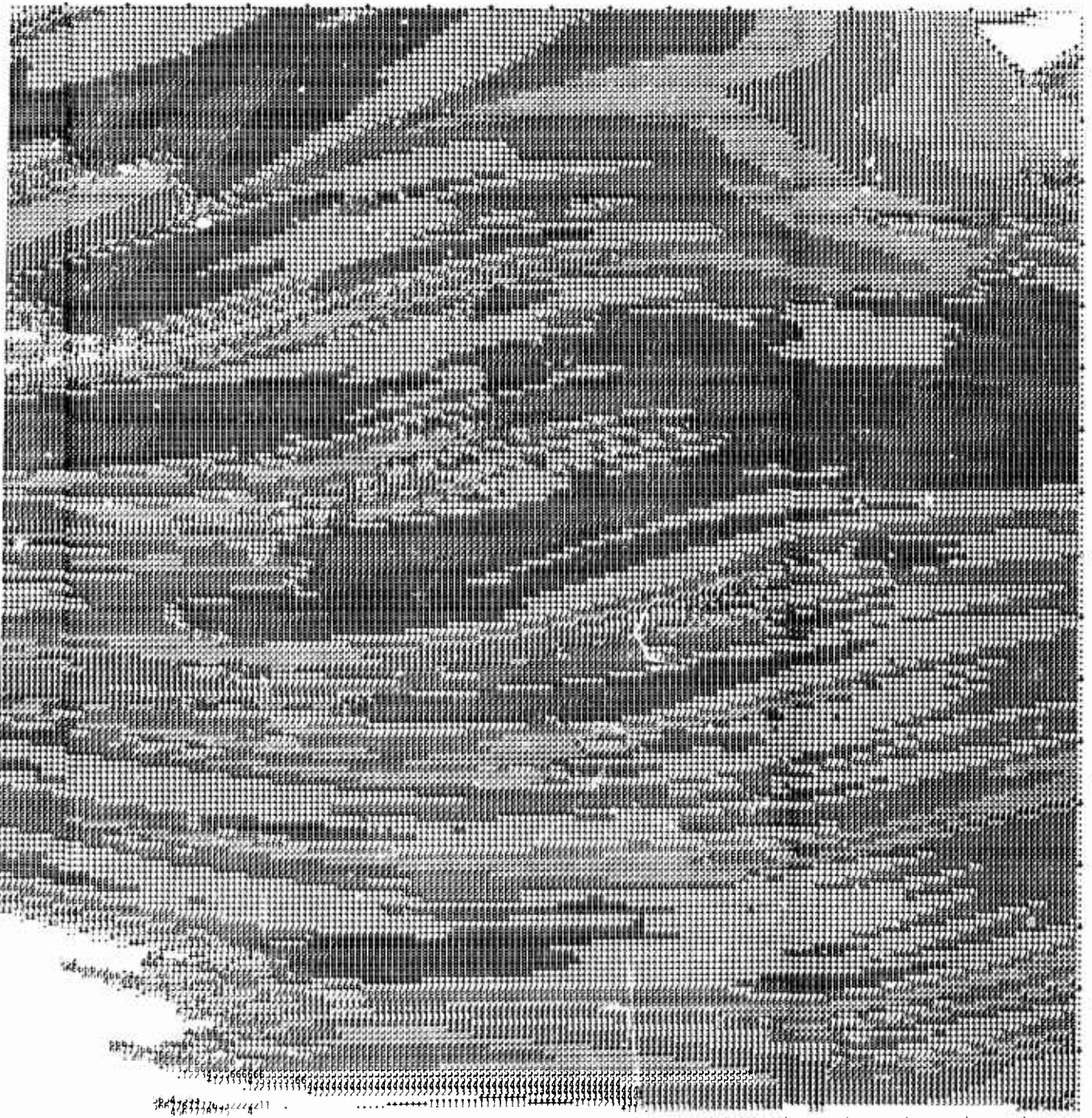




MARCH

B-3

5642554224-11

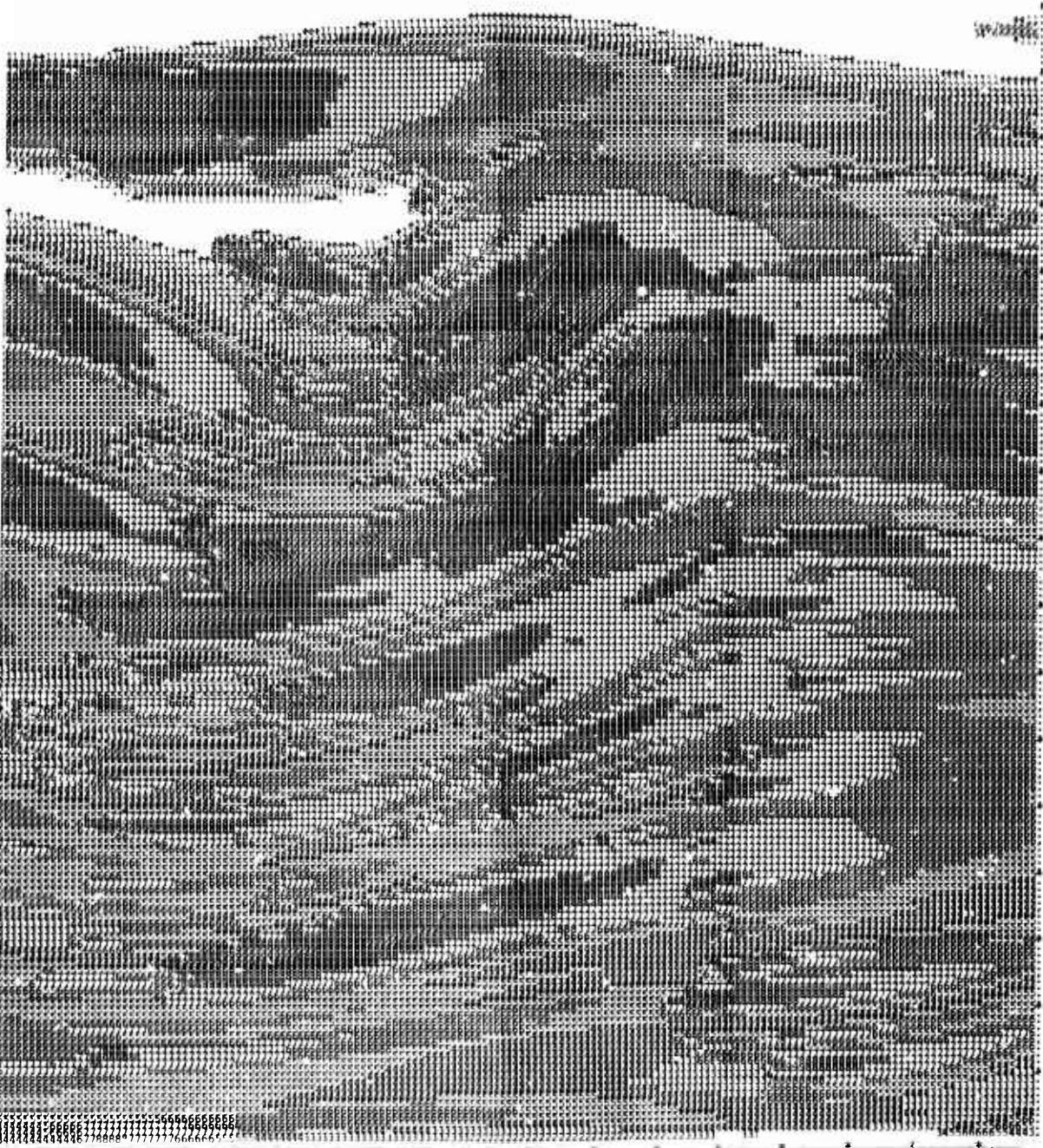


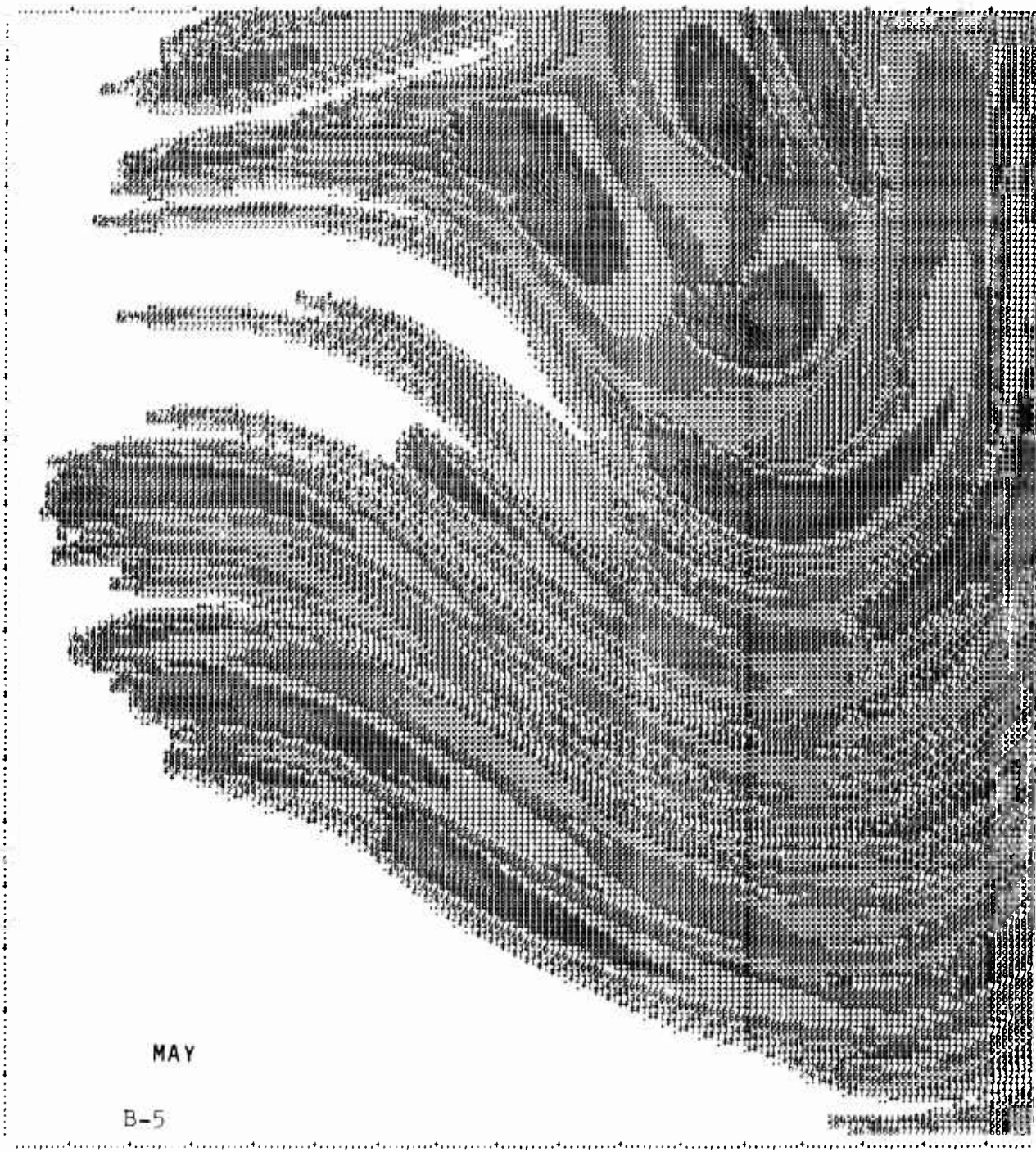


APRIL

B-4

✓

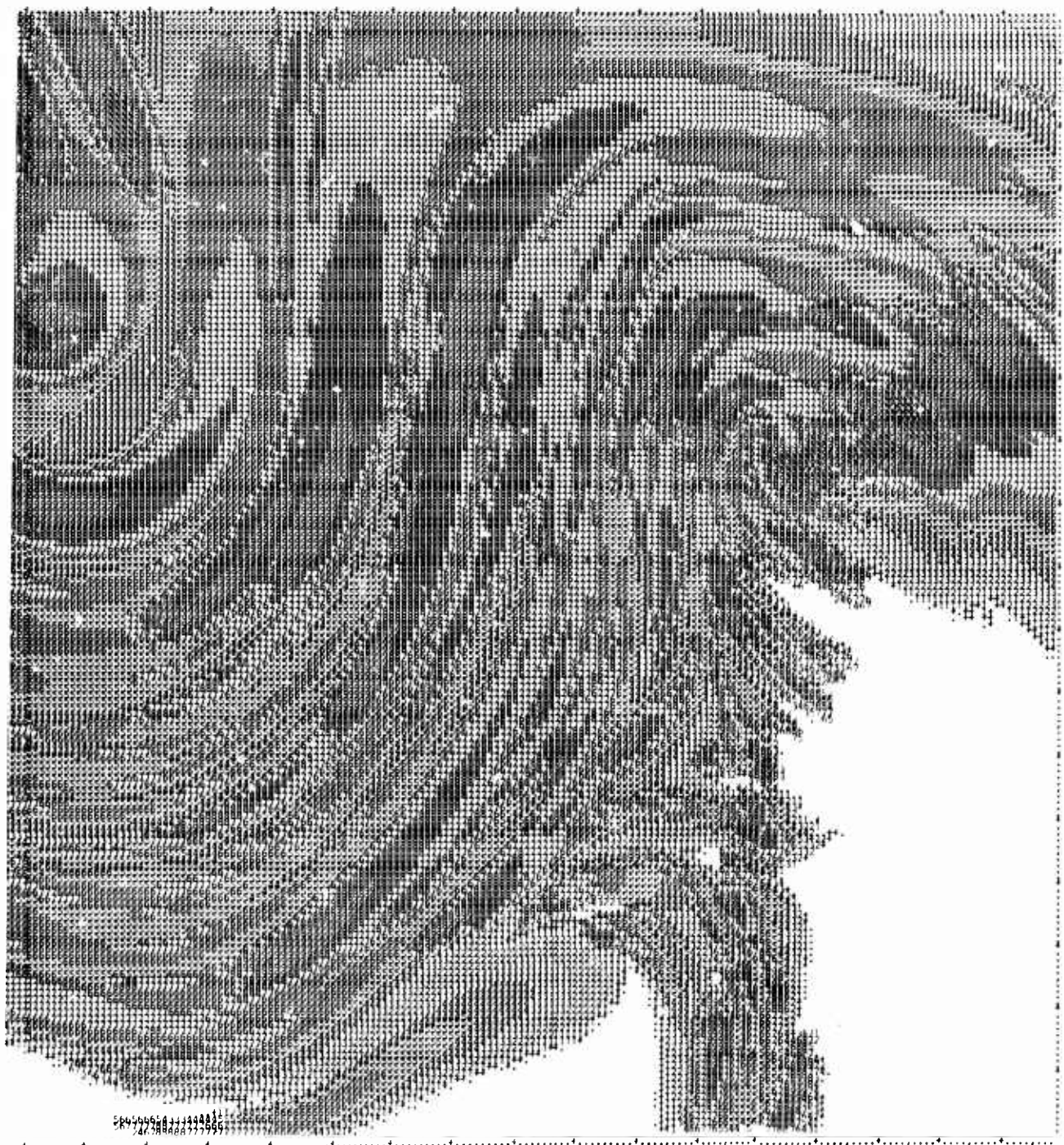




MAY

B-5

247 780841179977 11116.8





JUNE

B-6

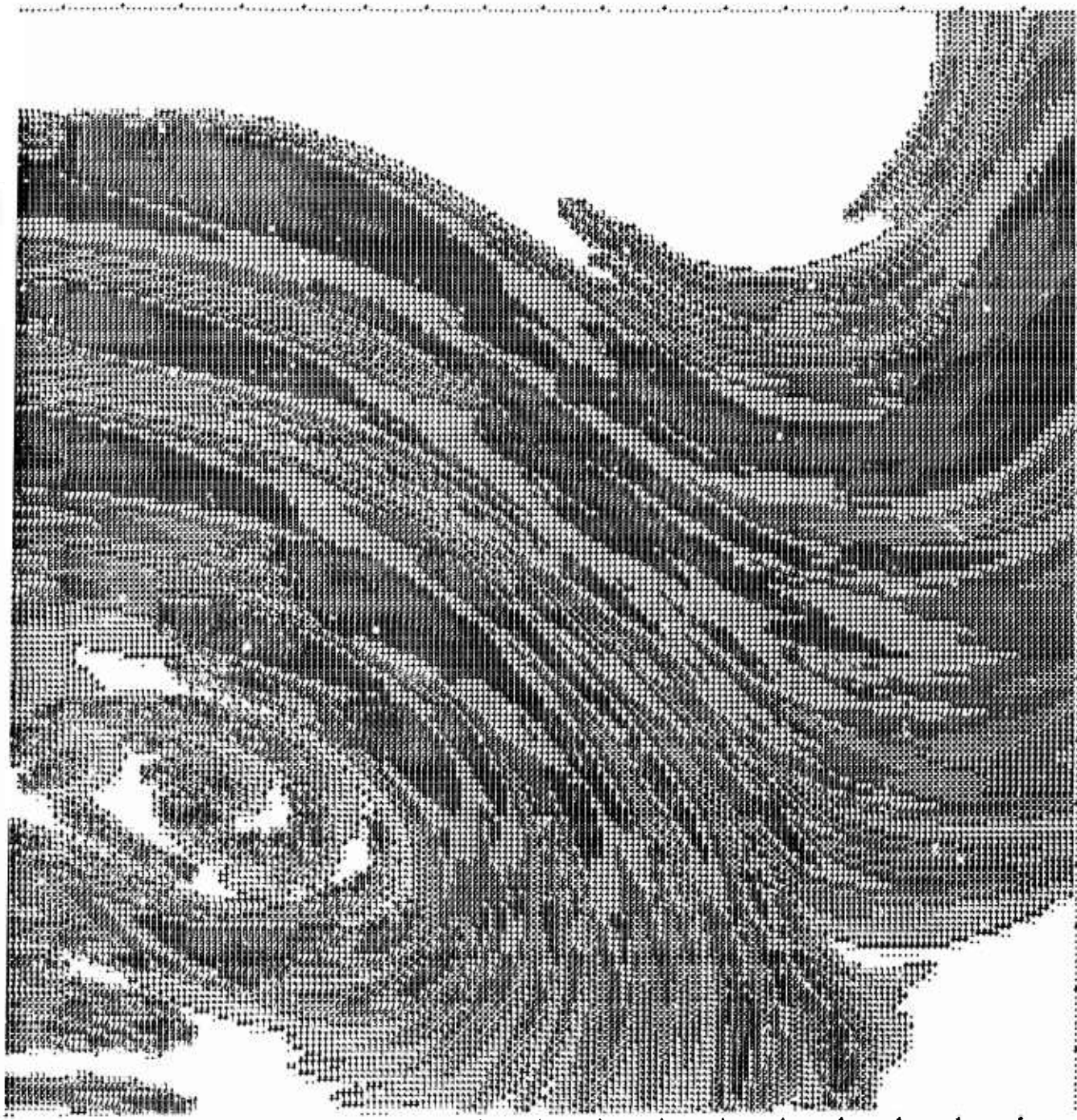
✓





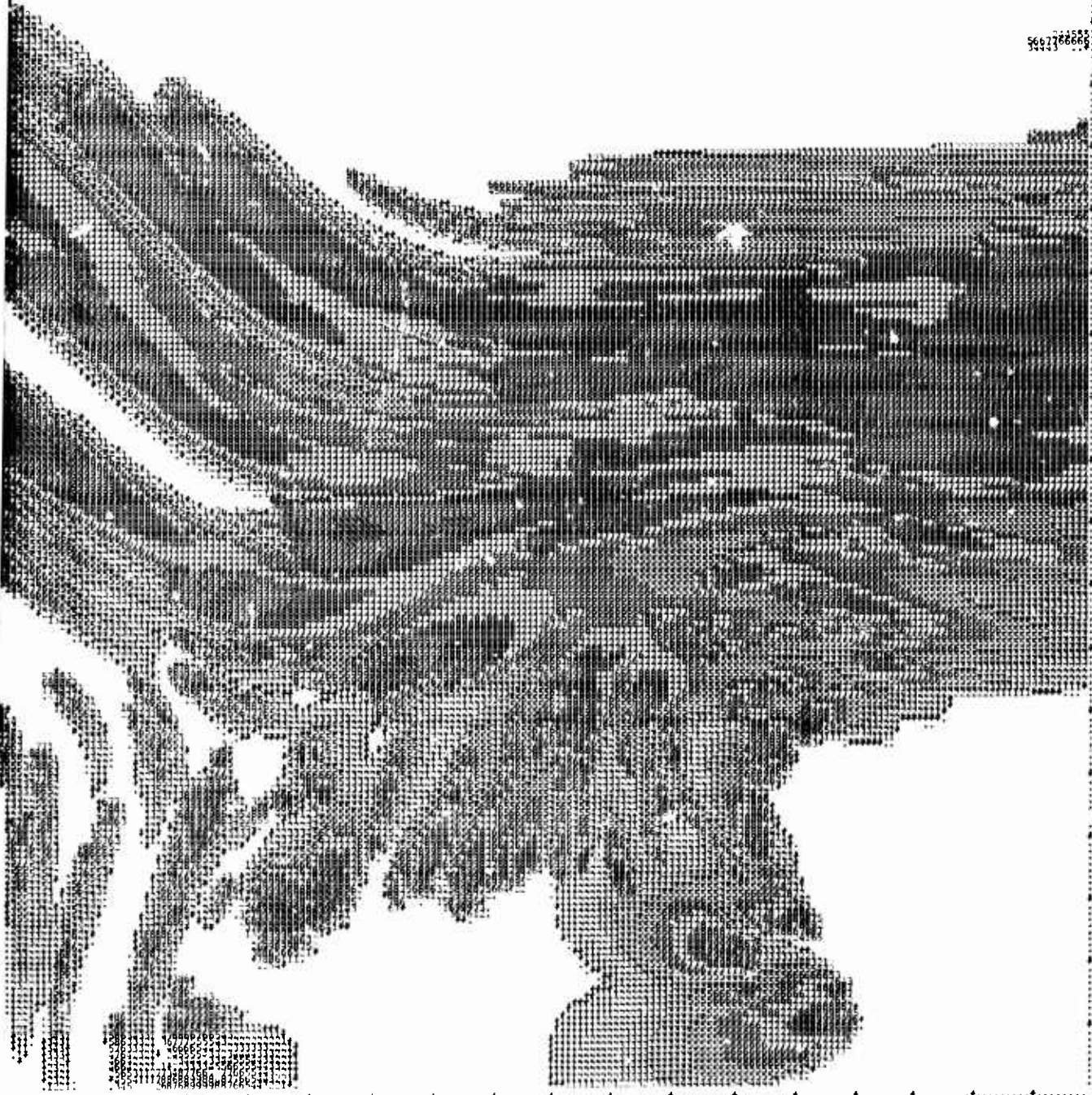
JULY

B-7



2

56278666





SEPTEMBER

B-9

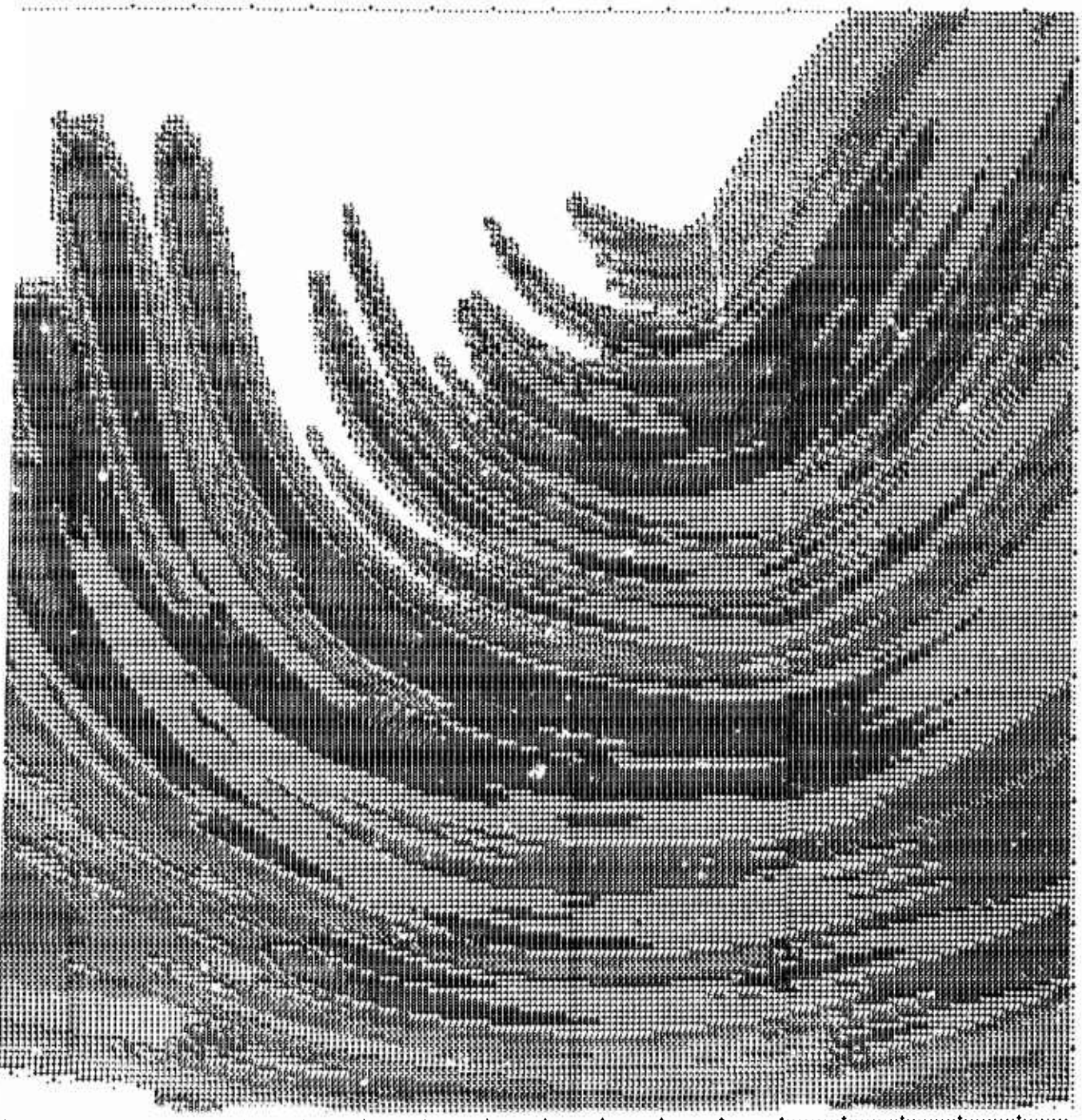


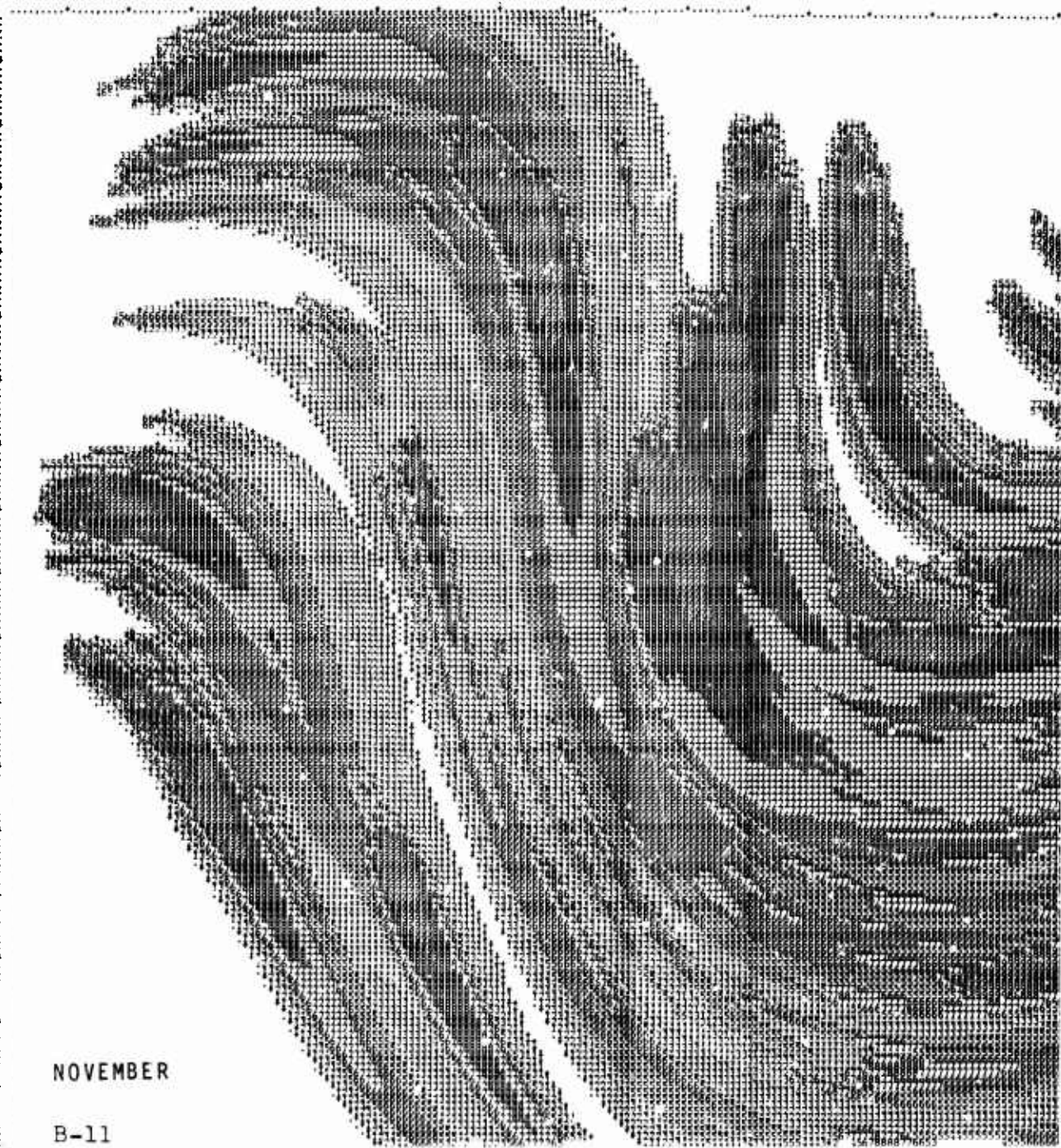


OCTOBER

B-10

2

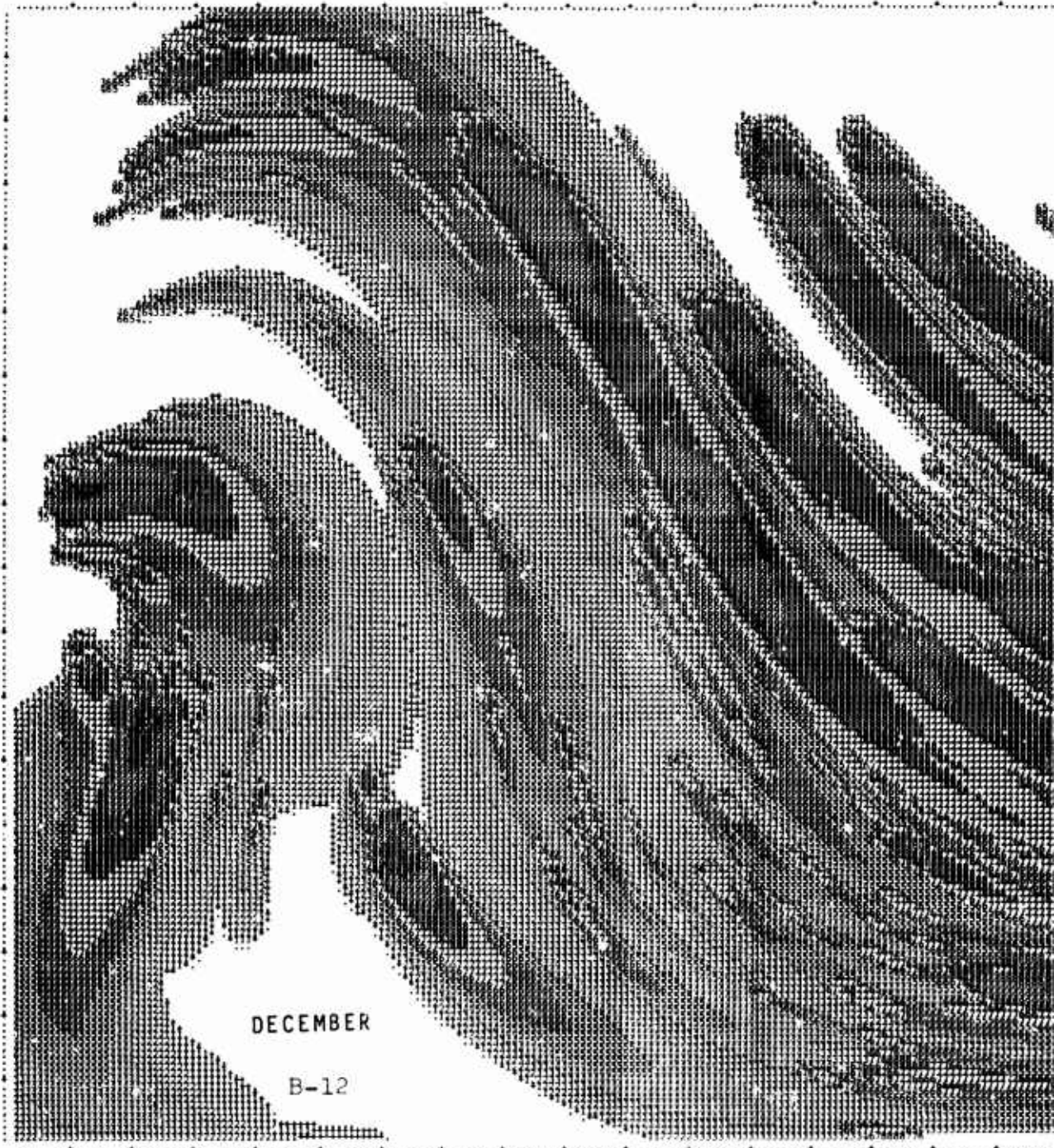




NOVEMBER

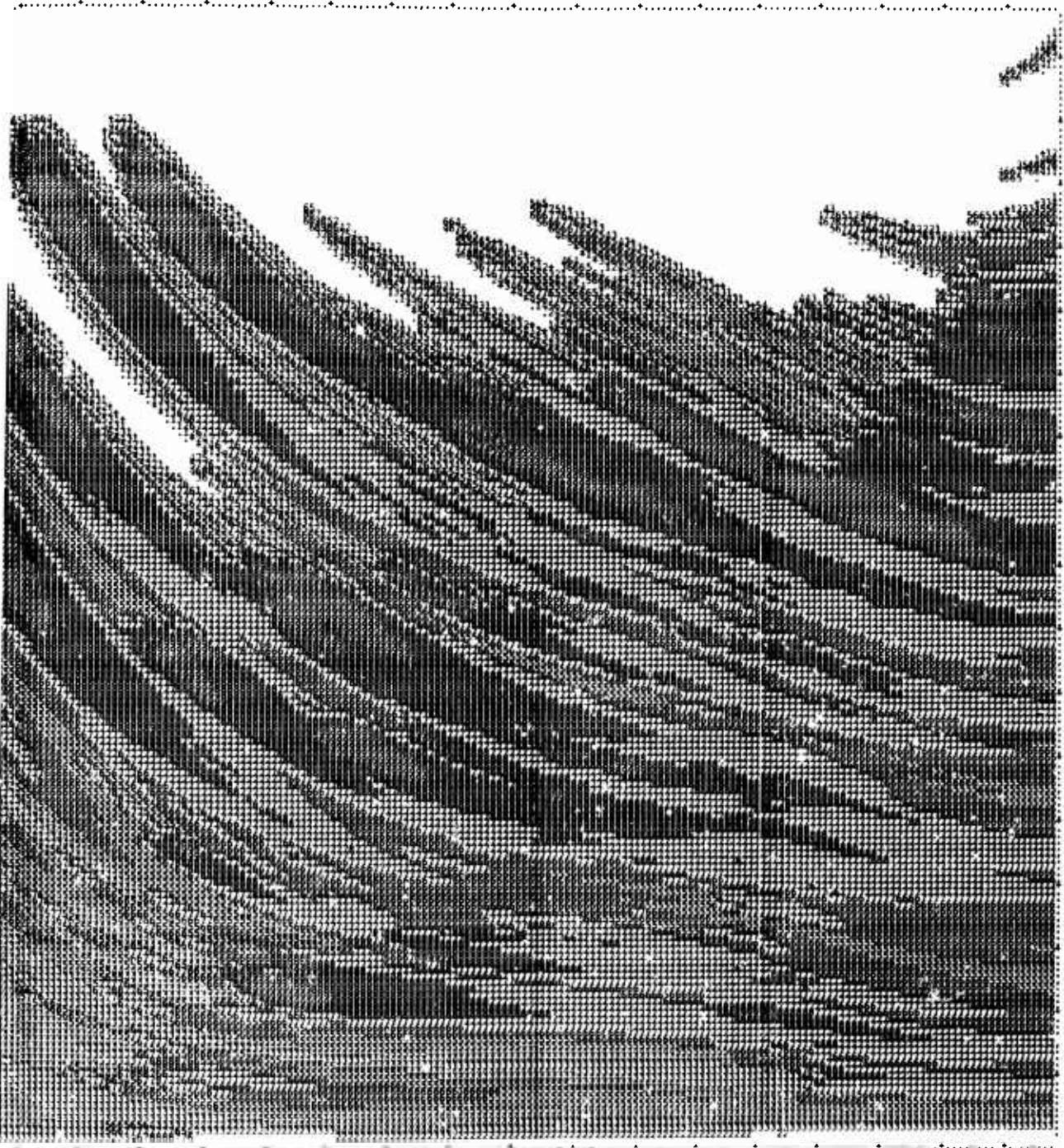
B-11





DECEMBER

B-12



Appendix C
COUNTERFORCE ATTACK, HIGH DOSE RANGE

FALLOUT MAPS FOR ATTACK B (COUNTERFORCE ATTACK)
IN THE HIGH DOSE RANGE

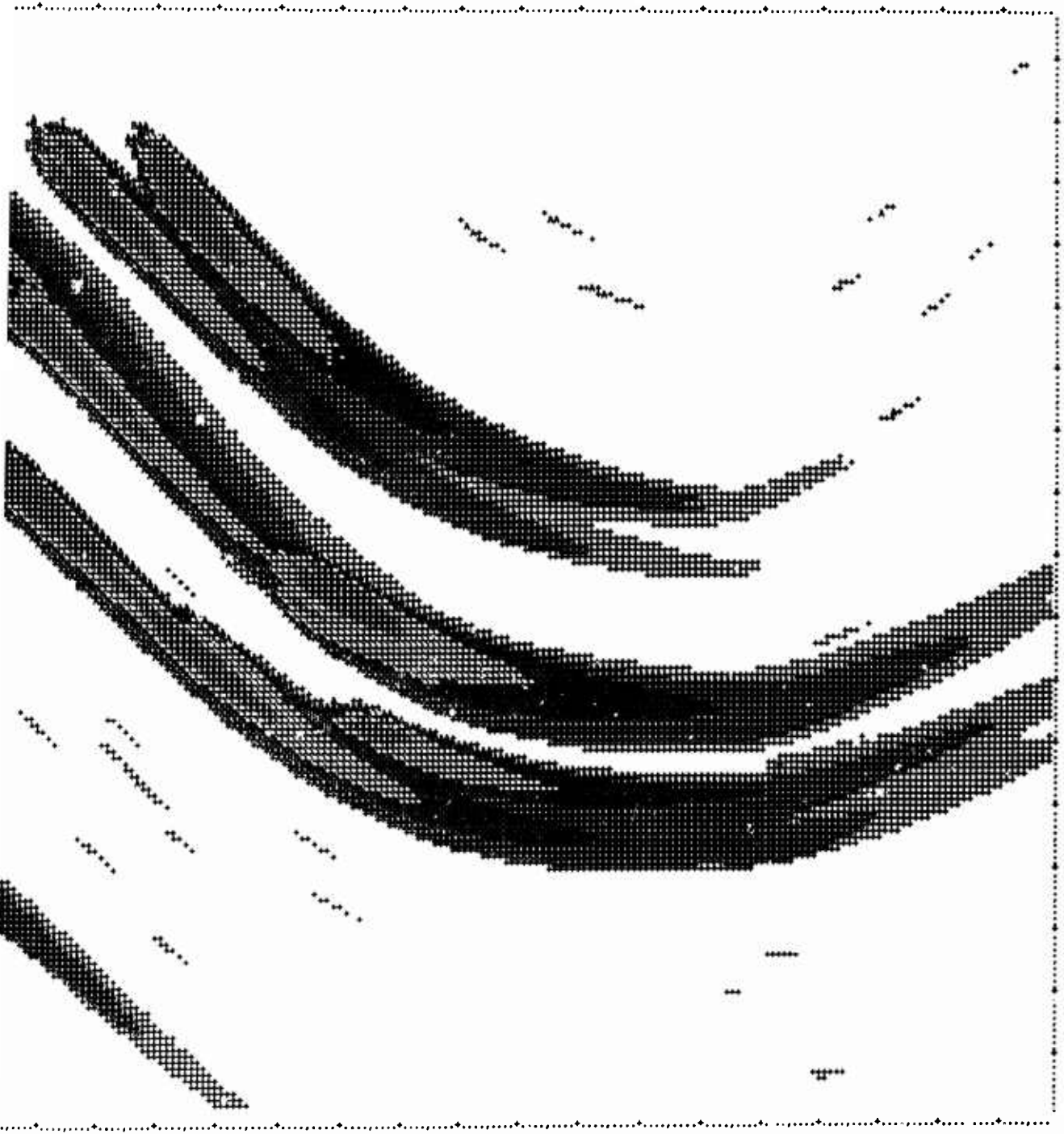
Figures C-1 through C-12 present maps of biological fall-out dose deposition for attack B (the counterforce attack) for each month of the year. The dose ranges chosen emphasize sheltering requirements. The symbol definitions are:

Symbol	Dose Range (Roentgens)
Blank	
+	Dose < 500
A	$500 \leq \text{Dose} < 1,000$
B	$1,000 \leq \text{Dose} < 2,000$
C	$2,500 \leq \text{Dose} < 5,000$
D	$5,000 \leq \text{Dose} < 10,000$
E	$10,000 \leq \text{Dose} < 30,000$



JANUARY

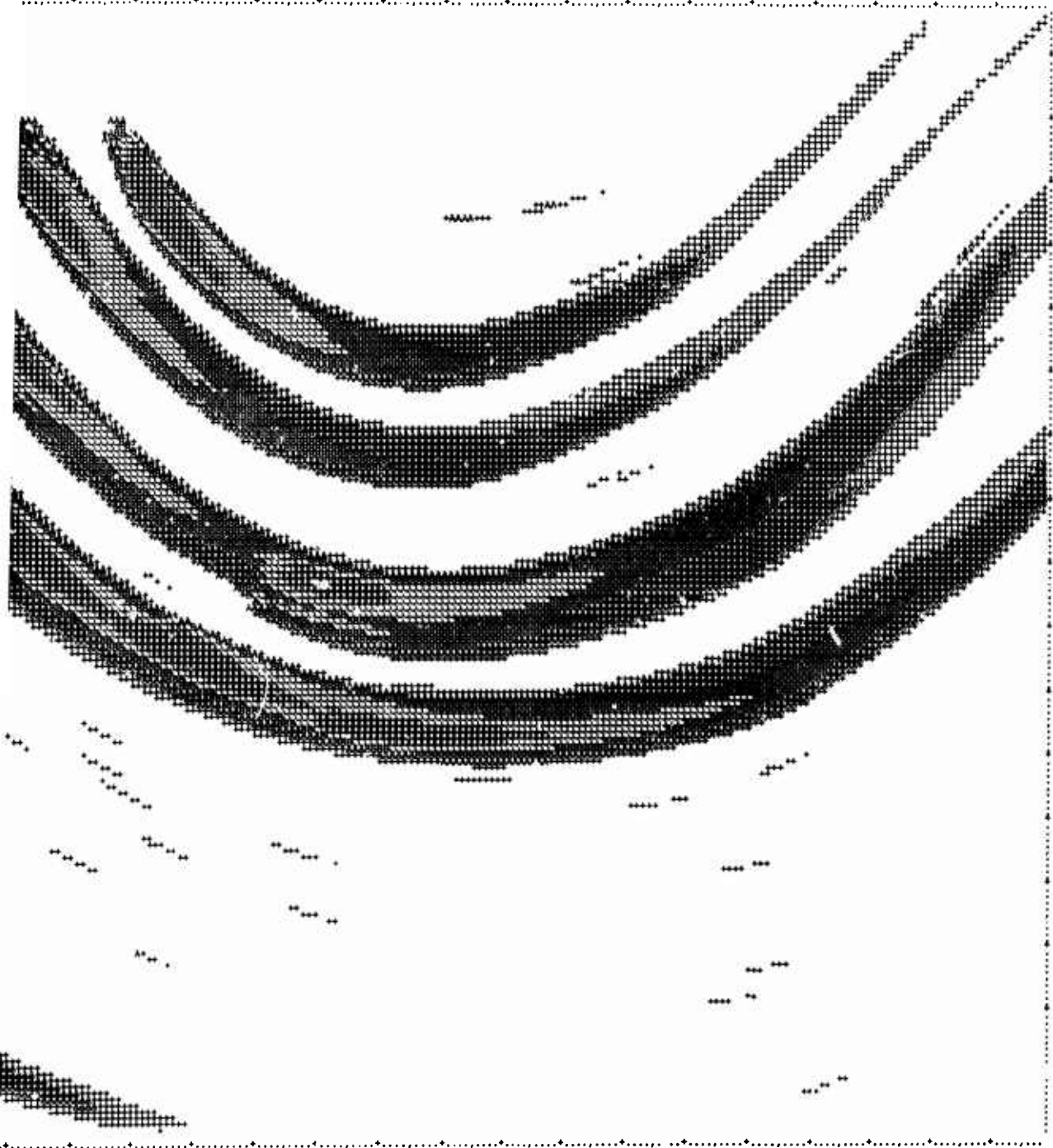
C-1



FEBRUARY

C-2

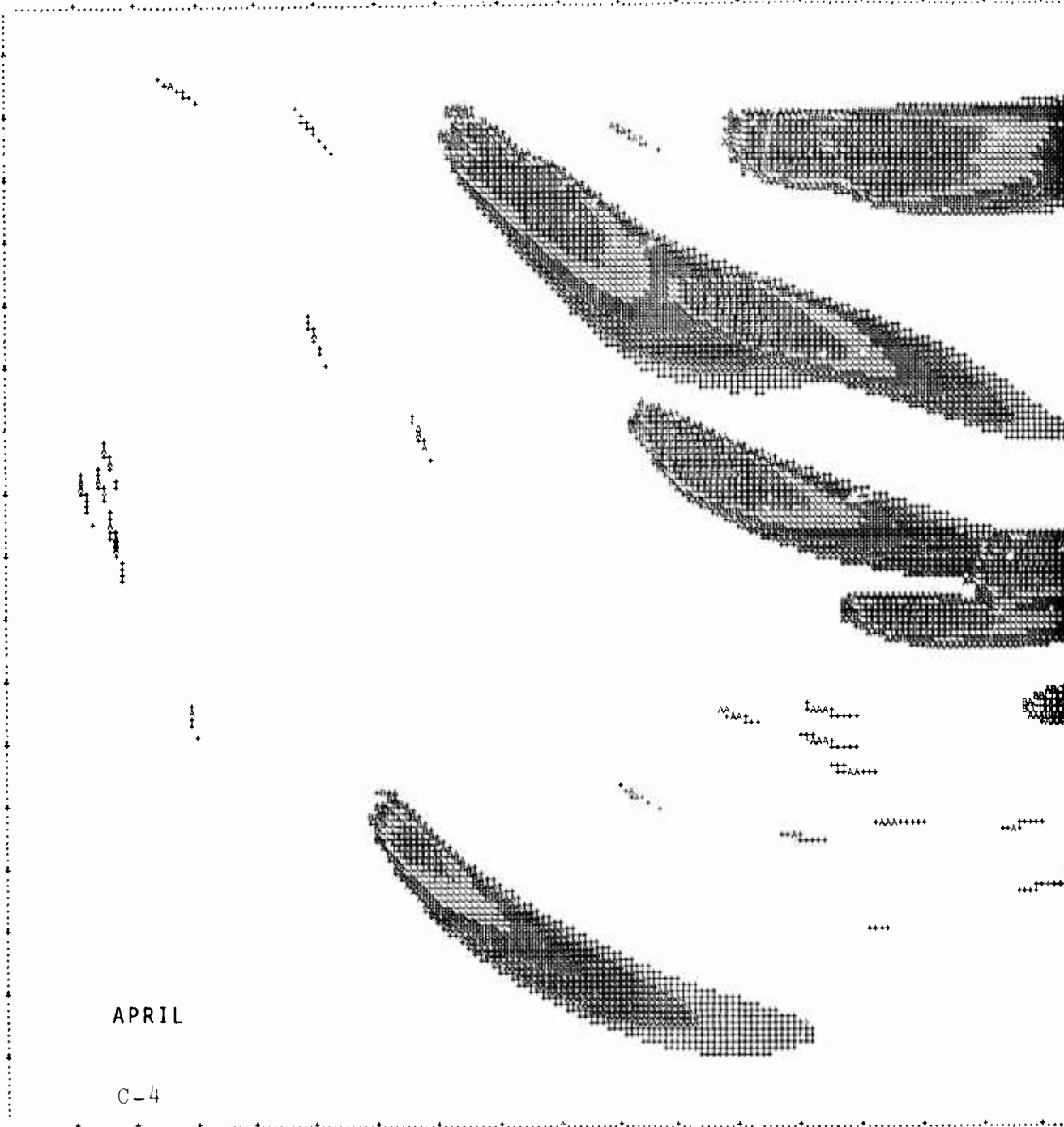




MARCH

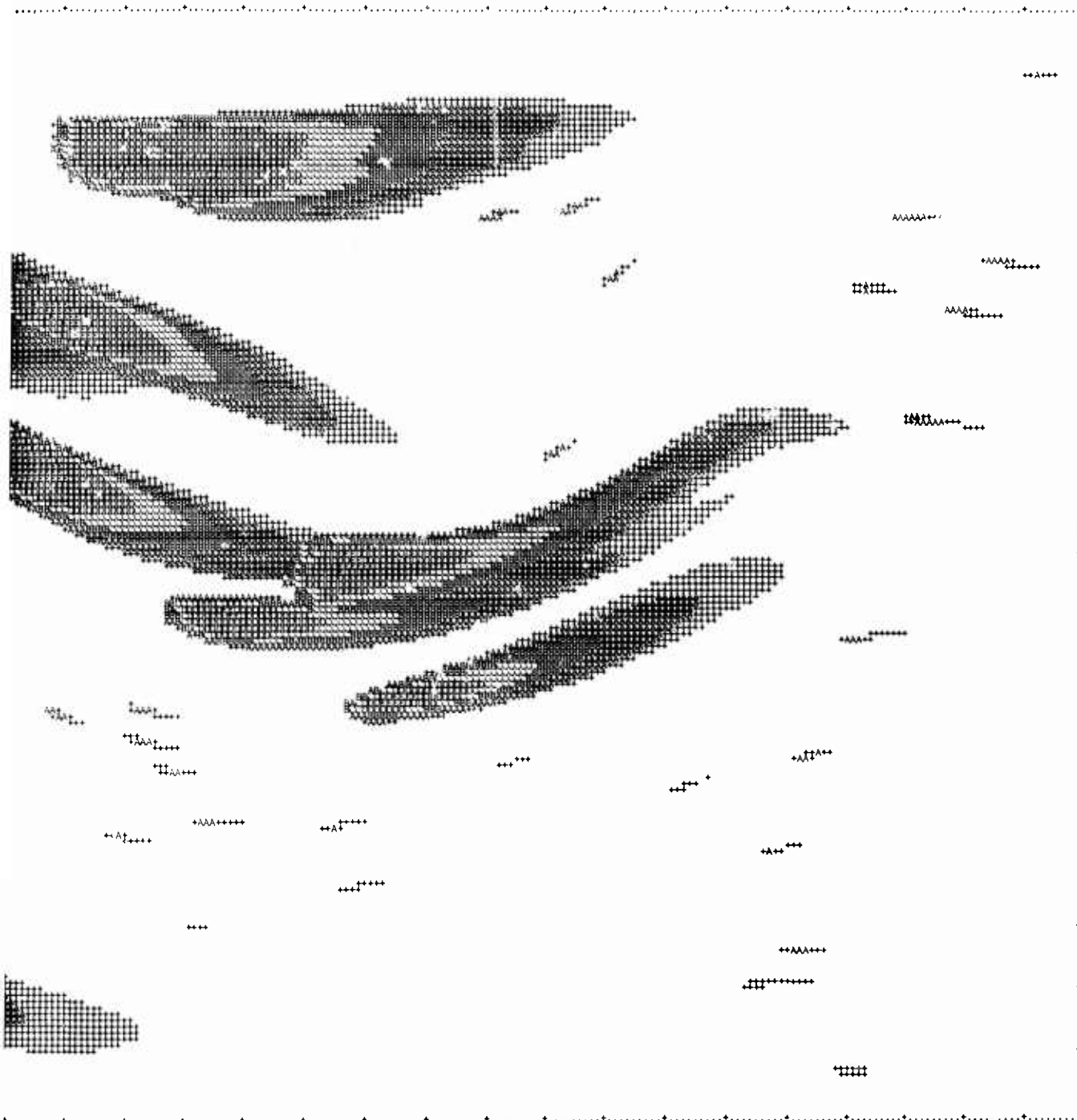
C-3





APRIL

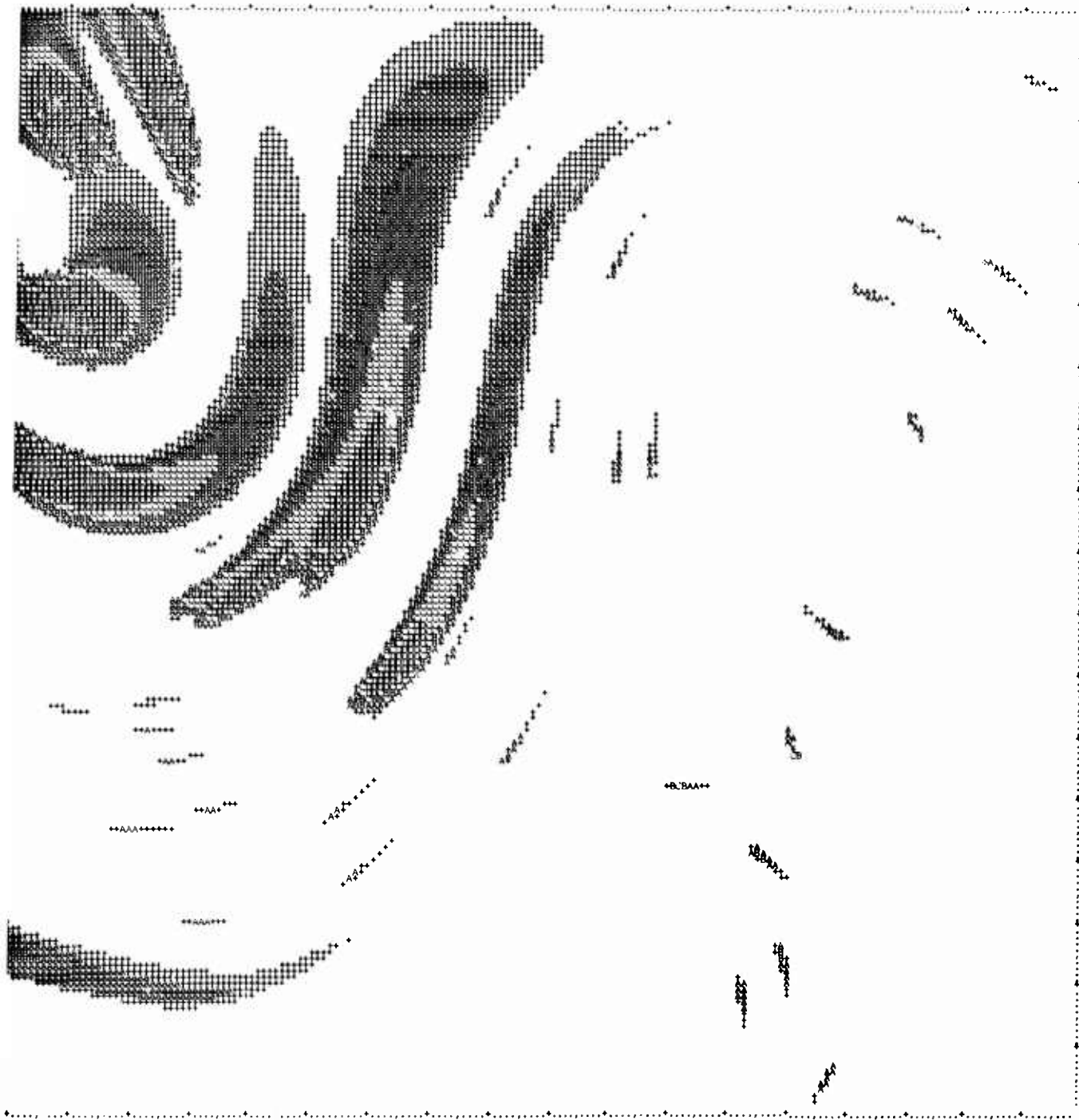
C-4

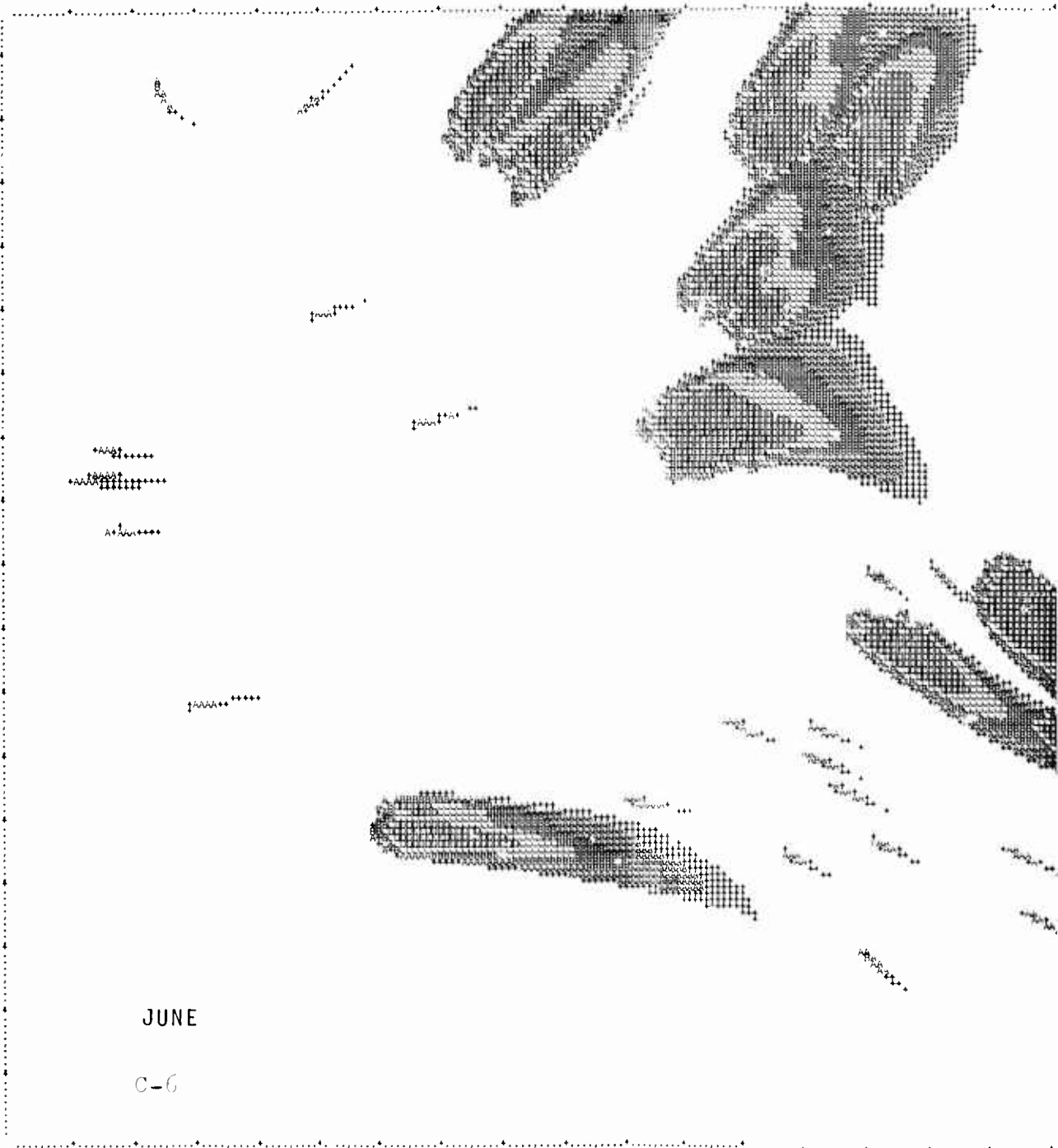




MAY

C-5





JUNE

C-6



AAAAA++

AAAAA++

AAAAA++

AAAAA++

AAAAA++
AAAAA++
AAAAA++

AAAAA++



AB

AAAAA++

AAAAA++

AAAAA++

AB

AB

AB

AB

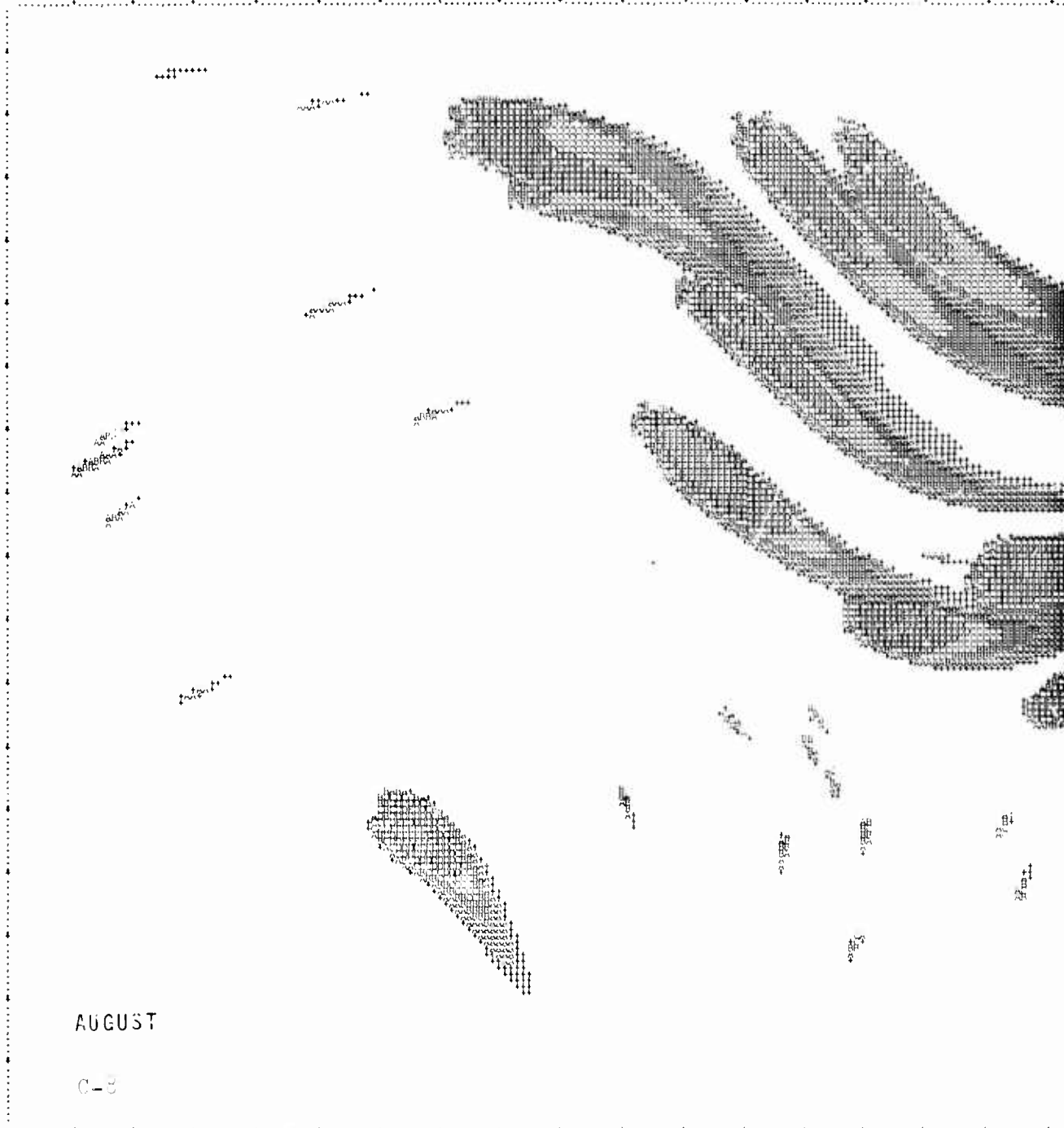
AAAAA++

AAAAA++

JULY

C-7





AUGUST

C-8



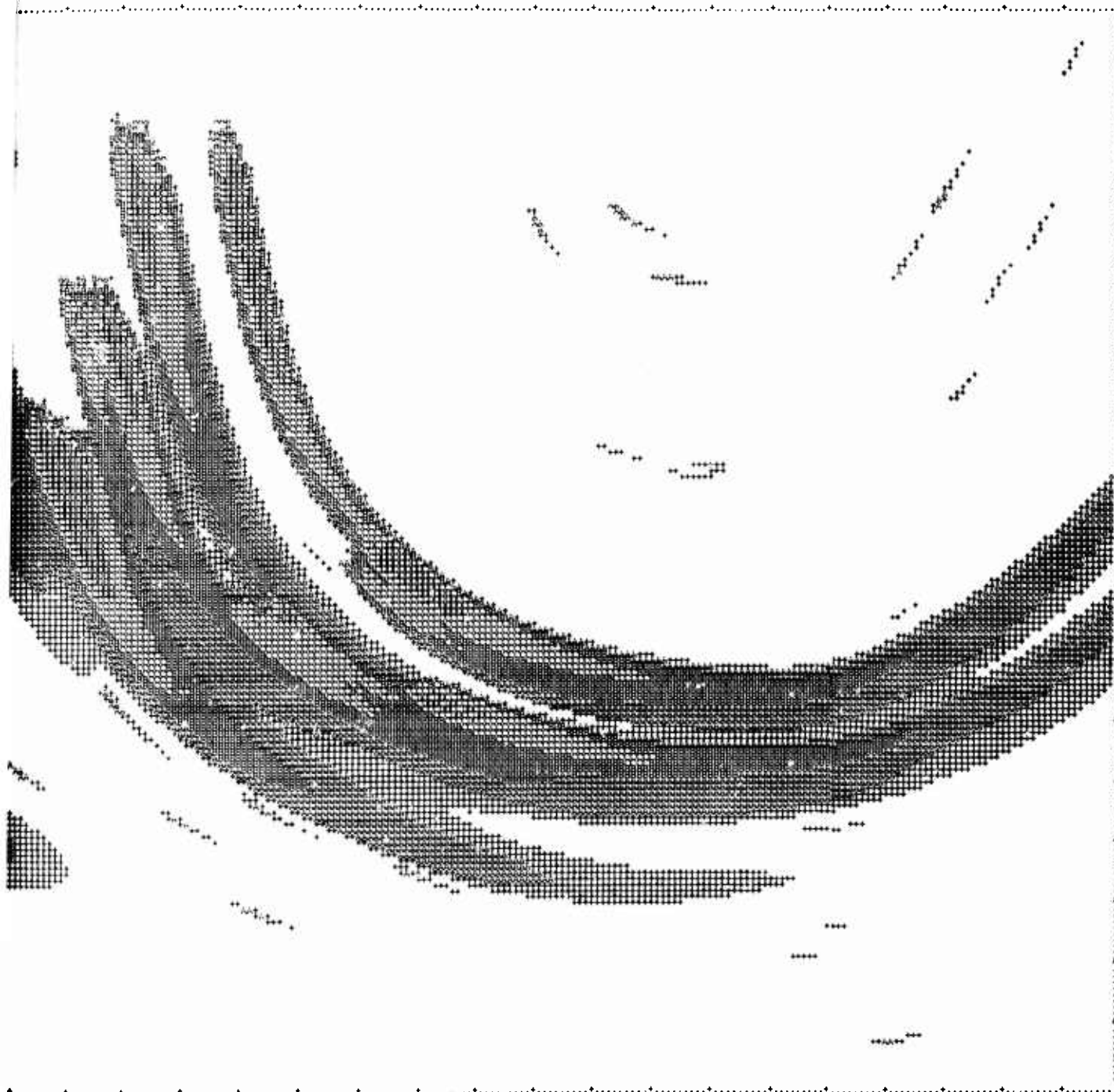






OCTOBER

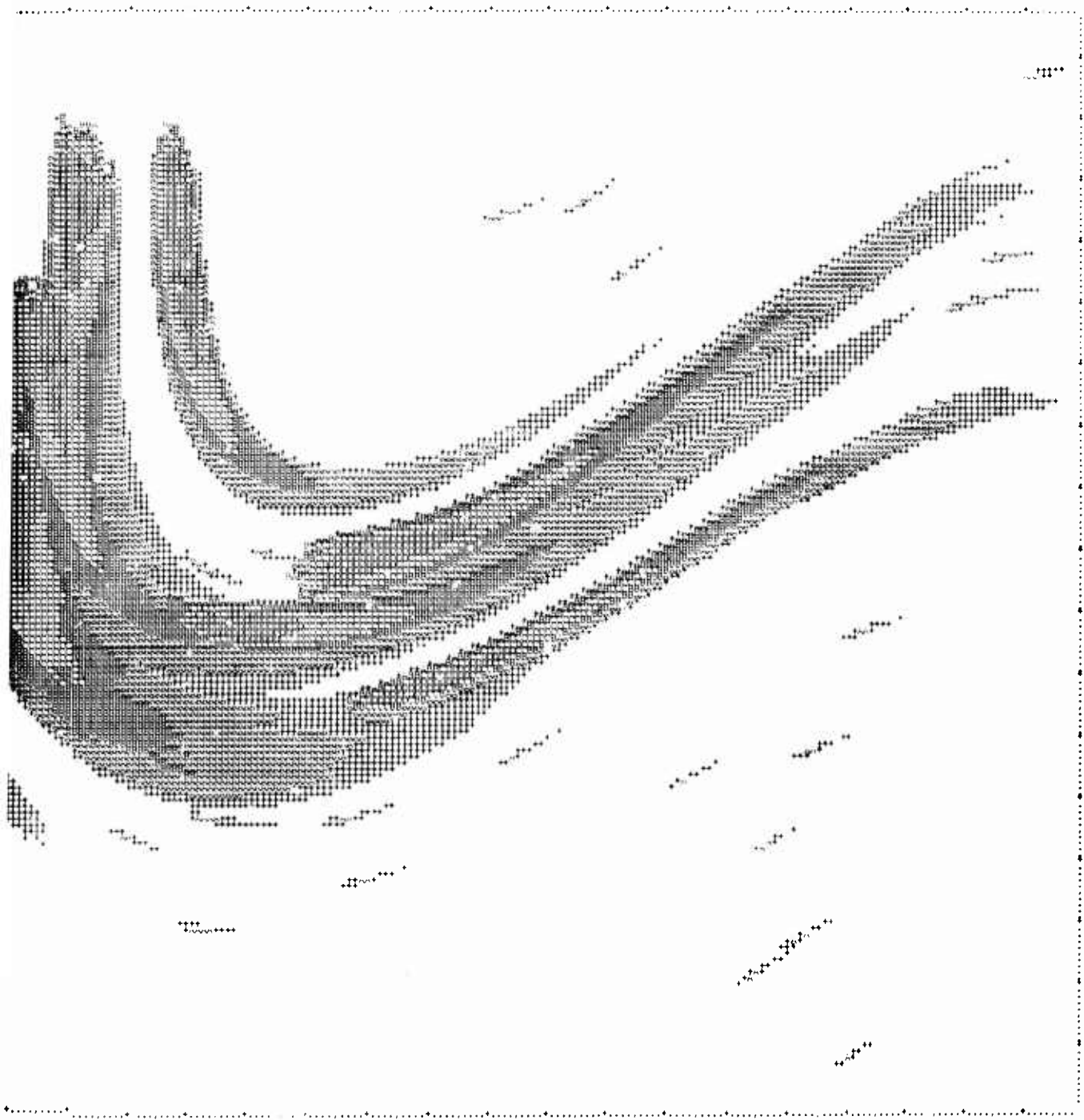
C-10

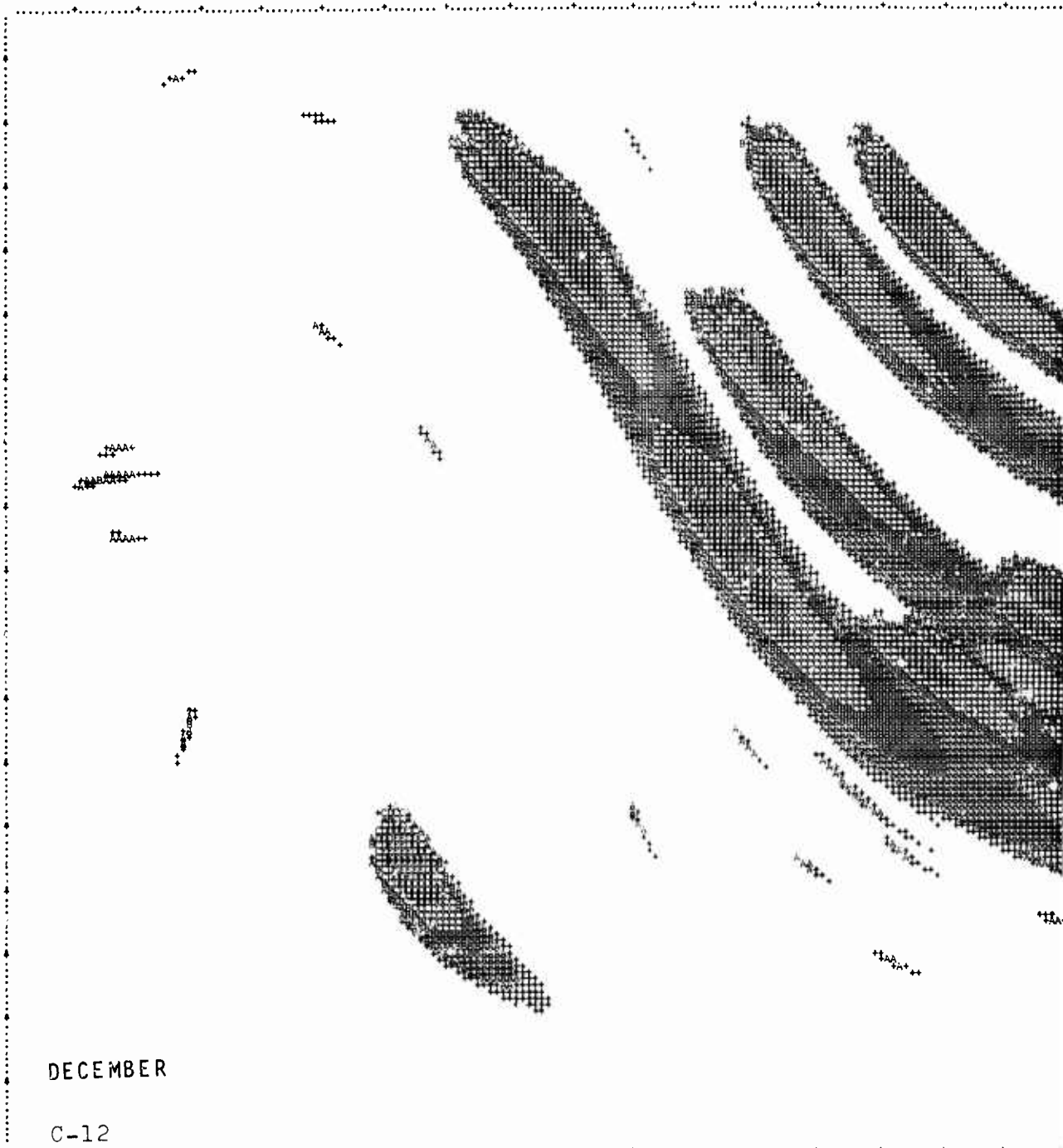




NOVEMBER

0-11





DECEMBER

C-12



Appendix D

COUNTERFORCE ATTACK, LOW DOSE RANGE

FALLOUT MAPS FOR ATTACK B (COUNTERFORCE ATTACK)
IN THE LOW DOSE RANGE

Figures D-1 through D-12 present maps of biological fall-out dose deposition for attack B (the counterforce attack) for each month of the year. The dose ranges chosen allows estimating dose levels within a factor of about three. The symbol definitions are:

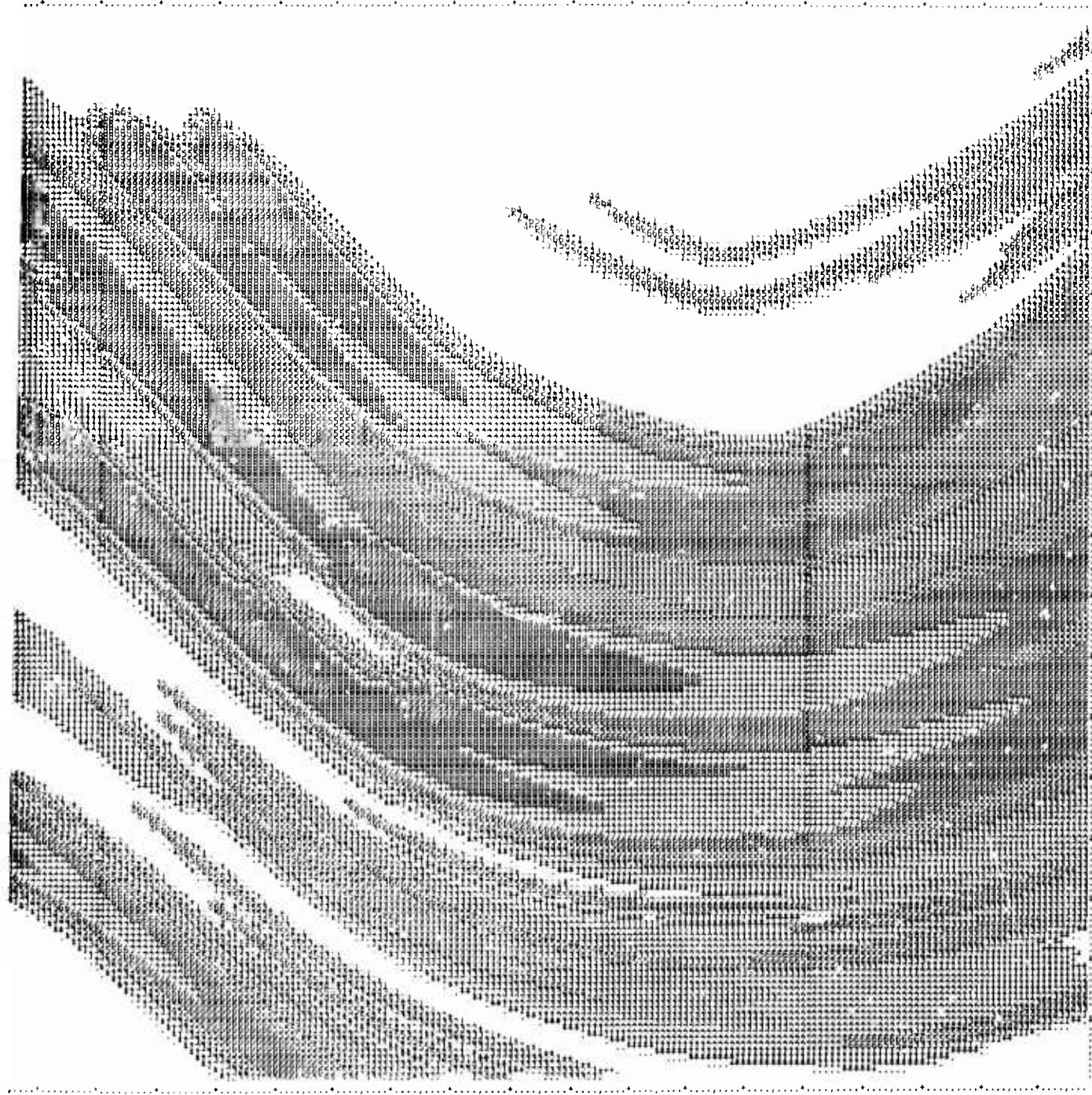
Symbol ¹	Dose Range (Roentgens)
Blank	Dose < 0.1
o	$0.1 \leq \text{Dose} < 0.3$
+	$0.3 \leq \text{Dose} < 1$
1	$1 \leq \text{Dose} < 3$
2	$3 \leq \text{Dose} < 10$
3	$10 \leq \text{Dose} < 30$
4	$30 \leq \text{Dose} < 100$
5	$100 \leq \text{Dose} < 300$
6	$300 \leq \text{Dose} < 1,000$
7	$1,000 \leq \text{Dose} < 3,000$
8	$3,000 \leq \text{Dose} < 10,000$
9	$10,000 \leq \text{Dose} < 30,000$
0	$30,000 \leq \text{Dose}$

PRECEDING PAGE BLANK-NOT FILMED



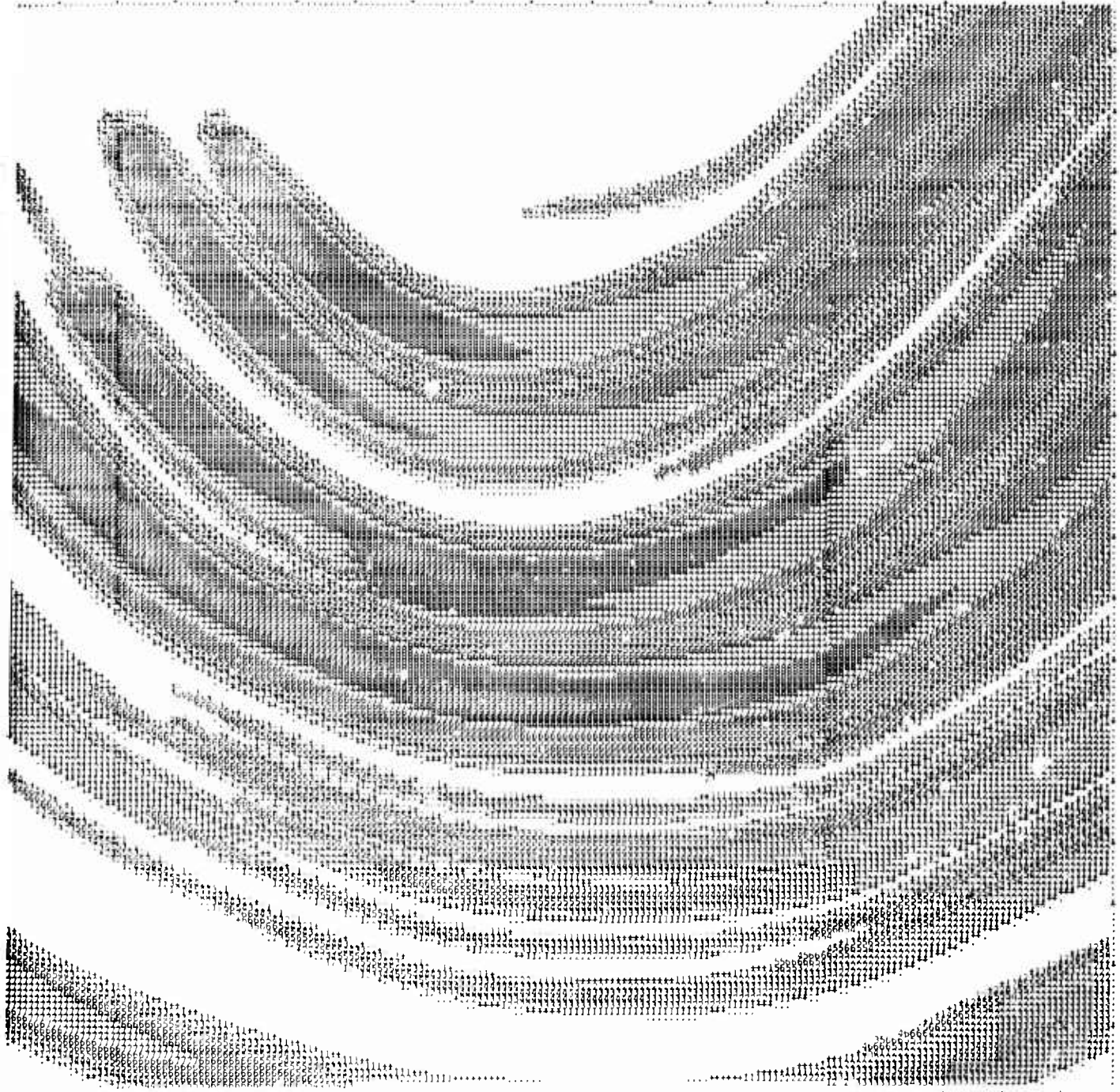
JANUARY

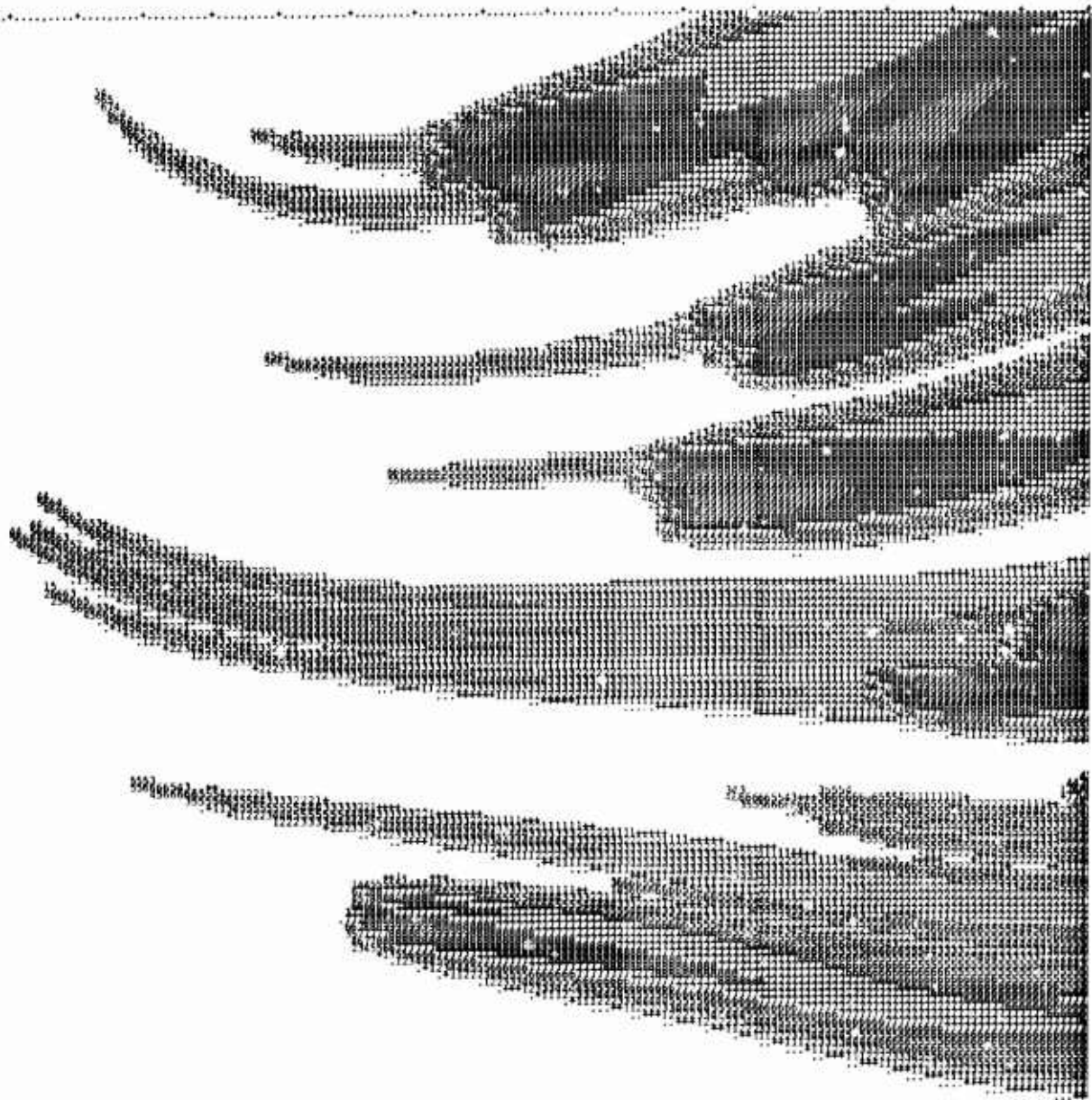
D-1



FEBRUARY

D-2

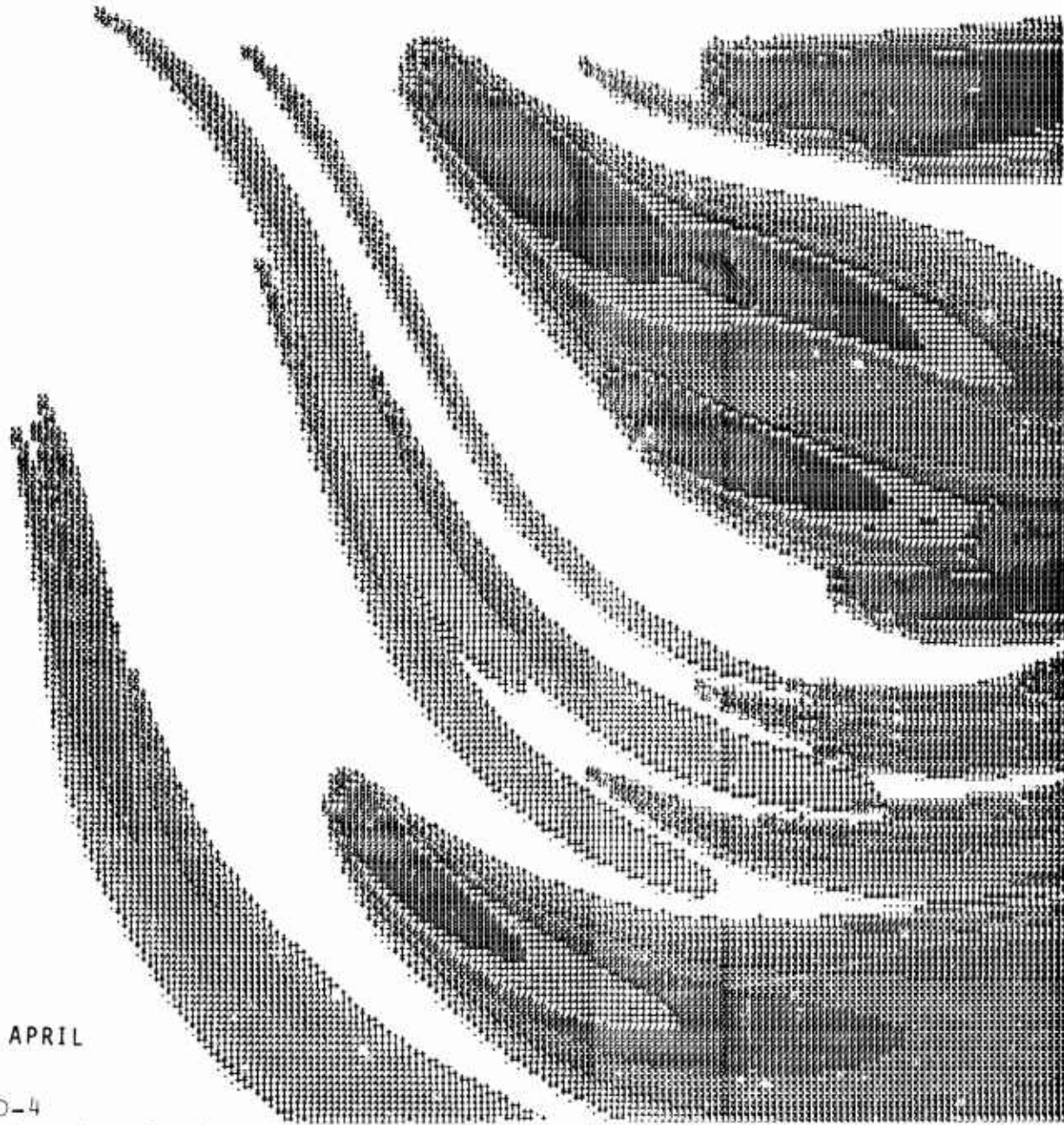




MARCH

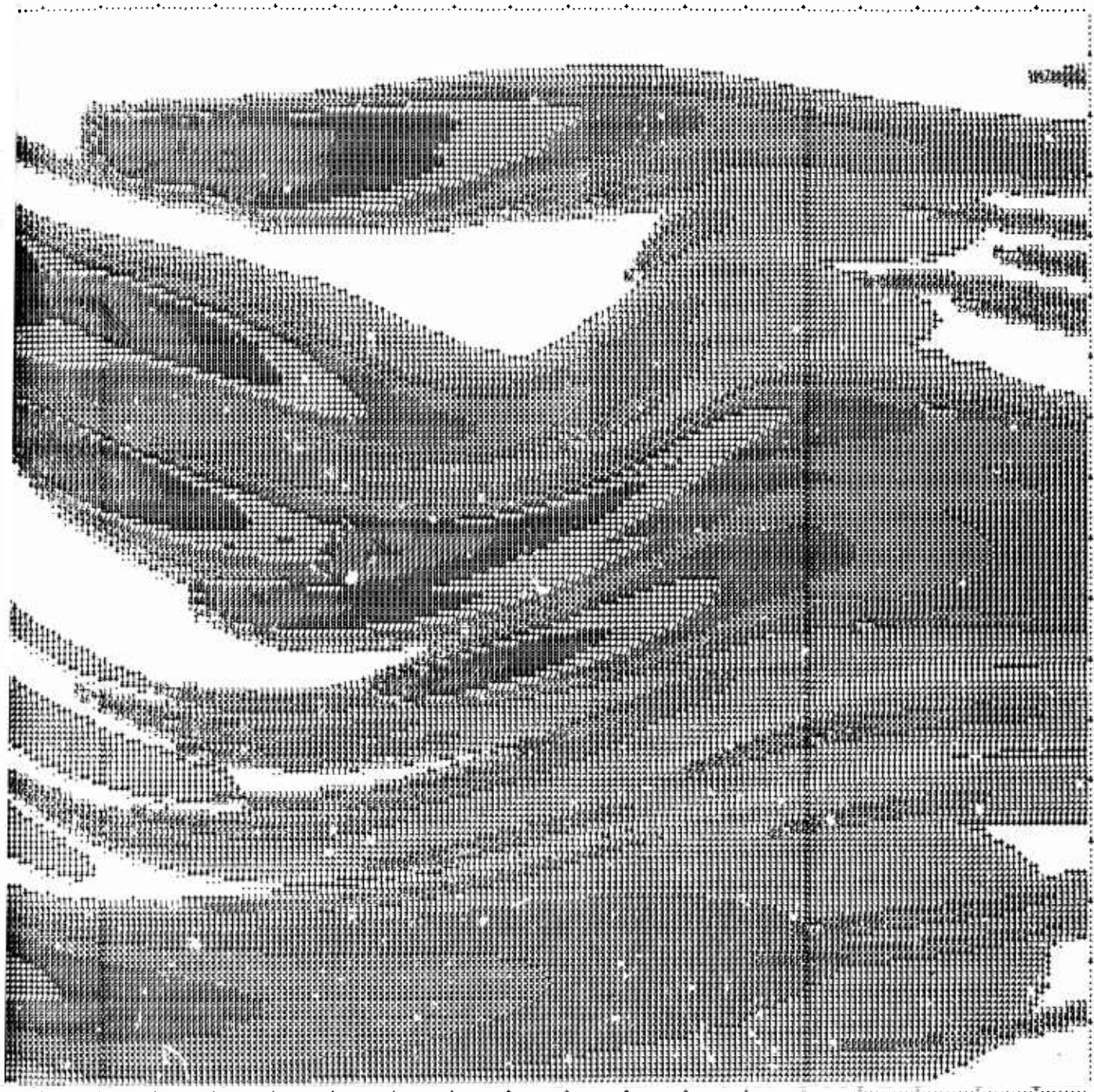
D-3





APRIL

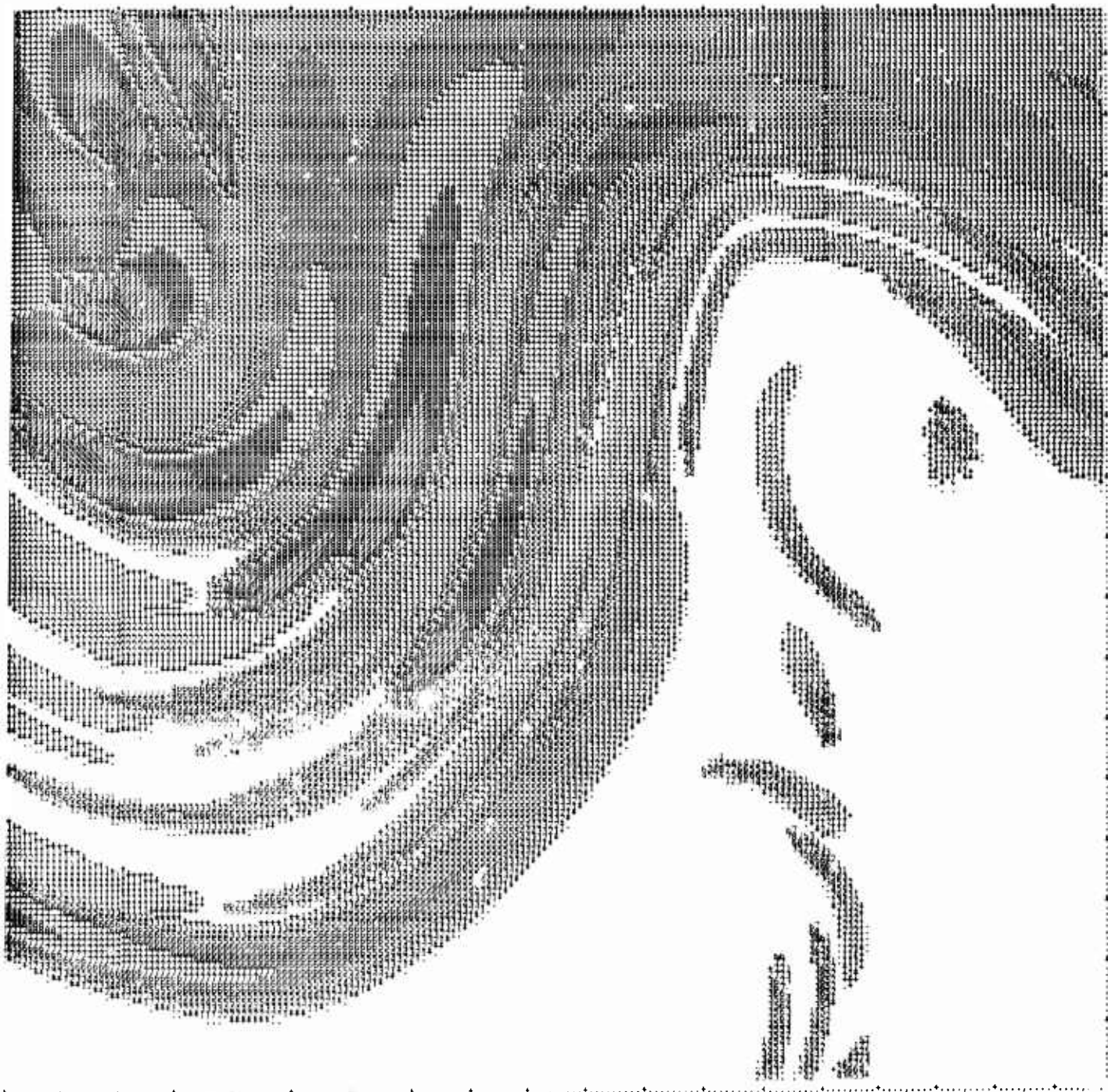
D-4





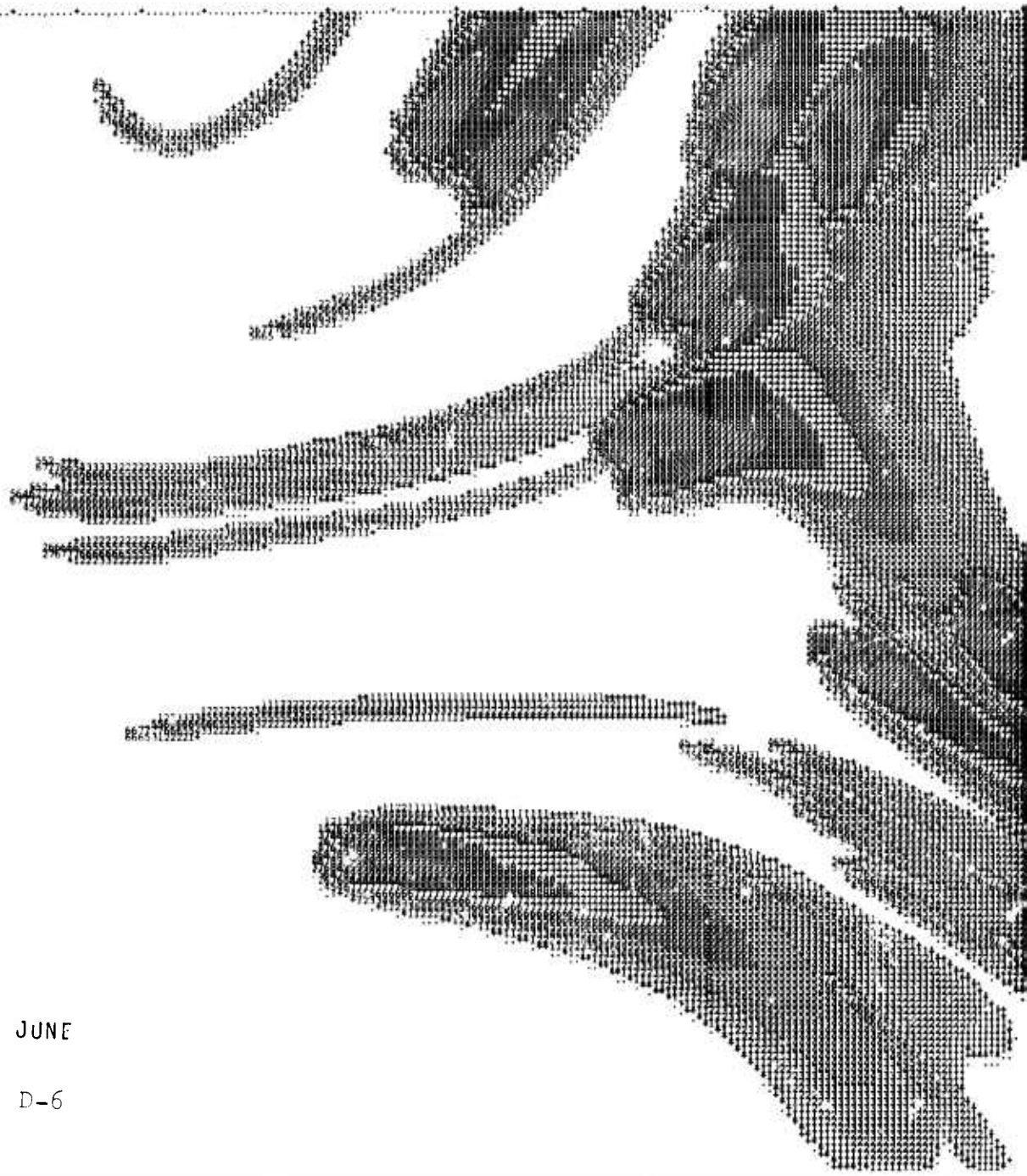
MAY

D-5



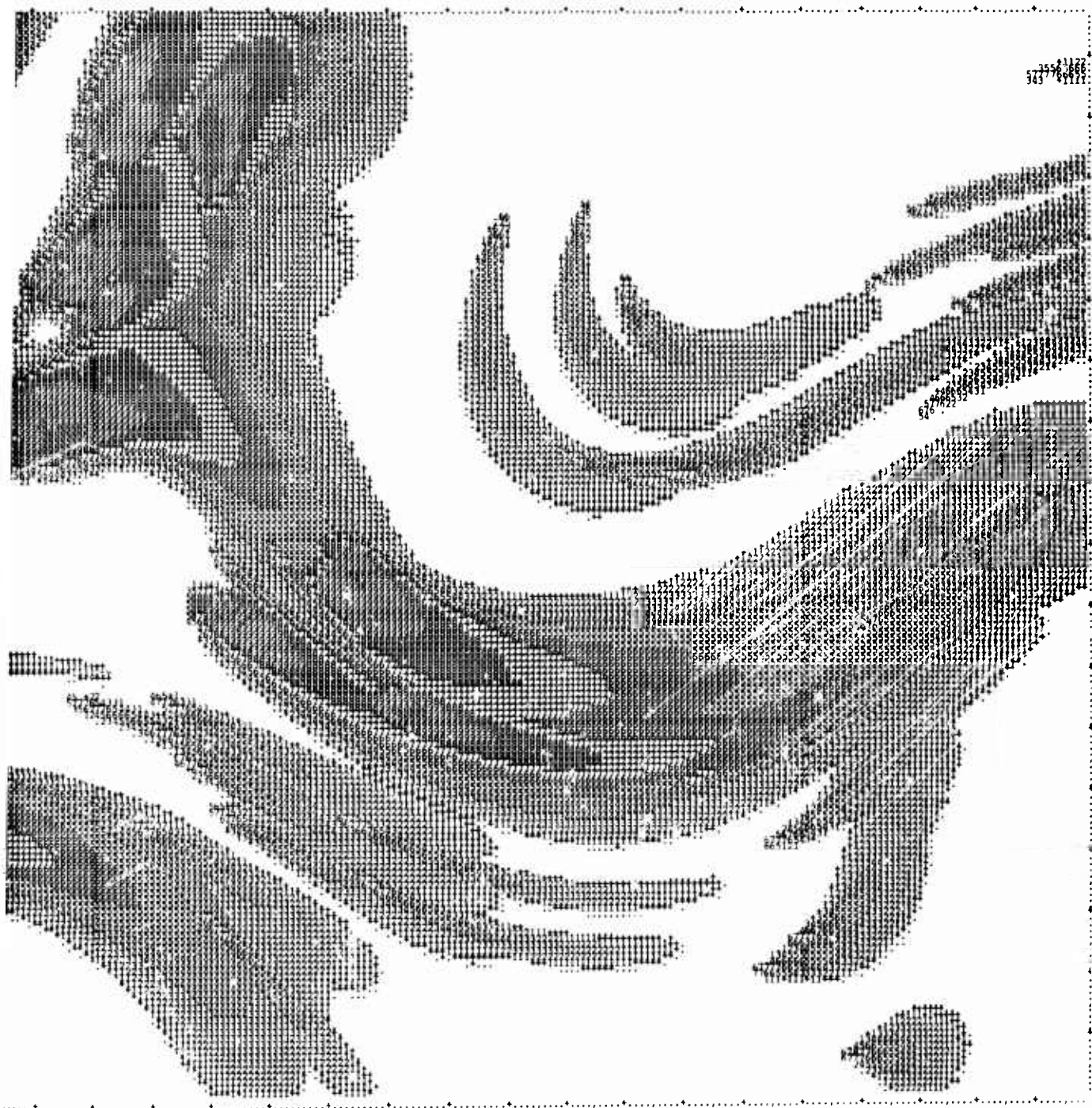
D-11/12

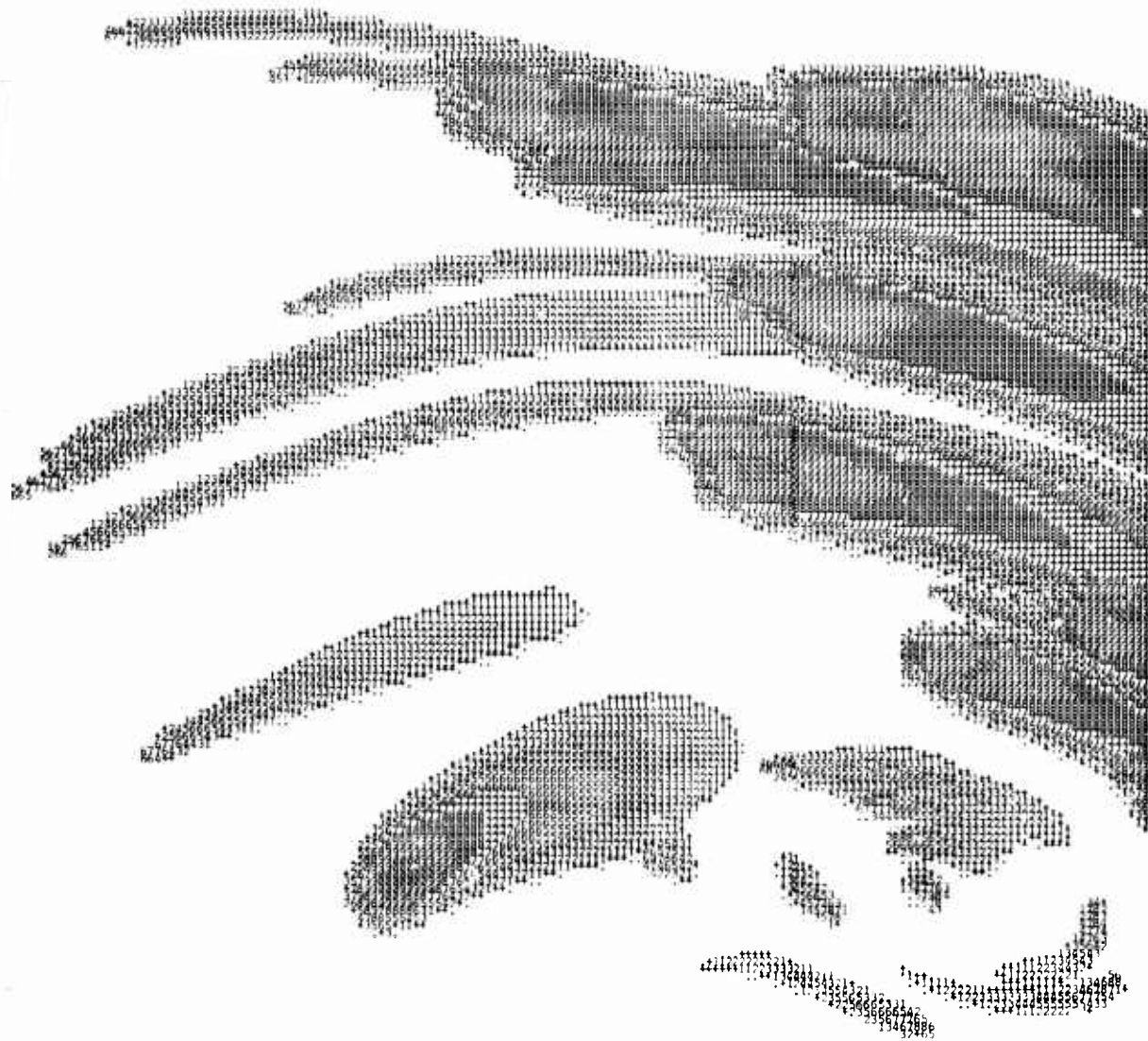
PRECEDING PAGE BLANK - NOT FILMED



JUNE

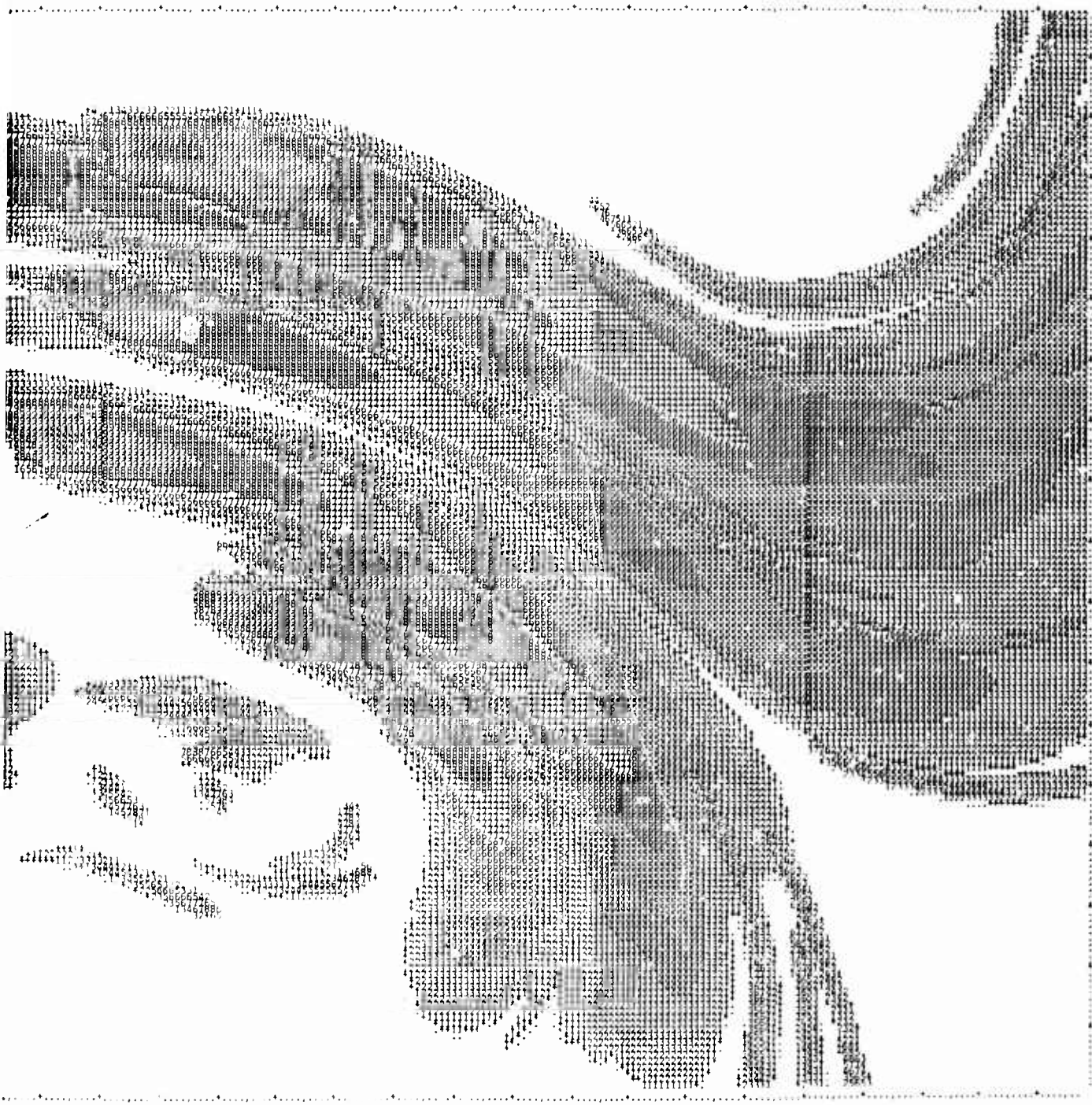
D-6

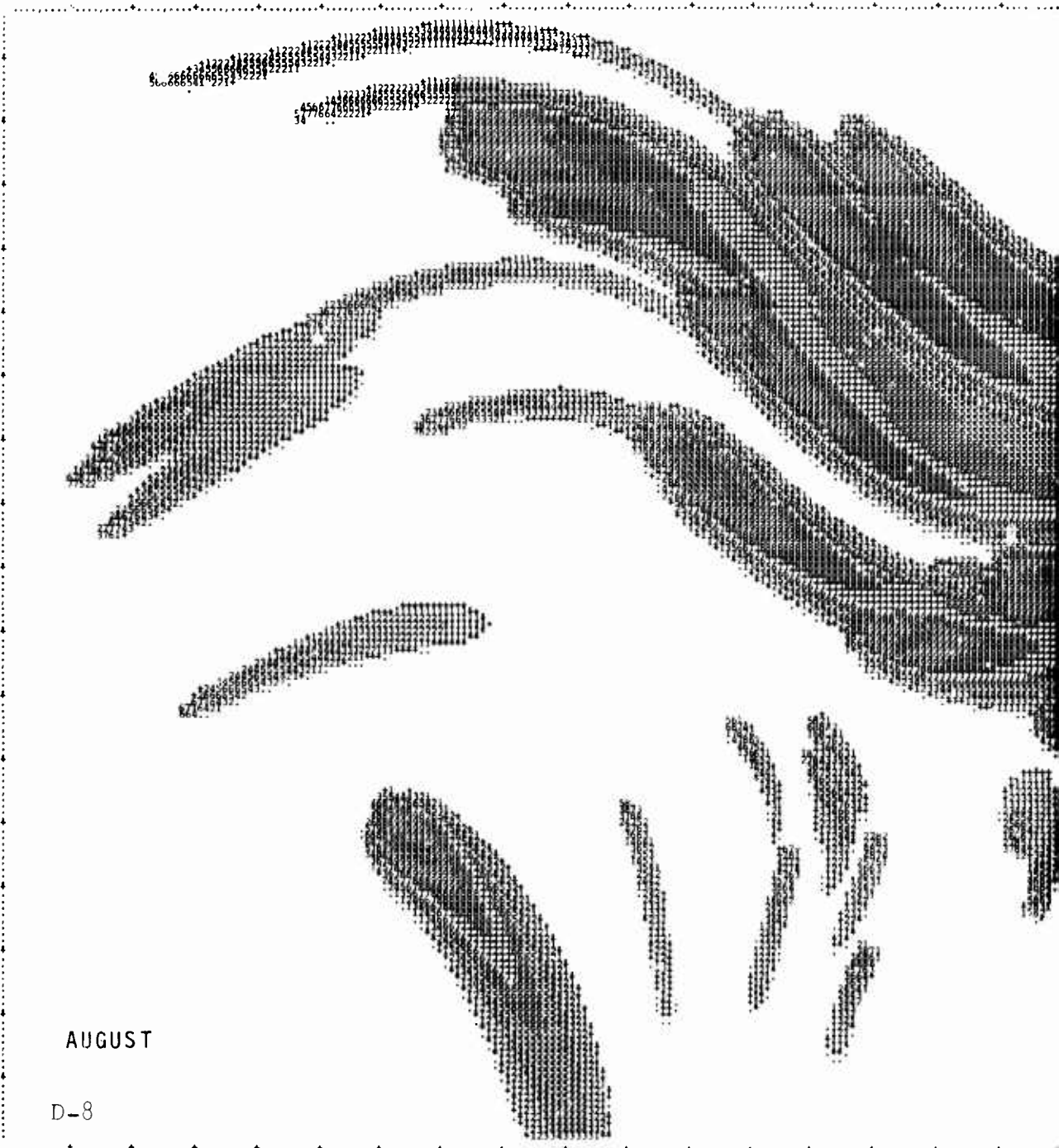




JULY

D-7





AUGUST

D-8

304736688



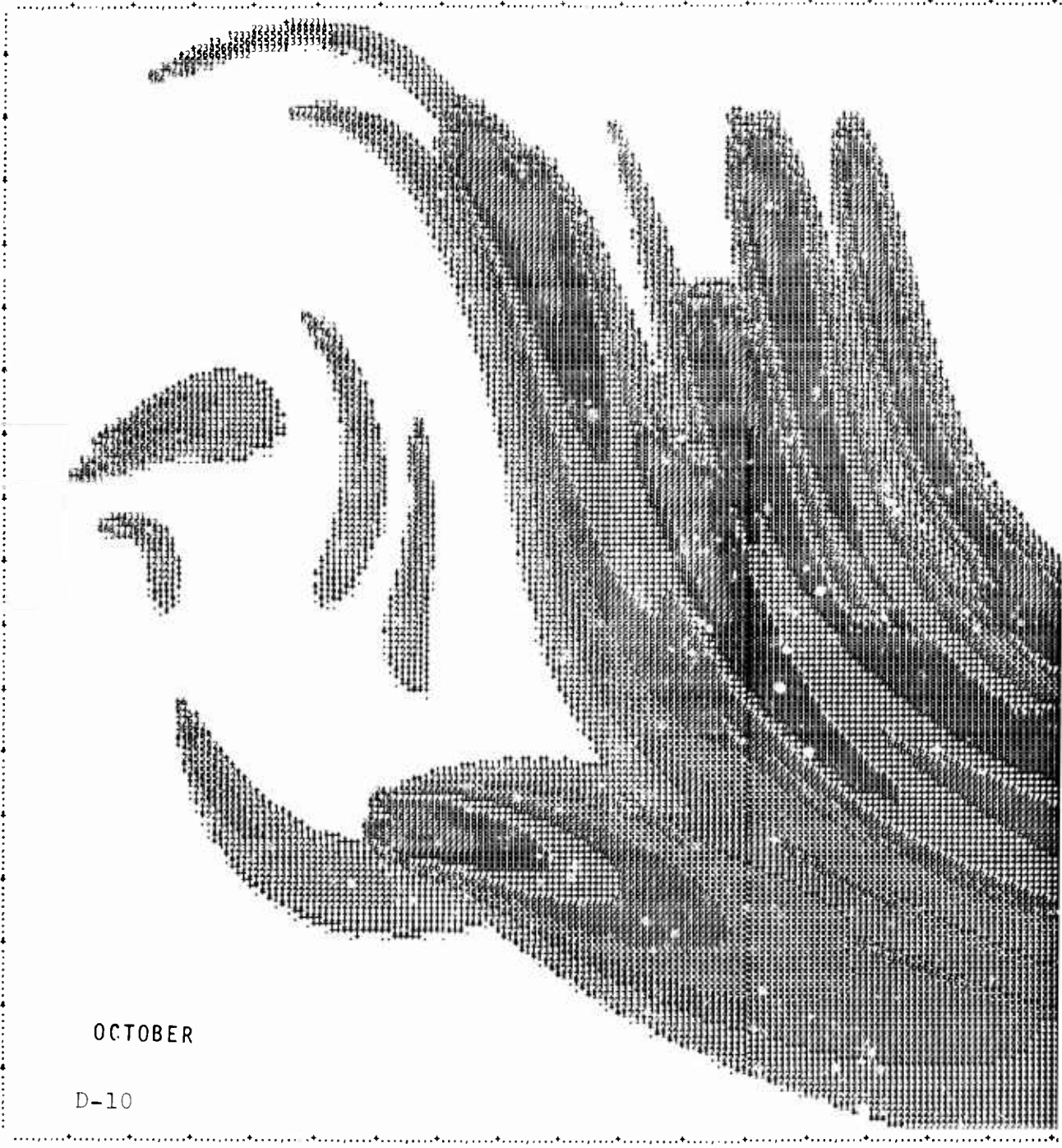


SEPTEMBER

D-9

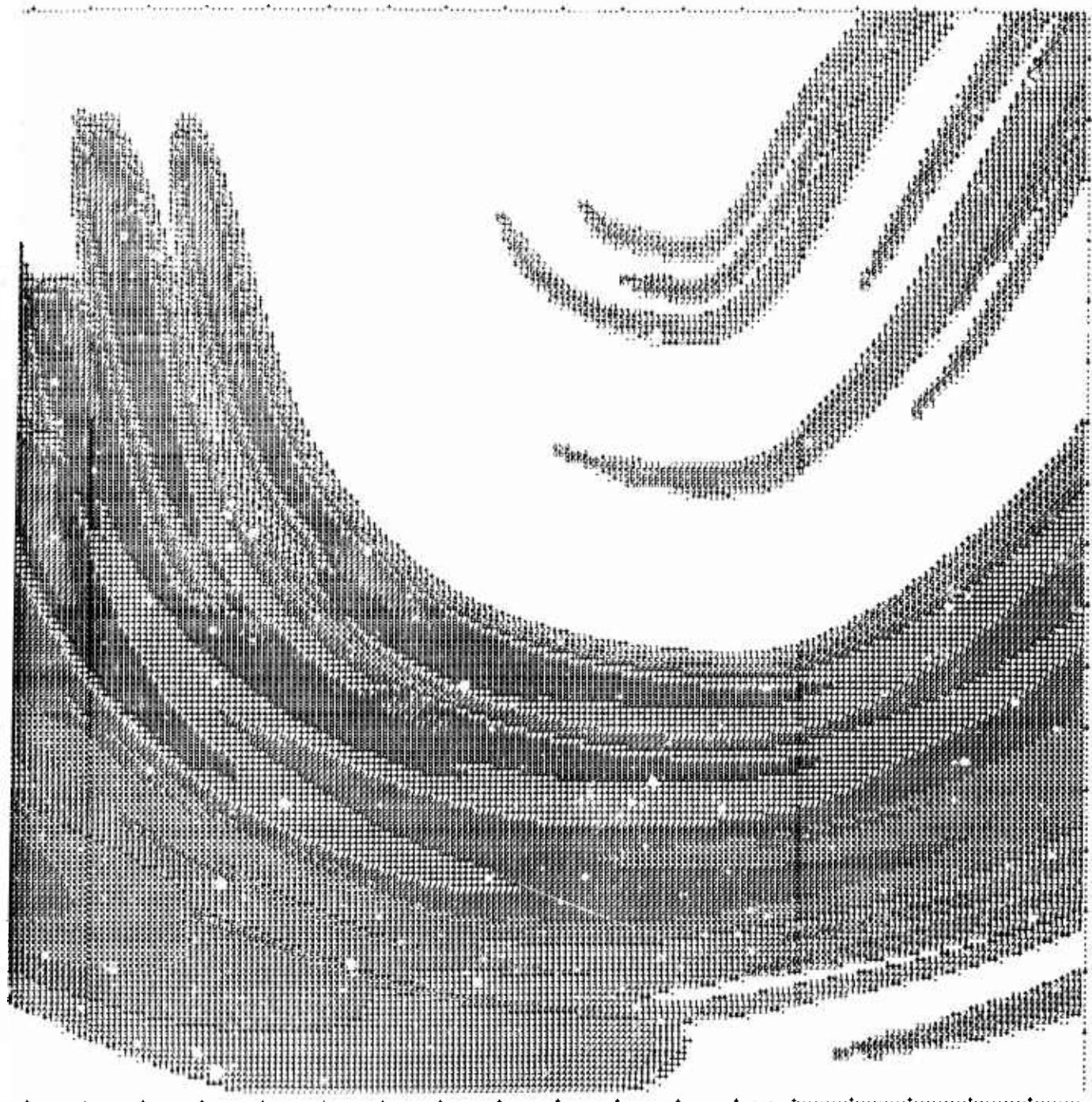


47656458385
144499



OCTOBER

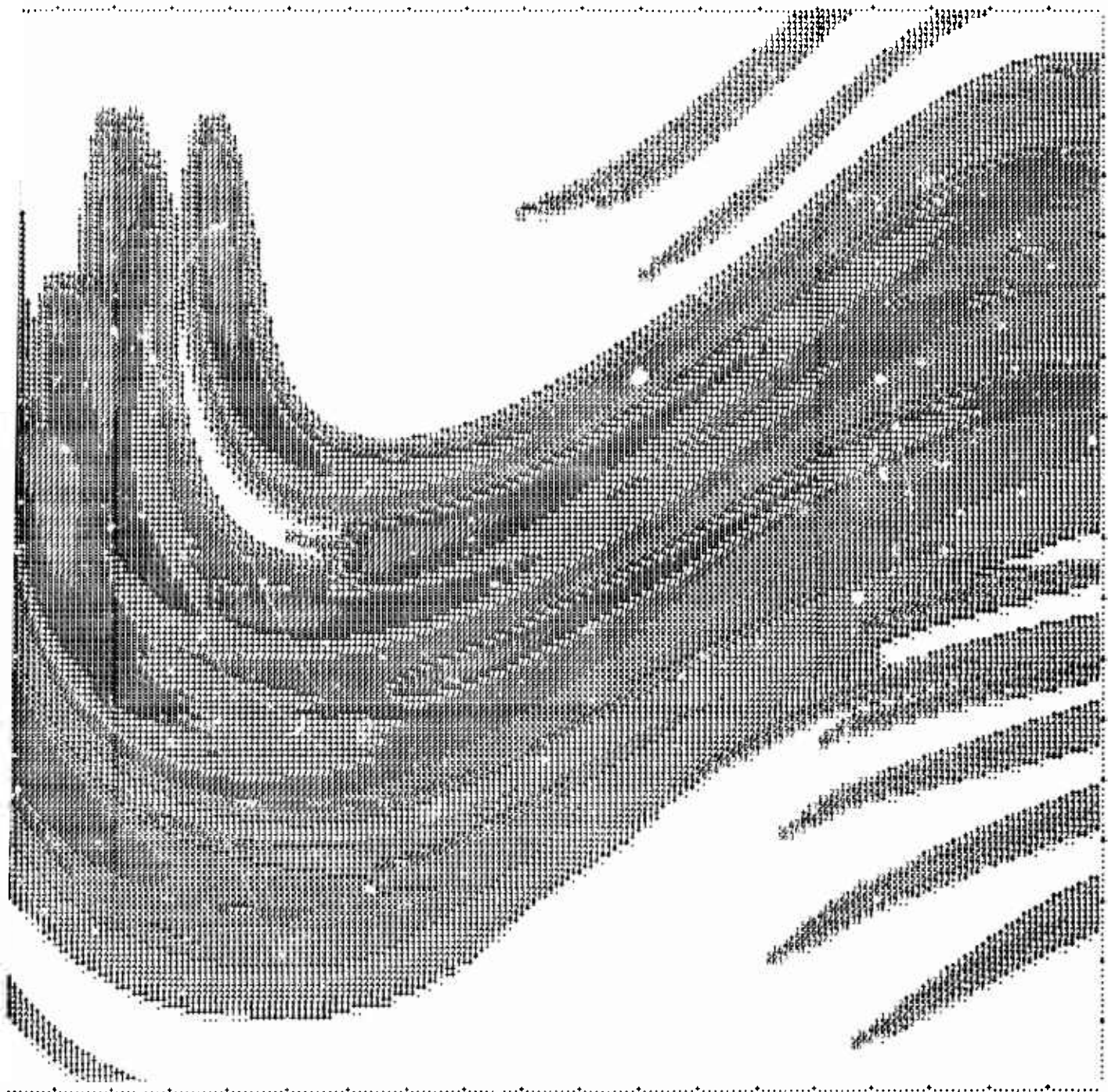
D-10





NOVEMBER

D-11

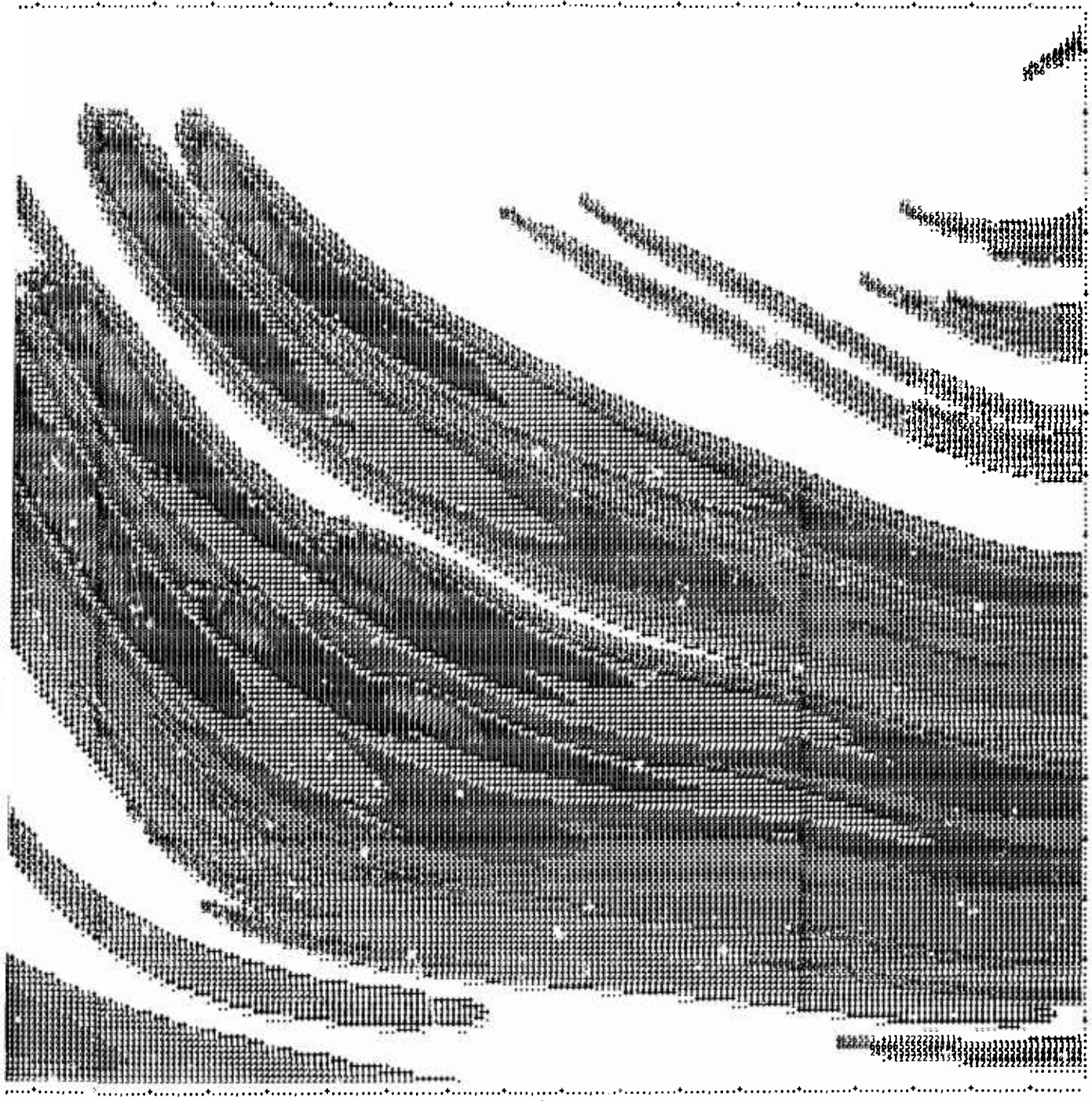


D-23/24



DECEMBER

D-12



DISTRIBUTION LIST

DISTRIBUTION LIST:

NUMBER OF COPIES

<p>FEMA Federal Emergency Management Agency Plans and Preparedness Studies, Research and Development ATTN: Program Operations Washington, D.C. 20472</p>	<p>60</p>
<p>Mr. J. Thomas Hughes Federal Emergency Management Agency U.S. Fire Administration Washington, D.C. 20472</p>	<p>1</p>
<p>U.S. Government, Executive Office of the President:</p>	
<p>Mr. Philip M. Smith Associate Director Natural Resources & Commercial Services Office of Science and Technology Policy Executive Office Building Washington, D.C. 20500</p>	<p>1</p>
<p>U.S. Department of Defense DOD Agencies:</p>	
<p>Defense Technical Information Center Cameron Station Alexandria, VA 22314</p>	<p>12</p>
<p>Command and Control Technical Center Department of Defense Room 2E312 Pentagon Washington, D.C. 20301</p>	<p>1</p>
<p>Mr. Carl Wiehle Defense Intelligence Agency ATTN: CKW DB-4C2 Washington, D.C. 20301</p>	<p>1</p>
<p>Mr. Tom Kennedy Defense Nuclear Agency Washington, D.C. 20305</p>	<p>1</p>
<p>U.S. Department of Defense, U.S. Army:</p>	
<p>Assistant Secretary of the Army (R&D) ATTN: Assistant for Research Washington, D.C. 20301</p>	<p>1</p>

U.S. Army Combined Arms Combat
Development Activity
Fort Leavenworth, KA 66027

2

Director, Army Materials and
Mechanics Research Center
ATTN: Technical Library
Watertown, Massachusetts 02172

1

U.S. Army Training and Doctrine
Command
Fort Monroe
Hampton, VA 23651

1

Chief of Engineers
Department of the Army
ATTN: ENGEME-RD
Washington, D.C. 20314

1

Director, U.S. Army Ballistic
Research Laboratory
ATTN: Document Library
Aberdeen Proving Grounds, MD 21005

1

Mr. William Taylor
Ballistic Research Laboratories
Aberdeen Proving Grounds, MD 21005

2

Chief Joint Civil Defense
Support Group
Office, Chief of Engineers
Department of the Army
ATTN: ENGMC-D
Washington, D.C. 20314

1

Director
U.S. Army Engineer Waterways
Experiment Station
ATTN: Document Library
P.O. Box 611
Vicksburgh, Mississippi 39180

1

Mr. W.L. Huff
U.S. Army Engineer Waterways
Experiment Station
Post Office Box 631
Vicksburgh, Mississippi 39180

1

U.S. Department of Defense, U.S. Navy:

Chief of Naval Research
Washington, D.C. 20306

Dis-2

1

U.S. Naval Civil Engineering Laboratory
ATTN: Document Library
Port Hueneme, CA 93041

1

Naval Ship Research and Development Center
ATTN: Mr. Tom Amrhein
Code 857
Washington, S.C. 20034

1

U.S. Department of Defense, U.S. Air Force:

Civil Engineering Center/AF/PRECET
Wright Patterson Air Force Base
Ohio 45433

1

Air Force Weapons, Lab.
ATTN: SUL Technical Library
Kirtland Air Force Base
Albuquerque, New Mexico 87117

1

AFWL/Civil Engineering Division
Kirtland Air Force Base
Albuquerque, New Mexico 87117

1

U.S. Department of Agriculture, U.S. Forest Service:

Dr. Craig Chandler, Director
Forest Fire & Atmospheric Science Research
U.S. Forest Service
Department of Agriculture
Washington, D.C. 20250

1

Mr. A. P. Brackebusch
Forest Fire Research
Northern Forest Fire Laboratory
Missbula, Montana 59801

1

U.S. Forest Service
ATTN: Dr. A. Broido
P.O. Box 245
Berkeley, CA 94710

1

U.S. Department of Commerce, National Bureau of Standards:

Fire Research Library
National Bureau of Standards
Technology Building 225
Washington, D.C. 20234

1

Mr. Irwin A. Benjamin
Building Research Division
National Bureau of Standards
Washington, D.C. 20234

1

Mr. William Parker
National Bureau of Standards
Room B66, Technology Building
Washington, D.C. 20234

1

Dr. John Rockett
National Bureau of Standards
Center for Fire Research
Building 225, Room A17
Washington, D.C. 20234

1

Dr. Lewis V. Spencer
National Bureau of Standards
Room C313-Building 245
Washington, D.C. 2023

1

Mr. Samuel Kramer, Chief
Office of Federal Building
Technology
Center for Building Technology
National Bureau of Standards
Washington, D.C. 20234

1

U.S. Department of Energy, Headquarters:

Department of Energy
Military Application Office
Washington, D.C. 20545

U.S. Department of Energy Laboratories:

Mr. Norman J. Alvares
Lawrence Livermore National Laboratory
University of California
P. O. Box 808, L-Stop 442
Livermore, CA 94550

1

Chief Robert C. Purington
Lawrence Livermore National Laboratory
University of California
P.O. Box 808, L-Stop 519
Livermore, CA 94550

1

Oak Ridge National Laboratory
ATTN: Librarian
P.O. Box X
Oak Ridge, Tennessee 37830

1

Dr. Conrad V. Chester
Oak Ridge National Laboratory
P.O. Box X
Oak Ridge, Tennessee 37830

1

Emergency Technology Division
Oak Ridge National Laboratory
P.O. Box X
ATTN: Librarian
Oak Ridge, Tennessee 37830

1

Dr. Clarence R. Mehl
Division 1112
Sandia National Laboratories
Box 5800
Albuquerque, New Mexico 87185

1

Other Organizations in U.S.:

Mr. Arthur D. Caster
Chairman, Coordination Committee
on Civil Defense
American Society of Civil Engineers
2864 McFarlan Park Drive
Cincinnati, Ohio 45211

1

Dr. Robert Fristrom
Applied Physics Lab JHU
Johns Hopkins Road
Laurel, MD 20810

1

Mr. Ronald Drzewoeclo
Calspan Corporation
P.O. Box 235
Buffalo, New York 15221

1

Center for Planning and Research, Inc.
2483 East Bayshore - Suite 104
Palo Alto, CA 94303

1

Mr. Richard Laurino
Center for Planning and Research, Inc.
2483 East Bayshore - Suite 104
Palo Alto, CA 94303

1

Scientific Service Inc.
517 E. Bayshore
Redwood City, CA 94063

1

Mr. John Rempel
Center for Planning and Research, Inc.
2483 E. Bayshore - Suite 104
Palo Alto, CA 94303

1

Mr. Walmer (Jerry) Strobe
Center for Planning and Research, Inc.
5600 Columbia Pike (Suite 101)
Bailey's Crossroads, VA 22041

1

The Dikewood Corporation
1608 Bradbury Drive
University Research Park
Albuquerque, New Mexico 87112

1

Factory Mutual Research Corp.
ATTN: Dr. Ray Friedman
1151 Boston-Providence Turnpike
Norwood, Massachusetts 02062

1

Higgins-Auld & Associates Engineers
ATTN: Cornelius J. Higgins
2601 Wyoming Blvd., Suite H-1
Albuquerque, New Mexico 87112

1

Hudson Institute
Quaker Ridge Road
Croton-on-Hudson
New York 10520

1

Dr. Anatole Longinow
IIT Research Institute
10 West 35th Street
Chicago, Illinois 60616

1

Mr. Thomas Waterman
IIT Research Institute
10 West 35th Street
Chicago, Illinois 60616

1

Dr. Leo A. Schmidt
Institute for Defense Analyses
400 Army-Navy Drive
Arlington, VA 22202

1

Los Alamos Scientific Laboratory
ATTN: Document Library
Los Alamos, N.M. 87544

1

The RAND Corporation
ATTN: Document Library
1700 Main Street

Dis-6

1

Mr. Howard McClennon, President 1
International Association of Fire Fighters
915 16th Street, N.W.
Washington, D.C. 20006

Mr. Don Sachs 1
Kaman Nuclear
Garden of the Gods Road
Colorado Springs, Colorado 80901

Mr. Peter S. Hughes 1
Los Alamos Technical Associates, Inc.
P.O.Box 410
Los Alamos, New Mexico 87544

Director 1
Lovelace Foundation
5200 Gibson Boulevard, S.E.
Albuquerque, New Mexico 87108

Mr. Kenneth Kaplan 1
Management Science Associates
P.O. Box 239
Los Altos, CA 94022

Dr. Laurence Pietrzak 1
Mission Research Corp.
735 State Street, P.O. Drawer 719
Santa Barbara, CA 93102

Dr. Geoffrey N. Berlin 1
Modeling Systems, Incorporated
Ten Emerson Place
Suite 4-J
Boston, Massachusetts 02210

Mr. H.L. Murphy 1
H. L. Murphy Associates
P.O. Box 1727
San Mateo, CA 94401

National Council on Radiation 1
Protection & Measurements
7910 Woodmont Avenue
Bethesda, MD 20014

National Fire Protection Association 1
Library
470 Atlantic Avenue
Boston, Massachusetts 02210

Dr. Harold L. Brode
Pacific-Sierra Research Corp.
1456 Cloverfield Blvd.
Santa Monica, CA 90403

1

Dr. Richard Small
Pacific-Sierra Research Corp.
1456 Cloverfield Blvd.
Santa Monica, CA 90403

1

Mr. Fred Sauer
Physics International Company
2700 Merced Street
San Leandro, CA 94577

1

The RAND Corporation
ATTN: Document Library
1700 Main Street
San Monica, CA 90401

1

R&D Associates
ATTN: Dr. Henry Cooper
1401 Wilson Blvd.
Rosslyn, VA 22209

1

Mr. Edward Hill
Research Triangle Institute
Post Office Box 12194
Research Triangle Park, N.C. 27709

1

Harvey G. Ryland
Ryland Research, Inc.
5266 Hollister Ave., Suite 324
Santa Barbara, CA 93111

1

Dr. John Cockayne
Senior Scientist
Science Applications, Inc.
1710 Goodridge Drive
P.O.Box 1303
McLean, VA 22101

1

Dr. Marvin Drake
Science Applications, Inc.
P.O.Box 2351
1200 Prospect Street
La Jolla, CA 92037

1

Fire Research Section
Department of Structural Research
Southwest Research Institute
8500 Culebra Road
San Antonio, Texas 78206

1

Mr. Raymond Alger
SRI International
Menlo Park, CA 94025

1

Dr. Jana Backovsky
SRI International
Menlo Park, CA 94025

1

Mr. Clay P. Butler
SRI International
Menlo Park, CA 94025

1

Mr. Dick Foster
SRI International
1611 Kent Street
Arlington, VA 22209

1

Dr. Thomas C. Goodale
SRI International
Menlo Park, CA 94025

1

Mr. Stanley Martin
SRI International
Menlo Park, CA 94025

1

Dr. Fred Offensend
SRI International
Menlo Park, CA 94025

1

Mr. Tom Blake
Systems, Science & Software
P.O.Box 1620
La Jolla, CA 92138

1

Technology & Management Consults.
330 Washington Street
Suite 613
Marina Del Rey, CA 90291

1

Mr. Joseph E. Minor Texas Tech University Lubbock, Texas 79408	1
Dr. Francis E. Fendell TRW One Space Park (R1/1038) Redondo Beach, CA 9017	1
Dr. William F. Christian Underwriters Laboratories, Inc. 333 Pfingsten Road Northbrook, Illinois 60062	1
Professor A. Murty Kanury Department of Aerospace and Mechanical Engineering University of Notre Dame Notre Dame, Indiana 46556	1
Dr. Forman Williams Department of the Aerospace and Engineering Sciences University of California San Diego La Jolla, CA 03027	1
Prof. R. K. Pefley University of Santa Clara Santa Clara, CA 95063	1
Foreign Organizations:	
Mr. Ashton M. Patterson Canadian Defense Research Staff 2450 Massachusetts Ave., N.W. Washington, D.C. 20008	1
The Information Center Forest Fire Research Institute 331 Cooper Street Ottawa Ontario CANADA KIA 043	1
Dr. Ing, P.G. Seeger Forschungstelle für Brandschutztechnik University of Karlsruhe (TH) 75 Karlsruhe 21 Postfach 63380 West Germany	1

Dr. Vilhelm Sjolin
Research Institute of National Defense
Forsvarets Forskningsanstalt
Stockholm 80, Sweden

1

Individuals
No Organizational Affiliation:

Dr. Matthew G. Gibbons
5424 Lawton Avenue
Oakland, CA 94618

1

Dr. Don Scheuch
430 Golden Oak Drive
Portola Valley, CA 94025

1

Dr. Steve J. Wiersma
658 Princeton Avenue
Sunnyvale, CA 94087

1

Dr. Roger Sullivan
System Planning Corporation
1500 Wilson Boulevard - Suite 1500
Arlington, VA 22209

1

INTERNAL IDA DISTRIBUTION

H. Williams
PAD, 10A9

1

E. Kerlin
PAD, 10A15

1

J. Grotte
PAD, 10D27

1

B. Anderson
PAD, 10A27

1

J. Bracken
PAD, 10D31

1

R. Jakobovits
PAD, 10A21

1

R. Kuenne
10D12

1

D. Moody
PAD, 10D15

1

E. Doherty
PAD, 10C2

2

Control and Distribution

7

I. Schmidt
PAD, 10D23

17

A Study of Twenty-Four Nationwide Fallout Patterns from Twelve Winds, (IDA Paper P-1604) by Leo A. Schmidt, Unclassified, Institute for Defense Analyses, September 1981, 344 pages (Contract FEMA EMW-C-0377, Work Unit 4112C)

Abstract

The research conducted under this contract deals with an assessment of fallout deposition resulting from two different types of attacks on the continental United States (counterforce-only and counterforce plus countervalue) given twelve typical wind patterns--one for each month of the year. Representations of fallout deposition are given in two categories--one accenting higher dose ranges to indicate shelter requirements and the other accenting lower dose ranges to present the complete spectrum of the fallout threat.

The research is reported in descriptive presentation of the model, the winds, the attack and the results. Appendices present the fallout deposition maps.

A Study of Twenty-Four Nationwide Fallout Patterns from Twelve Winds, (IDA Paper P-1604) by Leo A. Schmidt, Unclassified, Institute for Defense Analyses, September 1981, 344 pages (Contract FEMA EMW-C-0377, Work Unit 4112C)

Abstract

The research conducted under this contract deals with an assessment of fallout deposition resulting from two different types of attacks on the continental United States (counterforce-only and counterforce plus countervalue) given twelve typical wind patterns--one for each month of the year. Representations of fallout deposition are given in two categories--one accenting higher dose ranges to indicate shelter requirements and the other accenting lower dose ranges to present the complete spectrum of the fallout threat.

The research is reported in descriptive presentation of the model, the winds, the attack and the results. Appendices present the fallout deposition maps.

A Study of Twenty-Four Nationwide Fallout Patterns from Twelve Winds, (IDA Paper P-1604) by Leo A. Schmidt, Unclassified, Institute for Defense Analyses, September 1981, 344 pages (Contract FEMA EMW-C-0377, Work Unit 4112C)

Abstract

The research conducted under this contract deals with an assessment of fallout deposition resulting from two different types of attacks on the continental United States (counterforce-only and counterforce plus countervalue) given twelve typical wind patterns--one for each month of the year. Representations of fallout deposition are given in two categories--one accenting higher dose ranges to indicate shelter requirements and the other accenting lower dose ranges to present the complete spectrum of the fallout threat.

The research is reported in descriptive presentation of the model, the winds, the attack and the results. Appendices present the fallout deposition maps.

A Study of Twenty-Four Nationwide Fallout Patterns from Twelve Winds, (IDA Paper P-1604) by Leo A. Schmidt, Unclassified, Institute for Defense Analyses, September 1981, 344 pages (Contract FEMA EMW-C-0377, Work Unit 4112C)

Abstract

The research conducted under this contract deals with an assessment of fallout deposition resulting from two different types of attacks on the continental United States (counterforce-only and counterforce plus countervalue) given twelve typical wind patterns--one for each month of the year. Representations of fallout deposition are given in two categories--one accenting higher dose ranges to indicate shelter requirements and the other accenting lower dose ranges to present the complete spectrum of the fallout threat.

The research is reported in descriptive presentation of the model, the winds, the attack and the results. Appendices present the fallout deposition maps.



WASHINGTON

MONTANA

CANADA

IDAHO

NORTH DAKOTA

MINNESOTA

OREGON

WISCONSIN

MICH

WYOMING

SOUTH DAKOTA

CALIFORNIA

NEVADA

UTAH

NEBRASKA

IOWA

ILLINOIS

COLORADO

MISSOURI

KANSAS

ARIZONA

NEW MEXICO

OKLAHOMA

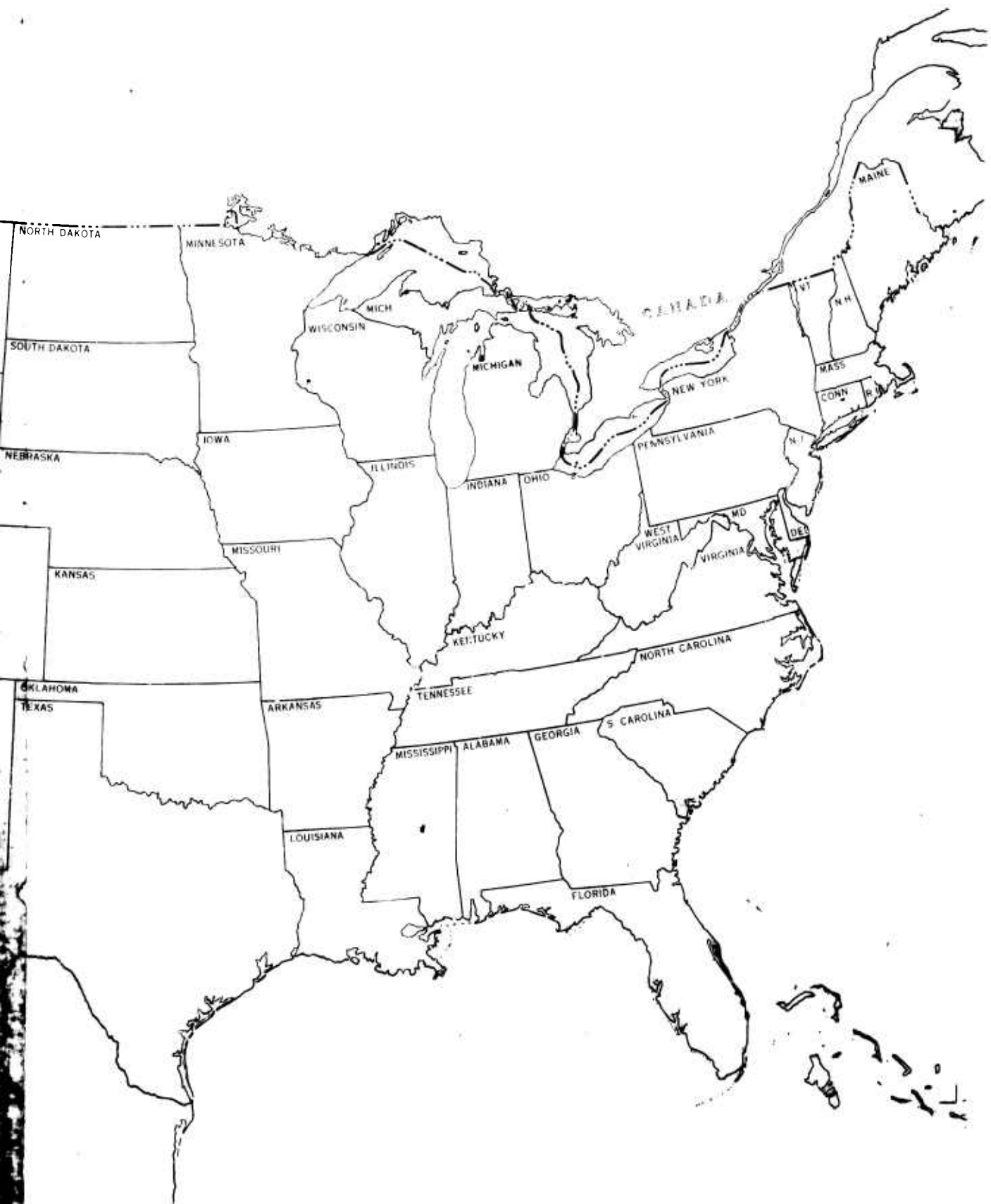
TEXAS

ARKANSAS

MEXICO

LOUISIANA

MISS



NORTH DAKOTA

MINNESOTA

SOUTH DAKOTA

NEBRASKA

IOWA

KANSAS

MISSOURI

OKLAHOMA

TEXAS

ARKANSAS

LOUISIANA

WISCONSIN

MICH

MICHIGAN

ILLINOIS

INDIANA

OHIO

KY: TUCKY

TENNESSEE

MISSISSIPPI

ALABAMA

GEORGIA

FLORIDA

NORTH CAROLINA

S CAROLINA

PENNSYLVANIA

NEW YORK

VT

N.H.

MASS

CONN

R.I.

N.J.

WEST VIRGINIA

MD

VIRGINIA

DE

MAINE

CANADA